Abstract

DAWOOD, MINA MAGDY RIAD. Bond Characteristics and Environmental Durability of CFRP Materials for Strengthening Steel Bridges and Structures. (Under the direction of Dr. Sami Rizkalla.)

This dissertation presents the findings of a research program that was conducted in two parts to investigate the bond behavior and environmental durability of carbon fiber reinforced polymer (CFRP) materials for strengthening steel bridges and structures.

The first part of the research consisted of an experimental and analytical research program to investigate the bond characteristics of CFRP lap-splice joints. The experimental program included a total of eight double-lap shear tests and ten steel beam tests. The main parameters considered include the geometric configuration of the plate ends, the length of the splice plates and the use of mechanical anchorage near the plate ends. A finite element analysis was conducted to determine the distribution of the stresses within the adhesive layer for different splice configurations. The findings indicate that the presence of the reverse tapered plate end reduced the magnitude of the peak stresses in the adhesive layer thereby increasing the tension strength of the splice joints. Increasing the splice length and installing additional mechanical anchorage did not enhance the strength of the joints. Based on the findings, a method is proposed to design lap-splice joints for implementation of the proposed CFRP system on longer-span flexural members.

The second part of the research consisted of a total of 44 steel-CFRP double-lap shear tests to study the environmental durability of the proposed CFRP strengthening system. The specimens were exposed to accelerated corrosion conditions and subsequently loaded monotonically to failure. The additional use of a silane adhesion promoter or a glass fiber insulating layer, to enhance the bond durability, was also studied. The findings indicate that the presence of the glass fiber layer enhanced the initial bond strength of the system, while the use of a silane adhesion promoter was essential to ensure the durability of the system. The findings of this research program demonstrate that, with proper detailing, the proposed CFRP system can be effectively used for strengthening of steel bridges and structures.

Bond Characteristics and Environmental Durability of CFRP Materials for Strengthening Steel Bridges and Structures

by
Mina Magdy Riad Dawood

A dissertation submitted to the Graduate Faculty of
North Carolina State University
in partial fulfillment of the
requirements for the Degree of
Doctor of Philosophy

Civil Engineering

Raleigh, North Carolina
2008

APPROVED BY:

Dr. Sami Rizkalla Chair of the Advisory Committee	Dr. Murthy Guddati Advisory Committee Member
Dr. Kara Peters Advisory Committee Member	Dr. Emmett Sumner Advisory Committee Member

Dedication

To Mira, with love…

Biography

Mina Dawood received his Bachelor of Science degree in Civil Engineering in 2003 from the University of Manitoba. He then moved to North Carolina to pursue his graduate studies at North Carolina State University under the direction of Dr. Sami Rizkalla. He completed his thesis on the fatigue and overloading behavior of steel-concrete composite beams strengthened with high modulus CFRP materials and received his Master of Science degree in 2005. He continued his research on the use of high modulus CFRP materials for strengthening steel bridges and structures at North Carolina State University in pursuit of his Doctoral degree. He also participated in research on the use of high strength steel reinforcing bars as flexural reinforcement for concrete structures, and on the development of a fiber optic system for structural health monitoring of civil infrastructure.

Acknowledgements

It is with profound appreciation and humility that I offer my gratitude to those organizations and individuals who have made my graduate career an opportunity for immense professional and personal growth.

This research was supported by the National Science Foundation (NSF) Industry/University Cooperative Research Center (I/UCRC) on Repair of Buildings and Bridges with Composites (RB^2C). Funding and materials were provided by Mitsubishi Chemical FP America Inc.; the personal dedication and participation of Mr. Akira Nakagoshi and Mr. Takashi Aikawa are greatly appreciated. Fyfe Co. LLC donated the glass fiber reinforced polymer (GFRP) materials for the environmental durability study.

My personal thanks are also extended to North Carolina State University for the opportunities with which it has presented me.

The tireless guidance and mentorship of my academic and personal advisor, Dr. Sami Rizkalla, are paramount to my success in my studies and in my life. Dr. Rizkalla is a truly inspirational role model with a genuine interest in the success of each of his students. Thank you. The support of my advisory committee, Dr. Murthy Guddati, Dr. Emmett Sumner and Dr. Kara Peters, cannot be overlooked. Their guidance and thorough review helped to maintain the integrity of this research. Dr. Paul Zia and Dr. Rudolf Seracino, although they were not directly involved in the preparation of this dissertation, were instrumental in my academic growth.

The experimental components of this research could not have been completed without the support of the technical staff at the Constructed Facilities Laboratory, Mr. Jerry Atkinson, Mr. William Dunleavy and Mr. James (Lee) Nelson. Several members of the International Institute for FRP in Construction (IIFC) working group on FRP-Strengthened Metallic Structures reviewed the details of the environmental durability study prior to implementation

of the experimental program. The thorough review and insightful comments of Dr. Len Hollaway, Dr. Riadh Al-Mahaidi, and Dr. Xiao-Ling Zhao are greatly appreciated.

The administrative assistance of Mrs. Renee Howard, Mrs. Diana Lotito, and Mrs. Amy Yonai was essential to ensure that the project, and my graduate career, progressed on schedule and on budget.

My colleagues at the Constructed Facilities Laboratory cannot be forgotten. The advice and friendship of Dr. Wonchang Choi, Dr. Owen Rosenboom, Dr. Hatem Seliem, and Mr. Gregory Lucier, who brought a fresh new perspective to my research, is sincerely appreciated. The friendship of every member of the CFL family will remain with me indefinitely.

I offer my sincere gratitude to my parents for the incomparable role they have played in my life. Their love, their role model and their ceaseless prayers have made me into the person that I am today. The love and support of my newest family members, and in-laws to be, Uncle Alfred, Tante Hoda and Monica, are meaningful to me beyond words.

To my dear fiancée Mira, thank you for your love and for the special place you have in my life. I thank God for you always.

I thank God for orchestrating my life more perfectly than I could imagine.

Table of Contents

List of Tables

List of Figures

Chapter 1: Introduction

The use of fiber reinforced polymer (FRP) materials in civil infrastructure for the repair and strengthening of reinforced concrete structures and also for new construction has become common practice. Based on the successful implementation of this technique for reinforced concrete, researchers have also investigated the use of CFRP materials for repair and strengthening of steel structures. While the use of CFRP materials has been demonstrated to enhance the strength of steel flexural members, the relatively low modulus of CFRP materials compared to steel has typically resulted in minimal enhancement of the elastic behavior of the strengthened members. However, the development of high modulus carbon fibers, with an elastic modulus approximately three times that of structural steel, challenged researchers to establish a CFRP system to enhance the strength and serviceability of steel structures.

The development of a high modulus CFRP strengthening system for steel bridges and structures began at North Carolina State University in 2002 through funding by the National Science Foundation (NSF) Industry/University Cooperative Research Center (I/UCRC) on Repair of Buildings and Bridges with Composites (RB^2C). An extensive experimental and analytical research program was conducted to develop a suitable system to use high modulus carbon fibers for strengthening and repair of steel bridges and structures (Schnerch, 2005). The system development included selection of suitable adhesives to bond carbon fiber materials to steel surfaces and selection of a suitable high modulus CFRP pultruded product which could be used to enhance the strength and serviceability of steel flexural members. A series of large-scale tests were conducted to evaluate the feasibility of the proposed strengthening system for strengthening steel highway and telecommunications infrastructure. The research findings demonstrated that the proposed strengthening system was capable to enhance the flexural strength and stiffness of steel-concrete composite bridge girders by up to 45 percent and 36 percent respectively.

Based on the successful use of the proposed strengthening system, further research was conducted by the author to evaluate the performance of the strengthening system under severe loading conditions (Dawood, 2005; Dawood et al., 2007). The research findings demonstrated that the strengthening system can be used to increase the allowable live load level of typical steel-concrete composite beams. The findings further indicated that, even under the effect of the increased live load, beams strengthened with the proposed high modulus CFRP system exhibited superior performance under overloading and fatigue loading conditions compared to unstrengthened beams.

The successful implementation of high modulus CFRP materials for enhancing the strength and serviceability of steel bridges and structures led to the need to evaluate practical aspects related to the detailing and environmental durability of the proposed strengthening system which is the main focus of the research presented in this dissertation.

1.1 RESEARCH SIGNIFICANCE

This dissertation describes a research program, which was conducted in two parts, to evaluate the bond characteristics, and the environmental durability of the proposed high modulus CFRP strengthening system.

The objective of the first part of the research is to develop a suitable splice joint for high modulus CFRP materials used to strengthen steel flexural members. These types of joints are necessary in order to use CFRP systems to strengthen longer-span steel bridges and structures. Due to the high flexural rigidity of pultruded, high modulus CFRP plates, they cannot be easily coiled for transportation. This necessitates that the pultruded plates be cut to length and shipped straight to the job site. The producers of the high modulus CFRP material indicated that the maximum length of the CFRP plates which can be readily transported is approximately 7 m. In order to retrofit longer-span steel bridges and structures, it is therefore necessary to splice adjacent lengths of the CFRP plates. The relatively short length and high

flexural rigidity of CFRP splice plates makes them particularly susceptible to debonding mechanisms which typically initiate from the plate end. Therefore, a thorough understanding of the bond characteristics of CFRP plates is essential to establish an effective lap-splice type connection for strengthening steel structures. In order to develop a suitable CFRP splice joint, an experimental and analytical study was conducted, as outlined in the first part of this dissertation.

The objective of the second part of the research study is to evaluate the environmental durability of CFRP materials bonded to steel surfaces. Since bridges are typically exposed to a wide range of environmental conditions, the environmental durability of a strengthening system is essential to ensure the long-term performance of the system. Three primary mechanisms of degradation can affect the long-term durability of bonded joints between steel and CFRP: degradation of the interfacial region between the adhesive and the steel surface, accelerated corrosion of the steel due to galvanic coupling with the CFRP materials and degradation of the material properties of the adhesive itself. All three of these factors were studied in the experimental program which was conducted in the second part of this research.

1.2 SCOPE & ORGANIZATION OF THE DISSERTATION

This dissertation is organized in two major parts. The first part consists of five chapters which present the experimental and analytical research that was conducted to evaluate the bond characteristics and structural performance of CFRP splice joints bonded to steel surfaces. The second part consists of four chapters which present the experimental research that was conducted to study the environmental durability of the proposed strengthening system.

Chapter 2 presents a review of the research that has been conducted related to strengthening steel structures with CFRP materials. Major emphasis is placed on the research related to the characteristics of bonded joints between CFRP materials and steel surfaces.

Chapter 3 presents the details of the experimental program that was conducted to evaluate the bond and splice characteristics of CFRP plates. The experimental program included a total of eight double-lap shear specimen tests and ten tests of steel flexural members.

The results of the experimental program are presented in Chapter 4. The relevant results related to the measured strains and deflections and the observed behavior of the bonded joints are presented. Details of the experimental results are presented in Appendix A.

Chapter 5 presents the details of the finite element analysis that was conducted to evaluate the bond characteristics of the CFRP splice joints. The finite element results are presented and compared to the findings of the experimental program. A design method is presented as a tool to determine the design strength and to design the suitable location of spliced joints for application to longer-span steel flexural members.

The major findings of the bond and splice study, and recommendations for future work related to bond are presented in Chapter 6.

The remaining chapters present the second part of the research program which was conducted to study the environmental durability of the bond between CFRP materials and steel surfaces.

Chapter 7 presents a review of the literature related to the previous research that was conducted to study the environmental durability of adhesively bonded joints.

Chapter 8 describes the details of the experimental program that was conducted to study the environmental durability. The test specimens, materials, testing program and test setup that were used are described.

Chapter 9 presents the results of the experimental program. The environmental durability is evaluated based on the degradation of the strength and stiffness of the tested specimens. The

degradation of the basic material characteristics is also presented. Details of the experimental results are presented in Appendix B.

The conclusions of the environmental durability study are presented in Chapter 10 along with recommendations for future work related to the environmental durability of the bond between CFRP materials and steel surfaces.

Part I:
Bond & Splice Study

Chapter 2: Background

The use of fiber reinforced polymer (FRP) materials for repair and strengthening of metallic structures has been demonstrated in aerospace, marine, automotive and manufacturing industries. In civil engineering, FRP materials have been successfully used for repair and strengthening of reinforced concrete structures and this technique has become a commonly accepted practice for repair of reinforced and prestressed concrete civil infrastructure. The successful use of FRP materials in these other fields has recently led to research on the use of FRP materials for strengthening and repair of metallic structures for civil engineering applications. Many of the advances which have been made in other industries can be directly applied to FRP strengthening of metallic structures. However, the use of FRP materials for repair and strengthening of metallic civil infrastructure poses many unique challenges. In aerospace, automotive and manufacturing industries relatively thin FRP laminates are typically installed in controlled environments using sophisticated installation techniques which require elevated cure temperatures and complex surface treatments. Civil infrastructure applications necessitate the use of relatively thick FRP materials which are typically installed on site using simple installation techniques, ambient-temperature cure adhesives and simple surface preparation techniques. Debonding of FRP materials bonded to reinforced concrete structures is typically governed by the tension strength of the concrete surface. By comparison debonding of FRP systems for strengthening metallic structures typically occurs in the adhesive or FRP materials and careful selection of these components is essential to the satisfactory performance of the strengthening system. For the past 10 years research has been focused on addressing the specific problems associated with the use of FRP materials for strengthening and repair of metallic, specifically steel, civil infrastructure.

A number of state-of-the art review papers have been published which summarize the research findings related to the use of FRP for strengthening metallic structures. In 2002, Hollaway and Cadei discussed different techniques for installation of FRP materials on

metallic structures. They focused on surface preparation techniques, material selection and installation requirements as well as briefly discussing environmental durability issues. They presented a number of specific field applications, primarily in the United Kingdom, which illustrate the ease and effectiveness of using FRP materials for rehabilitation of metallic structures.

In 2003, Shaat et al. presented a review of the research related to the flexural behavior of steel members strengthened with FRP materials. They demonstrated that FRP materials could be effectively used to enhance the strength and stiffness of steel flexural members. They identified that further research was needed to study the use of high-modulus CFRP materials for strengthening steel-concrete composite girders. They also identified the need for further research on the bond behavior and environmental durability of CFRP strengthened steel structures and also on the use of FRP for strengthening compression members.

In 2004, Buyukozturk et al. reviewed the research related to debonding of FRP materials from steel surfaces. They identified four possible debonding mechanisms including adhesive failure at the steel-adhesive interface, cohesive failure within the adhesive layer, cohesive failure at the adhesive-FRP interface and delamination within the FRP material itself. They also identified two main analytical approaches which were commonly used to evaluate debonding of FRP materials including stress-based approaches and fracture mechanics-based approaches. They identified a need for additional development of debonding models, continued experimental research to validate the current analytical models, and development of suitable failure criteria to predict debonding of FRP materials. The also identified the need to extend the existing debonding models to include the effects of fatigue loading, to study environmental durability of bonded strengthening systems and to develop non-destructive analysis methods to evaluate bond integrity.

In 2007, Zhao and Zhang conducted a state-of-the art review of FRP strengthening for steel structures. They identified the significant, rapid developments which have been recently

made on the understanding of the bond behavior of FRP materials bonded to steel surfaces. They also discussed the recent developments related to strengthening of tubular steel structures and repair of cracked steel structures with FRP materials. They identified the need for future research related to development of bond-slip relationships for FRP materials bonded to steel surfaces. Additional research needs that were identified included investigation of the lateral-torsional stability of FRP strengthened steel flexural members and development of a fatigue crack propagation model.

This chapter presents an up-to-date review of the research related to strengthening steel structures with FRP materials. The following sections discuss the research related to flexural behavior, bond characteristics, repair of cracked steel members, strengthening of tubular structures, field applications and design guidelines related to the use of FRP materials for strengthening steel structures.

2.1 FLEXURAL BEHAVIOR OF STEEL BEAMS STRENGTHENED WITH CFRP

A number of studies have been conducted to evaluate the suitability of using CFRP materials for repair or strengthening of steel flexural members. Researchers have studied the use of FRP material for repair of naturally corded steel girders (Mertz & Gillespie, 1996), strengthening of plain steel beams (Nouredine, 1996; Patnaik & Bauer, 2004), repair of overloaded steel-concrete composite beams (Sen et al., 2001), repair of notched steel (Liu et al., 2001) and steel-concrete composite beams (Tavakkolizadeh & Saadatmanesh, 2003b), strengthening undamaged steel-concrete composite girders (Tavakkolizadeh & Saadatmanesh, 2003c) and repair of steel-concrete composite beams with simulated corrosion damage (Al-Saidy et al., 2004). A detailed review of these previous studies is presented by Dawood (2005).

The findings of the previous research indicate that the presence of the CFRP can help to increase the ultimate strength and post-elastic stiffness of typical steel beams. Further, the

presence of the CFRP helped to reduce the strain in the tension flange thereby increasing the yield load of the strengthened beams. In the case of steel beams with natural or simulated damage of the tension flange, installation of the CFRP typically restored the lost strength of the beam to levels comparable to those of the undamaged girders. The previous studies focused on the use of conventional modulus CFRP materials, which typically have a modulus of elasticity less than or equal to that of structural steel. Consequently, in order to achieve a significant increase of the elastic stiffness of the member, a significant amount of strengthening materials must be applied. A similar trend was identified in a recent study by Colombi and Poggi (2006a) who reported a maximum increase of the elastic stiffness of 14 percent for steel beams strengthened with up to 2 layers of CFRP plates with an elastic modulus approximately equal to that of steel.

Alternatively, high modulus CFRP materials have been proven to be effective in increasing the elastic stiffness and ultimate strength of steel-concrete composite beams (Schnerch, 2005). A high-modulus CFRP system was developed for strengthening steel-concrete composite bridge girders. The system development included selection of an appropriate adhesive to bond CFRP materials to steel surfaces. Based on a series of small-scale flexural tests, a two-part epoxy adhesive was selected to bond CFRP plates to steel surfaces for strengthening steel flexural members. The selected adhesive was capable of achieving the rupture strength of the CFRP strips within a development length of 100 mm. Once a suitable adhesive was selected, a series of large-scale steel-concrete composite beams were tested to evaluate the effectiveness of different intermediate and high-modulus CFRP strengthening systems. The proposed high modulus CFRP system was capable of increasing the elastic stiffness and ultimate strength of the tested beams by up to 36 percent and 45 percent respectively. It was also demonstrated that prestressing the CFRP plates prior to bonding them to the steel surface could help to increase the efficiency of the strengthening system.

In a partner study, the overloading and fatigue behavior of steel-concrete composite beams, strengthened using the proposed high modulus CFRP system, was investigated (Dawood et

al., 2007). The findings indicated that installation of the strengthening system helped to increase the elastic stiffness, yield load and ultimate strength of the tested steel-concrete composite beams. Additionally, the presence of the CFRP helped to reduce the residual deflections of the strengthened beams due to the effect of overloading conditions. This suggests that, due to the presence of the CFRP materials, a strengthened beam can remain in good serviceable condition even after experiencing severe overloading conditions. The fatigue test results indicated that the strengthened beams were capable of sustaining 3 million loading cycles with a simulated increase of the live load level of 20 percent without exhibiting any degradation of the measured elastic stiffness. These results are similar to those obtained in a previous study of naturally deteriorated steel beams strengthened with conventional modulus CFRP materials (Miller et al., 2001). The results of the latter study indicate that the strengthened beams were capable of sustaining up to 10 million loading cycles under typical field loading conditions without any indications of debonding of the CFRP.

The tests reported in the literature identified several different failure modes for typical steel or steel-concrete composite beams strengthened with CFRP materials. These include local or global buckling or instability (Mertz and Gillespie, 1996; Columbi & Poggi, 2006a), excessive deflection (Sen et al., 2001; Columbi & Poggi, 2006a), debonding of the CFRP materials(Liu et al., 2001; Tavakkolizadeh and Saadatmanesh, 2003b,c), rupture of the CFRP materials (Tavakkolizadeh and Saadatmanesh, 2003c; Patnaik and Bauer, 2004; Al-Saidy et al, 2004; Schnerch 2005; Dawood et al., 2007) and, in the case of steel-concrete composite beams, crushing of the concrete deck prior to rupture of the CFRP (Tavakkolizadeh and Saadatmanesh, 2003b; Al-Saidy et al., 2004). In practical applications, instability can be prevented by providing adequate lateral bracing to the structure. Deflections can be evaluated based on the transformed moment of inertia of the strengthened member and checked to ensure that they are within acceptable limitations. Rupture of the CFRP and crushing of the concrete can be evaluated using a moment-curvature analysis and the

allowable live load level can be designed to prevent these modes of failure. However, debonding of the CFRP is typically an unexpected failure mode which can be difficult to account for in the design process. To help prevent the occurrence of a premature debonding failure, some researchers have implemented additional mechanical anchorage by bolting or clamping the CFRP laminates (Sen et al., 2001). However, caution should be exercised when bolting CFRP materials to prevent longitudinal splitting of unidirectional CFRP products.

2.2 BOND CHARACTERISTICS OF CFRP MATERIALS TO STEEL SURFACES

Due to the uncertainty and the sudden nature of debonding modes of failure, considerable research has been conducted to evaluate the bond characteristics of CFRP materials. Experimental research was conducted to develop a fundamental understanding of the behavior of bonded joints. To fully understand the nature of the stress transfer in bonded joints, a number of analytical studies have been conducted to predict the distribution of stresses in the adhesive layer. Due to the complex nature of the stresses, researchers have also used finite element analysis techniques to evaluate the variation of the bond stresses along the length and through the thickness of the adhesive layer. Other researchers have studied different techniques to reduce the stress concentration near the ends of typical bonded joints by implementing different geometric configurations near the plate ends. Additional research has focused on the use of fracture mechanics techniques to evaluate the bond strength. The research conducted in each of these areas is reviewed in the following sections with particular emphasis on the bond behavior between CFRP materials and steel surfaces.

2.2.1 Experimental Studies

A number of experimental studies have been conducted to evaluate the behavior of bonded joints under different loading conditions. These experimental studies can be broadly divided into two categories: testing of tension type specimens and testing of flexural members. Finally, a number of novel experimental studies have been conducted including a study of

non-destructive evaluation of bonded joints and also an application of nanotechnology to enhance the strength of the bond between epoxy adhesives and steel surfaces. The research conducted in each of these areas is reviewed in the following sections.

2.2.1.1 Experimental studies on tension specimens

Miller et al. (2001) conducted tension tests on a series of continuous steel plates with CFRP strips bonded to each face as part of a research program to develop a CFRP system for strengthening steel structures. They concluded that, for the tested bond configuration, 98 percent of the force transfered to the CFRP plates occurred within a 100 mm zone near the end of the CFRP strengthening plate. Similarly, Lam et al. (2004) tested a series of steel-CFRP double-lap shear coupons and concluded that increasing the overall bond length from 100 mm to 300 mm did not significantly increase the bond strength of the joint for the particular combination of materials tested. This was due to the presence of significant bond stress concentrations near the ends of the CFRP and steel materials. However, increasing the bond length did help to increase the maximum ductility of the bonded joints. In the same study it was demonstrated that increasing the axial stiffness of the CFRP splice plates, by increasing the thickness of the CFRP plates, significantly increased the tension strength of the system.

Other testing indicates that increasing the bond length is essential to maintain the damage tolerance of bonded joints subjected to fatigue loading (Matta et al., 2005). Fatigue tests of steel-CFRP double lap shear specimens indicated that fatigue loading led to propagation of cracks which initiated within the center of the joints. The presence of the cracks resulted in a stiffness degradation of up to 40 percent for the tested double-lap shear specimens. The authors suggested that for shorter bond lengths, propagation of the crack may have led to complete debonding under the effect of the applied fatigue loading.

Xia and Teng (2005) conducted a series of tests to develop a stress-slip curve for CFRP materials bonded to steel surfaces. CFRP strips were bonded to stiff steel blocks and tested in a longitudinal pull-off type configuration. This is similar to the approach used to develop stress-slip relationships for CFRP materials bonded to concrete surfaces. Test results indicated that the measured stress-slip relationship was essentially bilinear with linear ascending and descending branches. The measured peak shear strength of the bond between CFRP and steel surfaces was approximately five to six times greater than the typical measured bond strength to concrete surfaces; however, the measured maximum slip was similar to that for CFRP materials bonded to concrete (Zhao and Zhang, 2007). The proposed stress-slip approach may be appropriate to model the bond of CFRP to cracked steel members. However, the observed failure typically occurred away from the end of the CFRP plate. Therefore, this approach may not accurately represent the effect of the typical plate end debonding type failures which can govern the behavior of steel members strengthened with high modulus CFRP materials.

Other researchers have investigated the effectiveness of using adhesive bonding in combination with mechanical anchorage of the CFRP plates to the steel surface (Colombi and Poggi, 2006b). The test specimens consisted of a continuous steel tension specimen with CFRP strips bonded to each face. A hole was subsequently drilled through the assembly and bolts were installed for two of the tested specimens. The test results indicated that the bolts were engaged after debonding of the CFRP strips from the steel surface. Failure occurred due to splitting of the longitudinal CFRP strips. The test results did not conclusively indicate whether or not the additional use of bolts increased the joint strength.

Photiou et al. (2006a) studied the bond behavior of intermediate and high modulus CFRP prepreg materials bonded to steel surfaces using a compatible adhesive film for strengthening steel structures. This type of strengthening system is similar to that used in aerospace applications. They found that the bond strength of the proposed system was higher than that obtained using typical two-part cold cure epoxy adhesives which are typically used in civil

infrastructure applications. They also found that the intermediate modulus CFRP strengthening system gave higher failure loads than the high modulus system due to the relatively low failure strain of the latter. The study also indicated, however, that the strength of the high modulus system could be increased by adding a glass fiber prepreg layer between the steel and the CFRP. The presence of the glass fiber layer resulted in a more gradual transfer of shear stresses from the steel to the CFRP thereby increasing the strength of the system.

Al-Emrani and Kliger (2006b) developed a new type of tension specimen to evaluate the propagation of debonding for yielded steel members. The specimen consisted of a dog bone shaped steel tension coupon with CFRP strips bonded on each face. The gradual taper of the width of the coupon was designed to simulate the gradual progression of yielding in the tension flange of a steel beam away from the plastic hinge region. The authors identified that, for certain strengthening systems, debonding could possibly initiate at the center of the bonded region rather than initiating at the plate ends. This type of failure mode was observed for steel members that were strengthened using conventional CFRP materials and a stiff adhesive with a relatively low strain capacity. The high level of plastic strains which formed due yielding of the steel near the center of the bonded joint resulted in the formation of significant shear stress concentrations in the relatively stiff adhesive near the center of the bonded joint. Finite element analysis indicated that the magnitude of these stress concentrations was equal to or greater than the shear stress concentrations near the plate ends. Due to its relatively low strain capacity, the adhesive could not accommodate the high levels of strain in the steel member. Therefore, the stress concentrations led to debonding of the CFRP plate initiating at the center of the bonded joint rather than at the plate ends.

In another study, Bocciarelli et al. (2008) conducted fatigue tests of steel tension members reinforced with CFRP materials to develop S-N curves for the tested strengthening system. An analytical model was developed to determine the magnitude of the principal stress in the adhesive layer near the end of the CFRP plate. The magnitude of the principal stress was

related to the number of fatigue cycles required to achieve a given level of degradation of the stiffness of the strengthened steel member. The test results indicate that stiffness degradation was an indicator of imminent failure of the strengthening system, however, a safe level of stiffness degradation was not proposed.

2.2.1.2 Experimental studies on strengthened flexural members

Nozaka et al. (2005) used a specially designed testing fixture to evaluate the bond characteristics of CFRP materials used to strengthen cracked steel beams. A CFRP strip was bonded to two steel plates, similar to a tension splice configuration. The plates were subsequently bolted to a steel beam which had a specially fabricated notch in the tension flange and web at midspan. A total of 27 tests were conducted using two different types of CFRP plates and five different adhesives. The test results suggested that increasing the ductility of the adhesive helped to increase the maximum strain achieved in the CFRP strip. Increased loading resulted in progressive yielding of the adhesive which helped to reduce the magnitude of the stress concentrations at critical locations within the bonded joint. The results further indicated that increasing the number of layers of the CFRP joint increased the tension strength of the bonded joint and reduced the maximum measured strain in the CFRP prior to debonding. For one of the CFRP/adhesive combinations tested an effective bond length was defined. Increasing the bonded length beyond the effective bond length did not result in any significant increase of the tension strength of the bonded joint.

Lenwari et al. (2006b) tested a total of seven steel beams strengthened with conventional modulus CFRP strips of different lengths to evaluate the bond behavior of the strengthening system. Three different plate lengths were considered including 500 mm, 650 mm and 1200 mm. The beams strengthened with the shorter plate lengths failed by debonding while the beams strengthened with 1200 mm long plates failed by rupture of the CFRP. For all of the beams which failed by debonding, the applied moment at the location of the plate end, at the time of failure, was approximately equal regardless of the length of the CFRP plate. The

measured strains in the CFRP near the end of the strengthening plate indicated that a distance of approximately 100 mm was required for the measured strains to achieve conformance with the predicted strains obtained from an elastic-plastic section analysis. A similar trend was identified using a stress-based analysis which used differential equilibrium and compatibility to predict the shear stresses in the adhesive layer. The measured 100 mm length to achieve conformance of the stresses in the CFRP was independent of the length of the CFRP plate.

A similar study was conducted by Deng and Lee (2007a) who tested a series of simply supported steel beams that were strengthened with CFRP plates of different lengths. The test results indicated that increasing the length of the bonded CFRP plate helped to increase the debonding load of the strengthening system. This was because increasing the length of the CFRP plate moved the plate end closer to the support, to a region of lower moment. This consequently reduced the magnitude of the shear and normal (peeling) stresses in the adhesive near the plate end. The authors proposed an analytical model to predict the magnitude of the maximum adhesive principal stress near the plate end, which is a function of the magnitude of the moment at the end of the plate. They suggested that the debonding of the CFRP plates would occur when the principal stress reached a limiting value. Additionally, the test results indicated that increasing the thickness of the CFRP plate decreased the debonding load of the system. This suggests that increasing the plate thickness also increased the magnitude of the stress concentrations near the plate ends.

In a related study the authors tested a series of strengthened small-scale steel beams subjected to fatigue loading conditions (Deng and Lee, 2007b). Seven different loading ranges were considered and the crack propagation in the adhesive near the end of the strengthening plate was monitored. Failure occurred when the crack in the adhesive propagated past the midspan of the beam. Based on the test results, an S-N curve was developed for the specific adhesive that was used in the experimental program. The S-N curve was not a function of the geometry or material characteristics of the steel beam or the CFRP materials. The infinite

life fatigue threshold for the tested strengthening system was found to be approximately 30 percent of the ultimate failure stress under static loading conditions.

2.2.1.3 Experimental studies on the bond behavior of CFRP materials to steel

Recent research efforts have focused on establishing non-destructive techniques to evaluate the performance of adhesive bonds under typical service conditions. Matta et al. (2006) investigated the use of the acoustic emission technique to monitor the progression of damage in bonded joints between steel and CFRP. They considered two different joint configurations subjected to both static and fatigue loading conditions. The test results indicated that the acoustic emission technique was capable of detecting the accumulation of microcracking in the adhesive prior to any visible signs of damage being observed in the joint. The technique was also capable of accurately identifying the initiation and progression of the debonding failure. The location of the debonding, which typically occurred at the end of the CFRP plate or at the location of a crack-like discontinuity in the steel plate, was also accurately identified using the proposed method. For joints subjected to fatigue loading, the acoustic emission output was correlated with different stages of crack propagation that were observed using conventional methods.

Recent developments in nanotechnology have been applied to enhance the bond strength between epoxy adhesives and steel surfaces. Zhai et al. (2007) indicated that adding 2 percent of nano-Al_2O_3 by weight to a commercially available epoxy adhesive could increase the bond strength of the epoxy to steel surfaces up to 5 times. The strength increase was sensitive to the degree of surface roughness of the steel and was maximized for surfaces with moderate roughness. Chemical analysis of the steel surface of failed bond specimens suggested that the presence of the nano-Al_2O_3 resulted in the formation of a carboxyl group which was not observed on surfaces bonded with the unmodified adhesive. The formation of this new polar group was believed to enhance the strength of the interface between the

adhesive and the steel. This resulted in a change of the failure mode from an interfacial mode to a combined interfacial/cohesive mode.

2.2.2 Analytical Studies

A number of analytical studies have been performed to evaluate the distribution of stresses in bonded joints. These can generally be divided into two categories: those applicable to tension type bonded joints, such as single-lap and double-lap joints, and those applicable to flexural members, namely beams strengthened with an externally bonded plate. The analytical research conducted in each of these fields is reviewed in the following sections.

2.2.2.1 Analytical models developed for tension type bonded joints

Extensive analytical research on the stress transfer mechanisms in bonded joints has been conducted in the aerospace industry for the past 60 years. As a result, a number of analytical models exist to predict the distribution of stresses in typical bonded joints subjected to tension loading. While these models were typically developed for specific applications, the underlying assumptions do not typically limit the application of these models to specific materials. Therefore, they can generally be applied to a number of different applications in different industries including marine, automotive, manufacturing and civil infrastructure.

In 1944 Goland and Reissner developed an analytical model to calculate the distribution of shear and normal, or peeling, stresses in single lap shear bonded joints. Explicit solutions were obtained for two extreme cases: the case of a very stiff adhesive, and the case of a relatively flexible adhesive. The expressions for the shear and normal stresses were obtained on the basis of a plane strain analysis assuming that the adhesive joints were relatively wide. Additionally, the development assumed that the deformation and stress distribution of the joint could be represented as that of a cylindrically bent plate. Further, the analysis neglected the effect of the longitudinal stresses in the adhesive layer. Based on these assumptions, the

correct stress distributions were defined as those satisfying the boundary conditions while minimizing the strain energy of the system.

The proposed analytical model indicated the presence of significant shear and normal stress concentrations near the ends of the bonded joints. The normal stresses developed due to the geometric non-linearity of the joint which developed due to the eccentricity of the applied loads in the single lap joint. The analytical model further demonstrated that, for joints constructed using relatively stiff adhesives, the predicted stress concentrations dissipated within a relatively short distance away from the end of the plates equal to about two times the thickness of the adherends. For joints fabricated using relatively flexible adhesive, such as for metal adherends bonded with an epoxy adhesive, the stress concentration was significantly less severe and dissipated over a considerably longer distance. In both cases, the shear and normal stresses were taken to be constant throughout the thickness of the adhesive.

The expressions proposed by Goland and Reissner were developed for balanced single lap joints, that is, for joints between two sheets of the same adherend, subjected to longitudinal tension forces. In 1973, Hart-Smith used the same approach to develop expressions for the distribution of shear and normal stresses in double-lap shear joints between dissimilar materials (Cadei et al., 2004).

Both of the above models are based on linear-elastic behavior of the adhesive and the adherends. Later models were developed which take into account the non-linear material properties of the adhesive and adherends (Crocombe et al., 1990). The stress distribution obtained using a fully non-linear analysis was compared to the predicted stresses obtained from a non-linear finite element analysis and the results demonstrated good agreement.

The different lap-joint models that have been developed typically incorporated several different simplifying assumptions. The effect of these different assumptions on the

magnitude of the predicted maximum shear and normal stresses in an adhesive lap joint were evaluated for a number of different loading cases (Carpenter, 1991). The different assumptions evaluated included: the distribution of shear strain through the adhesive layer and the shear strain-displacement relationship, neglecting the shear deformation of the adherends, consistency of plane-stress and plane-strain assumptions used in different stages of the analysis, the completeness of the adhesive stress-strain relationship and the assumption of zero thickness of the adhesive layer. The study found that the predicted shear stresses were insensitive to the different assumptions considered. However, neglecting the shear deformation of the adherends had a significant effect on the magnitude of the maximum normal stress near the end of the adhesive joint. It was found that neglecting the shear deformation of the adherends could affect the magnitude of the calculated adhesive normal stress by up to 30 percent.

In 1999, Albat and Romilly, developed an analytical model, based on the approach of Hart-Smith, for double sided reinforcements and double-lap shear joints. The analysis considered joints with bonded plates of uniform thickness and also joints with tapered or stepped bonded cover plates. The analysis further proposed a correction factor to account for the effect of shear-lag in the adherends. The authors proposed analytical models to predict the shear stresses in the adhesive, the longitudinal stresses in the outer adherend and the longitudinal stresses in the inner adherend. However, an expression for the normal stresses in the adhesive was not presented. The expressions for the stresses in the outer adherend are particularly useful since these can be directly compared to the measured values obtained from strain gauges in experimental studies. A number of other researchers have confirmed that the expressions obtained by Albat and Romilly closely match the measured values obtained experimentally (Miller et al, 2001; Matta et al., 2005; Colombi and Poggi, 2006a). For double-lap shear coupons, shown schematically in Figure 2.1, the longitudinal stress in the outer adherened, σ_o, is given by Equation 2.1 for $0 < y < \ell$; the distribution of stresses is symmetric about the center of the joint.

$$\sigma_o = \frac{1}{2}\left(\frac{\frac{P}{E_o t_o} - 2(\alpha_i - \alpha_o)\Delta T}{t_o\left(\frac{1}{E_o t_o} + \frac{2}{E_i t_i}\right)}\right)\left(\cosh(\lambda y) - \frac{\sinh(\lambda y)}{\tanh(\lambda \ell)}\right) + \left(\frac{\frac{P}{E_i t_i} + (\alpha_i - \alpha_o)\Delta T}{t_o\left(\frac{1}{E_o t_o} + \frac{2}{E_i t_i}\right)}\right)\left(1 - \frac{\sinh(\lambda y)}{\tanh(\lambda \ell)}\right) \quad \text{(Eq. 2.1)}$$

where:

$$\lambda = \sqrt{\frac{\left(\frac{1}{E_o t_o} + \frac{2}{E_i t_i}\right)}{\left(\frac{t_i}{4G_i} + \frac{t_a}{G_a} + \frac{3}{8}\frac{t_o}{G_o}\right)}}$$

E = tensile modulus

α = coefficient of thermal expansion

ΔT = temperature change

G = shear modulus

subscripts o, i, and a refer to the outer and inner adherends and the adhesive respectively and the remaining variables are defined in Figure 2.1.

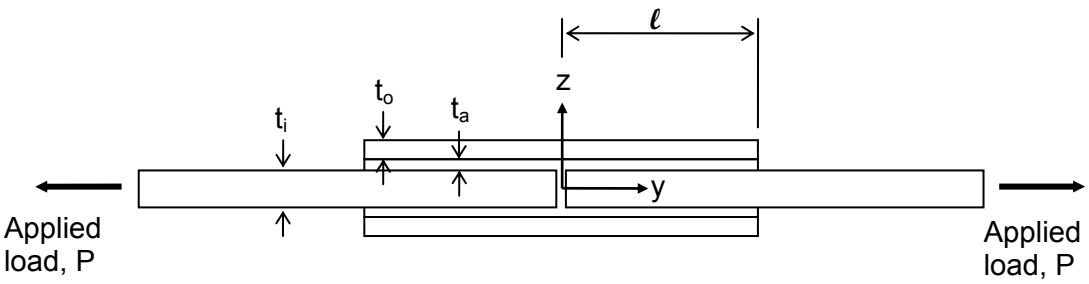

Figure 2.1 – Double-lap shear joint configuration considered by Albat and Romilly (1999)

The models discussed above are based on a common assumption that the bond stresses are constant through the thickness of the adhesive. Consequently, the expressions obtained for the shear stresses typically do not satisfy the zero shear stress boundary condition at the free edge of the adhesive. In a recent study Diaz et al. (2008) developed a model in which a double-lap shear joint was modeled using a series of stacked Reissner-Mindlin plates. A total of six plates were used to model the thickness of the joint including one plate for each of the outer adherends, one plate for each adhesive layer and two plates for the inner adherend. Consequently, each adhesive layer incorporated two interfaces which allowed different stresses to be calculated at each of the adhesive-adherend interfaces. The analysis results indicated that the peak shear stresses typically occurred a small distance away from the plate end rather than directly at the end of the joint as predicted by others. Additionally, the findings indicated that the assumption of constant bond stresses through the adhesive thickness can result in an over-prediction of the maximum shear stresses by up to 25 percent.

2.2.2.2 Analytical models for beams strengthened with externally bonded plates

A number of similar analytical models have been developed to predict the distribution of bond stresses in the adhesives for beams strengthened with externally bonded plates. The typical analysis approach involves considering differential equilibrium and strain compatibility for an infinitesimal element of the adhesive along the length of the plated

beam. Similarly to the case of tension loaded bonded joints, these models typically predict the presence of significant shear and normal stress concentrations in the adhesive near the plate ends.

One such model was developed by Täljsten (1997) to predict the shear and normal stresses in the adhesive layer for reinforced concrete beams strengthened with externally bonded FRP plates. This model was later used by Colombi and Poggi (2006a) to predict the longitudinal stresses in the CFRP plate for three steel beams that were strengthened with one or two layers of CFRP plates and subsequently tested to failure. The predicted stresses closely matched the stresses that were determined experimentally.

Smith and Teng (2001) evaluated the various assumptions of a number of different analytical models including the one previously developed by Täljsten. They identified that most of the available solutions did not account for the effect of the axial deformation of the beam member and/or bending deformations of the beam and/or the strengthening plate. They stated that these assumptions were appropriate when the flexural rigidity of the plate was small compared to that of the beam, such as for reinforced concrete beams strengthened with FRP materials. However, for applications in which the flexural rigidity of the plate was significant, such as for steel members strengthened with high modulus CFRP materials, these assumptions may lead to inaccurate prediction of the adhesive stresses. Therefore, the authors developed a new analytical model which accounted for the axial and flexural deformations of the beam and the strengthening plate. This model was later revised by Schnerch (2005) to account for the effect of thermally induced bond stresses. A parametric study conducted by the latter author indicated that the magnitude of bond stresses due to thermal fluctuations can be equal to or even exceed those due to typical mechanical loading.

The previous models were developed for beams strengthened with plates of uniform thickness. This allowed the development of closed form solutions for the shear and normal stresses which can be directly implemented for design purposes. In another study, Deng et

al. (2004) developed an analytical model for beams reinforced with tapered CFRP plates, shown schematically in Figure 2.2(a). The model requires a numerical solution technique due to the variation of the thickness of the strengthening plate near the plate end. The model predicts that the presence of a tapered plate end helps to reduce the magnitude of the adhesive stresses near the end of the strengthening plate. The model further indicates that increasing the length of the taper, ℓ, and decreasing the thickness of the plate at the end of the taper, t, further helps to decrease the magnitude of the stress concentration. A similar numerical solution approach was used by Schnerch (2005) to predict the stresses for reverse tapered plate ends, such as that shown schematically in Figure 2.2(b), and by Stratford and Cadei (2006) to predict the bond stresses near defects or voids in the adhesive. The latter study indicated the presence of significant stress concentrations near locations of defects in the adhesive. Such defects can be particularly damaging if they occur near the plate end. The analysis of Stratford and Cadei further indicates that the stresses near the plate end due to the effect of prestressing the CFRP materials can be up to five times higher than the stresses induced by mechanical loading only.

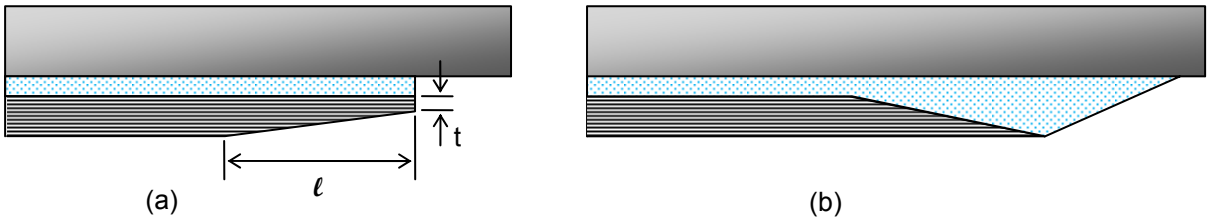

Figure 2.2 – Schematic representation of (a) tapered and (b) reverse tapered plate ends

Al-Emrani and Kliger (2006a) developed an analytical model to study the shear stresses near the plate ends of a steel beam strengthened with externally bonded, prestressed CFRP materials. The model did not include an expression for the normal stress component in the adhesive. The model was used to evaluate the effect of different parameters on the magnitude of the shear stress concentration near the plate end. The analysis indicated that decreasing the shear modulus, G, or increasing the thickness, t, of the adhesive reduced the

magnitude of the peak shear stresses in the adhesive. Further, it was found that the adhesive shear stresses were more sensitive to the magnitude of the prestrain that was applied to the FRP materials than they were to the modulus or thickness of the FRP plate.

The previous models considered only elastic material properties of the steel, FRP plate and the adhesive. However, other researchers have demonstrated that plasticity of the steel beam can have a significant effect on the distribution of bond stresses in the adhesive (Sebastian, 2005; Youssef, 2006). Sebastian (2005) demonstrated analytically that yielding of the tension flange of a strengthened steel beam can induce significant shear stresses in the adhesive layer near the elasto-plastic region of the beam. The findings of the study further indicated that assuming a rigid bond, and neglecting the flexibility of the adhesive, can result in an over-prediction of the maximum adhesive shear stress by up to 65 percent. Youssef (2006) conducted another analysis to predict the shear and normal stresses in an adhesive layer for a steel beam strengthened with GFRP plates. Within the elastic range, the maximum shear and normal stresses in the adhesive were predicted to occur near the ends of the FRP plate. This is similar to the trend obtained from the expressions developed by others using elastic analyses. However, after the yielding of the steel beam occurred, the model predicted the formation of significant shear and peeling stress concentrations near the plastic hinge region of the beam near one of the loading points. This was due to the excessive yielding of the steel beam in the plastic hinge region while the FRP materials remained elastic. At higher load levels the magnitude of the stresses near the location of the plastic hinge was greater than the magnitude of the stresses near the plate ends.

A common assumption among all of the previously studied analytical models is that the bond stresses are constant through the thickness of the adhesive layer. This assumption is necessary to simplify the analysis and, in certain cases, to decouple the differential equations which are used to obtain the distribution of shear and peeling stresses along the length of the adhesive. Other researchers have conducted higher-order, linear analyses which account for the variation of the bond stresses through the thickness of the adhesive (Rabinovich and

Frostig, 2000; Shen et al., 2001). Rabinovich and Frostig found that near the plate end the adhesive stresses varied significantly between the beam-adhesive and plate-adhesive interfaces. However, this difference diminished rapidly and, at a distance away from the plate end equal to the thickness of the adhesive, the stresses at both interfaces were essentially equal. Both of the analyses, by Rabinovich and Frostig (2000) and Shen et al. (2001), indicated that the adhesive shear and peeling stresses increase by increasing the stiffness or thickness of the FRP plate, decreasing the length of the FRP plate or decreasing the thickness of the adhesive layer.

2.2.3 Finite Element Analysis

A number of different researchers have used finite element analysis as a tool to evaluate the magnitude of bond stresses in different configurations of bonded joints. A number of the previously reported studies additionally used finite element analysis to confirm the results of the proposed analytical models. The proposed analytical models and the finite element results typically showed good agreement. Finite element analysis can also be used to evaluate the bond stresses in complex joint configurations which prohibit the development of simple closed form expressions for the bond stresses. Finite element analysis also provides an effective tool to evaluate the effect of geometric or material non-linearity on the behavior of bonded joints.

Adams and Peppiatt (1977) conducted a series of axially symmetric finite element analyses to study the distribution of bond stresses for bonded tubular lap joints subjected to tensile and torsional loading. They also studied different techniques to reduce the bond stresses near the ends of the adhesive joints. They found that the presence of an adhesive fillet near the end of the bonded joint can help to significantly reduce the magnitude of the bond stresses in the adhesive. The effect was more significant for joints subjected to tension loading then it was for torsionally loaded joints. They further found that partially tapering the tubular adherends

to form a scarf joint did not reduce the bond stresses enough to justify the added complexity of the manufacturing process.

Harris and Adams (1984) conducted a non-linear finite element analysis of aluminum single lap joints made using four different types of adhesives. The adhesives ranged from a brittle, essentially linear-elastic adhesive to a ductile essentially elastic-plastic adhesive. The presence of an adhesive fillet at the end of the joint was also considered. A two-dimensional, plane strain analysis was conducted and the non-linear material properties of the adhesive and the adherends were considered in the analysis. The analysis also accounted for the geometric non-linearity of the problem which occurred due to rotation of the bonded joint to accommodate the eccentricity of the applied loads in the single-lap joint configuration.

The analysis results indicated the presence of two stress concentrations in the adhesive: one near the end of the adhesive fillet and the other near the end of the lap-spliced plate. The analysis demonstrated that the geometric non-linearity of the joint helped to reduce the magnitude of the predicted adhesive stress concentrations. Plasticity of the adherends can also help to reduce the magnitude of the predicted stresses. The findings of the research further indicate that adhesive plasticity helps to reduce the magnitude of the stress concentrations near the ends of the bonded joint by allowing redistribution of the stresses to the less stressed portions of the splice joint. Based on the research findings, the authors proposed two different failure criteria for adhesively bonded joints. For brittle adhesives a maximum principal stress criterion was recommended while for ductile adhesive a maximum principal strain criterion was proposed. It should be noted that the finite element analysis indicated that the adhesive near the end of the lap-spliced plate was in a state of triaxial tension. Therefore, in order to apply the maximum principal strain failure criterion, the adhesive should maintain its ductile characteristics when subjected to a state of triaxial tension, not only when loaded uniaxially.

Richardson et al. (1993) conducted linear-elastic, two and three dimensional finite element analyses of adhesive joints subjected to different combinations of cleavage and shear stresses. They found that the adhesive joint remained in a state of plane strain over approximately 80 percent of the width of the joint. Near the edges of the joint the adhesive was found to be in a state of plane stress. Therefore, the authors found that it is generally acceptable to model typical bonded joints by a two-dimensional plane-strain analysis which represents the mid-plane of the adhesive joint. However, the authors proposed the use of a correction factor to modify the magnitude of the applied load in the two dimensional analysis to account for the non-uniform distribution of the applied load across the width of the specimen. They suggested that the magnitude of the correction factor should be obtained by conducting an initial three-dimensional analysis to evaluate the distribution of stresses in the adhesive across the width of the bonded joint.

Sebastian (2003) conducted a non-linear finite element analysis to evaluate the bond stresses in the adhesive for an indeterminate steel beam strengthened with CFRP laminates. The laminates were bonded to the tension side of the beam which varied between the top and bottom flanges at different locations along the continuous member. The laminates were terminated at the points of inflection along the beam as determined by an elastic analysis. The adhesive layer was modeled by a series of linear, shear and rotational springs while the beam and the strengthening plates were modeled by layered frame elements with translational and rotational degrees of freedom. The findings of the analysis indicated that, due to yielding of the steel beam at the locations of highest moment, the locations of the points of inflection along the beam can shift. This shift of the locations of the points of inflection can result in a significant increase of the adhesive shear stresses at the plate ends that are near the points of inflection. Further, the shift of the points of inflection can result in a reversal of the stresses in the strengthening plate from tension to compression. This could induce premature buckling of the strengthening materials. The author notes, however, that the majority of the life of a typical structure is spent in the linear regime. Therefore, such a

migration of the points of inflection is unlikely to occur and would likely only occur once. Therefore, while this behavior should be checked, it would not likely govern the design of the strengthening system. The findings further indicated that implementing a reverse tapered plate end configuration, such as that shown in Figure 2.2(b), could help to reduce the adhesive stresses near the plate end and delay the debonding of the strengthening materials.

In a later study, Sebastian (2006) used a similar finite element model to study the effects of the steel constitutive properties on the adhesive stresses in the yield zone of a steel beam strengthened with an FRP plate. The effect of the strain hardening modulus of the steel on the adhesive stresses was considered. The analysis also considered the effect of gradual yielding of the steel, rather than a sharp elastic-perfectly plastic stress-strain curve with a well defined yield plateau. The analysis results indicated that the peak adhesive shear stress in the yield zone of the beam was sensitive to the strain hardening modulus of the steel. A small strain hardening modulus, equal to approximately 5 percent of the elastic modulus of the steel, resulted in a reduction of the maximum adhesive shear stress of 2.5 times for one loading case. The results also indicated that the adhesive shear stresses in the areas of relatively low moment were sensitive to the gradual or abrupt nature of the yielding of the steel. Gradual yielding of the steel resulted in higher adhesive shear stresses in regions of low moment compared to the case of an elastic-perfectly plastic stress strain curve. Further findings of the analysis indicated that changing the adhesive modulus did not significantly change the adhesive shear stresses in the yield zone of the beam. However, increasing the elastic modulus of the FRP significantly reduced the adhesive shear stresses in the yield zone since the stiffer FRP helped to constrain the yielding of the steel beam. Increasing the FRP modulus also increased the magnitude of the stresses near the end of the FRP plate.

2.2.4 Effect of Plate End Configuration on Bond Behavior

As demonstrated, the experimental and analytical research that has been conducted to date indicates the presence of significant stress concentrations in the adhesive layer near the plate

ends of bonded joints. Researchers have investigated a number of different geometric configurations of the plate ends to help reduce the magnitude of these stress concentrations. In 1986, Adams et al. conducted a comprehensive finite element analysis to investigate the effect of the plate end configuration on the adhesive strength and failure load of bonded CFRP-steel double lap shear joints. The different plate end configurations, shown in Figure 2.3 included square, tapered, reverse tapered, adhesive fillet, and reverse tapered with an adhesive fillet. Several different taper angles, θ, were considered. A two-dimensional, non-linear, plane strain analysis was conducted. The geometric and material non-linearity of the joint was considered. The adhesive was modeled as an elastic-perfectly plastic material with a maximum principal strain failure criterion. A maximum transverse tension stress failure criterion was used to model the interlaminar failure of the CFRP.

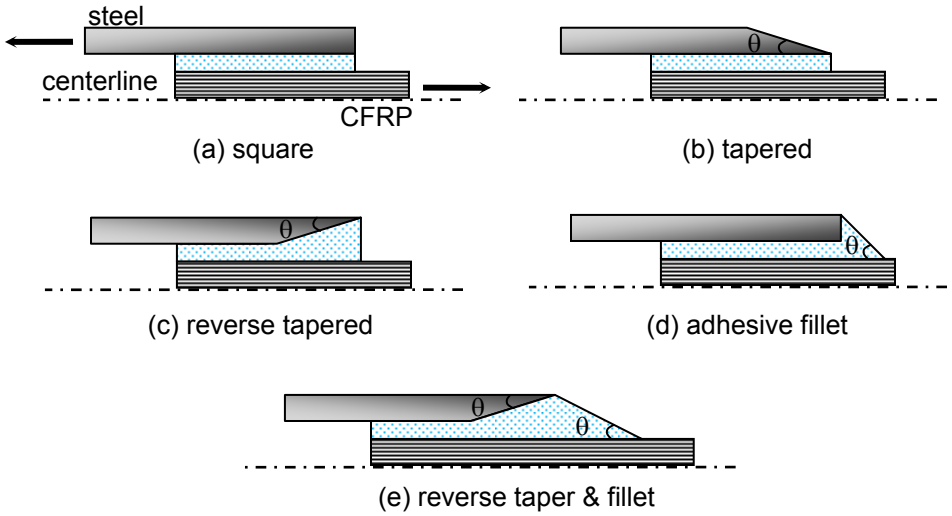

Figure 2.3 – Plate end configurations considered by Adams et al. (1986)

The analysis results indicated that tapering the steel adherend only, either using a taper or a reverse taper, without incorporating an adhesive fillet, did not significantly reduce the magnitude of the transverse tension stress in the CFRP. However, the presence of an adhesive fillet helped to uniformly distribute the transverse stresses over a larger area of the

CFRP. Therefore, the presence of the adhesive fillet helped to reduce the magnitude of the transverse stresses in the CFRP near the plate end by up to 75 percent compared to the square plate end case. Implementation of a reverse taper and adhesive fillet with a taper angle, θ, of 17^o resulted in an 87 percent reduction of the transverse tension stress as compared to the square plate end case. A similar trend was observed experimentally. Based on the experimental results, a taper angle of 30^o was found to yield the greatest increase of strength of the bonded joint. For smaller taper angles, the failure mode shifted from interlaminar in the CFRP to a cohesive failure within the adhesive. A similar study was conducted by Hildebrand in 1994 on FRP-metal single lap joints. The findings of that study indicated that the presence of a reverse tapered plate end with an adhesive fillet at the end of the metal adherend could increase the joint strength by up to 4.7 times.

The behavior of the reverse tapered plate end configuration with an adhesive spew fillet was further studied by Belingardi et al. (2002). They conducted a two-dimensional, linear, plane strain analysis of steel-GFRP single lap-shear coupons with different fillet and taper angles. The analysis results were used to evaluate the magnitude of the shear and normal stress components at different locations in the adhesive layer. The results indicated that significant adhesive shear and normal stress concentrations typically formed near the corner of the adherend at the start of the taper. The results further indicated that reducing the taper angle helped to reduce the magnitude of the normal stress concentration by up to 10 times and the shear stress concentration by up to four times for a taper angle of 45^o. For taper angles greater than 45^o, a secondary stress peak typically formed near the end of the adhesive spew fillet. For fillet angles greater than 60^o, the magnitude of this secondary peak was greater than the magnitude of the stress concentration near the start of the taper.

Sancaktar and Nirantar (2003) conducted a plane-stress finite element analysis and experimental study to evaluate the behavior of aluminum and steel single lap joints with tapered adherends. In this study both adherends were tapered and the adhesive thickness was

left uniform along the length of the bonded joint. Two different adhesives were considered, a brittle adhesive and a relatively ductile adhesive. The analysis results indicated that the presence of the taper helped to reduce the magnitude of the peak shear and normal stresses by up to 31 and 57 percent respectively. The stress concentrations were found to be higher for bonded joints made with aluminum adherends rather than steel adherends. The authors suggested that this was due to the greater effect of geometric non-linearity for the less stiff adherends. This trend was confirmed experimentally. The experimental results further indicated that higher failure loads were achieved using the more ductile adhesive.

Wang et al. (2005) tested a series of bonded aluminum double-lap shear specimens, with different taper angles for the outer adherends, under fatigue loading conditions. The results indicated that the presence of the tapered plate end helped to increase the load required for fatigue crack initiation in the adhesive. Decreasing the taper angle also helped to increase the measured fatigue life of the bonded specimens. For specimens with adherends with a 3^o taper, fatigue failure of the bulk aluminum adherend occurred before crack initiation in the adhesive layer was observed. Finite element analysis results indicated that the increase of the crack initiation load and the fatigue life of the specimens were likely due to the reduction of the stresses in the adhesive due to the presence of the taper. However, the increase of crack initiation load did not appear to be proportional to the reduction of the adhesive stresses. A fracture mechanics analysis further indicated that the presence of the taper helped to reduce the magnitude of the strain energy release rate near the end of the joint. The fracture mechanics analysis further indicated that the crack initiation and propagation would occur at the interface between the adhesive and the central adherend which was also observed experimentally.

Recently, Gao et al. (2006b) investigated the effect of tapering the ends of a six-layer CFRP laminate used to strengthen reinforced concrete beams. The taper of the end of the CFRP was achieved by stepping individual layers of the CFRP laminates. Different taper configurations were achieved by stepping different numbers of layers and by varying the

length of the steps. The tested beams typically failed by plate end debonding either at the CFRP-concrete interface or by cover delamination. The presence of the taper only had a minimal effect on the measured load and deflection at failure with typical increases ranging between 3 to 9 percent. In a related study, a finite element analysis was conducted to evaluate the effect of the different taper configurations on the stresses at the interface between the CFRP and the reinforced concrete beam (Gao et al., 2006a). The results indicated a significant reduction of the interfacial stresses due to the presence of the taper. However, since the majority of the tested beams failed by cover delamination, it is possible that the predicted reduction of stresses at the interface did not represent the stress distribution at the failure location.

2.2.5 Fracture Mechanics Based Approaches

In addition to the stress-based approaches, which are commonly used in civil engineering applications, a number of researchers have also developed fracture mechanics based approaches to predict debonding. Based on the theory of stress singularity at biomaterial wedges, Lenwari et al. (2002) proposed a failure criterion to evaluate the debonding load for steel beams strengthened with CFRP plates. The proposed failure criterion suggested that failure of the bonded joint would occur when the calculated stress intensity factor at the adhesive-steel interface, reached a critical value. The critical stress intensity factor was determined experimentally from a series of double-lap shear specimen tests. The proposed failure criterion was used to predict the failure load for a series of tested steel beams that were strengthened using the same CFRP strengthening system. The findings indicate that the proposed method effectively identified the initiation of debonding of the CFRP plates.

In a related paper a parametric study was presented to evaluate the effect of different parameters on the magnitude of the stress intensity factors near the plate ends, which were calculated by the J-integral method (Lenwari et al., 2006a). The results indicated that increasing the thickness and modulus of the FRP plate increased the magnitude of the stress

intensity factors for a given load level and decreased the predicted debonding load of the strengthened beams. Similarly, increasing the adhesive modulus, decreasing the adhesive thickness and increasing the angle of the adhesive fillet near the end of the CFRP plate also increased the stress concentration factor near the end of the strengthening plate and decreased the predicted failure load. These results are similar to the trends predicted by the stress-based analysis approaches discussed previously.

Andresen and Echtermeyer (2006) studied the fracture characteristics of the bond interface between steel surfaces and CFRP materials bonded by an adhesive layer that was reinforced by a chopped fiber mat. Two different techniques were used to predict the strain energy release rate of the bond. The first method was based on the area under the measured load-deflection curve, which is a direct measure of the crack energy. The second method is based on the measured compliance of the bonded system. Both methods gave comparable values of the strain energy release rates and the findings indicated that the fracture mechanics approach can be applied even when the strengthening system includes a reinforced adhesive.

Using linear elastic fracture mechanics, Colombi (2006) evaluated the effect of different parameters on the strain energy release rate for metallic beams strengthened with externally bonded CFRP materials. The analysis demonstrated that the strain energy release rate is a function of the forces, and stresses at the bonded interface near the plate end. These parameters were evaluated using three techniques. In the first method, the stresses where evaluated using a transformed section analysis, which neglects the effect of the stress concentration near the end of the CFRP plate. The second approach implemented a stress-based bond analysis, similar to that developed by Stratford and Cadei (2006), which accounts for the shear and normal stresses in the adhesive layer and the effect of the stress concentration near the plate end. In the third method the stresses were evaluated using a finite element analysis. The analysis results indicate that the strain energy release rate is not sensitive to the technique used to evaluate the stresses near the plate end. For a specific example beam the three methods predicted the strain energy release rate to within 3 percent

of each other. The analysis further indicated that the discrepancy between the three approaches increased as the elastic modulus of the CFRP increased. This was attributed to the fact that the transformed section analysis did not account for the effect of the stress concentration near the plate end and the stress-based bond analysis did not account for the flexural stiffness of the strengthening plate. Both of these factors become more prominent as the modulus of the CFRP is increased. The analysis presented by Colombi demonstrated that the fracture mechanics approach can be used in conjunction with other stress-based analysis tools. However, no method was proposed to evaluate the magnitude of the critical strain energy release rate which would govern the debonding strength of a bonded CFRP strengthening system.

2.3 REPAIR OF CRACKED STEEL MEMBERS USING CFRP MATERIALS

A number of researchers have studied the use of CFRP materials to repair cracked steel structures. Bassetti et al. (2000) investigated the use of CFRP materials to repair cracked riveted steel girders from a decommissioned historic railway bridge subjected to fatigue loading. The results indicated that the presence of the CFRP materials helped to reduce crack opening displacements which dramatically reduced the magnitude of the stress intensity factor near the end of the crack. The results further indicated that prestressing the CFRP materials prior to installation helped to promote crack closure effects which further reduce the crack growth rates. The results demonstrated that prestressed CFRP materials could even be used to halt the propagation of cracks due to fatigue loading.

Tavakkolizadeh and Saadatmanesh (2003a) tested a total of 20 small scale steel beams to evaluate the fatigue performance of a CFRP system used to repair cracked steel beams. The presence of a crack was simulated by notching the tension flanges of the beams. Seven different stress ranges in the steel beam were considered ranging from 69 MPa to 379 MPa to develop S-N curves to predict the fatigue life of the strengthened beams. The test results

indicated that the presence of the CFRP could reduce the crack propagation rates and increase the fatigue life of the strengthened beams by up to 3.4 times.

Colombi et al. (2003a) conducted a finite element study to evaluate the effect of CFRP materials on the performance of cracked steel members. The analysis results indicated that the presence of the CFRP materials was more beneficial for members with long cracks in which the CFRP patch partially covered the end of the crack. In this case, the presence of the CFRP helped to reduce the stress intensity factor near the end of the crack. For shorter cracks the analysis indicated that the CFRP materials should be prestressed prior to installation to achieve any significant reduction of the crack growth rate. The results further indicated that shear-lag in the flexible adhesive layer reduced the effectiveness of the repair. A companion study was also conducted by the same authors to study the effect of the crack propagation on the debonding of the CFRP patch (Colombi et al., 2003b). The analysis indicated that the size of the debonded region near the end of the crack had a significant effect on the stress intensity factor at the tip of the crack in the steel member. The size of the debonded region was affected by the thickness of the adhesive layer. Thinner adhesive layers resulted in a greater extent of debonding due to an increase of the debond crack strain energy release rate. Later, the first author proposed analytical models to predict the stress intensity factor and crack opening displacements (Colombi, 2004) and the retardation of the crack growth rate for fatigued elements (Colombi, 2005).

Jones and Civjan (2003) conducted a series of fatigue tests on steel tension members, with different configurations of crack sensitive details which were retrofit with different configurations of CFRP materials. The test results indicated that installing the CFRP materials as a preventative measure prior to formation of the cracks achieved the greatest increase of the life of the fatigue sensitive details. However, the CFRP systems tested were also effective as a repair technique for already cracked members. Increasing the length of the CFRP patches was shown to moderately increase the fatigue life of the system. However, longer patches also resulted in a decrease of the scatter of the test results indicating the

increased reliability of the system. The results further indicated that in order to be effective the CFRP patches should be applied to both sides of the cracked member. Installing the CFRP on only one side of the member resulted in bending effects which significantly reduced the effectiveness of the CFRP patch. A similar bending effect for specimens repaired with a single sided CFRP patch was reported by Lam et al. (2006).

In a recent study Shaat and Fam (2008) tested a total of 11 steel-concrete composite beams with a simulated crack in the tension flange which were subsequently repaired with different configurations of CFRP materials. Both conventional and high modulus CFRP materials were considered for the repair application. The test results indicated the presence of a significant stress concentration in the CFRP materials and the steel beam near the location of the crack. For the beams repaired with high modulus CFRP materials, the presence of the stress concentration led to failure due to rupture of the CFRP materials. This was attributed to the relatively low failure strain of the high modulus CFRP materials. Alternatively, the beams strengthened with conventional CFRP materials typically failed by debonding of the CFRP sheets. The test results typically indicated that the beams repaired with high modulus CFRP sheets exhibited greater stiffness increases than the beams repaired with conventional CFRP materials. Alternatively, the beams repaired with conventional CFRP materials exhibited more ductile behavior. The test results further indicated that bonding the CFRP materials to both the upper and lower surfaces of the tension flange did not provide any significant advantage over systems in which the CFRP was only bonded to the bottom surface of the tension flange. In a companion study Fam et al. (2008) tested a series of beams with simulated damage representing 50 percent and 100 percent loss of the cross-sectional area of the tension flange. They found that the simulated damage representing 50 percent loss of the flange area did not result in a significant loss of the flexural capacity or stiffness of the beams. Therefore, implementation of the CFRP repair systems did not significantly improve the performance of the beams.

In another application, GFRP materials were used to retrofit cracked aluminum truss sign post structures, which are commonly used in North American highway infrastructure, and which are susceptible to fatigue induced cracking (Pantelides et al., 2003). Due to the complex geometry of the welded joints of the aluminum truss structures, the application technique of the GFRP had to be carefully considered to ensure that the glass fibers were properly oriented in the directions subjected to the highest tension loading. The test results indicated that the GFRP repair system can be designed to ensure that the capacity of the repair is equal to or greater than the initial strength of the unrepaired, undamaged welded connection.

2.4 STRENGTHENING OF TUBULAR AND SLENDER MEMBERS

The use of CFRP materials for retrofit of tubular and thin-walled steel structures has also recently gained research attention. The research in this relatively new field has focused on studying the bond behavior, flexural behavior and axial compression behavior of the strengthened members.

2.4.1 Bond Behavior

Jiao and Zhao (2004) investigated the use of CFRP materials to strengthen the heat affected zone of butt-welded very high strength circular steel tubes. Initial tests of un-welded tubes that were spliced together only by bonding CFRP materials to the outside of the tubes indicates that the bond behavior is similar to that of typical double-lap shear type specimens. The tests of the un-welded and welded joints indicated the existence of a critical bond length. Increasing the bond length beyond the critical length did not increase the strength of the bonded joint. The results further indicated that CFRP materials could be used to recover the lost yield strength in the heat affected zone for very high strength circular steel tubes.

The behavior of CFRP materials bonded to hollow tubular steel sections was also investigated by Fawzia (2007). She tested a total of six tubular steel specimens which consisted of two lengths of very high strength steel tubes which were butted together and joined by bonding five layers of high modulus CFRP materials to the outer surfaces of the tubes. Bond overlap lengths ranging from 40 mm to 85 mm were considered. The test results were compared to results obtained from typical double-lap shear coupons which were fabricated using the same CFRP materials. The test results indicated that the curvature of the steel tubes did not have any effect on the bond behavior of the FRP materials. The magnitude of the measured strains was approximately 50 percent lower at the outer CFRP layer compared to the measured strain at the inner CFRP layer. This suggests the presence of a considerable shear-lag effect in the FRP materials, which were installed by hand using a wet layup procedure. A similar trend was observed for both circular, tubular specimens and conventional double-lap shear specimens.

2.4.2 Flexural Behavior

Photiou et al. (2006b) studied the behavior of rectangular hollow steel sections strengthened with FRP materials and loaded in four point bending. They tested two different strengthening configurations. In the first configuration the CFRP materials were bonded only to the tension flange of the beam. In the second configuration the CFRP materials were wrapped up the sides of the beams and extended up to the neutral axis. The tests indicated that extending the CFRP strengthening up the sides of the beam helped to confine the failure to a very localized region. By contrast, the beams with CFRP bonded only to the tension flange exhibited nearly total debonding of the CFRP after failure. An experimental study conducted by Zhao et al. (2006) further demonstrated that bonding CFRP materials to the sides of rectangular hollow steel sections can help to increase the bearing strength of the members. The presence of the CFRP materials typically changed the failure mode of the web from a web buckling type failure to a web yielding type failure.

Seica and Packer (2007) conducted an experimental program to develop a CFRP strengthening system for hollow circular steel flexural members used in underwater applications. To study the effect of the curing conditions on the performance of the strengthening system, four members were strengthened and allowed to cure underwater while two were strengthened and cured using conventional methods in air. The test results indicated that strengthening and curing the members conventionally in air increased the flexural strength and ductility compared to an unstrengthened member. The members strengthened underwater did not achieve the same level of strength and ductility as the members strengthened in air. However, the strengthening systems that were installed underwater did result in moderate increases of strength and ductility compared to the unstrengthened member.

The flexural behavior of tapered, twelve sided, hollow steel towers, similar to those used in the communications industry to support cellular antennae, has also recently been studied (Lanier et al., 2007). The members were retrofit with different configurations of high and intermediate modulus CFRP materials. The test results indicated that failure was typically due to local buckling near the base of the steel tube, accompanied by delamination and rupture of the CFRP, or due to crushing of the CFRP materials on the compression face of the member. The results indicated that the presence of the CFRP materials could help to increase the elastic stiffness of the towers; however, due to the relatively low failure strain of the CFRP materials, significant increases of the flexural capacity of the members were not achieved.

2.4.3 Axial Compression Behavior

Shaat and Fam (2006) studied the behavior of short and long hollow square steel columns strengthened with different configurations of externally bonded CFRP materials. For short columns, the presence of the CFRP materials helped to increase the column capacity by up to 18 percent by delaying the occurrence of local buckling of the column walls. The greatest

enhancement was achieved by wrapping the columns with two layers of carbon fibers oriented in the transverse direction. For the long columns the presence of the CFRP helped to delay global buckling of the slender compression members thereby increasing the axial load carrying capacity by up to 23 percent. The authors indicated that the behavior of the columns was highly dependent on the nature of local imperfections in the column, and therefore no correlation could be made between the strength increase and the amount of CFRP materials applied. The effect of the initial imperfections and the number of CFRP layers applied were later uncoupled in a non-linear analytical study conducted by the same authors (Shaat and Fam, 2007). The analysis indicated that increasing the amount of CFRP, for a given level of out-of-straightness, increased the axial load carrying capacity of the strengthened member by up to 39 percent. The results further indicated that the CFRP strengthening system was more effective for slender columns with a higher degree of initial out-of-straightness.

In another study, Bambach and Elchalakani (2007) studied the plastic behavior of short square hollow steel columns strengthened with CFRP materials under large deformations. The test results indicated that the presence of the CFRP helped to increase the plastic strength of the columns at large levels of axial deformation. The increase of the plastic strength was greater for members with a higher slenderness ratio. The presence of the CFRP also helped to increase the energy dissipation of the columns compared to un-retrofit columns. In contrast to the strength increase, the increase of the energy dissipation was greater for members with lower slenderness ratios. The authors also proposed an analytical model to predict the response of the strengthened members in the plastic range which demonstrated reasonable correlation with the experimental results. The experimental and analytical study was later extended to evaluate the performance of the strengthened square hollow steel columns under axial impact loading (Bambach et al., 2008). The results confirmed that the strengthening system helped to increase the crushing load and specific energy absorption of the members under impact loading by up to 82 percent and 52 percent respectively.

Other researchers have conducted experimental and finite element investigations to study the effect of CFRP strengthening on the buckling behavior of cold-formed steel lipped C-channel short and long columns (Silvestre et al., 2008). These members are characterized by various different, and relatively complex buckling modes. Therefore, careful consideration of the orientation and location of the CFRP materials is necessary. The presence of the CFRP helped to increase the axial capacity of the short and long columns by up to 15 percent and 20 percent respectively. The experimental and analytical results both indicated that, for short columns, the CFRP was most effective when bonded to the web and flanges of the section and that minimal enhancement was achieved by bonding the CFRP to the lips of the channel. For long columns, both the experimental and analytical results indicate that additionally bonding CFRP to the channel lips is beneficial.

2.5 FIELD APPLICATIONS

A number of field applications have been conducted in North America to demonstrate the effectiveness of CFRP systems for strengthening steel bridges and structures. These include demonstration projects in Delaware, Iowa and Oregon.

In Delaware, bridge 1-704, which carries southbound I-95 traffic over Christina Creek, was retrofit using conventional modulus CFRP materials (Miller et al., 2001). The bridge, which consists of concrete slab on steel girder superstructure, was not in need of strengthening; however, the demonstration project provided an opportunity to evaluate the long-term durability of the strengthening system subjected to actual environmental conditions. Only a single girder was strengthened for the demonstration project. Load testing before and after the retrofit indicated that the presence of the CFRP helped to reduce the measured strain in the tension flange of the steel girder by approximately 15 percent.

In a second demonstration project, the Ashland Bridge in Delaware was strengthened using the same strengthening system (Chacon et al., 2004). The bridge consists of steel floor

girders spanning between two steel through girders with a reinforced concrete deck slab resting on the floor girders. In a related repair, the bridge deck was removed. Two of the steel floor girders were retrofit and a new concrete deck was cast to act in complete composite action with the floor girders. In this way the CFRP strengthening system contributed to supporting part of the dead load of the structure.

In Iowa, the positive moment regions of four girders of a bridge over Walnut Creek in Pottawattamie County were strengthened with conventional CFRP materials (Wipf et al., 2005). The CFRP was bonded to both the bottom and the top of the tension flange at different locations. Two of the strengthened girders were originally designed to act in complete composite action with the concrete bridge deck while the other two were originally designed to be non-composite. Analysis of the structure indicated that the CFRP system increased the stiffness of the girder by 1.2 percent per layer of CFRP materials. Load testing revealed that the measured strains on the tension flange of the girder were similar prior to and after the strengthening. This was likely due to the relatively small amount of CFRP materials that were applied and the relatively low modulus of the conventional CFRP materials.

In another project a steel girder bridge over Willow Creek, west of Bayard, Iowa, was strengthened with unbonded external CFRP post-tensioning strands (Lee et al.,2005). The steel girders supported a non-composite reinforced concrete deck. Load testing indicated that the installation of the strengthening system did not significantly increase the stiffness of the girders. However, strain measurements indicated that the post tensioning induced a negative moment equal to approximately 3 percent to 5 percent of the moments induced by the live load. Additional load tests after two years of service indicated essentially no change of behavior during that time. After two years the post tension was removed to evaluate the post tensioning losses. The average measured post tensioning loss represented approximately 5 percent of the applied post tensioning force.

Based on the results of an experimental program, a proprietary CFRP strengthening system was used to strengthen the Sauvie Island Bridge in Oregon (Mosallam, 2005). The strengthening system consisted of a CFRP laminate bonded to an aluminum honeycomb core. The purpose of the aluminum core was to increase the distance from the CFRP plate to the neutral axis of the strengthened beam thereby increasing the stiffness of the beam. The installation on the actual bridge was successfully completed in 5 hours.

2.6 DESIGN GUIDELINES

A number of different guidelines have been published internationally which are applicable to the design and installation of externally bonded CFRP systems for retrofit of bridges and structures.

In 1999 the Institution of Structural Engineers in the United Kingdom published the "Guide to the structural use of adhesives". This document presents general recommendations regarding good practice in the use of adhesives for structural applications. It does not give specific or detailed recommendations regarding the calculation of the strength or durability of structural adhesive joints. However, the document does recommend the use of partial safety factors when determining the design strength of adhesive joints. These partial factors are intended to account for the variability of different parameters including the material characteristics, method of application, type of loading, environmental conditions and fatigue loading of the adhesive joints. In combination, these partial safety factors can potentially result in an overall safety factor of up to twenty, which may be overly conservative for practical application of adhesives in infrastructure applications.

In 2001 the Institution of Civil Engineers in the United Kingdom published the first design guide specifically related to the design and installation of FRP strengthening systems for metallic structures (Moy et al., 2001). Structural design principals are presented which can be used by practitioners to evaluate the strength of a metallic structure strengthened with FRP

materials. The guide recommends the use of a transformed section analysis to evaluate the behavior of strengthened beams in the elastic range. The use of an elastic-plastic moment-curvature analysis is recommended to assess the behavior of strengthened beams beyond the elastic range.

A similar flexural analysis approach is recommended in the CIRIA guidelines which were later published also in the UK (Cadei et al., 2004). These guidelines also describe the effect of temperature and initial strains and stresses, in the metallic beam and the FRP strengthening materials, on the behavior of the strengthened members. The detailed calculation of adhesive shear and normal stresses is also presented. The guidelines recommend that, to prevent debonding of the strengthening system, the calculated principal stress in the adhesive should not exceed a critical value. The limiting value of the adhesive stress should be determined from lap-shear tests using the same strengthening materials and methods that will be used in the actual application. Based on the measured failure load, the appropriate lap-splice theories can be applied to back calculate the value of the limiting principal stress, which can then be used for design purposes.

Recently guidelines were established for the design and installation of high modulus CFRP materials for strengthening of steel concrete composite beams (Schnerch et al., 2007). The proposed flexural design guidelines are based on a moment-curvature analysis which satisfies the conditions of equilibrium and compatibility. The flexural design of the strengthening system should satisfy three criteria. For serviceability, the combined effect of the dead load and the increased live load should not exceed 60 percent of the increased yield moment capacity of the strengthened member. For safety, the effect of the applied load, after applying a suitable load factors, should not exceed the ultimate moment strength of the strengthened member after applying a suitable reduction factor. For redundancy of the system, the combined effect of the dead load and increased live load should not exceed the residual strength of the unstrengthened member. The design of the adhesive joint to prevent debonding follows similar recommendations to those provided by Cadei et al. (2004).

Most recently an Italian guideline has been published by the National Research Council (2007). The fundamental design approaches for flexure and bond are similar to those proposed by the CIRIA document. The design guidelines recommend the use of material partial factors, similar to those proposed by the Institution of Structural Engineers. However, for a typical CFRP strengthening system, the combination of the proposed safety factors would result in an overall factor of safety of approximately 5.3, which is considerably more reasonable than the factor of 20 previously proposed.

Chapter 3: Experimental Program

This chapter outlines the experimental program that was conducted to evaluate the bond and splice behavior of the proposed CFRP strengthening system. The objective of the experimental program is to develop a method for splicing CFRP strips to facilitate implementation of the proposed strengthening system to longer span bridges and structures. The experimental program was conducted in two stages. The first stage consisted of testing eight double-lap shear specimens. Different geometric configurations of the CFRP plate ends were considered to help reduce the bond stress concentration and to increase the bond strength of the splices. The second stage consisted of testing ten large-scale steel beams to study the behavior of the spliced connections under flexural loading conditions. The parameters studied include the geometry of the plate end, the length of the splice plate and the additional use of mechanical anchorage to help increase the splice capacity. All of the tested specimens were instrumented with electrical resistance strain gauges to measure the strain at the surface of the CFRP plates. This chapter presents details of the double-lap shear specimen tests followed by details of the steel beam tests.

3.1 DOUBLE-LAP SHEAR SPECIMEN TESTS

The first stage of the experimental program consisted of testing eight double-lap shear specimens. These tests provided a relatively simple way to evaluate the effect of different parameters on the bond behavior of the CFRP strips. The following sections describe details of the test specimens, materials, test setup and instrumentation used in the experimental program.

3.1.1 Test Specimens

The test specimens for the experimental program consisted of two 8 mm thick x 38 mm wide main CFRP plates which were bonded together using two 4 mm thick x 38 mm wide CFRP splice plates. A schematic of a typical specimen is shown in Figure 3.1.

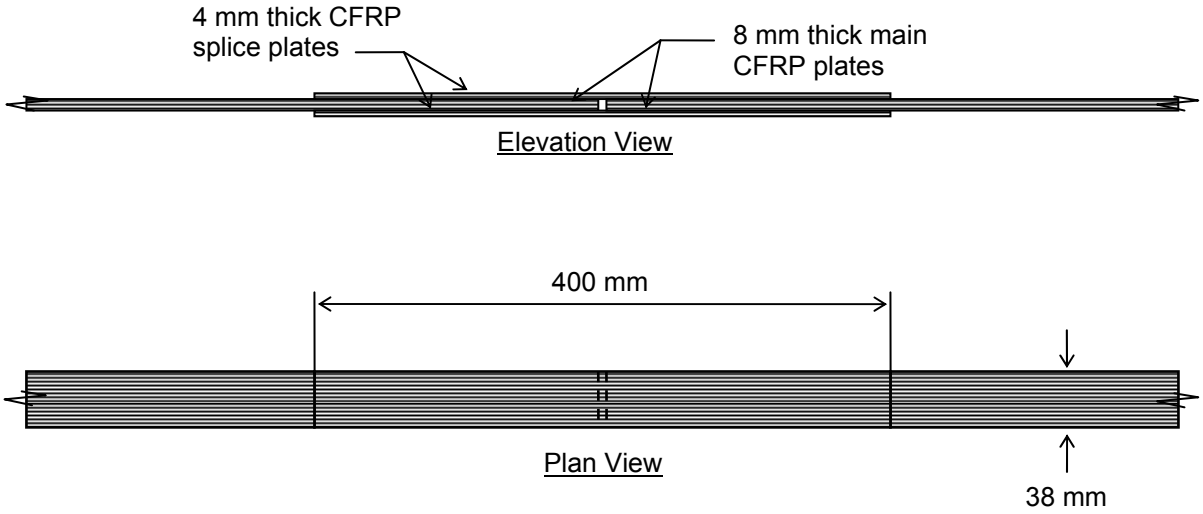

Figure 3.1 – Schematic of typical CFRP double-lap shear specimens

The testing program for the double-lap shear specimen tests is given in Table 3.1. Multiple repetitions of the same specimen configuration were tested to confirm the repeatability of the test results. Each specimen configuration was assigned a three part identifier. The first part of the identifier indicates the overall length of the splice plate, in millimeters. The second part indicates the plate end detail. The third part indicates the presence of the steel clamp.

Table 3.1 – Double-lap shear specimen test matrix

Specimen ID	Plate end detail	Mechanical anchorage	Splice Length (mm)	Repetitions
400-S	S	None	400	3
400-T1	T1	None		1
400-T2	T2	None		2
400-U	U	None		1
400-U-C	U	Steel clamp		1

A total of four different plate end details were investigated as shown schematically in Figure 3.2. The square end represents the simplest and most commonly used joint detail. To reduce the bond stress concentrations, different combinations of reverse tapered and rounded plate ends were implemented at the end of the CFRP splice plate and at the end of the main CFRP plate within the center of the joint, as outlined in Figure 3.2(a). Taper angles and fillet angles of approximately 20^o were considered in the experimental study. Typical square, tapered and rounded plate ends are shown in Figure 3.2(b), (c) and (d) respectively. The use of a steel clamp at the ends of the splice plate, shown in Figure 3.2(e), was also considered to help resist the normal stresses near the plate end and to increase the tension strength of the splices.

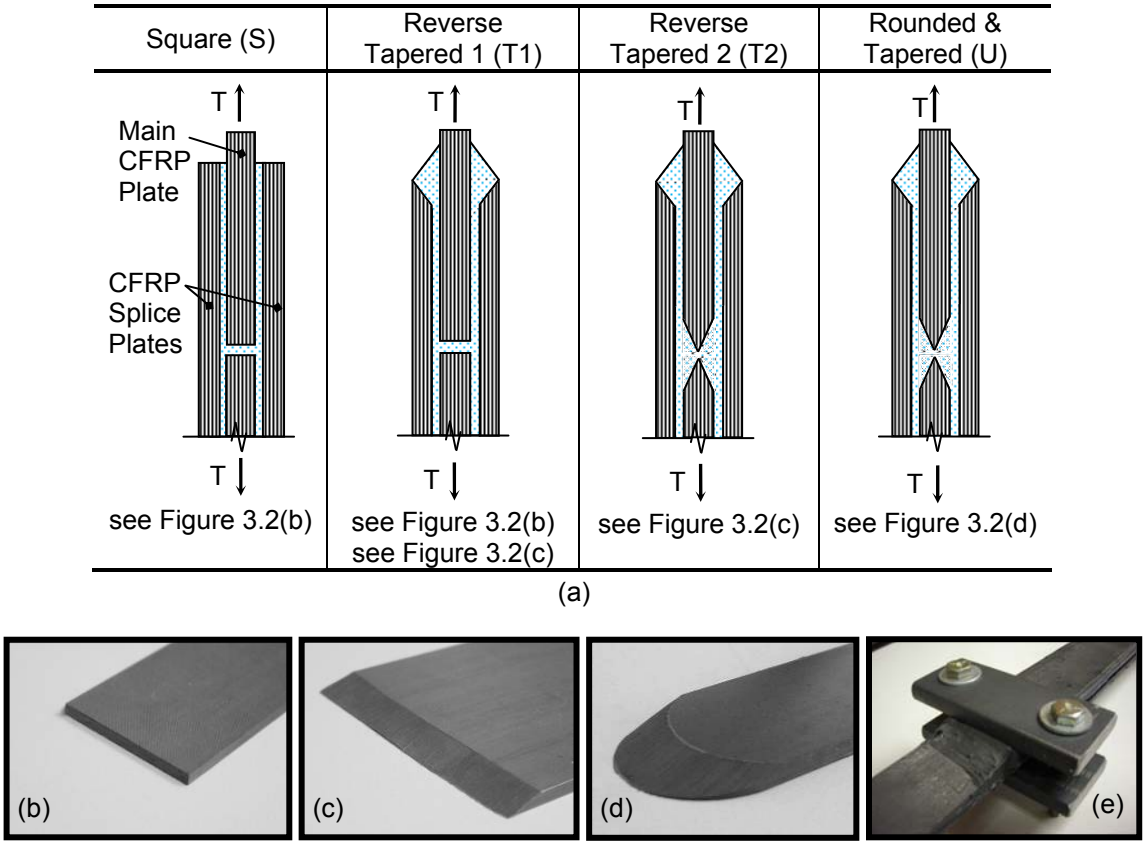

Figure 3.2 – (a) Schematic of tested splices (b) square plate end (c) tapered plate end, (d) rounded & tapered plate end (e) clamped plate end

All of the specimens were fabricated using a consistent technique to minimize the variability of the test results due to fabrication. Prior to bonding, the required plate end details were fabricated using simple power tools that are easily accessible in most typical workshops. The 8 mm thick main CFRP plates were fabricated by bonding together two 4 mm thick CFRP strips. The plates were clamped together to minimize the bond line thickness, excess adhesive was removed and the adhesive was allowed to cure for at least 12 hours at room temperature. The main plates were then aligned in a jig with a 1 mm to 2 mm gap left between the plate ends and the first CFRP splice plate was bonded to the surface. The plates were bonded using the SP Spabond 345 two part epoxy adhesive. E-glass spacer beads with a nominal diameter of 1 mm, manufactured by MoSci Corporation, were mixed into the

adhesive to help maintain a consistent adhesive thickness. Approximately 1 gram of beads was used per 100 grams of adhesive. The adhesive was applied liberally to ensure complete coverage of the CFRP strips and to help minimize the formation of air voids in the adhesive layer. A uniform pressure was applied to the splice plate to squeeze out any excess adhesive and the adhesive was allowed to cure at room temperature for at least 12 hours. The second splice plate was bonded using a similar technique. The CFRP plates were fabricated with a glass fiber peel ply layer which minimized the requirement for surface preparation. In some cases, excessive adhesive spewed onto an exposed surface of the CFRP. In these cases the cured adhesive was removed by light abrasion and the surface was wiped clean with methanol prior to bonding. Aluminum tabs were bonded to the ends of the main CFRP plates to prevent damage during griping.

3.1.2 Materials

The primary materials used in this stage of the experimental program included the CFRP and the adhesive. Each of the materials was tested according to the appropriate ASTM standards to determine their respective mechanical properties. The results of the tests are presented in the following sections.

3.1.2.1 CFRP Material Properties

The CFRP materials consisted of a pultruded, high modulus CFRP strip, ePLATE HM, which is distributed by Mitsubishi Chemical FP America Inc. The tensile properties of the CFRP were determined according to ASTM D3039-00. Three straight, 12 mm wide CFRP coupons were fabricated and tested in tension using an 890 kN MTS hydraulic testing machine. The measured stress-strain relationship of the CFRP up to failure is shown in Figure 3.3. The chord modulus of the CFRP was measured between strain values equivalent to 25 percent and 50 percent of the measured ultimate strain of the CFRP respectively. The

measured elastic modulus, failure strain and tension strength of the CFRP coupons are given in Table 3.2. All of the tested CFRP tension coupons failed due to rupture of the CFRP.

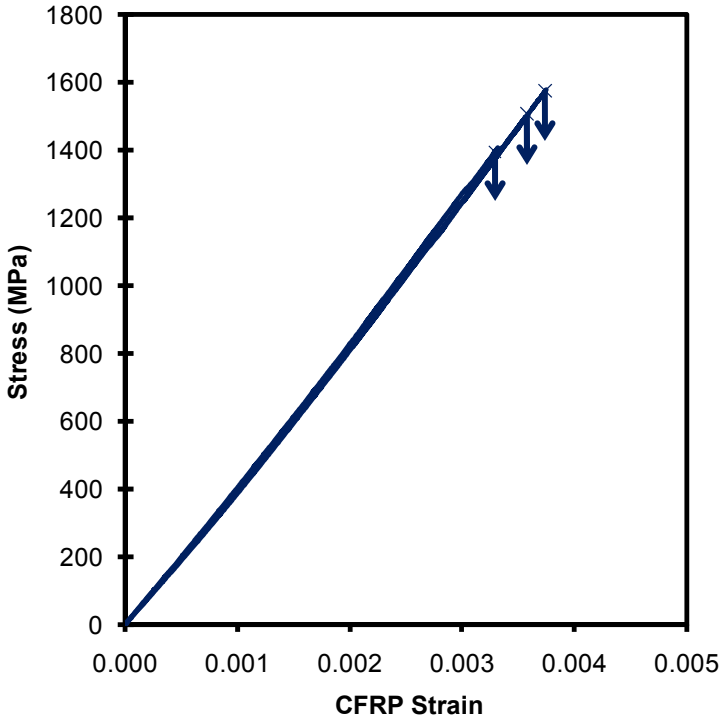

Figure 3.3 – Measured tensile stress-strain curve of the CFRP strips

Table 3.2 – Measured tensile properties of the CFRP plates

Coupon ID	Tensile Modulus (MPa)	Ultimate Tensile Strain	Tensile Strength (MPa)
CFRP-0-1	418,000	0.00329	1400
CFRP-0-2	418,000	0.00374	1570
CFRP-0-3	419,000	0.00358	1500
Average	418,000	0.00354	1490
Standard Deviation	580	0.00023	90
Coefficient of Variation	0.14%	6.5%	6.0%

3.1.2.2 Adhesive Material Properties

The tensile properties of the adhesive were determined according to ASTM D638-02 (Dawood, 2005). A 5.2 mm thick plate of the cured adhesive was fabricated and the adhesive was allowed to cure for one week. Dog-bone shaped tension coupons were cut from the plate. The coupons were tested in tension using a 90 kN Instron screw-driven universal testing machine. The measured stress-strain relationship of the adhesive is given in Figure 3.4. The tensile chord modulus of the adhesive was determined between 2 percent and 25 percent of the measured failure load of the adhesive. The measured elastic modulus, failure strain and tension strength of the adhesive coupons are given in Table 3.3. All of the tested adhesive coupons failed in a brittle manner due to rupture.

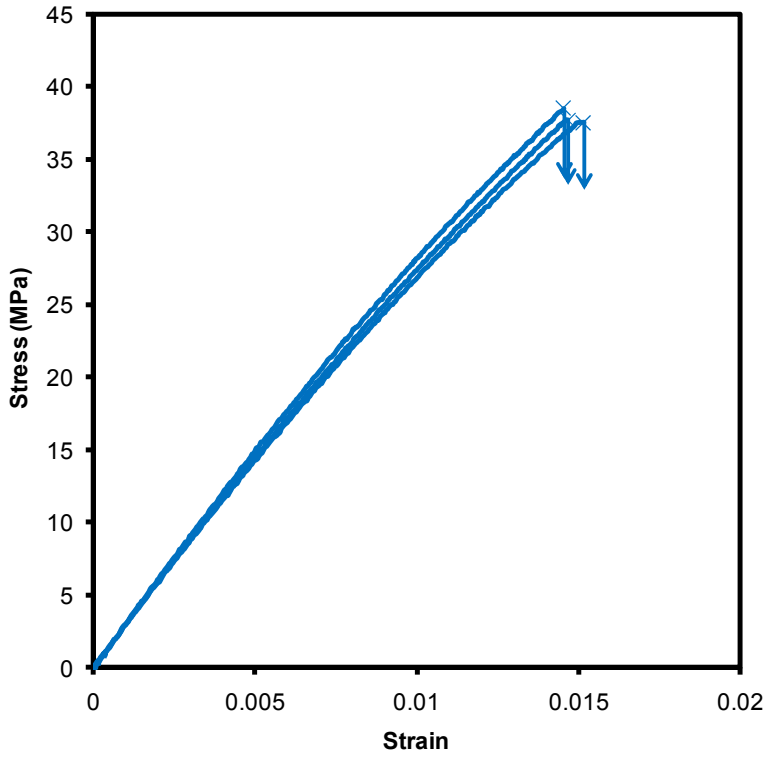

Figure 3.4 – Measured tensile stress-strain curve of the cured adhesive

Table 3.3 – Measured tensile properties of the cured adhesive

Coupon ID	Tensile Modulus (MPa)	Ultimate Tensile Strain	Tensile Strength (MPa)
Epoxy-0-1	2920	0.0151	37.5
Epoxy-0-2	3050	0.0145	38.5
Epoxy-0-3	2970	0.0147	37.7
Average	2980	0.0148	37.9
Standard Deviation	70	0.0003	0.5
Coefficient of Variation	2.3%	2.0%	1.3%

3.1.3 Instrumentation

The strain at different locations along the double-lap shear coupons was measured using conventional electrical resistance strain gauges. The strain gauges were bonded to the surface of the CFRP along the longitudinal centerline of the specimens. The strain gauge layout for the different test specimens is shown schematically in Figure 3.5. Multiple repetitions of the same test configuration are identified by the number in parentheses after the specimen identifier. The presence of the steel clamps on specimen 400-U-C interfered with the placement of strain gauges on the CFRP splice plate for this specimen. The specimen was instrumented with two strain gauges placed on the main CFRP plate 25 mm from the end of the splice plate.

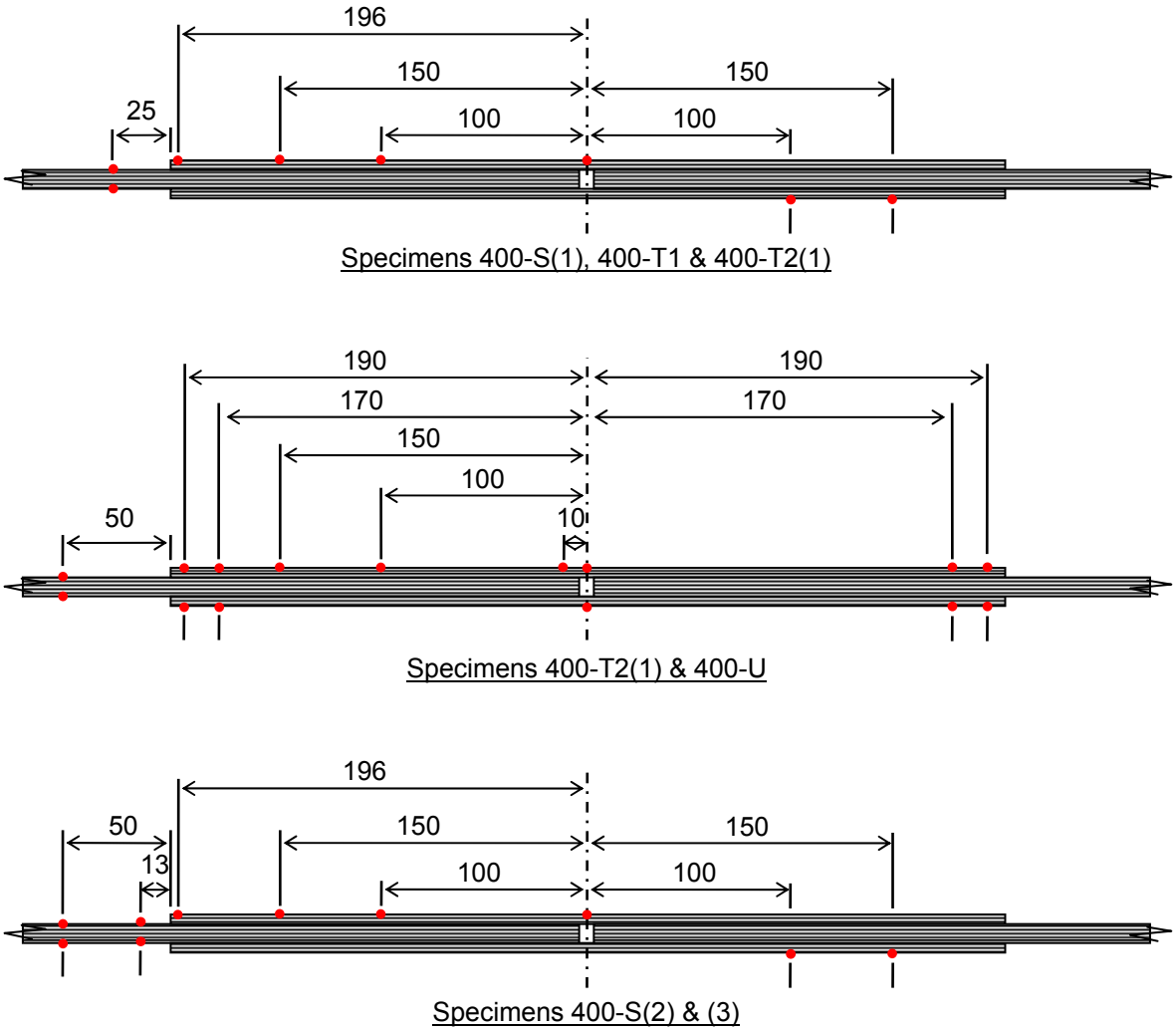

Figure 3.5 – Strain gauge layout for the tested double-lap shear specimens

3.1.4 Test Setup

All of the double-lap shear specimens were tested in direct tension by an 890 kN hydraulic MTS testing machine using a constant displacement rate of 0.5 mm/min. The machine load and stroke and the measured strain were recorded using a data acquisition system connected to a personal computer. The typical test setup is shown in Figure 3.6.

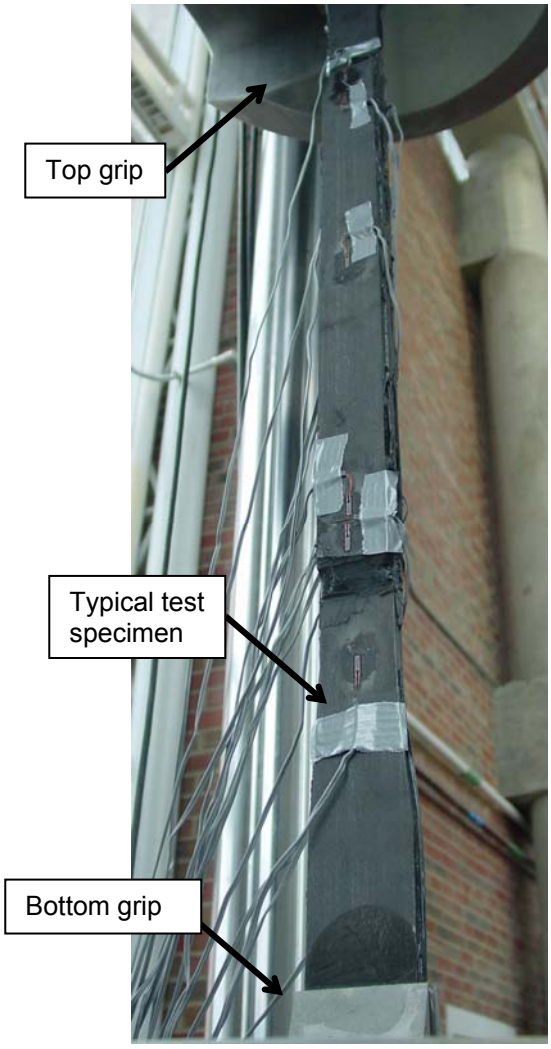

Figure 3.6 – Typical test setup for double-lap shear specimens

3.2 STEEL BEAM TESTS

A total of 10 large-scale steel beam tests were conducted to study the behavior and bond characteristics of CFRP splices under flexural loading conditions. The objective of the study is to develop a splice joint to facilitate implementation of the strengthening system to long-span steel girders. The details of the test specimens, materials, instrumentation and test setup are presented in the following sections.

3.2.1 Test Specimens

The typical test beams, shown schematically in Figure 3.7, consisted of a W12x30 wide flange steel beam. A standard steel channel was welded to the compression flange of the beam to simulate the presence of a reinforced concrete deck. Transverse stiffeners were fabricated from 9.5 mm thick steel plates and installed at the support locations and at the loading points, as shown in the figure, to prevent local instability of the web. Three such beams were fabricated using A992 or A572 Gr. 50 steel.

The beams were designed using a moment curvature analysis to ensure that the behavior was similar to that of typical steel-concrete composite beams (Dawood, 2005). Two different sizes of steel channels, C9x15 and C9x13.4, were used to fabricate the three different beams. The moment curvature analysis indicated that the difference of the nominal dimensions of the steel channel would not significantly affect the flexural behavior of the tested beams. To confirm that all three beams had similar flexural stiffnesses, an initial loading cycle was conducted within the elastic range for each of the unstrengthened beams prior to installation of the CFRP. The coefficient of variation of the measured flexural stiffnesses of the three beams was 1.0 percent.

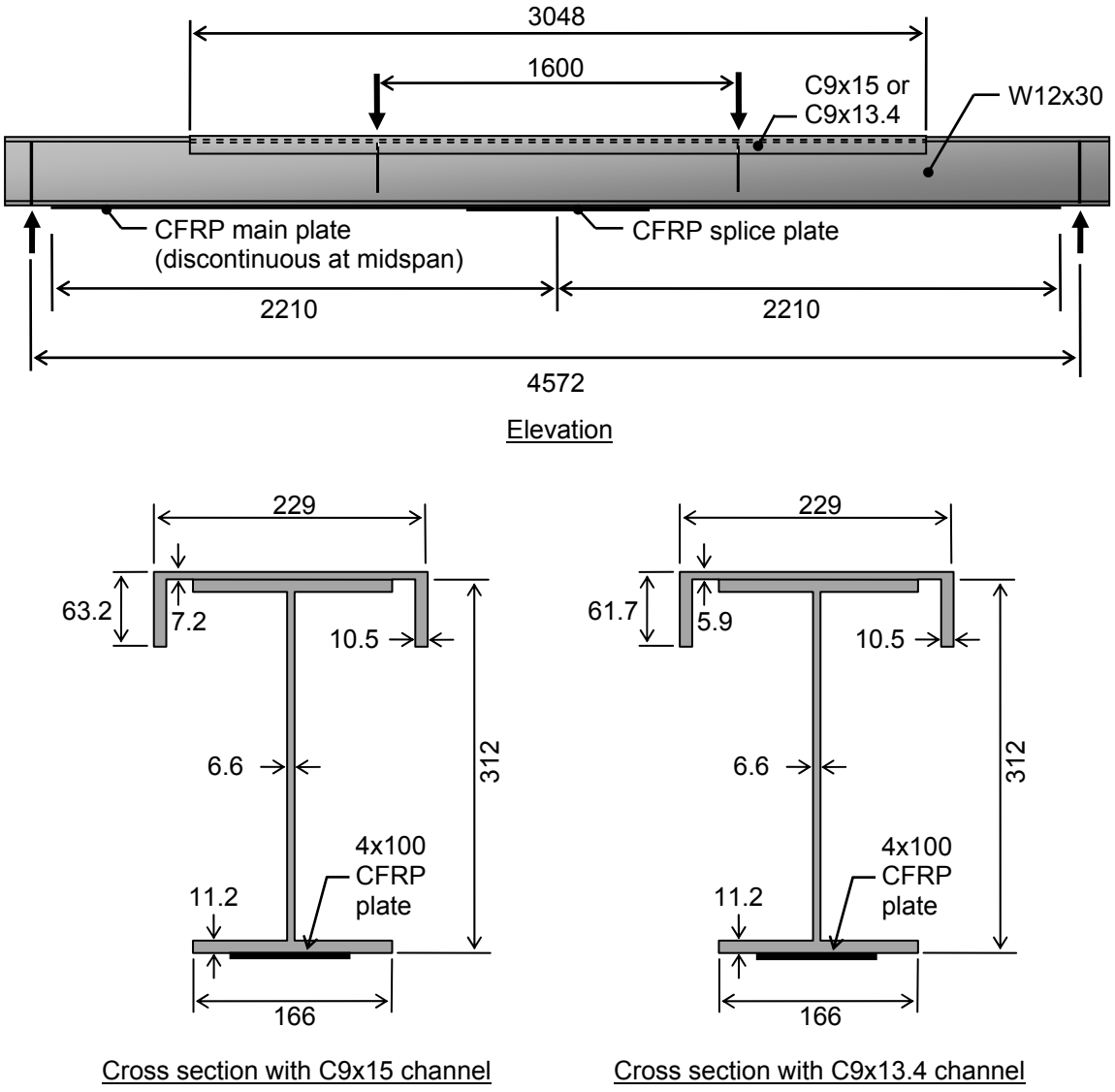

All dimensions in millimeters

Figure 3.7 – Schematic of typical steel test beam used for the bond & splice study

A typical test beam is shown in Figure 3.8(a). Each beam was strengthened using two 2210 mm long x 100 mm wide x 4 mm thick main CFRP plates which were butted together at midspan, as shown in Figure 3.8(b), to simulate a discontinuity of the main CFRP plate. To provide continuity of the strengthening system, a CFRP splice plate was subsequently

bonded to the main CFRP plates as shown in Figure 3.8(c). This type of detail is required to strengthen typical long-span steel girders.

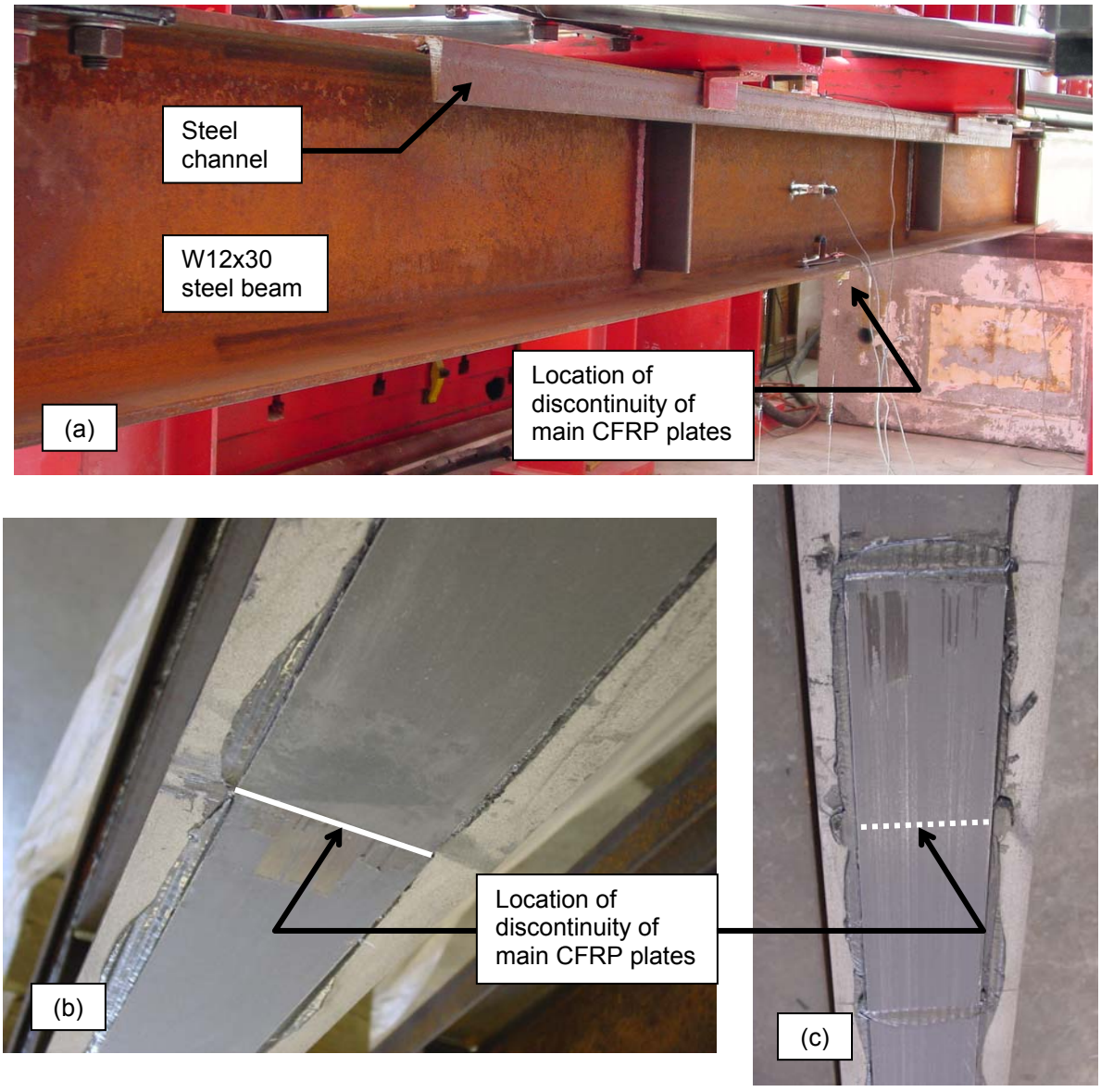

Figure 3.8 – (a) Typical steel test beam (b) Discontinuity of main CFRP strengthening plate (c) Typical 400 mm long CFRP splice plate

The complete test program is given in Table 3.4. A total of 10 tests were conducted and nine different splice configurations were considered. Three parameters were considered in the study: the length of the splice plate, the plate end detail and the presence of two different types of mechanical anchorage. The plate end details that were considered, shown in

Figure 3.9, were similar to those tested in the double-lap shear specimen tests. Two different types of mechanical anchorage were considered including a specially fabricated steel clamp and a transverse CFRP wrap. Each splice configuration was assigned a three part identifier. The first part indicates the overall length of the splice plate in millimeters. The second part indicates the plate end detail. The third part indicates the type of mechanical anchorage used, 'C' for the steel clamp and 'W' for the CFRP wrap.

Table 3.4 – Test program for the steel beam tests

Specimen ID	Splice Length (mm)	Plate end detail	Mechanical Anchorage	Repetitions
800-S	800	S	None	2
800-T2		T2	None	1
800-U		U	None	1
800-U-C		U	Steel clamp	1
400-S	400	S	None	1
400-S-W			CFRP Wrap	1
400-T2		T2	None	1
400-T2-W			CFRP Wrap	1
200-T2-W	200	T2	CFRP Wrap	1

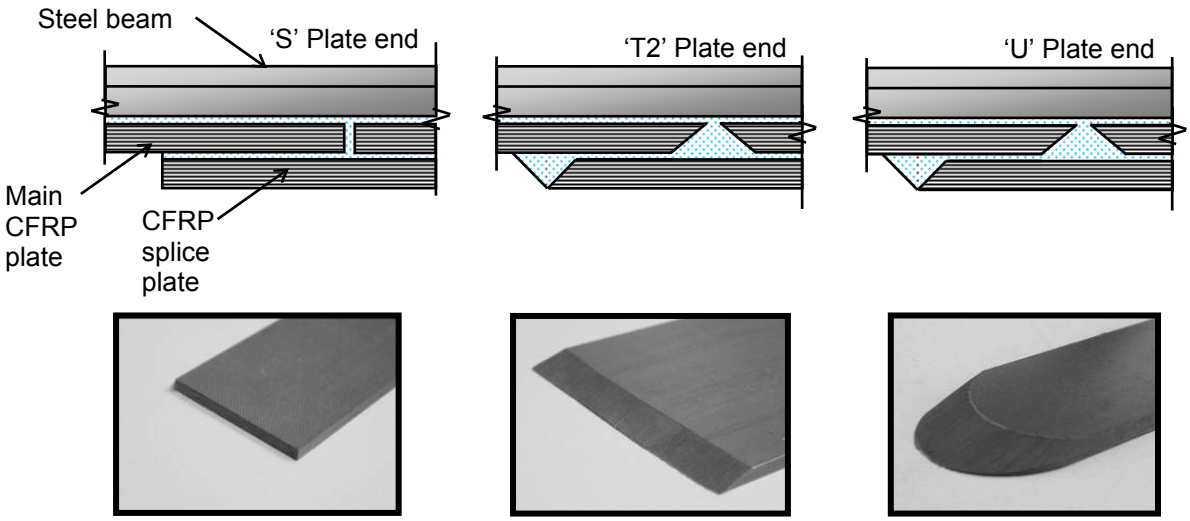

Figure 3.9 – Plate end configurations for tested steel splice beams

All of the tested steel beams remained essentially elastic throughout the experimental program. Therefore, after each test, the CFRP was removed from the tension flange of the beam, the beam was strengthened using a different splice configuration and subsequently retested.

The installation of the CFRP was conducted according to the recommendations provided by Schnerch et al. (2007). The surface of the steel was degreased by brushing with acetone, abraded by grit blasting and brushed again with acetone. The CFRP strips were bonded using the SP Spabond 345 two part epoxy adhesive. To maintain the thickness of the bond line, glass spacer beads were mixed with the epoxy. Approximately 1 gram of beads was mixed with every 100 grams of epoxy. The CFRP strips were fabricated with a glass fiber peel ply layer which was removed immediately prior to bonding. The adhesive was applied liberally to the surface of the CFRP to minimize the formation of air voids within the adhesive layer. The CFRP strips were applied to the surface and clamped in place using a wooden clamping system. The adhesive was allowed to cure for at least 12 hours at room temperature.

The strengthening was conducted in two days. On the first day the steel surface was prepared and the main CFRP plates were installed. The adhesive was allowed to cure for at least 12 hours. On the second day the excess adhesive was removed from the surface of the main CFRP plate by light abrasion. Contaminants were removed from the surface by wiping with methanol. The CFRP splice plate was installed and clamped, and the adhesive was allowed to cure.

Three tests were conducted to study the effect of installing a transverse CFRP wrap around the splice plate. A typical CFRP wrap is shown in Figure 3.10. The dry CFRP fibers were wrapped from the top of the tension flange on one side of the beam, around the bottom of the CFRP to the other side of the tension flange. The fibers were oriented in the transverse direction to help resist the peeling stresses that could possibly develop near the plate end. The fibers were bonded to the beam using the Sikadur 330 two part epoxy paste. The CFRP wrap was extended approximately 40 mm past the end of the splice plate to provide additional anchorage near the plate end.

Figure 3.10 – Typical transverse CFRP wrap

One test was conducted to study the effect of installing a specially fabricated steel clamping system near the plate end locations. The steel clamping system, shown in Figure 3.11, consisted of three steel plates that were tightened together using high-strength structural bolts. The clamps were installed at the locations where the highest magnitude of peeling stresses was expected to occur. These included at each end of the splice plate and at the center of the splice. To simulate the installation of the clamps in a typical field application, it was desirable to prevent direct electrical contact between the steel clamps and the CFRP splice plate to avoid possible galvanic corrosion. Therefore the steel plates were bonded to the CFRP and to the steel tension flange using a 1 mm thick layer of adhesive prior to installation of the steel bolts. The adhesive was allowed to cure and the steel bolts were tightened to apply an average confining pressure of approximately 25 MPa at the clamp locations.

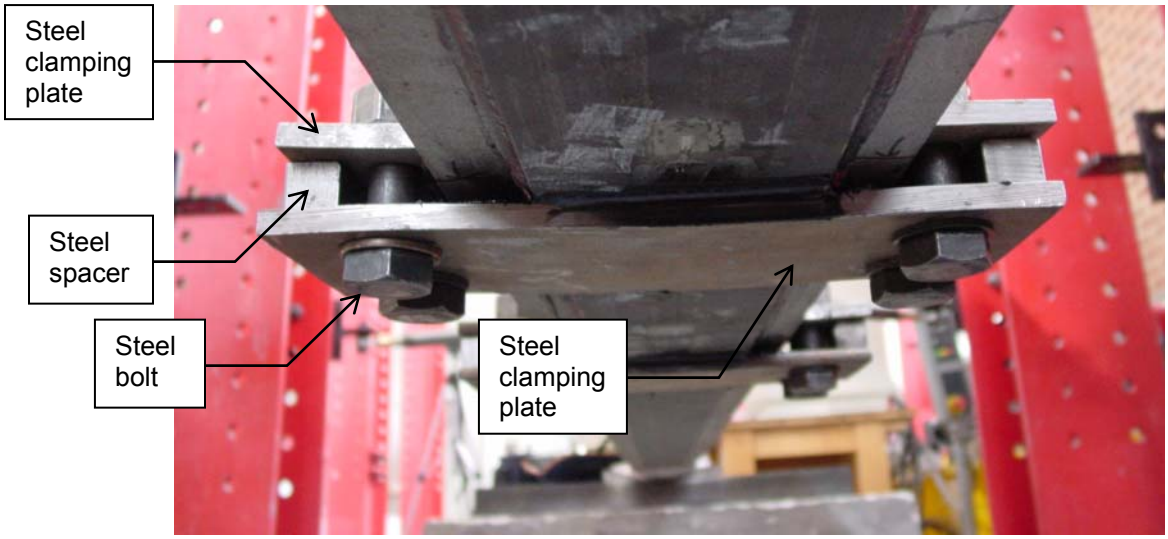

Figure 3.11 – Typical steel clamp assembly

3.2.2 Materials

The CFRP and adhesive materials that were used in this stage of the experimental program were the same as the materials used for the double-lap shear specimen tests and reported previously in this chapter. The material properties of the steel were determined by testing steel tension coupons according to ASTM A370-02. The tested beams were fabricated at two different times using two different batches of steel. The first batch of steel was used to fabricate the first beam while the second and third beams were fabricated using the second batch of steel. Independent material properties were measured for the web and the flange of the wide flange beams and for the steel channels. The measured elastic modulus, E, and yield strength, f_y, of the steel are presented in Table 3.5.

Table 3.5 – Measured steel material properties for the tested splice beams

	Beam 1			**Beams 2 & 3**		
	Web	**Flange**	**Channel**	**Web**	**Flange**	**Channel**
E (MPa)	209,000	208,000	205,000	211,000	223,000	N/A*
f_y (MPa)	403	373	340	388	358	N/A*

* Properties not tested

3.2.3 Instrumentation

Each of the steel beams was instrumented to measure the strain and deflection at various locations as shown in Figure 3.12. The strain at different locations along the steel beam was measured using strain gauge based displacement transducers, known as PI gauges, with a gauge length of 200 mm. The steel strains were measured at three locations on the midspan cross-section of the beam: the top surface of the beam, the mid-height of the web and the top surface of the tension flange. The midspan deflection of the beam was measured by two string potentiometers, one on either side of the longitudinal centerline of the beam. The deflection at each support was measured by a linear potentiometer.

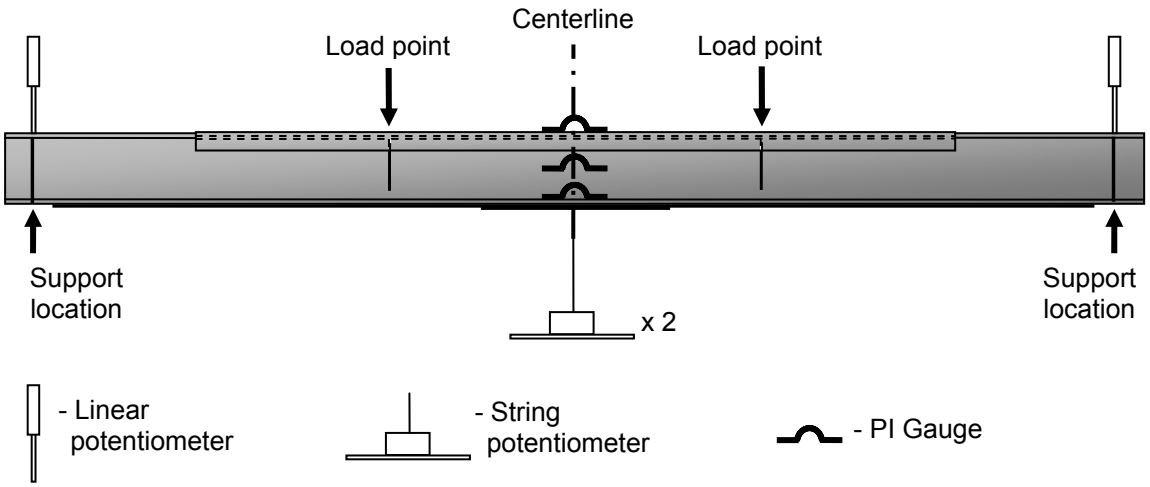

Figure 3.12 – Strain and deflection measurements on steel splice beams

The localized strain at the surface of the CFRP plates was measured using conventional electrical resistance strain gauges. The strain gauges were placed along the longitudinal centerline of the beam at the locations shown in Figure 3.13. The numbers in the figure indicate the distance from the splice centerline to the respective strain gauges in millimeters.

Due to the presence of the transverse CFRP wrap on beam tests 400-S-W, 400-T2-W and 200-T2-W, strain gauges could not be placed directly on the surface of the CFRP splice plate. Therefore, electrical resistance strain gauges were installed on the CFRP wrap near each of the plate ends to measure the transverse strain. The measured strain was used to evaluate the magnitude of the force in the CFRP wrap that was resisting the peeling at the end of the splice plate. Two longitudinal strain gauges were also installed on the main CFRP plate approximately 100 mm away from each end of the splice plate.

Similarly, due to the presence of the steel clamps, strain gauges could not be effectively installed on the CFRP splice plate for splice configuration 800-U-C. Therefore, only two longitudinal strain gauges were installed on the main CFRP plate approximately 40 mm away from each end of the splice plate.

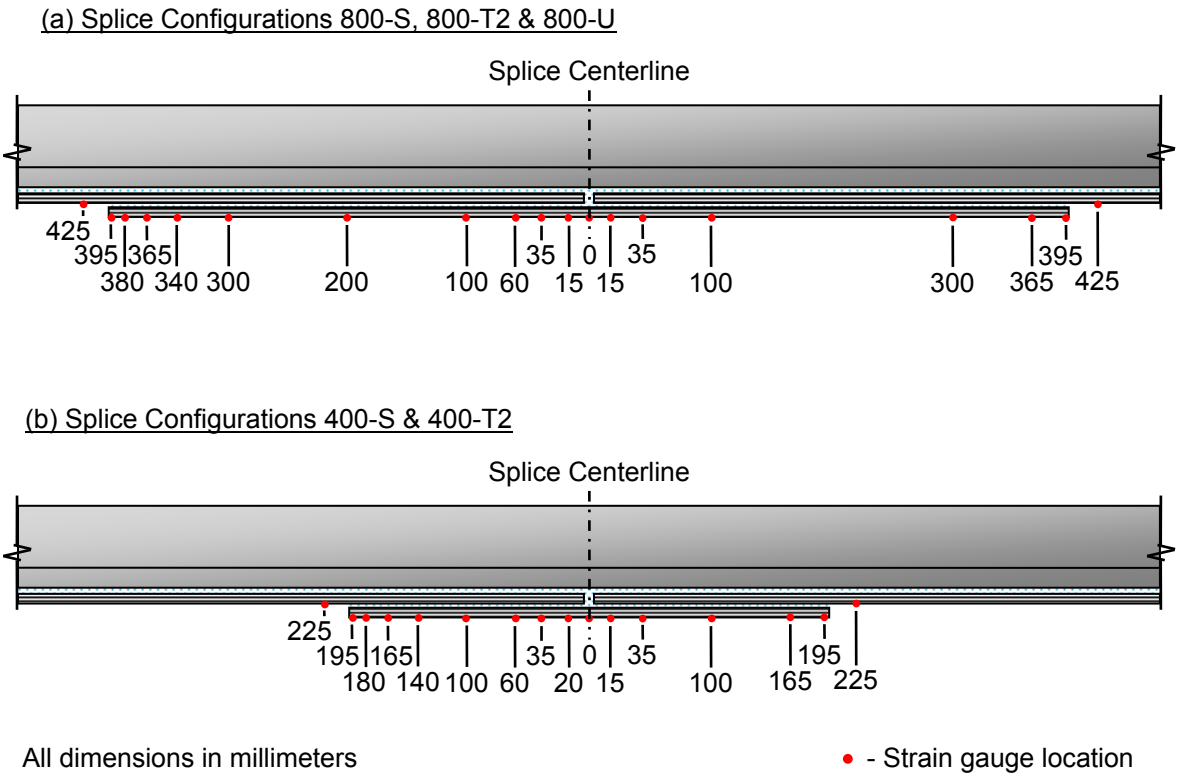

Figure 3.13 – Typical strain gauge locations for (a) 800 mm long splice configurations and (b) 400 mm long splice configurations

3.2.4 Test Setup

The typical test setup is shown in Figure 3.14. All of the beams were tested in a four point bending configuration with a span of 4570 mm and a 1600 mm long constant moment region. The load was applied using an 890 kN MTS hydraulic actuator and a steel spreader beam. The beams were supported on steel plates resting on 100 mm thick neoprene pads. Steel lateral braces were attached to the spreader beam at four locations and to the test beams at the support locations to prevent lateral movement and instability of the test beams. The load was applied at a constant displacement rate of 0.5 mm per minute and data was record using a data acquisition system connected to a personal computer.

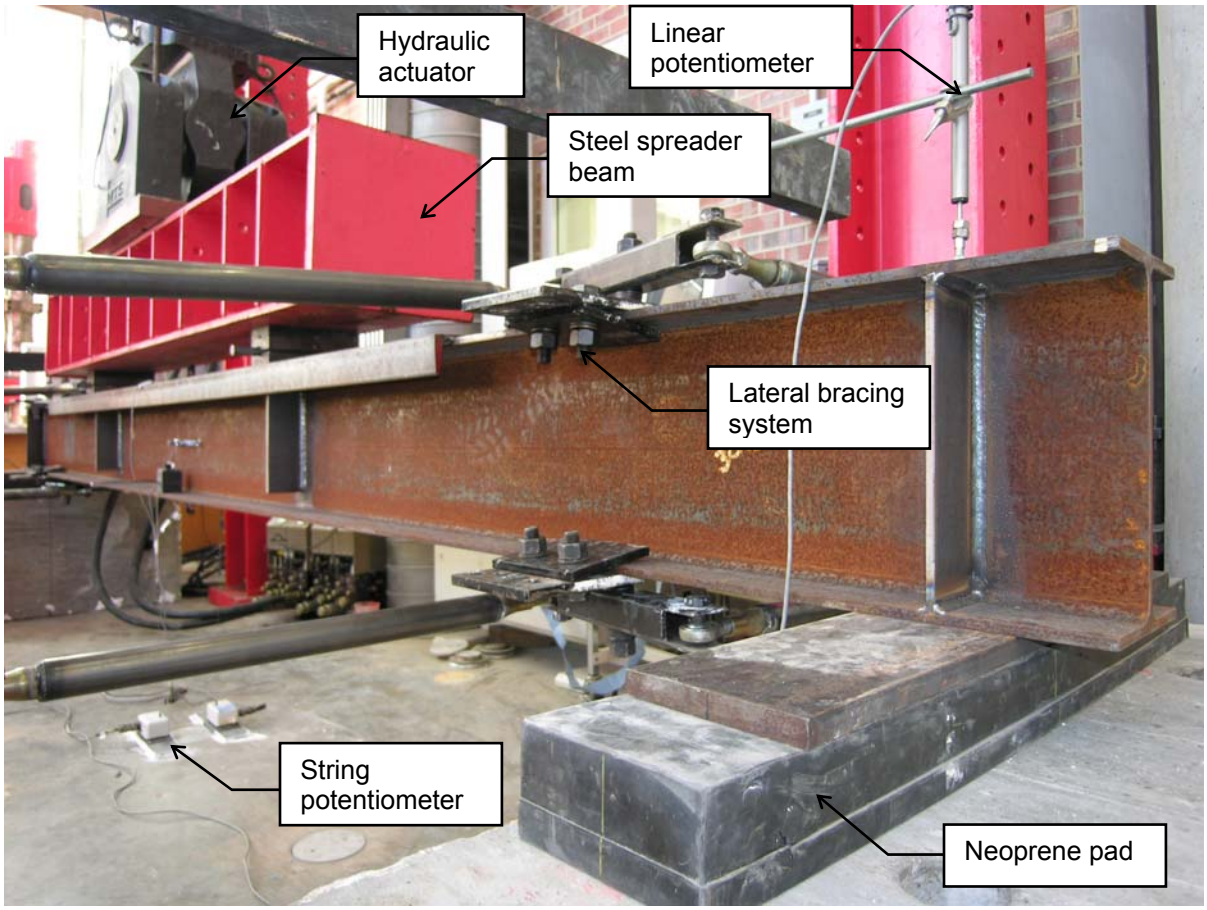

Figure 3.14 – Typical test setup for steel beam tests

Chapter 4: Experimental Results & Discussion

This chapter presents the results of the experimental program that was conducted to study the bond and splice behavior of the proposed high modulus CFRP system for strengthening steel structures. The experimental program was conducted in two stages. The first stage consisted of eight double-lap shear specimen tests while the second stage consisted of 10 steel beam tests. The results of the double-lap shear specimen tests are presented in detail in Section 4.1. The results of the steel beam tests are presented in Section 4.2. For the beam tests, the results of selected tests are presented in detail in this chapter. The results of the remaining tests are summarized in this chapter. The results are provided in detail in Appendix A. The effect of the different parameters studied, including plate end configuration, different types of mechanical anchorage used and splice length are also discussed.

4.1 RESULTS OF THE DOUBLE-LAP SHEAR SPECIMEN TESTS

The first stage of the experimental program consisted of eight double-lap shear specimen tests. All of the tested specimens consisted of two 8 mm thick main CFRP plates which were bonded together by two 4 mm thick x 400 mm long CFRP splice plates. Four different splice configurations were considered as described in Chapter 3. The effect of a steel clamp assembly on the joint strength is also presented. All of the specimens were tested in monotonic tension and strains were measured at different locations along the surface of the CFRP splice plate.

4.1.1 Behavior of the square plate end specimens, 400-S

Three of the tested coupons included square plate end geometries at all plate ends, including at the end of the CFRP splice plates and at the end of the main CFRP plates within the center of the joints. All three of the tested coupons failed suddenly due to debonding of the CFRP

splice plate as shown in Figure 4.1. Typically a mixed mode failure was observed with some of the adhesive remaining bonded to the main CFRP plate and some of the adhesive bonded to the CFRP splice plate. Inspection of the failure surfaces suggested that the failures typically occurred within a thin layer of resin at the surface of the CFRP. However, several cracks and diagonal failure planes were observed in the adhesive layer, which suggests that the failure may also have been partially cohesive within the adhesive layer.

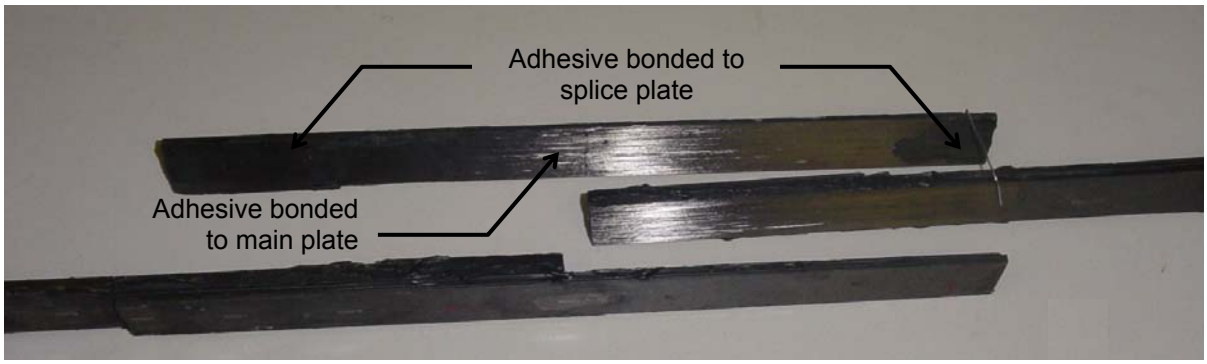

Figure 4.1 – Typical failure mode for the double-lap shear specimens with square plate ends

The measured load-strain behavior of the splice plate at the center of the joint is shown in Figure 4.2(a) for all three of the tested coupons. The predicted load-strain behavior of a continuous CFRP coupon without a splice joint is shown by the dashed line in the figure for comparison purposes. Inspection of the figure indicates that, initially, the measured strains at the surface of the CFRP splice plate were considerably lower than the predicted strains for the continuous CFRP. During fabrication of the specimens, a 1 mm to 2 mm wide gap was left between the ends of the main CFRP plates, which was subsequently filled with adhesive. The adhesive within the gap region may have possibly helped to transfer shear stresses across the joint thereby decreasing the measured strain at the surface of the splice plate. During testing a cracking sound was heard which was accompanied by a sudden increase of the measured strain, shown in Figure 4.2(a), at the 42 kN, 46 kN and 50 kN load levels for the three specimens respectively. This suggests cracking of the adhesive occurred within the

center of the joint. This was confirmed using a non-linear finite element analysis as described in Chapter 5.

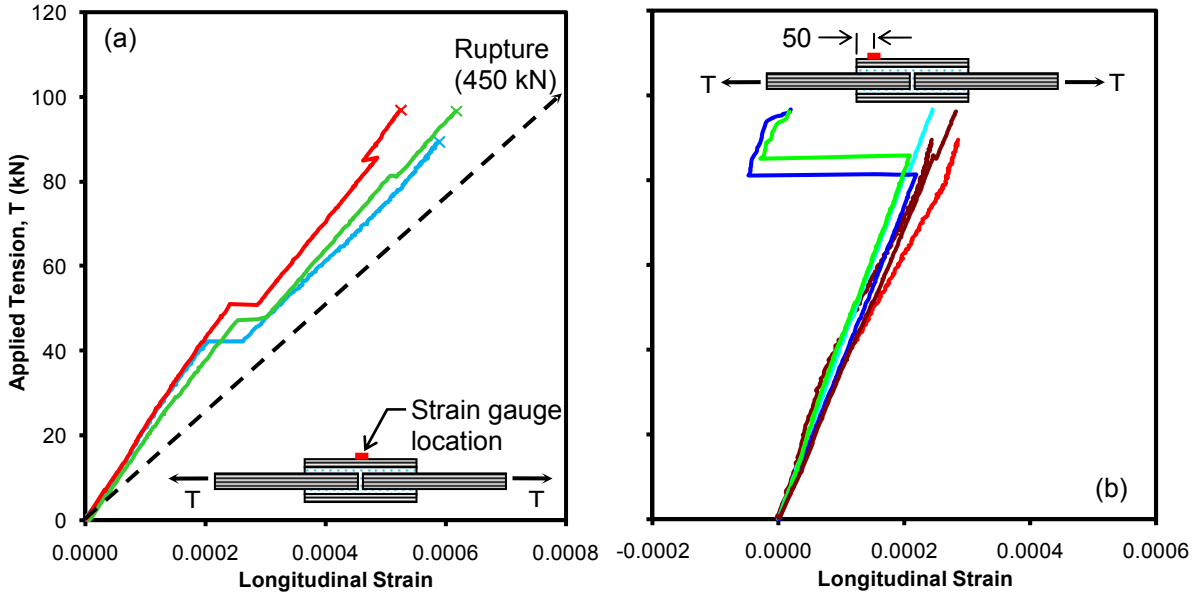

Figure 4.2 – Measured strains for the tested 400-S double-lap shear specimens at: (a) center of the splice joint and (b) 50 mm from the end of the splice plate

Figure 4.2 (b) shows the measured strain 50 mm away from the end of the splice plate for all three of the tested double-lap shear specimens with the square plate ends. Two gauges were installed on each specimen at similar locations. The figure indicates an essentially linear load-strain response for all of the specimens. However, two of the gauges indicated a sudden decrease of strain at the 81 kN and 85 kN load levels respectively which was accompanied by a cracking sound during testing. The sudden decrease of strain could possibly be due to cracking of the adhesive layer near the plate end. Propagation of the crack beyond the location of the strain gauges may have relieved some of the longitudinal strain in the splice plate at the gauge location. Inspection of the failure surface for one of the test specimens indicated the presence of a sizeable air void near one end of one of the splice plates. The presence of this void may have induced premature cracking of the adhesive.

Distribution of the measured strain along the length of the CFRP splice plate is shown in Figure 4.3 for all three tested coupons with the square plate ends at a load level of 80 kN. The selected load level is slightly lower than the measured failure loads of the tested specimens. The strain distribution was also calculated using an analytical model proposed by Albat & Romily (1999) which was developed for a similar specimen configuration. Inspection of the figure indicates that the measured strains closely match the trend predicted by the analytical model. The results of the analytical model indicate the presence of a stress concentration in the adhesive near the ends of the splice plate and also near the center of the joint which is indicated by the high gradient of strains in these regions. All three of the tested coupons failed at load levels from 89 kN to 97 kN due to sudden debonding of one or both of the CFRP splice plates. The observed debonding failure was likely due to the presence of the stress concentrations. Due to the sudden brittle nature of the failure the location of the initiation of the debonding, whether at the center of the joint or near the end of the splice plate, could not be identified.

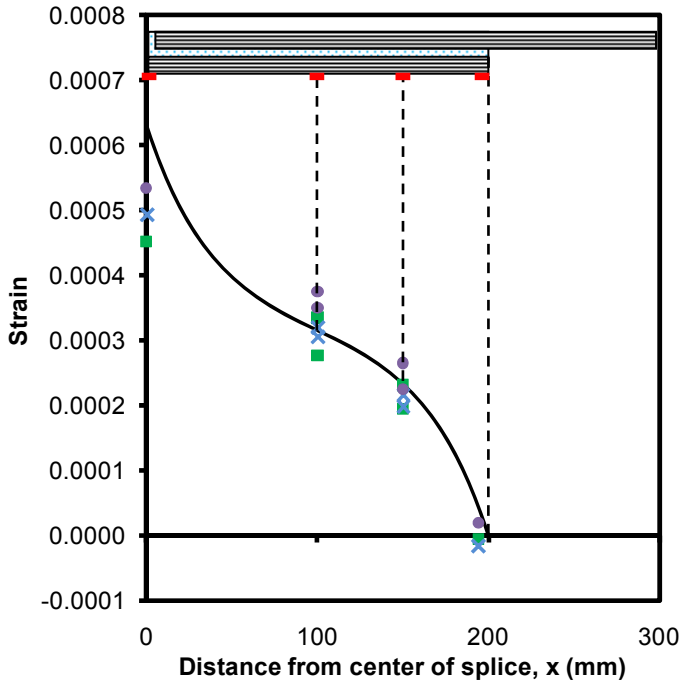

Figure 4.3 – Strain distribution along splice plate length for square plate end configuration

4.1.2 Effect of the plate end configuration

To reduce the stress concentrations near the plate ends, several different plate end configurations were considered in the experimental program as described in Chapter 3. The T1 configuration included a reverse tapered detail at the ends of the CFRP splice plates. However, the ends of the main CFRP plates within the center of the joint were left square. The T2 configuration included tapered plate ends at the ends of the splice plates and within the center of the joint. The U configuration included rounded and tapered plate ends at all locations.

Figure 4.4 presents the measured strain at the surface of the CFRP splice plates at the center of the joint for the 400-T1, 400-T2 and 400-U specimen configurations. The numbers in parentheses at the end of the specimen identifiers in the figure indicate multiple repetitions of the same specimen configuration. Inspection of the figure indicates that the measured strain for the 400-T1 configuration increased suddenly at the 41 kN and 144 kN load levels. This indicates progressive cracking of the adhesive within the center of the joint which is similar to the behavior that was observed and previously described for the 400-S specimen configurations. The cracking of the adhesive was likely due to a stress concentration within the center of the joint due to the square end configuration of the main CFRP plates. This suggests that the presence of the taper at the ends of the splice plates did not affect the magnitude of the stress concentration near the center of the joint. Both the 400-T2 and 400-U specimen configurations included modified plate end geometries within the center of the splice joint which helped to reduce the stress concentration at this location. Therefore, similar cracking behavior was not observed for these specimen configurations.

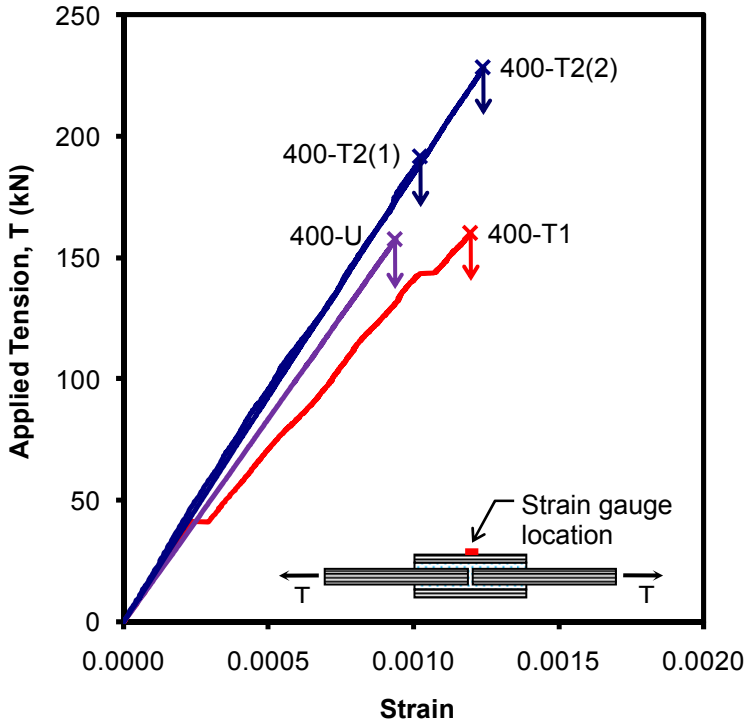

Figure 4.4 – Measured strain at the center of the splice for the double-lap shear specimens

All of the tested coupons failed by debonding of one or both of the CFRP splice plates in a similar manner as the 400-S test specimens with square plate ends. Table 4.1 presents the measured failure load and maximum measured strain on the surface of the main CFRP plate for all of the tested double-lap shear specimens. The results presented in the table indicate that the maximum measured CFRP strain was significantly lower than the rupture strain.

Inspection of Table 4.1 indicates that providing a reverse taper only at the ends of the splice plate, such as for the T1 configuration, resulted in a 70 percent increase of the measured tensile strength compared to the square plate end configuration. This suggests that the presence of the reverse taper helped to reduce the magnitude of the localized stress concentration near the end of the splice plate. This trend was confirmed by the results of the finite element analysis which was used to determine the stresses throughout the adhesive layer as discussed in Chapter 5.

Table 4.1 – Experimental results for the tested double-lap shear specimens

Specimen ID	Tension Strength (kN)	ε_{max}	$\varepsilon_{max}/\varepsilon_{CFRP,u}$
400-S(1)	89	0.00078	0.22
400-S(2)	97	0.00086	0.24
400-S(3)	97	0.00088	0.25
400-T1	160	0.00129	0.36
400-T2(1)	191	0.00148	0.42
400-T2(2)	228	0.00160	0.45
400-U	157	0.00119	0.34
400-U-C	284	0.00200	0.56

Test results, presented in Table 4.1, further indicate that providing reverse tapers at the end of the splice plate and also within the center of the joint, such as for the T2 configuration, increased the average measured tension strength of the tested specimens by 120 percent compared to the square plate end configuration. The results of the finite element analysis presented in Chapter 5 and the observed cracking behavior of the 400-T1 specimen indicate that the selected length of the splices was adequate to prevent any interaction between the stress concentrations at the two locations. Therefore, it is likely that the observed difference of the measured strength between the T1 and T2 configurations represents the statistical variation of the bond strength.

Providing rounded and tapered plate ends at all locations, such as for the 400-U specimen configuration, resulted in a 70 percent strength increase compared to the square plate end configuration. While this may indicate that the U configuration was less effective than the T2 configuration, it may also represent the inherent variability of the bond strength of the strengthening system.

Comparison of the results for specimen 400-U and 400-U-C indicates that the presence of the steel clamp assemblies near the plate ends and at the center of the joint increased the tension strength of the coupons by 80 percent. This suggests that the steel clamps confined the plate

end region and helped to resist the peeling stresses which typically develop due to the eccentricity between the main CFRP plates and the splice plates.

4.2 RESULTS OF THE STEEL BEAM TESTS

The second stage of the experimental program consisted of ten steel beam tests. The beams were strengthened with CFRP plates with a splice joint at midspan as described in Chapter 3. The different parameters that were studied included the plate end configuration, the length of the splice plate and two different methods to mechanically anchor the splice plate including a transverse CFRP wrap and a steel clamp assembly. The behavior of the tested beams with square plate ends is described in detail in the following section. The effect of the different parameters on the splice behavior is summarized and detailed results for the remaining beam tests are presented in Appendix A.

4.2.1 Behavior of the square plate end specimens, 400-S & 800-S

Three of the tested beams included splices with square plate ends at all locations, including at the ends of the splice plate and at the ends of the main CFRP plates within the center of the splice. For two of the beam tests, 800-S(1) and 800-S(2), an 800 mm long splice plate was installed while for the remaining test, 400-S, a 400 mm long splice plate was installed. The measured load-deflection behavior of all three beams is shown in Figure 4.5. The dashed line in the figure represents the predicted load-deflection behavior of the strengthened beam, without any splice joint, past rupture of the CFRP, based on a moment-curvature analysis. All three of the tested beams failed due to debonding of the splice plate prior to yielding of the steel beam. The measured failure loads were 178 kN, 205 kN and 180 kN for the 800-S(1), 800-S(2) and 400-S splice configurations respectively. This corresponds to approximately 40 to 45 percent of the estimated increased yield load of the strengthened beam. Test results indicated that increasing the length of the splice plates did not significantly affect the measured failure load. The finite element analysis, described in detail

in Chapter 5, indicated that increasing the splice length from 400 mm to 800 mm did not affect the distribution of the adhesive stresses near the end of the CFRP splice plates. This highlights the need to incorporate different plate end geometries to reduce the bond stress concentration near the plate ends and to increase the tension strength of the splice joints.

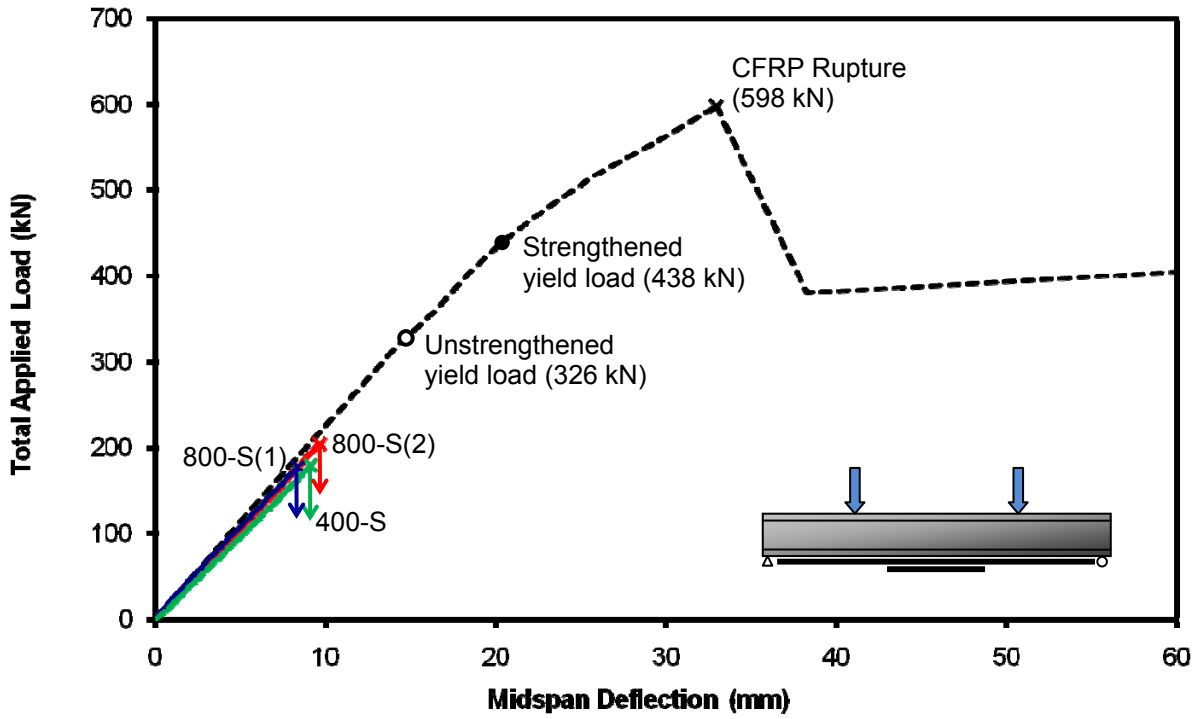

Figure 4.5 – Load-deflection behavior of the splices with square plate ends

All three of the tested splices failed due to debonding of the splice plates prior to yielding of the steel beam. The typical observed failure, shown in Figure 4.6(a), was a mixed mode interfacial/interlaminar failure near the surface of the FRP. The typical location of the failure surface is indicated schematically by the dashed line in Figure 4.6(b). The failure surface extended from one end of the splice plate along the interface between the splice plate and the first main CFRP plate to the center of the splice. At the center of the splice the failure surface shifted to the interface between the second main CFRP plate and the steel surface.

The splice plate remained bonded to the second main CFRP plate which partially debonded from the steel surface.

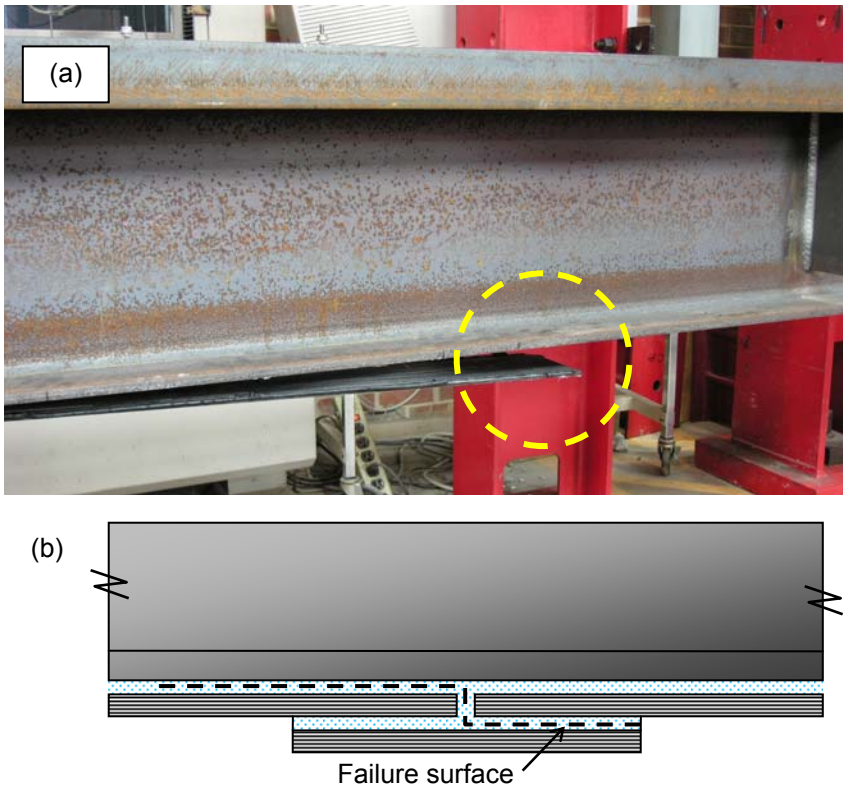

Figure 4.6 – (a) Typical debonding failure of CFRP splice plate with square plate ends (b) Typical location of the failure surface

Throughout the experimental program the longitudinal strains were measured at different locations along the surface of the CFRP splice plates and the main CFRP plates. The measured strains for the 800-S(2) splice configuration are plotted in Figure 4.7(a) for different load levels up to failure of the beam. The figure indicates the gradual development of the tension strain along the length of the splice plate. The horizontal dashed line in the figure indicates the calculated strain in the CFRP, immediately prior to failure, as determined by a moment-curvature analysis. The analysis assumed perfect bond between the steel beam and the CFRP strengthening system and did not account for the presence of the splice. The

figure indicates that the measured strain at the center of the splice immediately prior to failure was equal to the calculated strain obtained from the moment curvature analysis at the same load level. This indicates that the tension force in the CFRP was totally transferred to the CFRP splice plate. This further indicates complete composite action between the spliced CFRP strengthening system and the steel beam.

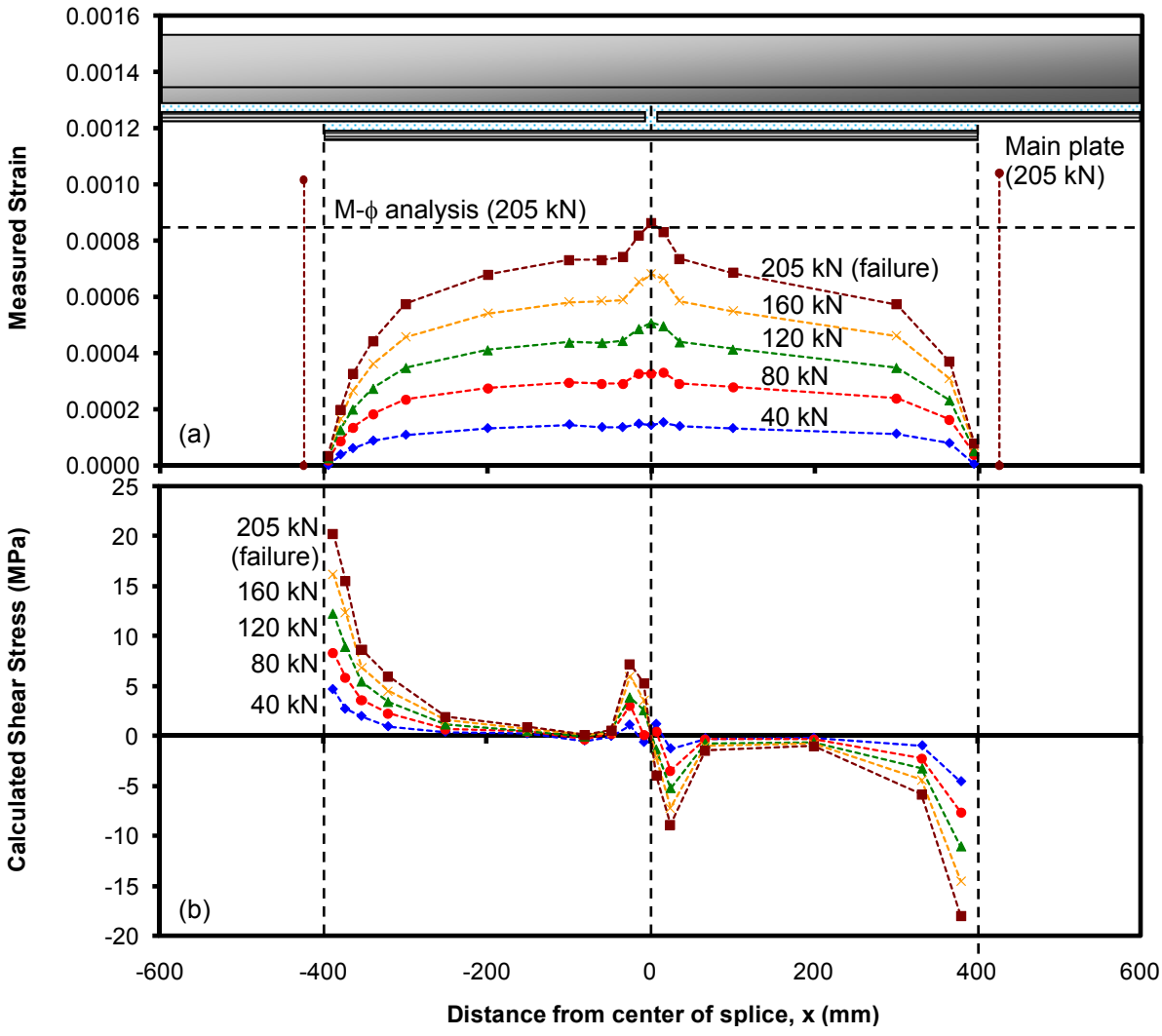

Figure 4.7 – (a) Measured strains at the surface of the CFRP splice plate and (b) calculated shear stress distribution in the adhesive layer

The measured strains at the surface of the main CFRP plate near both ends of the splice plate are also shown in Figure 4.7(a). The measured strains were approximately 18 percent higher than the calculated strain obtained from the moment-curvature analysis. This indicates the presence of a longitudinal stress concentration in the main CFRP plate near the end of the CFRP splice plate. The presence of such a stress concentration was confirmed by the results of the finite element analysis presented in Chapter 5.

The measured strains at the surface of the splice plate were used to determine the distribution of the shear stress in the adhesive layer. The average adhesive shear stress between two adjacent gauges was calculated by considering equilibrium of the CFRP splice plate. Considering two gauges, located at positions x_i and x_{i+1}, respectively, the average adhesive shear stress, $\bar{\tau}$, between the gauges was calculated as:

$$\bar{\tau} = \frac{\varepsilon_{i+1} - \varepsilon_i}{x_{i+1} - x_i} E_{CFRP} t_{CFRP} \qquad \text{(Eq. 4.1)}$$

where:

ε_{i+1} = measured strain at location x_{i+1}

ε_i = measured strain at location x_i

E_{CFRP} = tensile modulus of the CFRP splice plate

t_{CFRP} = thickness of the CFRP splice plate

The calculated distribution of the shear stresses is plotted in Figure 4.7(b) for different load levels, up to failure. The calculated average shear stress along each interval between two gauges, determined using Eq. 4.1, was assumed to occur at the midpoint of the interval. Inspection of the figure indicates the presence of significant shear stress concentrations near the ends of the CFRP splice plates and also near the center of the splice. The calculated

shear stresses away from these locations were relatively low. Further, the calculated stress concentration near the end of the splice plate was significantly higher than the stress concentration near the center of the joint. This suggests that the failure of the splices initiated at one end of the splice plate and propagated towards the center of the splice. This is consistent with the trend obtained from the finite element analysis described in Chapter 5 and the failure mode that was observed experimentally.

A similar trend of the measured strains and the calculated shear stresses was observed for the other two tested splices, 800-S(1) and 400-S. The detailed results are presented in a similar format in Appendix A.

4.2.2 Comparison of different splice configurations

The experimental program included a number of different splice configurations. Two additional plate end configurations, configurations T2 and U, were considered in the program, which were similar to those considered for the double-lap shear specimen tests. An additional three tests were conducted to study the effect of anchoring the splice plate using a transverse CFRP wrap. Mechanical anchorage of the splice plate using a specially fabricated steel clamp assembly was also considered for one test. The measured failure loads of the tested beams are presented in Table 4.2 for the different splice configurations. The table also compares the measured failure loads, P_{max}, to the calculated yield load of the unstrengthened beam, $P_{y,u}$ and the increased yield load of the strengthened beam, $P_{y,s}$. The maximum measured strains at the surface of the main CFRP plate, ε_{max}, are also given in the table and compared to the measured rupture strain of the CFRP, $\varepsilon_{CFRP,u}$.

Table 4.2 – Test results for the steel beam tests with different splice configurations

Beam ID	Failure Load (kN)	$P_{max}/P_{y,u}$	$P_{max}/P_{y,s}$	ε_{max}	$\varepsilon_{max}/\varepsilon_{CFRP,u}$
800-S(1)	178	0.55	0.41	0.00082	0.23
800-S(2)	205	0.63	0.47	0.0010	0.28
800-T2	408	1.25	0.93	0.0023	0.65
800-U	343	1.05	0.78	0.0015	0.42
800-U-C	308	0.94	0.70	0.0014	0.40
400-S	180	0.55	0.41	0.00085	0.24
400-S-W	200	0.62	0.61	0.00087	0.25
400-T2	340	1.04	0.78	0.0015	0.42
400-T2-W	218	0.67	0.50	0.00088	0.25
200-T2-W	236	0.72	0.54	0.00092	0.26

The effects of the different parameters studied in the experimental program, including the plate end configuration, the CFRP wrap and the steel clamp assembly, are presented in the following sections. The discussions in the following sections refer to Table 4.2 for comparison purposes. The general trend of the behavior for all of the tested splices was similar to that described in the previous section for the splices with square plate ends. The notable differences in the observed behavior are discussed in the following sections. The measured strains and calculated shear stress distributions for splice configurations 400-S, 800-S(1), 400-T2, 800-T2 and 800-U are presented in Appendix A.

4.2.2.1 Effect of the plate end configuration

In addition to the square plate ends, two additional plate end configurations, configurations T2 and U, were considered in the experimental program. The T2 configuration included reverse tapered plate ends at the ends of the splice plate and at the ends of the main CFRP plates at the center of the joint. The U configuration included rounded and tapered plate ends at all locations. All of the tested splice configurations failed by debonding of the CFRP splice plate prior to yielding of the steel beam. The observed failure mode was similar to that described for the square plate end configurations.

Comparison of the measured failure loads for the 800-S and 800-T2 configurations in Table 4.2 indicates that the reverse tapered plate end configuration increased the strength of the splice by approximately 115 percent. Comparison of the 400-S and 400-T2 results in the table indicates an 80 percent increase of strength relative to the square plate end configuration. A similar trend was observed for the tested double-lap shear specimens and the measured increase of the tension strength of the splices was comparable. The results suggest that the presence of the reverse tapered plate end configuration helped to decrease the magnitude of the stress concentration near the plate ends thereby increasing the strength of the splice. This trend was confirmed by the results of the finite element analysis which are presented in Chapter 5. However, this effect could not be directly observed experimentally since the spacing of the strain gauges was too coarse to precisely determine the magnitude of the peak shear stresses in the areas of high strain gradients near the plate ends. Further, the normal (peeling) and longitudinal (axial) stress components in the adhesive could not be directly measured.

Inspection of Table 4.2 further indicates that the measured failure loads of the beams with square plate ends, 800-S(1), 800-S(2) and 400-S, were less than the calculated yield load of the unstrengthened steel beams. By comparison, the measured failure load of the splices with reverse tapered plate ends, 800-T2 and 400-T2, was higher than the calculated yield load of the unstrengthened beam and approached the increased yield strength of the strengthened beam. This suggests that, for typical applications, the square plate end splices should be placed at locations of relatively low moment to prevent premature failure of the strengthening system by debonding of the splice plate. Alternatively, the tapered splice joints can be installed at locations of relatively high moment without compromising the integrity of the strengthening system. The results presented in Table 4.2 also indicate that, even if the tapered splices are installed at locations of relatively high moment, the strengthening system can still be used to enhance the serviceability of the strengthened beam.

Inspection of Table 4.2 indicates that the measured strength of the splice with the rounded and tapered plate ends, 800-U, was approximately 80 percent greater than the average measured strength of the square plate end splice configuration. Comparison of the results of the 800-U and 800-T2 splice configurations suggests that the rounded and tapered plate end configuration may be less effective than the reverse tapered plate end configuration. Alternatively, the measured difference of the failure loads may also represent the inherent variability of the bond strength. A similar trend was observed for the double-lap shear specimens.

4.2.2.2 Effect of the transverse CFRP wrap

Three different tests, 400-S-W, 400-T2-W and 200-T2-W were conducted to study the effect of a transverse CFRP wrap on the performance of the splice joint. The plate end configurations of the 400-S-W and 400-T2-W splices were similar to their unwrapped counterparts. The 200-T2-W configuration included a 200 mm long splice plate with reverse tapered plate ends at all locations which was subsequently wrapped with CFRP. The objective of the transverse CFRP wrap was to confine the splice location and to help resist the normal (peeling) stresses that developed near the ends of the splice plate.

The 400-T2-W test was halted when a loud cracking sound was heard which was similar to the debonding sound of the previously tested splices. Inspection of the splice indicated the presence of a small crack in the CFRP wrap near one end of the splice plate as shown in Figure 4.8. Similar cracking sounds were heard and similar cracks were observed during the tests of the 400-S-W and 200-T2-W splice configurations. However, the tests were continued until the measured load-deflection behavior indicated the onset of yielding of the steel beam. At this point the observed cracking pattern in the CFRP wrap had extended significantly, as shown in Figure 4.8, which indicated that the debonded CFRP splice plate was punching through the transverse CFRP wrap. At the conclusion of the tests, the CFRP wraps were removed to examine the failure surfaces for all three splice configurations.

Removal of the wraps indicated that in all three cases the splice plates had debonded in a similar manner to the unwrapped splice configurations. However, the separation was concealed by the presence of the CFRP wrap. This is not desirable for practical applications since failure of the splice would not be easily detected and may be overlooked during routine inspection of the strengthening system.

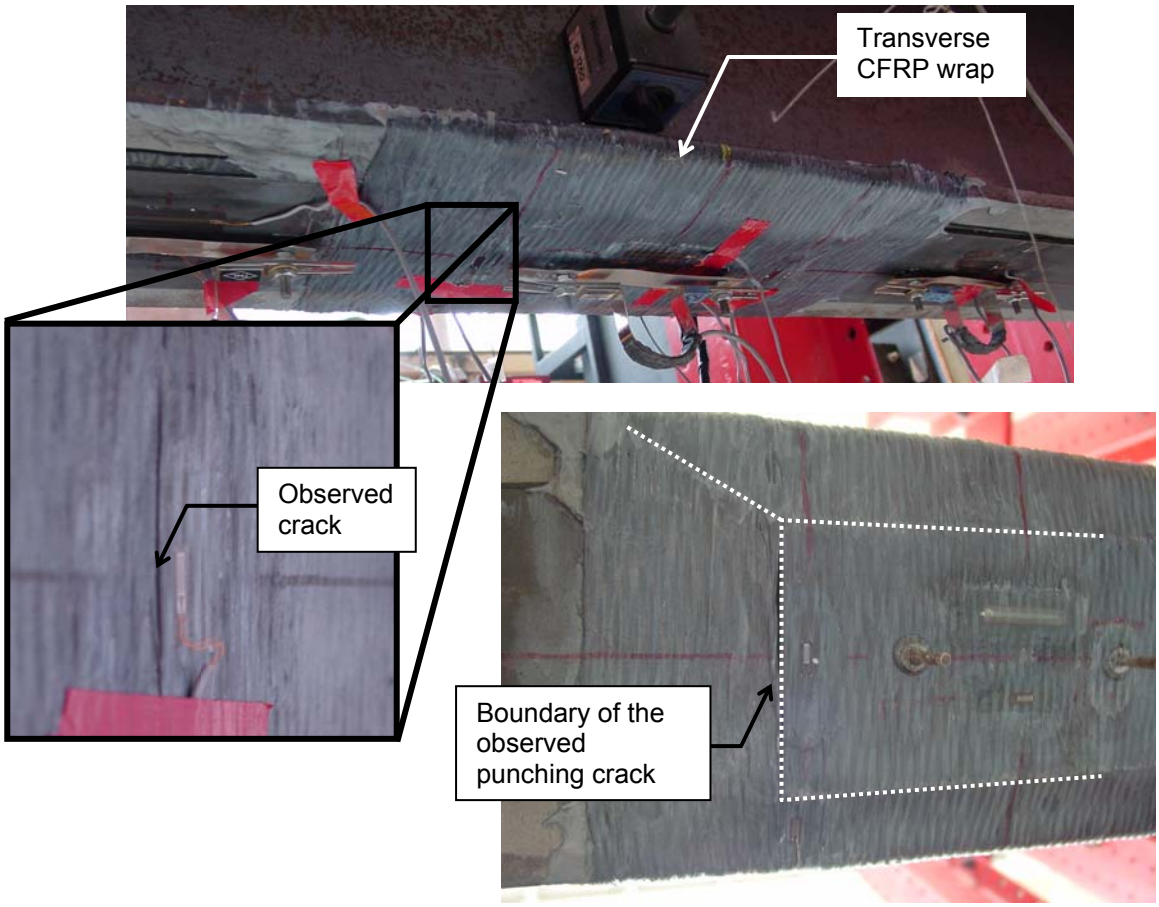

Figure 4.8 – Typical failure of a wrapped splice

Inspection of Table 4.2 indicates that the measured failure load of the 400-S-W splice configuration was approximately equal to that of its unwrapped counterpart, 400-S. This suggests that the presence of the CFRP wrap did not help to increase the strength of the

splice. Comparison of the measured failure load for splice configurations 400-T2-W and 400-T2 indicate that the measured failure load of the wrapped splice was lower than that of the unwrapped splice. This may possibly have been due to the presence of a defect or void in the adhesive layer which may have formed during fabrication or handling of the specimen and which was not detected prior to testing. Alternatively, the transverse CFRP wrap may have cracked prematurely during testing since the fibers in the wrap were oriented perpendicular to the primary direction of loading. Premature cracking of the wrap may have induced a stress concentration in the adhesive layer leading to premature debonding of the splice.

Strains were measured at several locations on the surface of the transverse CFRP wrap and on the main CFRP plate. The measured transverse strain on the surface of the CFRP wrap near one end of the CFRP splice plate is given in Figure 4.9 for the 200-T2-W splice configuration. The figure also presents the measured longitudinal strain on the surface of the main CFRP plate near the end of the splice plate. Inspection of the figure indicates that the measured longitudinal strain was tensile (positive) throughout the loading while the measured transverse strain was compressive (negative). If the CFRP wrap was helping to resist the normal (peeling) stresses near the end of the splice plate, the peeling of the splice plate would induce positive tensile strains in the transverse CFRP wrap. The measured compression strains suggest that the transverse strains in the CFRP wrap were dominated by Poisson effects rather than by peeling of the CFRP splice plate. The trend of the measured strains was confirmed by multiple gauges on all three of the tested beams with wrapped splice configurations.

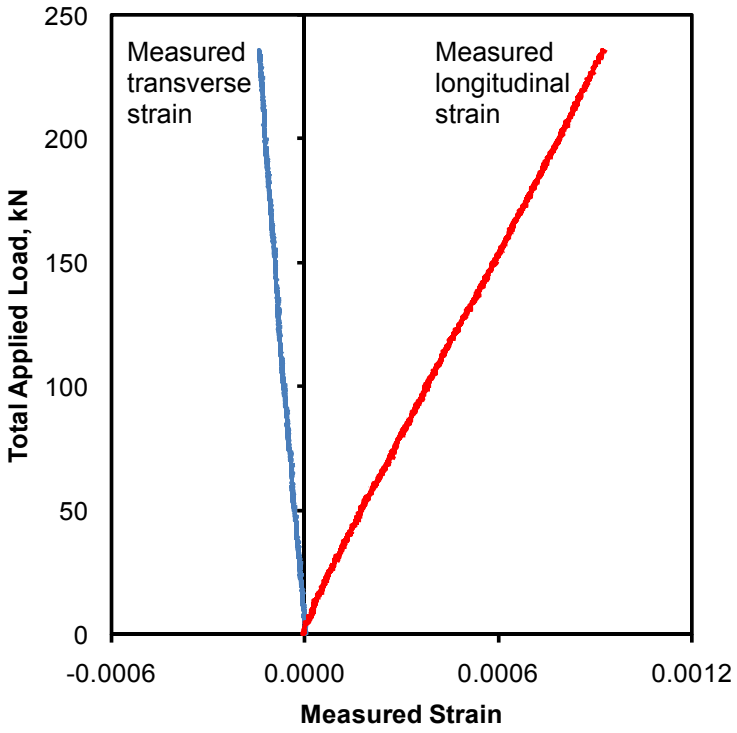

Figure 4.9 – Typical measured strains for the wrapped splice configurations

4.2.2.3 Effect of the steel clamp assembly

Beam 800-U-C was tested to investigate the performance of a specially fabricated steel clamp system. The splice configuration was similar to that of the 800-U specimen with the exception that steel clamps were installed at both ends of the splice plate and also at the center of the splice to help resist peeling stresses. The installation of the clamps is described in Chapter 3. Comparison of the maximum measured failure load for splice configurations 800-U and 800-U-C, given in Table 4.2, indicates that the presence of the steel clamps did not increase the measured splice capacity. Rather, the presence of the steel clamps may have slightly decreased the strength of the splice. The test of beam 800-U-C was halted after a loud cracking sound was heard similar to the debonding sound heard for the wrapped splices. The steel clamps were removed and the debonding of the splice plate was observed. Figure

4.10 shows one of the steel clamps near the end of the splice plate after the failure but prior to removing the clamps. The line in the figure clearly indicates a slight curvature of one the steel plates which is a part of the clamping system. As discussed in Chapter 3, the steel plates that made up the clamp assembly were first bonded to the beam prior to tightening the bolts. This was done to simulate an actual field application in which direct electrical contact between the steel clamp and the CFRP splice plate could possibly induce galvanic corrosion of the clamp or the steel beam. The adhesive was allowed to harden prior to tightening the steel bolts. The curvature of the steel plate, shown in Figure 4.10, was induced when the steel bolts were tightened to apply the clamping pressure at the end of the splice. Due to the presence of the cured adhesive between the steel clamp and the splice plate, the curvature of the plate may have possibly induced direct tension forces near the end of the splice. The presence of these tension forces near the plate end may explain the observed reduction of the measured failure load due to the installation of the steel clamp.

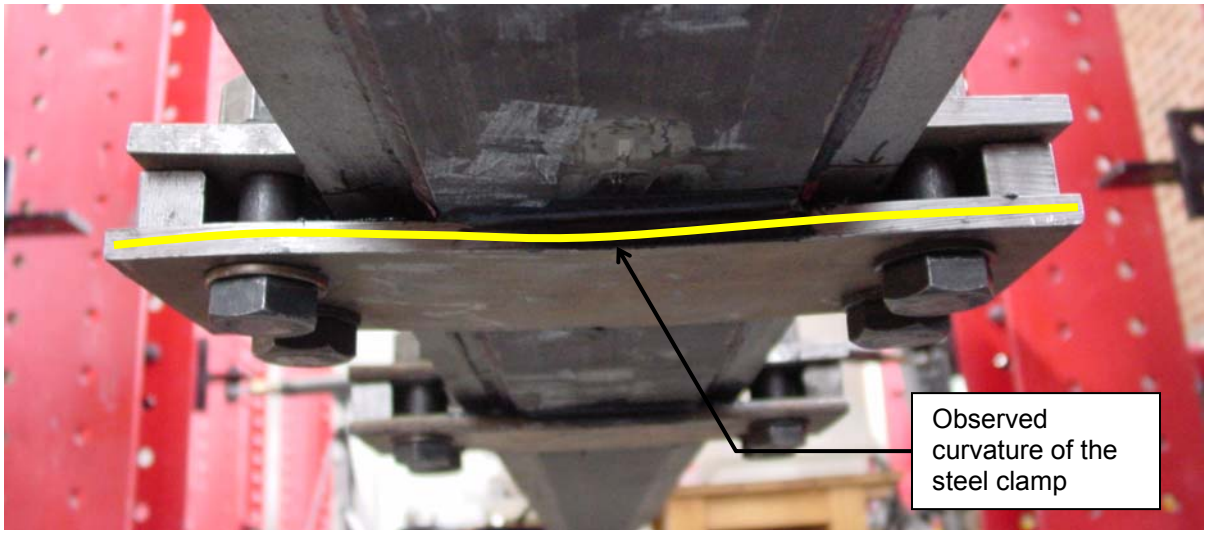

Figure 4.10 – Observed failure of the clamped, 800-U-C, splice configuration

The results of the double-lap shear specimen tests, which were presented previously in this chapter, indicate that, conceptually, a steel clamping system can be used to induce

compression stresses near the end of the splice plate and to increase the strength of the splice. The beam test results suggest that careful consideration of the design, detailing, and installation of the clamping system are essential to ensure that the clamps effectively confine the plate end region.

Chapter 5: Finite Element Analysis

The analytical phase of the research program was conducted in three stages. The first stage included a 3-D, non-linear finite element analysis of a 400 mm long double-lap shear specimen with square plate ends, similar to the specimen 400-S configuration. The analysis was conducted to investigate initiation and propagation of cracking which lead to failure of the double-lap shear specimen since this behavior could not be precisely observed experimentally. The second stage consisted of several 2-D linear plane-strain analyses of double-lap shear specimens with different taper angles near the plate end. The analyses were conducted to study the effect of the taper angle on the distribution of the adhesive stresses near the plate end. The effects of the adhesive modulus and adhesive thickness were also investigated. The final stage consisted of several 3-D linear analyses of beams strengthened with spliced CFRP strips. A global/local analysis approach was adopted to accurately capture the effect of the plate end detail on the distribution of adhesive stresses for splices loaded in flexure. Based on the analysis and the experimental results, a proposed design guideline for spliced connections of the proposed strengthening system is presented.

5.1 STAGE I: 3-D NON-LINEAR ANALYSIS OF A DOUBLE-LAP SHEAR SPECIMEN

In the first stage of the analytical portion of the research a non-linear, 3-D finite element analysis was conducted to evaluate the initiation and propagation of cracking throughout the adhesive layer. Due to the sudden nature of the failure which was observed experimentally it was difficult to identify whether the debonding failure initiated at the center of the splice joint or near the plate end. The non-linear finite element analysis was conducted and strain values were correlated with the strains measured from the experimental program to determine the debonding failure mechanism.

5.1.1 Description of the 3-D, non-linear finite element model

To determine the sequence of the debonding failure a CFRP double-lap shear specimen, shown in Figure 5.1, was modeled. The configuration of the specimen was selected to be similar to the configuration of the three 400-S type double-lap shear specimens which were tested during the experimental program. The two main CFRP plates were separated by a 2 mm gap which was filled with adhesive as shown in Figure 5.1. This is similar to the configuration of the specimens that were tested in the experimental program. Symmetry boundary conditions were applied in the three principal directions and, therefore, only $1/8^{th}$ of the specimen was modeled. A uniform pressure load was applied at the free end of the main CFRP plate to simulate the presence of a uniform tension load, T.

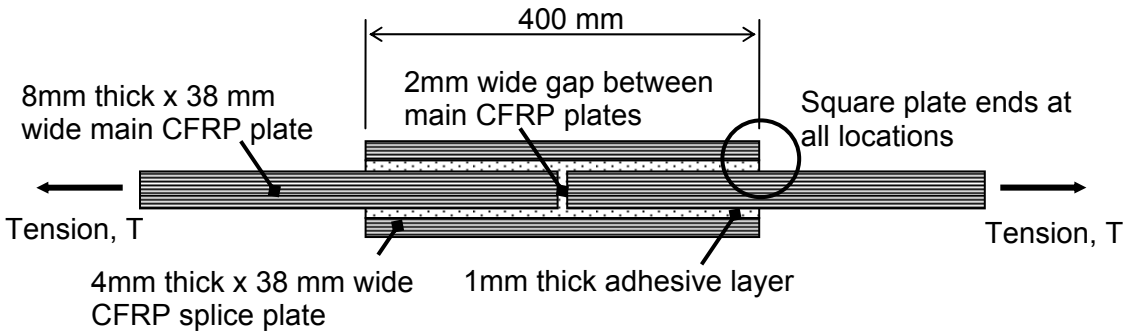

Figure 5.1 – Double-lap shear specimen configuration considered in the 3-D, non-linear FEA

The material properties used in the finite element analysis were based on the measured values from the experimental phase of the research. The CFRP plates were modeled as a linear-elastic, orthotropic material. The longitudinal and transverse elastic moduli were specified as 418,000 MPa and 10,200 MPa respectively. The shear modulus of the CFRP was specified as 3750 GPa. The Poisson's ratio of the CFRP was dependent on the loading direction and was taken to be within the range of 0.33 to 0.39 in all loading cases. The adhesive was modeled as a linear-elastic, isotropic material with modulus of elasticity and Poisson's ratio of 3000 MPa and 0.39 respectively. Since the constitutive relationship of the adhesive,

which was determined experimentally, was essentially linear, it was not necessary to consider the effect of the adhesive plasticity.

The CFRP material was modeled using the 8-node SOLID45 element with three translational degrees of freedom at each node and uniform reduced integration enabled. To simulate cracking, the adhesive was modeled using the SOLID65 8-node solid concrete element which is predefined in the ANSYS software package. The element has the capability to model the non-linear material characteristics related to cracking. The element can also simulate crushing behavior and the presence of internal reinforcing bars, however, these capabilities were disabled in the analysis. Cracking of the element occurs when the calculated principal stress at a given location exceeds the specified tension strength of the material. The location of the crack was simulated by reducing the shear stiffness of the material at the crack location. The shear stiffness was reduced by 95 percent and 90 percent for open and closed cracks respectively. Further, cracked elements cannot transmit tension stresses in the direction perpendicular to the crack. A maximum element size of 1 mm was implemented in all three principal directions. Thus, the adhesive layer was meshed by a single element through the thickness while the thickness of the CFRP splice plate was modeled using four elements. This mesh configuration was not intended to capture the detailed variation of stresses through the thickness of the adhesive layer. Rather, the objective of the 3-D, non-linear analysis was to gain a general understanding of crack initiation and propagation which led to the debonding failure mechanism of the double-lap splice specimens. Therefore, due to computational restrictions, the thickness of the adhesive layer was modeled by only a single element for the 3-D, non-linear analysis. The distribution of stresses at the adhesive-splice plate and adhesive-main plate interfaces was studied in detail using a 2-D, linear analysis with a highly refined mesh in the second stage of the analysis.

The tension strength of the bond interface between the CFRP and the adhesive was obtained from pull-off tests. A total of four pull-off tests were conducted. Typically a combined interfacial/interlaminar failure was observed near the surface of the CFRP material. The

average and maximum measured bond strengths were 18.4 MPa and 20.2 MPa respectively. The maximum measured pull-off strength was used as the specified tension strength of the bonded interface between the CFRP and the adhesive in the finite element model. The strength of the adhesive within the gap region between the ends of the two main CFRP plates was specified as 37.5 MPa which corresponds to the measured tensile strength of the adhesive.

5.1.2 Results of the 3-D, non-linear finite element analysis

Figure 5.2(a) compares the FEA and measured load-strain relationships at the center of the splice for joint configuration 400-S. The results indicate that the FE model accurately predicted the initial stiffness of the uncracked splice joint as can be seen in Figure 5.2(a). The finite element analysis predicted that the initial cracking of the adhesive would occur within the gap region between the main CFRP plates at a load level of 43 kN. This is identified in Figure 5.2(a) by the sudden increase of strain at the 43 kN load level. Inspection of the figure indicates that the measured strains from the tested specimens demonstrated a similar behavior. As the applied load was increased in the analysis, the FE model predicted additional cracking at the center of the joint at an applied load level of 64 kN. This additional cracking is shown in Figure 5.2(a) by the sudden increase of the strain at the 64 kN load level. This was accompanied by initial cracking of the adhesive near the end of the CFRP splice plate which extended approximately 30 mm from the plate end. As the applied load level was increased, the crack at the end of the splice plate continued to propagate as shown in Figure 5.2(b). The figure indicates that as the load level increased from the 64 kN to 82 kN the crack propagated from the end of the splice plate to a total length of 70 mm. This was followed by sudden total debonding of the splice plate at the 85 kN load level. Thus, the results of the non-linear analysis indicate that while initial cracking occurred at the center of the CFRP splice joint, failure of the splice was ultimately governed by debonding of the splice plate due to the crack formation and propagation near the end of the splice plate.

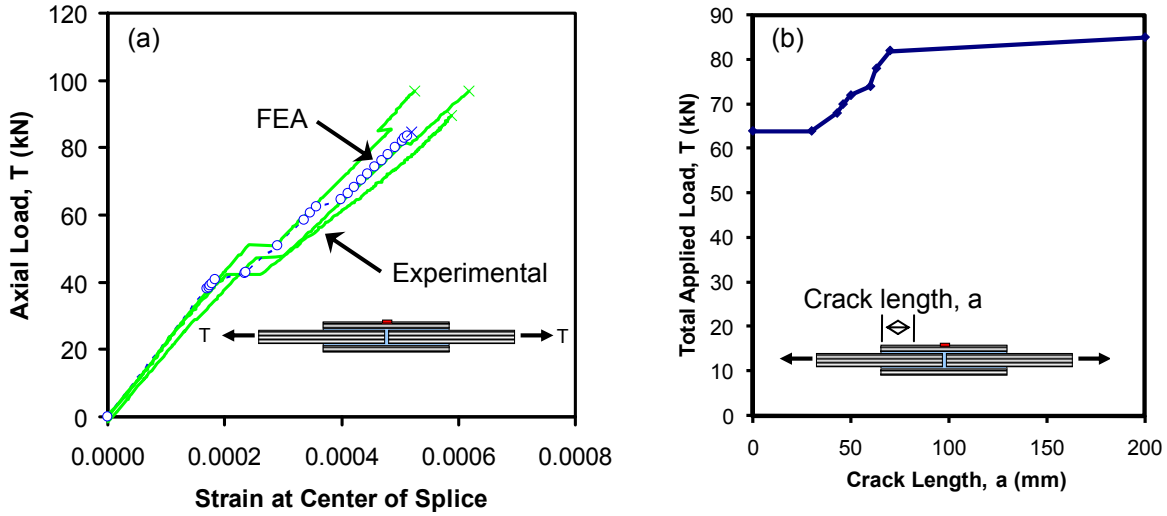

Figure 5.2 – Comparison of FEA results and measured experimental results for double-lap shear specimen 400-S

The analysis results indicated that the distribution of adhesive stresses was uniform across the width of the adhesive joint.

5.2 STAGE II: 2-D, LINEAR ANALYSIS OF DOUBLE-LAP SHEAR SPECIMENS

A linear, 2-D finite element analysis was conducted to evaluate the distribution of bond stresses near the ends of the splice plate for the tested double-lap shear specimens. The analysis was also used to determine the effect of implementing a reverse tapered plate end on the distribution of the bond stresses. The effect of the shear stiffness of the adhesive on the bond stresses was also investigated. The predicted stresses obtained from the finite element analysis were used to develop a quasi-empirical model to calculate the tension strength of high modulus CFRP double-lap shear specimens. The findings of the non-linear analysis which was conducted in the first phase of the analysis indicated that failure of the joint is governed by the crack initiation and propagation near the end of the CFRP splice plates. Therefore, the distribution of the stresses at this location was considered in detail for the 2-D analysis.

5.2.1 Description of the 2-D, linear finite element model

The basic configuration of the double-lap shear specimens considered in this phase of the analysis, shown in Figure 5.3, was similar to that considered in the previous phase. To evaluate the effect of the reverse tapered plate end, several analyses were conducted with different taper angles, θ, ranging from 20° to 90°. The 20° taper case represents the minimum practical taper angle for typical CFRP splice joints while the 90° case represents a square plate end as shown in the figure.

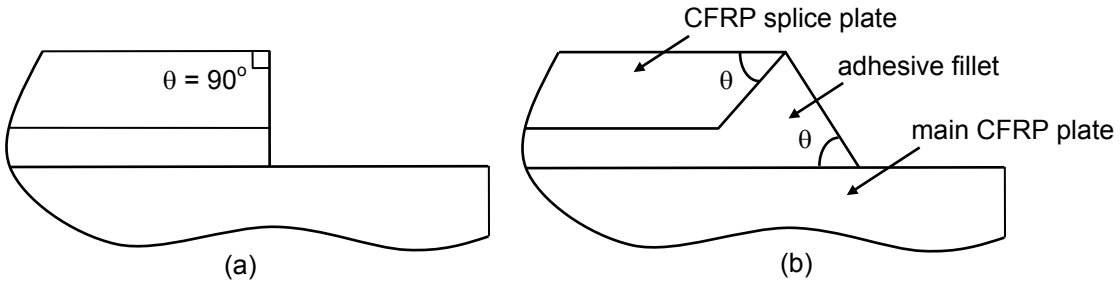

Figure 5.3 – Typical plate end configuration for (a) square and (b) tapered plate ends

To accurately capture the distribution of the bond stresses the mesh was refined locally near the end of the splice plate. A maximum element edge length of 0.2 mm was specified within a 40 mm long zone near the end of the splice plate. The adhesive layer was meshed by five elements through the thickness while the thickness of the CFRP splice plate was modeled using 20 elements. Thus, the model accurately captured the non-linear state of stress through the thickness of the adhesive. A coarse mesh, with a maximum element edge length of 1mm, was used away from the plate ends. A transition zone was also implemented to allow a smooth transition of the mesh from the fine mesh near the plate end to the coarse mesh elsewhere. The typical finite element mesh near the plate end is shown in Figure 5.4 (a) and (b) for 90° and 20° taper angles respectively.

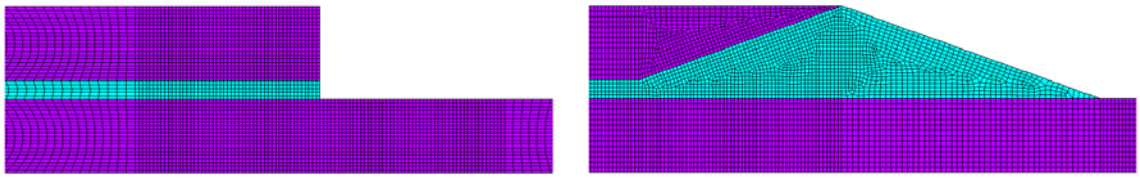

Figure 5.4 – Typical finite element mesh for (a) square and (b) 20° tapered plate ends

The specimens were modeled using the built-in 2-D, 8-node PLANE 82, plane-strain elements in the ANSYS software package. Quarter model symmetry was employed and a uniform pressure load was applied to the end of the main CFRP plate to simulate a tension load level of 38 kN. This load level is slightly lower than the initial cracking load of the specimen which was determined in the first phase of the analysis. The material properties for the CFRP and the adhesive were modeled in a similar manner as in the first phase of the analysis. Since a linear analysis was conducted at a given load level, less than the failure load of the specimen, the tension strength of the adhesive was not required in the analysis.

The effect of the shear stiffness of the adhesive was also considered in several of the analyses. The shear stiffness was varied by changing the thickness and elastic modulus of the adhesive layer. The thickness was varied in a range from 0.5 mm to 5.0 mm while the elastic modulus was varied in a range from 600 MPa to 6000 MPa. These represent the expected range of adhesive thicknesses and moduli which are typically used for structural applications.

5.2.2 Results of the 2-D, linear finite element analysis

The results of the finite element analysis were used to evaluate the distribution and magnitude of the bond stresses within the adhesive at several locations throughout the thickness of the adhesive layer. Since these stresses could not be accurately measured

experimentally, the finite element analysis represents a necessary tool to fully understand the behavior of the bonded joints. To confirm that the finite element model accurately represented the behavior of the bonded double-lap shear specimens, the predicted strains at the face of the CFRP splice plate were compared to the measured strains obtained for similar joint configurations in the experimental program. Figure 5.5(a) and (b) present the measured and predicted strains at the face of the CFRP splice plate for two of the tested configurations. Figure 5.5(a) shows the strain profile for the three tested specimens with the square plate ends, configuration 400-S, while Figure 5.5(b) shows the strain profiles for the two specimens with the 20^{o} tapered plate ends, 400-T2. In both figures the predicted strain is shown by the continuous curve while the markers indicate the measured strains at various locations along the splice plate. The figures demonstrate that the finite element model accurately predicted the strain behavior of the CFRP double-lap shear specimens. These results support the use of the proposed finite element model to evaluate the distribution of the bond stresses for the double lap shear specimens. It is interesting to note that the strain at the end of the tapered splice plate, shown in Figure 5.5(b), does not go to zero. This suggests that adhesive within the taper and fillet regions at the end of the splice plate are subjected to a longitudinal stress component.

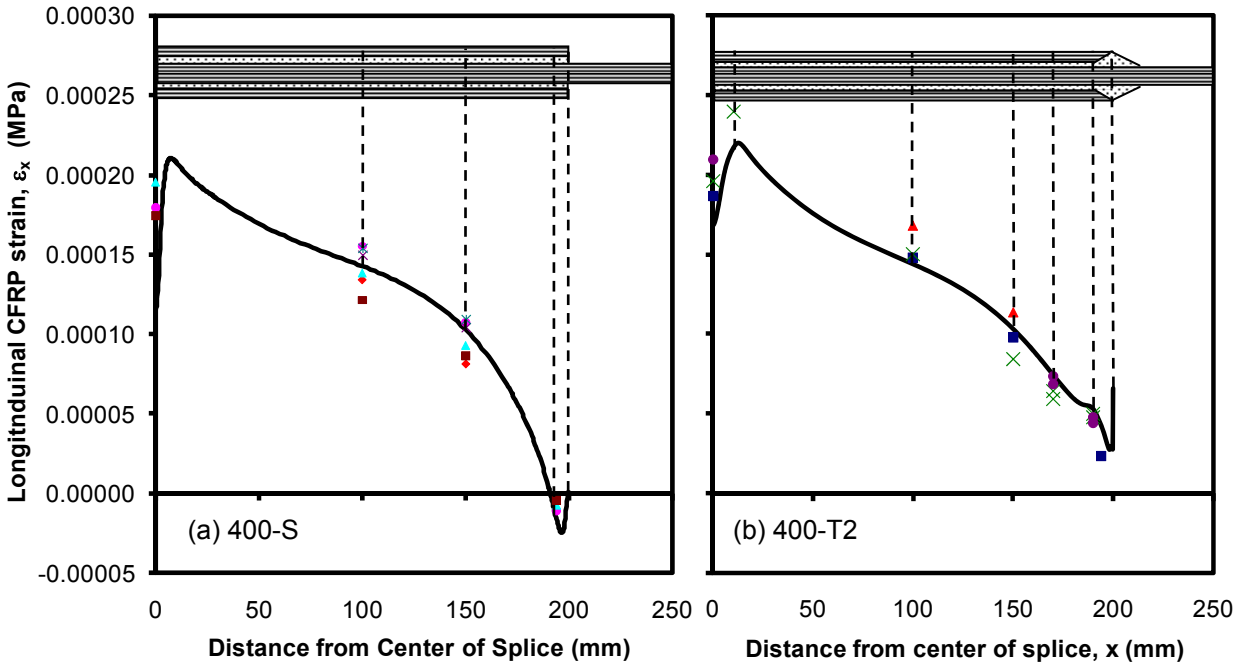

Figure 5.5 – Predicted and measured strains at the face of the CFRP splice plate for double-lap shear specimens with (a) square plate ends and (b) 20^o tapered plate ends

The finite element analysis results were used to evaluate the magnitude of the bond stresses near the ends of the CFRP splice plates for several different joint configurations. Inspection of the tested double-lap shear specimens after failure indicated that the failure surface typically propagated along the adhesive-main plate interface or along the adhesive-splice plate interface. Therefore, the stresses were considered along both interfaces to evaluate the effect of the reverse taper and to develop a suitable analytical model to predict the strength of the bonded joints. The effects of the taper angle on the distribution of the shear, normal (peeling), longitudinal (axial) and principal stress components at each interface are discussed in the following sections.

5.2.2.1 Shear Stress Distribution

The predicted shear stress distributions in the adhesive layer, at the splice plate and main plate interfaces, are shown in Figure 5.6 for different taper angles. Inspection of the figure indicates several interesting trends. Figure 5.6 indicates that the peak shear stress along the adhesive-splice plate interface occurs at the interior corner of the splice plate at the beginning of the taper. This location is marked by a dashed line in the figure, approximately 11 mm away from the end of the splice plate, for the 20^o taper case. Due to the geometric and material discontinuity at this location, a stress concentration forms as shown by the sharp peak in the stress distribution. As the taper angle increases and the taper becomes steeper, the location of the peak stress shifts towards the end of the splice plate as shown in the figure. However, the magnitude of the peak shear stress remains essentially constant regardless of the taper angle. A similar trend is observed at the adhesive-main plate interface. The peak shear stress occurs near the location of the corner of the splice plate and the magnitude of this peak stress remains essentially constant regardless of the taper angle. However, at the adhesive-main plate interface, for taper angels greater than 40^o, the finite element model also predicted the formation of a stress singularity at the end of the adhesive fillet. This singularity likely formed due to the sharp geometry at the end of the adhesive fillet.

Inspection of the figure indicates that the stresses at the adhesive-splice plate interface are generally higher than the stresses at the adhesive main plate interface. A similar trend was observed for all of the stress components considered.

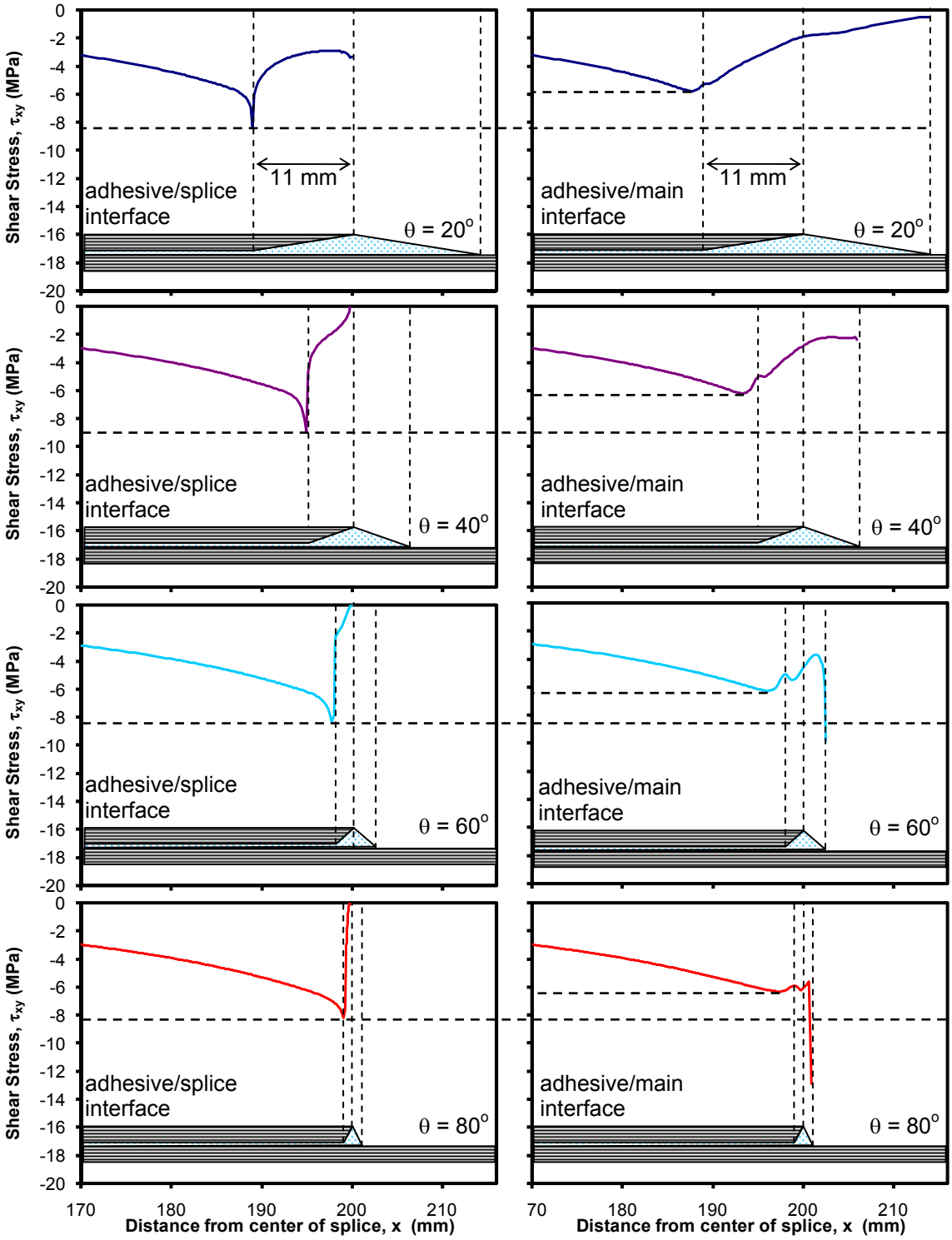

Figure 5.6 – Distribution of shear stresses at for different taper angles

5.2.2.2 Normal Stress Distribution

The predicted normal stress distributions in the adhesive layer, at the adhesive-splice plate interface and the adhesive-main plate interface, are presented in Figure 5.7 for different taper angles. Inspection of the figure indicates that, unlike for the shear distribution, the taper angle has a significant effect on the magnitude of the peak normal stress in the adhesive layer at both interfaces. Along both interfaces, for the case of a 20^o taper angle, the normal stresses are nearly zero. As the taper angle increases, and the geometry of the plate end becomes steeper, a sharp normal stress concentration formers near the interior corner of the splice plate. This demonstrates that the presence of the reverse taper helps to reduce the normal stress concentration near the plate end. The reduction of the normal stresses is likely due to the localized reduction of the flexural stiffness of the splice plate near the plate end. The localized reduction of the thickness of the splice plate increases the compliance of the tip of the plate. Therefore, the plate end can more easily conform to the curvature of the main plate which is induced by the eccentricity of the tension forces in the double-lap shear specimen. Additionally, locally increasing the thickness of the adhesive in the vicinity of the plate end helps to reduce the stiffness of the adhesive layer and further reduce the stress-concentration effect.

For taper angles greater than 40^o, a stress singularity begins to form at the main-plate interface near the end of the adhesive fillet as previously noted for the shear stress distribution.

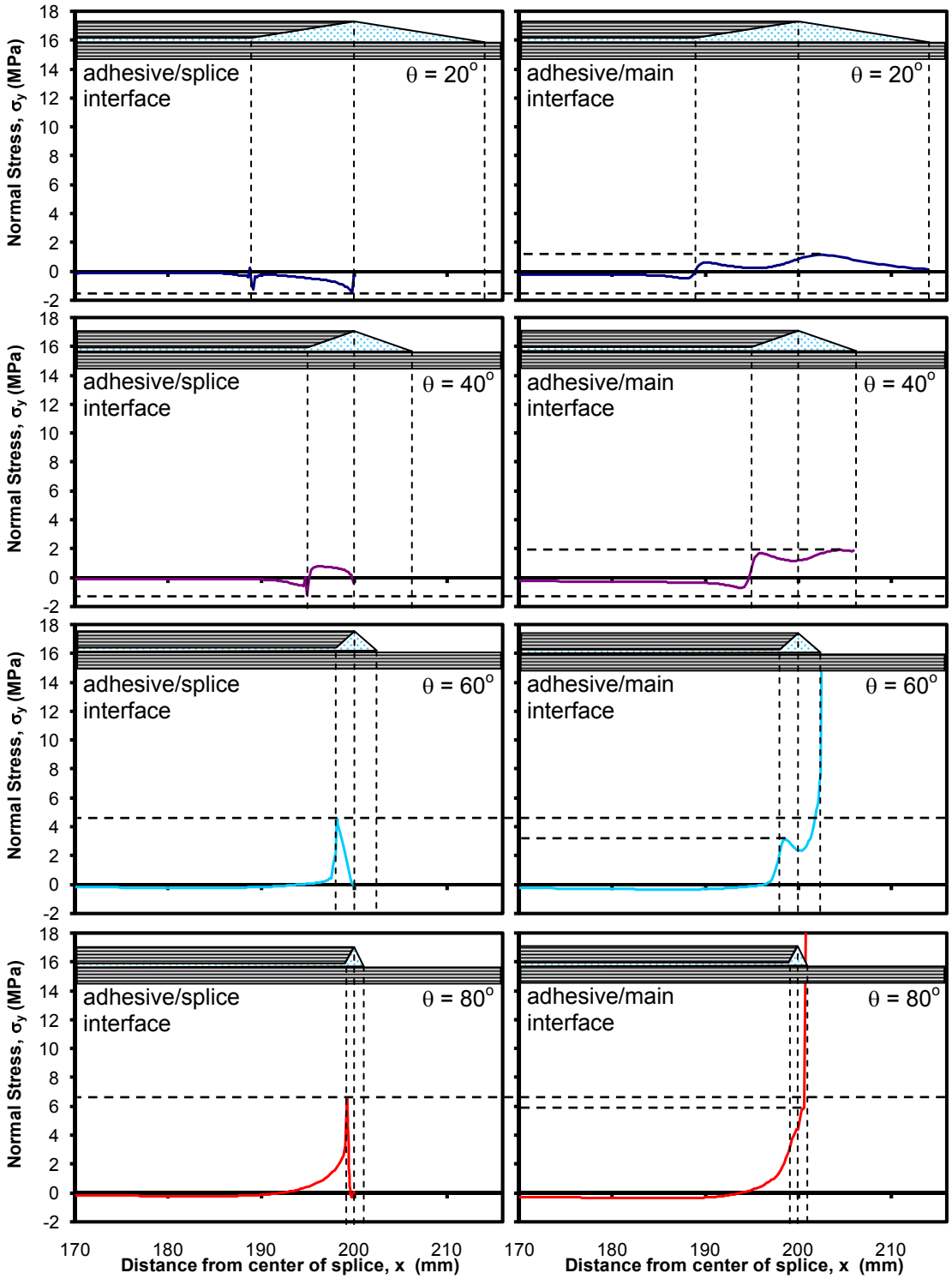

Figure 5.7 – Distribution of normal (peeling) for different taper angles

5.2.2.3 Longitudinal Stress Distribution

The predicted longitudinal stress distributions in the adhesive layer, at the adhesive-splice plate interface and the adhesive-main plate interface, are presented in Figure 5.8 for different taper angles. Conventionally the analysis of bonded joints has focused mainly on the effect of shear and normal stresses while neglecting the effect of the longitudinal stresses in the adhesive. However, comparison of Figure 5.7 and Figure 5.8 indicate that the longitudinal stresses in the adhesive layer near the end of the splice plate have a similar magnitude to the normal stresses and, therefore, should be considered. The longitudinal stress component is due to transfer of stresses from the adhesive to the end of the splice plate by direct axial tension. Inspection of Figure 5.8(a) indicates that the peak longitudinal stress along the splice plate interface typically occurs at the interior corner of the splice. Beyond this point, along the untapered portion of the splice plate, the longitudinal stress in the adhesive drops suddenly to zero. This is because the longitudinal stress cannot be transmitted to the CFRP along the untapered portion of the splice plate. The figure further indicates that increasing the taper angle from 20^o to 80^o also increases the magnitude of the peak longitudinal stress. Inspection of Figure 5.8(a) also indicates that as the taper angle decreases, the distribution of longitudinal stresses along the taper region becomes more uniform. This is due to the relatively long taper region over which the stresses are developed. Conversely, for large taper angles the longitudinal stress distributions exhibit a sharp stress concentration within the relatively short taper region. The distribution of longitudinal stresses at the adhesive-main plate interface is similar to the distribution of normal stresses at the same interface. For smaller taper angles the longitudinal stresses are minimal. The peak longitudinal stress increases as the taper angle increases and a longitudinal stress singularity begins to form near the end of the adhesive fillet for taper angles greater than about 40^o.

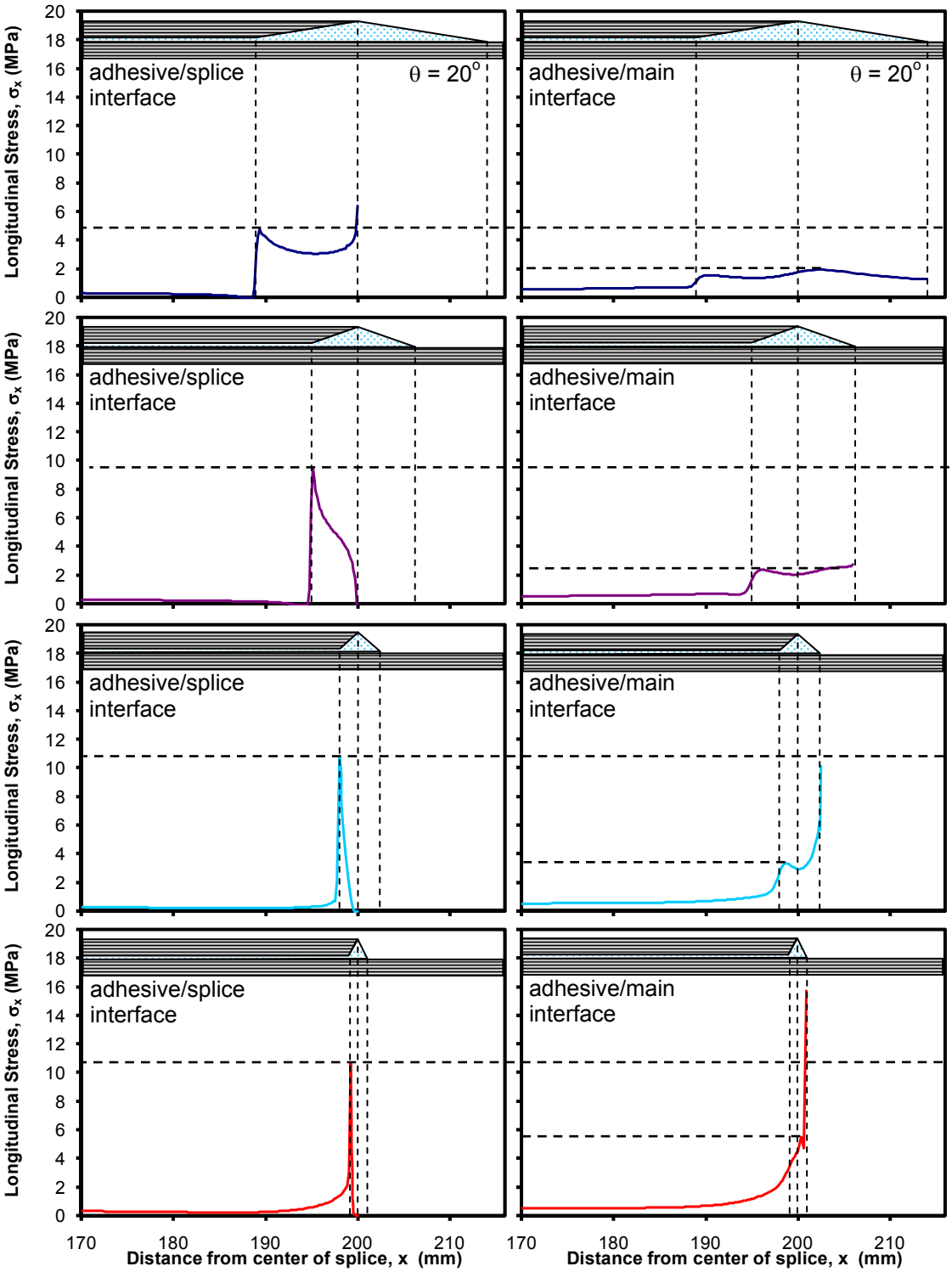

Figure 5.8 – Distribution of longitudinal (axial) stresses for different taper angles

5.2.2.4 Principal Stress Distribution

The predicted principal stress distributions in the adhesive layer, at the adhesive-splice plate interface and the adhesive-main plate interface, are presented in Figure 5.9 for different taper angles. The peak principal stress typically occurs at the splice plate interface at the interior corner of the splice plate. Increasing the taper angle, from 20^o to 80^o, results in a gradual increase of the magnitude of the peak stress. At the main plate interface the trend is similar with a peak stress occurring near the location of the corner of the taper and a stress singularity beginning to form at the end of the adhesive fillet for taper angles greater than 40^o. Consideration of the individual stress components indicates that for smaller taper angles the principal stress distribution at the splice plate interface is dominated by the shear and longitudinal stress components while for larger taper angles all three stress components contribute to the principal stress. At the main plate interface, for smaller taper angles the principal stress distribution is dominated by the shear component while the other two components contribute minimally. For larger taper angles, however, the normal and longitudinal stresses contribute more significantly to the principal stress at the main plate interface. This trend explains the sharp increase of the peak principal stress with increasing taper angle shown in Figure 5.9.

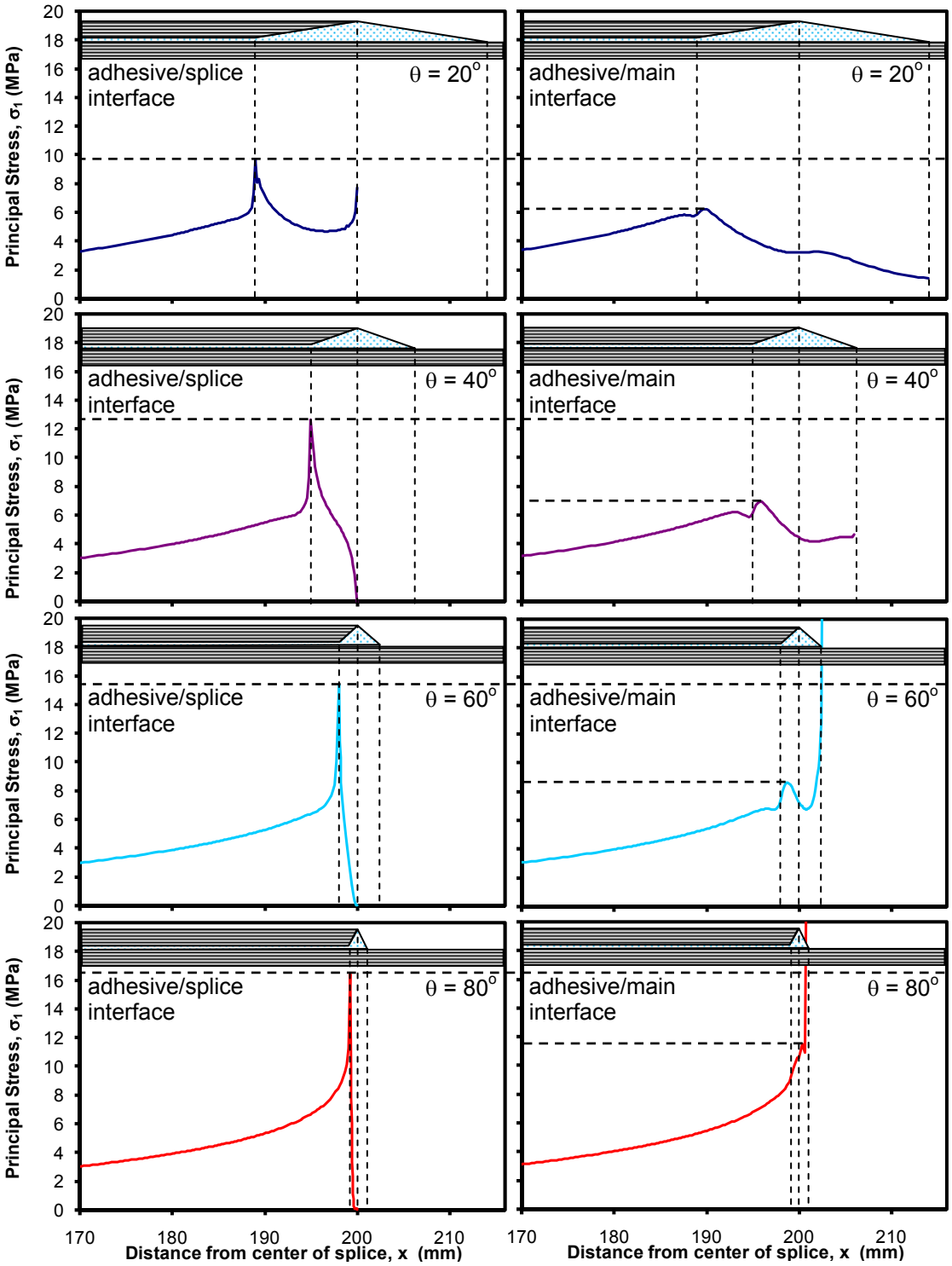

Figure 5.9 – Distribution of principal stresses for different taper angles

5.2.2.5 Effect of Adhesive Shear Stiffness

The effect of the shear stiffness of the adhesive was also considered in the analysis. The shear stiffness of the adhesive is proportional to the elastic modulus and inversely proportional to the thickness of the adhesive. Both parameters were varied to evaluate the effect of the adhesive stiffness on the distribution of stresses and the failure load of the double-lap shear specimens.

Four different shear moduli, 216 MPa, 360 MPa, 1080 MPa and 2160 MPa were considered in the analysis. Considering the Poisson's ratio of the adhesive, 0.39, the corresponding elastic moduli are 600 MPa, 1000 MPa, 3000 MPa and 6000 MPa. These represent the typical range of adhesive moduli which can be expected in most typical applications. The distribution of the principal stresses at the adhesive-splice plate interface near the end of the splice plate is shown for different adhesive moduli in Figure 5.10(a). The thickness of the adhesive and the taper angle were specified as 1.0 mm and 20^o respectively. The figure indicates that reducing the elastic modulus of the adhesive also reduces the magnitude of the principal stresses. Similarly, reducing the elastic modulus also reduces the magnitude of the individual stress components. The figure also indicates that increasing the elastic modulus has a significant effect on the magnitude of the stress singularity near the end of the adhesive fillet. A similar analysis was conducted for a double-lap shear specimen with a taper angle of 80^o at the plate end. The observed trends were similar to the 20^o taper angle case.

To evaluate the effect of the adhesive thickness on the stress distribution, four different adhesive thicknesses were considered: 0.5 mm, 1.0 mm, 3.0 mm and 5.0 mm. These represent the typical range of adhesive thicknesses that may be expected in practical applications. The distribution of principal stresses at the splice plate interface is shown in Figure 5.10(b) for different adhesive thicknesses and a taper angle of 20^o. The figure indicates that increasing the thickness of the adhesive layer decreases the magnitude of the

principal stresses at the splice plate interface. The trend is similar for the case of an 80° taper angle.

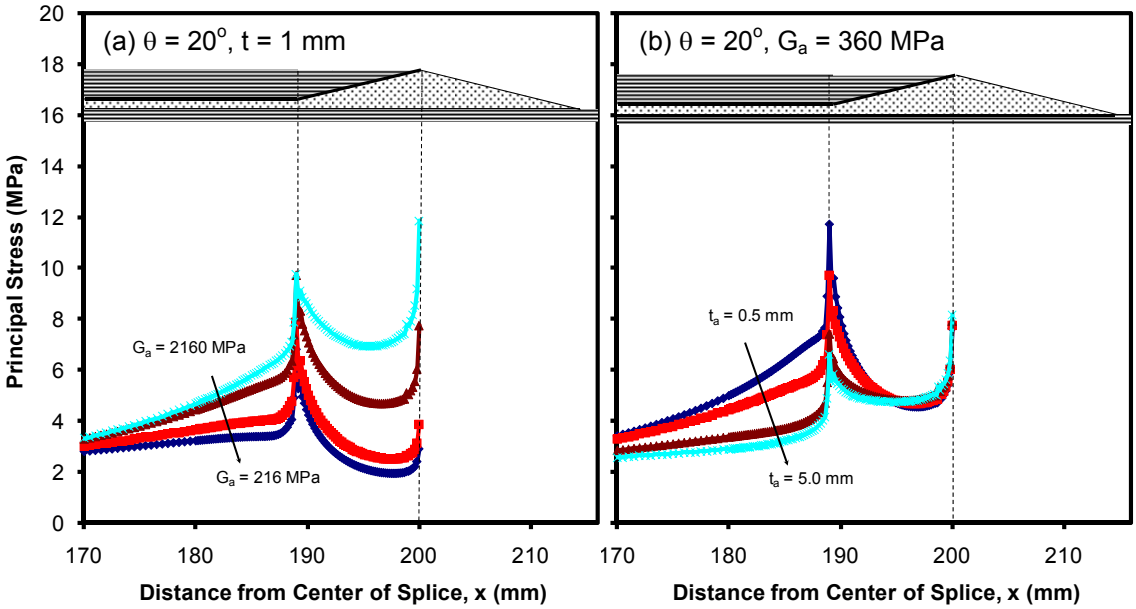

Figure 5.10 – Distribution of principal stresses for different (a) adhesive moduli and (b) adhesive thicknesses

As noted, the shear stiffness of the adhesive is proportional to the adhesive modulus and inversely proportional to the adhesive thickness. Therefore, it can be generally stated that increasing the adhesive shear stiffness also increases the magnitude of the principal stresses near the end of the splice plate.

5.2.2.6 Effect of Splice Length

The stress profiles presented in the previous sections indicate the presence of a significant stress concentration effect near the end of the CFRP splice plate. Inspection of the figures indicates that varying the different parameters, including the taper angle and the adhesive properties has a significant effect on the distribution of stresses, and the magnitude of the

maximum principal stress, in a localized zone near the end of the splice plate. However, a small distance away from the end of the splice plate, the stresses are unaffected by these parameters. In the case of a linear-elastic, brittle adhesive, such as the one used for the current research program, the failure of the bonded joint is governed by the magnitude of the maximum principal stress near the plate end. This behavior suggests that bonded joints are typically characterized by a critical length, ℓ_c. For splices that are shorter than this critical length the magnitude of the peak principal stress near the end of the splice plate can be affected by the presence of the stress concentration near the center of the splice joint. Therefore, increasing the splice length, up to the critical length, results in a corresponding increase of the tension strength. However, increasing the splice length beyond the critical length does not result in a significant increase of the strength of the splice. Different parameters can affect the magnitude of critical length including the modulus of the bonded plates (Fawzia, 2007) and the thickness of the plates.

To establish the critical length for the current CFRP system, a series of finite element analyses were conducted. Splice plate lengths ranging from 100 mm to 1200 mm were considered in the analyses. The analyses were conducted for taper angles of 20^o and 80^o. Figure 5.11(a) – (d) show the distribution of the adhesive principal stresses at the adhesive-splice plate interface for splice lengths of 100 mm, 200 mm, 400 mm and 1200 mm respectively. The ends of the main CFRP plate and the splice plate had taper angles of 20^o in all cases. Inspection of Figure 5.11(a) – (c) indicates that for splices less than 400 mm long increasing the splice length helps to decrease the magnitude of the peak principal stress near the end of the splice plate. This indicates an interaction between the stress concentrations near the center of the splice and near the end of the splice plate. However, comparison of Figure 5.11(c) and (d) indicates that increasing the splice length beyond 400 mm does not increase the magnitude of the peak principal stress near the plate end. Increasing the splice length beyond 400 mm only increases the length of the adhesive that is subjected to a

relatively low stress level. This suggests that, for the current strengthening system, the critical length, ℓ_c, is approximately 400 mm.

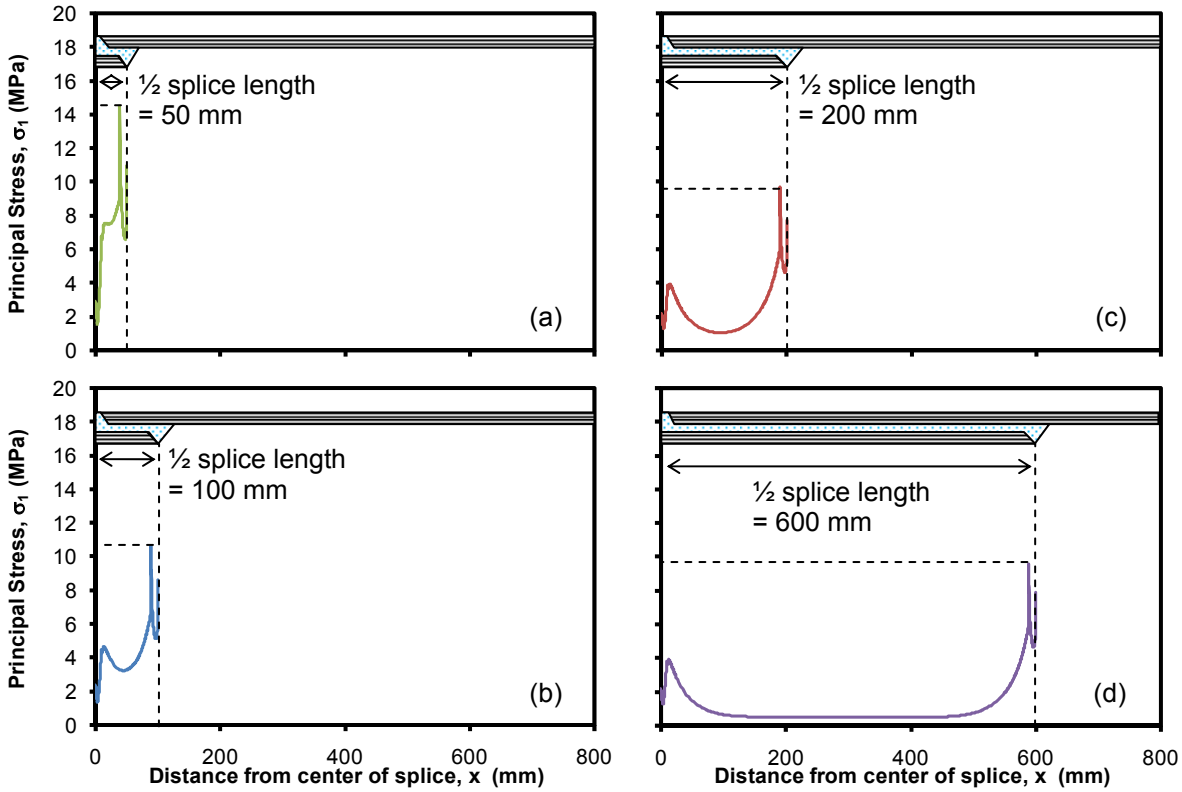

Figure 5.11 – Distribution of principal stresses for (a) 100 mm, (b) 200 mm, (c) 400 mm and (d) 1200 mm long splices with 20° reverse tapered plate ends.

Another set of analyses was conducted on splices with an 80° taper at the end of the splice plate. The same splice lengths were considered. Figure 5.12 shows the effect of the splice length on the maximum peak stress determined from the finite element analysis for splices with taper angles of 20° and 80°. Inspection of the figure indicates that increasing the splice length beyond 400 mm does not increase the magnitude of the maximum principal stress near the plate end, regardless of the taper angle. This suggests that, for the proposed strengthening system, the critical length of the splices is 400 mm. It is not recommended to

use splice lengths less than the critical length. For other CFRP systems, a similar approach can be used to evaluate the critical splice length, ℓ_c.

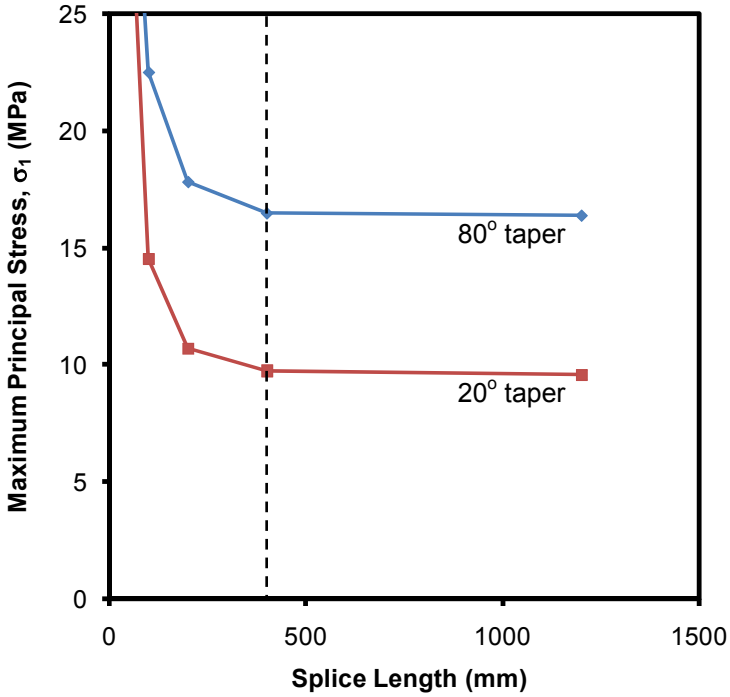

Figure 5.12 – Effect of splice length of maximum adhesive principal stress

5.2.2.7 Proposed Design Method

The typical geometry of a double-lap shear specimen is shown in Figure 5.13. For design purposes, it is convenient to express the strength of a double-lap shear specimen in terms of its basic tension strength, T_o:

$$T_o = f_a A_a \qquad \text{(Eq. 5.1)}$$

where:

f_a = adhesive tension strength

A_a = bonded surface area along which the tension force is transmitted

= $b_a \ell_a$

b_a = width of the adhesive joint

ℓ_a = overall bond length of the splice joint

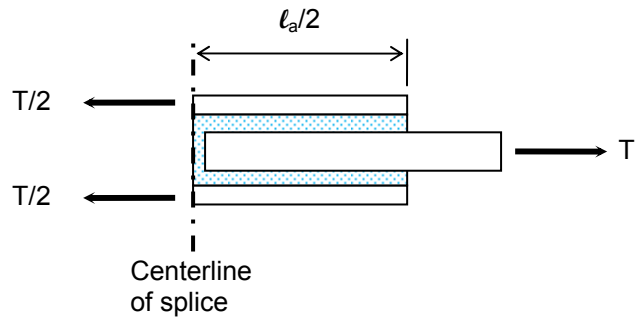

Figure 5.13 – Geometry of a typical double-lap shear specimen

This simple expression assumes that the adhesive is subjected to a uniform pure shear stress along the entire bonded length of the splice. Under these loading conditions, and assuming a brittle, linear-elastic adhesive such as the one used for the proposed strengthening system, the adhesive would fail when the maximum principal stress reached the pure tension strength of the adhesive. In a state of pure shear, the principal stress is equal to the applied shear stress. However, due to the effect of the stress concentrations near the end of the splice plate and due to the combined effect of shear, normal and longitudinal stresses, the basic strength of the joint cannot be achieved for typical double-lap shear specimens. Further, the shear stiffness of the adhesive also affects the magnitude of the stress concentration in the adhesive. Therefore, the design strength of the joint, T_n, can be calculated as:

$$T_n = \frac{T_o}{\psi_\theta \psi_a} \qquad \text{(Eq. 5.2)}$$

where:

ψ_θ = stress concentration factor to account for the effect of the taper angle

ψ_a = stress concentration factor to account for the effect of the adhesive properties

Based on the results of the finite element analysis two stress concentration factors were developed. The first, ψ_θ, accounts for the effect of the taper angle on the distribution of stresses near the plate end. To establish this factor, the results of several analyses with different taper angles ranging from 20^o to 80^o were considered. The adhesive thickness and shear modulus were kept constant at 1 mm and 1080 MPa respectively. The length of the splices considered in the analysis was 400 mm which is equal to the critical length of the proposed strengthening system. For each joint configuration, the stress concentration factor, ψ_θ, was defined as the ratio of the critical principal stress in the adhesive obtained from the finite element analysis, $\sigma_{1,crit}$, to the average adhesive shear stress due to the effect of the applied load, $\bar{\tau}$:

$$\psi_\theta = \frac{\sigma_{1,crit}}{\bar{\tau}} \qquad \text{(Eq. 5.3)}$$

where:

$\sigma_{1,crit}$ = critical principal stress obtained from finite element analysis with adhesive thickness and shear modulus of 1 mm and 1080 MPa respectively

$\bar{\tau}$ = calculated average shear stress due to applied load, T/A_a

T = applied tension force acting on the double-lap shear specimen

A_a = bonded surface area along which the tension force is transmitted

$= b_a \ell_a$

b_a = width of the adhesive joint

ℓ_a = overall bond length of the splice joint

The relationship between the taper angle, θ, and the stress concentration factor, ψ_θ, obtained from the finite element analysis is given in Figure 5.14. The peak stresses along both the splice plate interface and the main plate interface were considered. Along the adhesive-splice plate interface the peak stress was taken at the interior corner of the taper. It should be noted that, for the case of a square, 90^o plate end, the splice plate does not have an interior corner. Consequently, the peak stress for the 90^o case was lower than the peak stress for the 80^o taper angle. Thus the trend of the stress concentration factor curve was extrapolated from 80^o to 90^o as shown by the dashed portion of the curve in the figure.

At the main plate interface the peak stress was taken near the location of the peak stress in the adhesive which was near the interior corner of the splice plate. The effect of the stress singularity near the end of the fillet was neglected in the analysis. Due to the limitations of the fabrication process and the viscosity of the adhesive, the precise, sharp geometry which was modeled in the finite element analysis cannot be practically achieved. The fabrication process typically results in some amount of adhesive spewing from the end of the joint. This, combined with imperfections in the machining of the CFRP strip, makes the sharp geometry impractical to achieve. Therefore, the presence of a singularity near the end of the adhesive joint is unlikely. The absence of this singularity is confirmed by the relative consistency of the measured tension strength of the tested double-lap shear specimens with the square plate ends. The coefficient of variation of the measured failure load of the three tested specimens with square plate ends was less than 5 percent. If a stress singularity existed near the end of the adhesive joint, a considerably larger variation of the results would be expected.

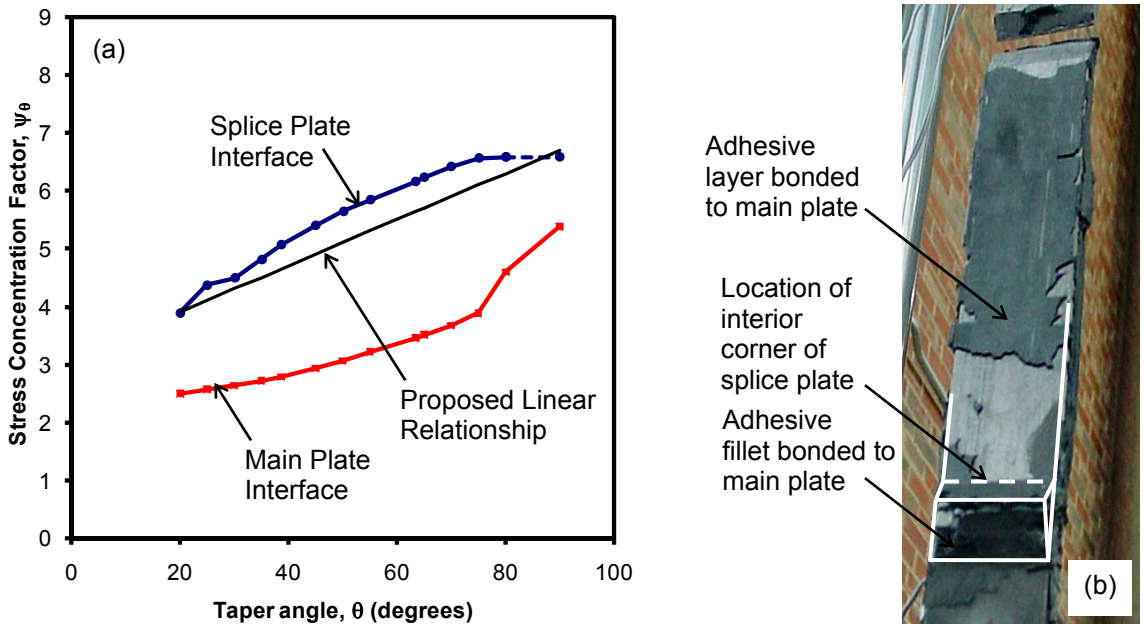

Figure 5.14 – (a) Effect of taper angle on the predicted stress concentration factor, ψ_θ (b) Failure at adhesive-splice plate interface

Inspection of Figure 5.14(a) indicates that the stress concentration factor at the splice plate interface is higher than at the main plate interface for all values of the taper angle, θ. This suggests that failure of the bonded joint likely initiates at the interior corner of the splice plate and propagates along the splice plate interface. The predicted failure mode is consistent with the typical failure mode that was observed for the tested 400-T2 specimens with a reverse-tapered plate end as shown in Figure 5.14(b). Figure 5.14(a) further demonstrates that reducing the taper angle of the plate end from 90° to 20° reduces the magnitude of the stress concentration factor at the splice plate interface by a factor of 1.7. The average measured failure load of the tested double-lap shear specimens with a 20° reverse taper at the end of the splice plate (configurations 400-T1 and 400-T2) was approximately 2 times greater than the average measured tension strength of the tested specimens with the square plate ends (configuration 400-S). The measured increase of the tension strength is consistent with the predicted reduction of the stress concentration factor.

To simplify the use of the stress concentration factor for design, a linear relationship between the stress concentration factor, ψ_θ, and the taper angle, θ, is proposed, as following and shown in Figure 5.14:

$$\psi_\theta = 0.04(\theta) + 3.1 \qquad \text{(Eq. 5.4)}$$

The proposed relationship represents a lower bound of the stress concentration factor obtained from the finite element analysis. The proposed equation accurately predicts the stress concentration to within 10 percent for all values of θ. Due to the absence of experimental data for joints with taper angles between 20^o and 90^o, and considering the inherent variability of the strength of bonded joints, the proposed linear relationship is considered to be acceptable for design purposes.

Based on the analysis results, a second factor, ψ_a, was established to account for the effect of the adhesive shear stiffness on the bond stress distribution. As discussed in the previous section, increasing the adhesive shear stiffness increased the magnitude of the stress concentration at the critical locations along the adhesive-splice plate and adhesive-main plate interfaces. As such, the second stress concentration factor was defined as:

$$\psi_a = \frac{\sigma_{1,crit} / \overline{\tau}}{\psi_\theta} \qquad \text{(Eq. 5.5)}$$

The calculated adhesive shear stiffness stress concentration factor, ψ_a, is shown in Figure 5.15. Several different analyses were considered to establish the trend of the stress concentration factor. Two different taper angles, 20^o and 80^o were considered. Four different adhesive thicknesses and four different adhesive moduli were considered as described previously. Figure 5.15 shows the effect of the adhesive shear stiffness on the stress concentration factor, at both the main plate and splice plate interfaces, for all of the splice configurations considered. In general the figure indicates a trend to increase the stress

concentration factor with an increase of the adhesive shear stiffness, regardless of the joint configuration. The figure also shows a proposed linear relationship to predict the stress concentration factor, ψ_a, based on the adhesive shear stiffness:

$$\psi_a = 0.0003(G_a/t_a) + 0.69 \qquad \text{(Eq. 5.6)}$$

where:

G_a = the adhesive shear modulus

t_a = the adhesive thickness

The proposed linear relationship represents an upper bound of the calculated stress concentration factor obtained from the finite element results.

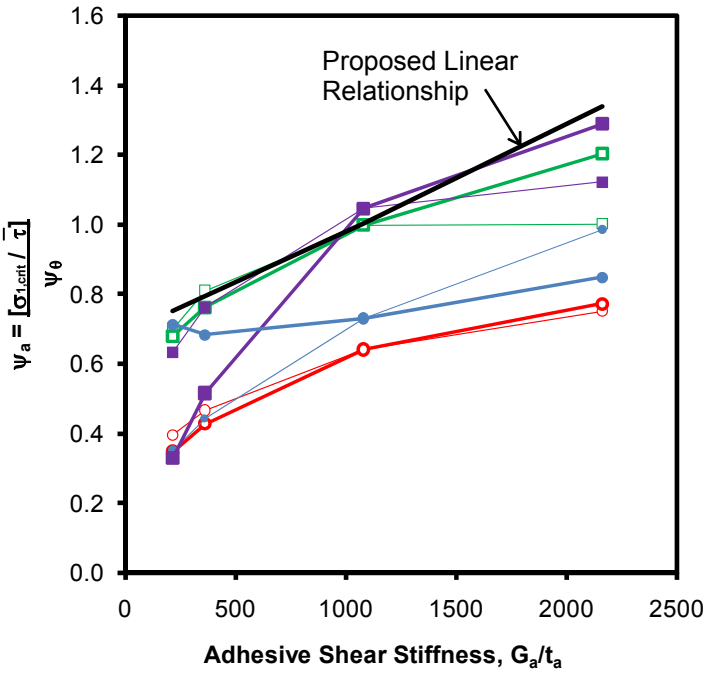

Figure 5.15 – Effect of adhesive stiffness on the predicted stress concentration factor, ψ_a

To maximize the capacity of a splice joint, for design purposes it is recommended that the splice length provided should exceed the critical length of the proposed strengthening system as defined in section 5.2.2.6. Since increasing the length of a splice beyond the critical length does not increase the tension strength of the joint, the calculation of the tension strength should be based on the critical length, ℓ_c, rather than on the overall splice length, ℓ_a. Therefore, based on the findings of the finite element analysis, the tension strength of a high-modulus CFRP splice can be calculated as:

$$T_n = \frac{f_a \ell_c b_a}{\psi_\theta \psi_a} \qquad \text{(Eq. 5.7)}$$

where:

f_a = adhesive tension strength

b_a = width of the adhesive joint

ℓ_c = critical length of the splice, 400 mm for the proposed CFRP system

ψ_θ = $0.04(\theta) + 3.1$

θ = taper angle near the end of the splice plate

ψ_a = $0.0003(G_a/t_a) + 0.69$

G_a = the adhesive shear modulus

t_a = the adhesive thickness

The proposed model was used to predict the tension strength of the tested double lap shear specimens with square, 400-S, and reverse tapered, 400-T1 & 400-T2, plate ends. Table 5.1

gives the measured and predicted strengths of the joints and the calculated stress concentration factors, ψ_θ and ψ_a.

Table 5.1 – Comparison of test results with proposed design equation

Specimen ID	Taper Angle	ψ_θ	G_a/t_a (N/mm^3)	ψ_a	Tension Strength (kN)		Measured/ Predicted
					Measured	Predicted	
400-S(1)	90^o	6.70	1080	1.01	89	85	1.05
400-S(2)					97		1.14
400-S(3)					97		1.14
400-T1	20^o	3.90			160	147	1.10
400-T2(1)					191		1.31
400-T2(2)					228		1.56

Inspection of the table indicates that in all cases the proposed model is conservative. The model typically over predicted the tension strength of the tested specimens with a 20^o taper near the plate end. This is largely due to the relatively large scatter of the experimental results and indicates the inherent variability of adhesive joints which necessitates a conservative approach to the design.

5.2.2.8 Stress Distribution in Main CFRP Plate

The distribution of the longitudinal strain at the surface of the main CFRP plate was also determined from the finite element analysis. Figure 5.16(a) and (b) show the distribution of the longitudinal tension strain at the surface of the main CFRP plate, near the end of the CFRP splice plate, for the square plate end and for a 20^o taper angle respectively, for an applied load level of 38 kN. The selected load level is slightly lower than the measured initial cracking load of the tested splices. In both cases the adhesive thickness was 1 mm and shear modulus was 1080 MPa. The measured strains obtained from the experimental program for similar specimens at the same load level are also shown in the figure.

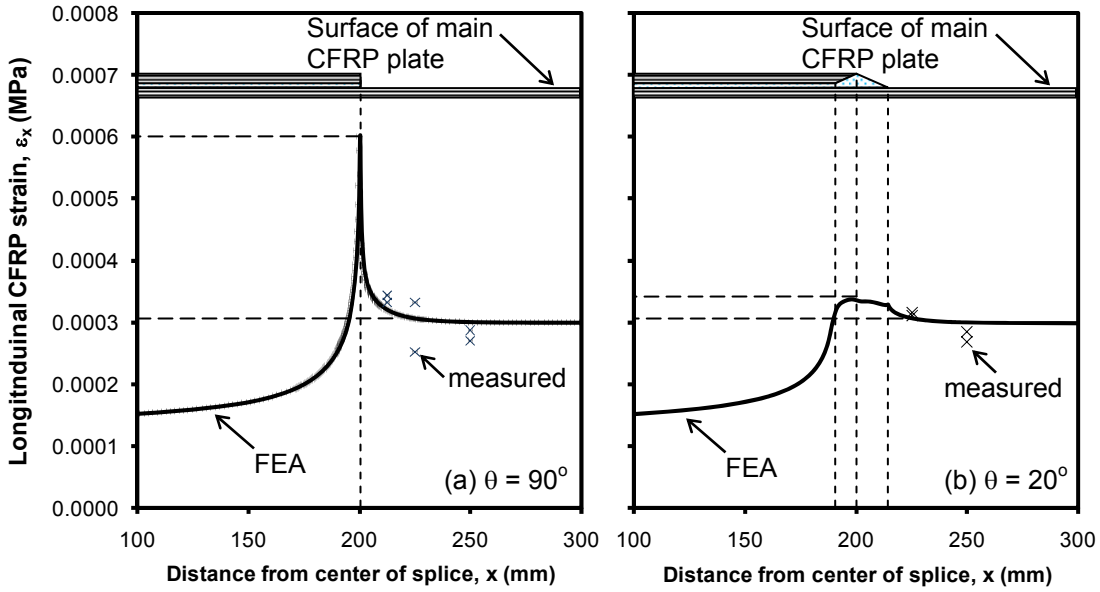

Figure 5.16 – Distribution of strain at the surface of the main CFRP plate for (a) a square plate end and (b) a 20° taper plate end

The analysis indicates a longitudinal strain and stress concentration in the main CFRP plate near the end of the CFRP splice plate as shown in Figure 5.16. The measured strains follow a similar trend to those obtained from the finite element analysis. For the square plate end configuration, the peak strain and stress that were determined from the finite element analysis were approximately twice the values away from the splice plate. However, since the sharp geometry that was specified in the analysis cannot be achieved practically, due to fabrication constraints, the actual stress concentration is likely much lower than that obtained from the analysis. For the 20° taper angle, the calculated peak stress was approximately 15 percent greater than the average calculated stress away from the splice plate which was similar to the measured strains. The results indicate the presence of a stress concentration in the main CFRP plate, which should be accounted for in the design. The magnitude of the stress concentration is significantly reduced by implementing a reverse tapered plate end configuration. However, the experimental results and the analysis indicate that, for typical splice joints, failure is governed by debonding of the splice plates at a much lower load than

the tensile rupture strength of the main CFRP plate. It should be also noted that for typical bridges and structures, splice are generally located away from locations of highest moment. Therefore, at the location of the splice joints, the tension force in the CFRP should be much less than the rupture strength of the main CFRP plate. Therefore, the presence of the stress concentration in the main CFRP plate will likely not induce premature rupture of the strengthening system, particularly for tapered splice plate configurations.

5.3 STAGE III: 3-D LINEAR ANALYSIS OF STEEL BEAMS STRENGTHENED WITH SPLICED CFRP STRIPS

The third stage of the analytical program consisted of a 3-D linear finite element analysis to investigate the behavior of bonded CFRP splice joints under flexural loading conditions. Several of the different splice configurations which were tested in the experimental program were also considered in the analysis. A global/local analysis approach was adopted. This approach made it possible to represent the global flexural behavior of the strengthened beams while also accurately representing the effect of the plate end geometry on the bond stresses. Based on the results of the analysis and the findings of the experimental program, guidelines are presented for the design of splice joints for steel flexural members strengthened using the proposed strengthening system.

5.3.1 Description of the 3-D, linear finite element model

To determine the distribution of bond stresses for CFRP splice joints used for flexural members, a 3-D, linear global/local finite element analysis was conducted. The global model, shown in Figure 5.17(a), represented the constant moment region of the typical CFRP-strengthened steel beams that were tested in the experimental program. Symmetry boundary conditions were considered to model only ¼ of the constant moment region. A constant moment was simulated by applying a linear gradient of pressures at the end of the model away from midspan which corresponds to the location of the applied load. The

applied pressure gradient simulated an applied moment of approximately 59 kN-m which corresponds to a total applied load of 80 kN. A maximum element edge length of 5 mm was considered in the analysis. While this level of mesh refinement was sufficient to represent the global flexural behavior of the steel beams, further refinement was required to accurately represent the geometry near the end of the splice plate.

To accurately represent the geometry and to determine the local stresses due to the stress concentration effect near the end of the CFRP splice plate a second local model was developed as shown in Figure 5.17(b). Due to the smaller size of the local model a higher level of mesh refinement was possible while maintaining a reasonable computation time. Therefore, in the region of the plate end, a maximum element edge length of 0.25 mm was specified in the through thickness direction. Thus, the thickness of the adhesive layer was modeled by 4 elements. For the rest of the local model the maximum element edge length ranged between 1 mm and 5 mm. Smaller element sizes were specified for the adhesive and CFRP materials closer to the end of the splice plate while larger element sizes were used away from the plate end and for the steel materials. The displacement boundary conditions for the local model were imported directly from the global model using a built-in algorithm in the ANSYS software. The local model was used to model the different geometries of the plate ends. The square plate end and taper angles of 20^o, 40^o, 60^o and 80^o were considered.

Both models were meshed using 20 node brick elements. Hexahedral elements were used for the global model while both hexahedral and tetrahedral elements were used for the local model to capture the geometry of the tapered plate ends. The material properties of the CFRP and adhesive were the same as those previously used for the double-lap shear models. The steel was modeled as a linear, isotropic material with elastic modulus and Poisson's ratio of 205,000 MPa and 0.3 respectively.

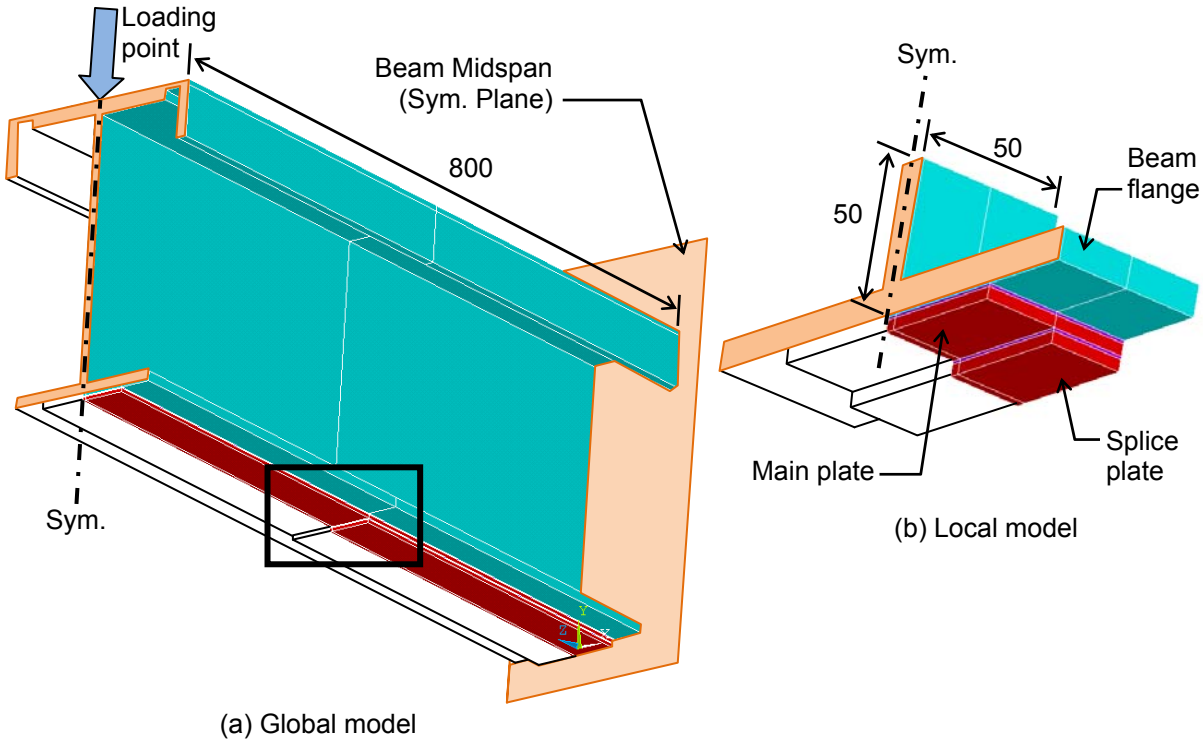

Figure 5.17 – Global and local finite element models for steel beams with CFRP splice plate

5.3.2 Validation of the 3-D, linear finite element model

The 3-D, linear finite element analysis was conducted to evaluate the distribution of the bond stresses for steel beams strengthened with spliced CFRP plates. To validate the model the calculated strains at the surface of the CFRP splice plates were compared to the measured values obtained from the experimental program as shown in Figure 5.18. Figure 5.18 (a) and (b) present the calculated and measured strains for 800 mm long and 400 mm long splice plates respectively. The different marker types indicate measured strains from different tests. The calculated strains were obtained from the global model, which did not include the details of the splice plate end geometry. Therefore, the measured strains from all of the tested splice configurations, regardless of the plate end geometry, were used to validate the results. The figure indicates generally good agreement between the finite element results and the

measured strains. These results support the use of the proposed finite element model to evaluate the distribution of the bond stresses for the steel beam tests.

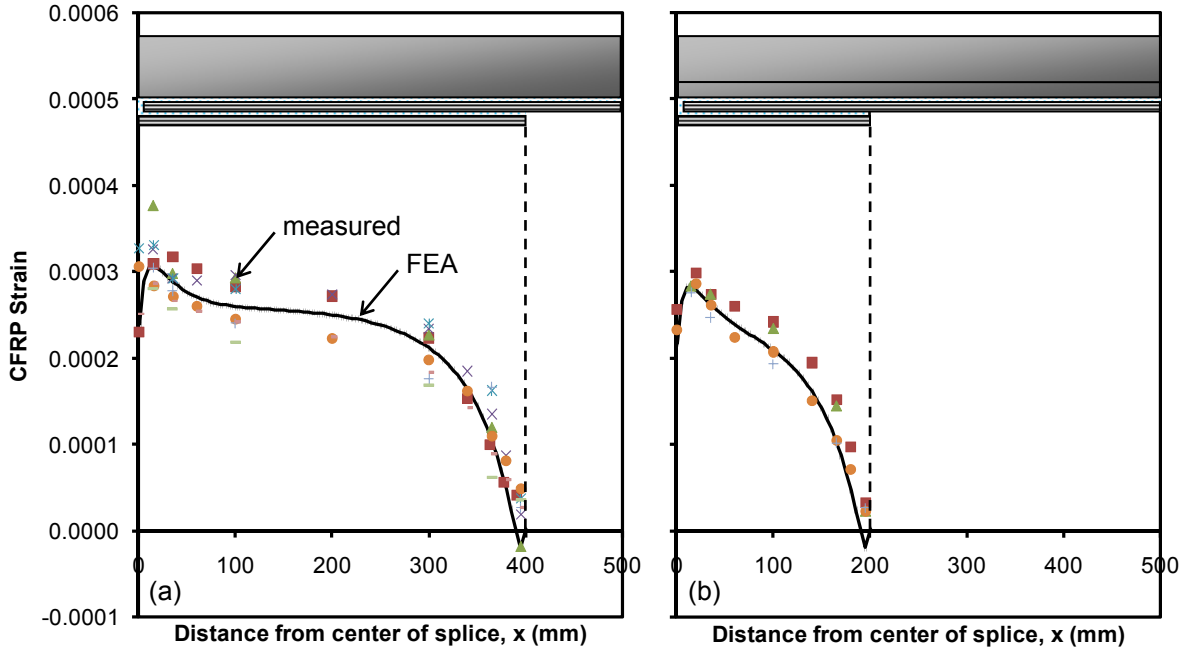

Figure 5.18 – Longitudinal strain distribution at surface of CFRP splice plate for beams with (a) 800 mm and (b) 400 mm long splice plates

The adhesive principal stresses near the end of the CFRP splice plate are shown in Figure 5.19 for a 400 mm long splice with square plate ends. The principal stresses at the adhesive-splice plate interface are shown in Figure 5.19(a) and (b) for the global and local analyses respectively. Both analyses indicate a significant stress concentration near the end of the splice plate, similar to the trend of the behavior observed in the analysis of the double-lap shear specimens.

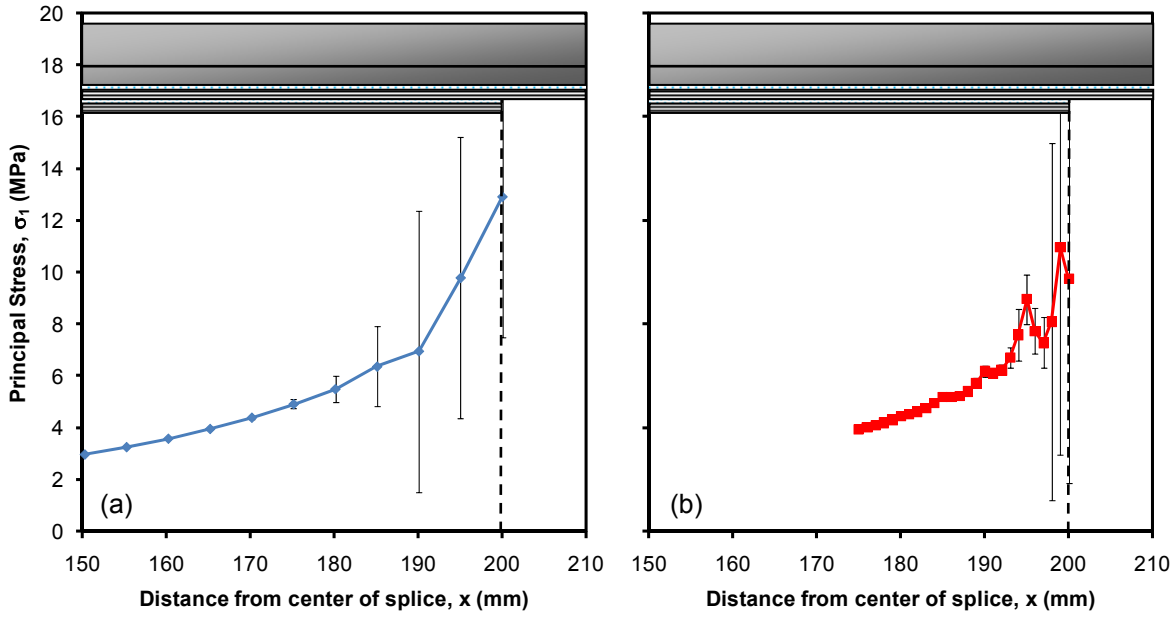

Figure 5.19 – Calculated principal adhesive stresses for a 400 mm long splice plate with square plate ends (a) Global model results (b) local model results.

The error bars shown in the figure indicate the discretization error of the calculated principal stresses. The calculated error was determined using an internal algorithm of the ANSYS program which calculates the difference between the nodal stress for a given element at a given node and the average of the calculated nodal stresses of all the elements connected to that node. The calculated errors give an indication of the precision of the calculated adhesive stresses and were used to select the boundaries of the local finite element model. Inspection of Figure 5.19(a) indicates that 25 mm away from the plate end the calculated error of the principal stresses using the global model was negligible. This indicates that the mesh refinement of the global model was sufficient to precisely calculate the adhesive stresses 25 mm away from the end of the splice plate. However, near the end of the splice plate the error of the calculated stresses is significantly higher, up to 78 percent, which indicates that a finer mesh is required to precisely calculate the adhesive stresses.

Inspection of Figure 5.19(b) indicates that the error of the adhesive stresses obtained from the local model was negligible up to 10 mm away from the plate end. The calculated errors were acceptable up to 3 mm away from the plate end which indicates satisfactory precision of the local finite element model.

Inspection of Figure 5.19(b) also indicates a slight oscillation of the calculated principal stresses near the end of the splice plate. The observed oscillations are confined to a zone approximately 5 mm away from the plate end. These oscillations are possibly due to slight variations of the localized curvature of the CFRP splice plate within this zone. Further mesh refinement could possibly help to identify the cause of these oscillations. However, the element size near the plate end for the current local model was specified as 0.25 mm. Therefore, the geometry of the current local model is far more precise than can be practically achieved for the actual bonded joints due to the limitations of the fabrication process. Therefore further mesh refinement may not be justified since the added precision of the plate end geometry cannot be physically achieved. Therefore a more highly refined model would not be an accurate representation of the actual bonded joints. The results indicate that the proposed global/local analysis approach adequately predicts the bond stresses in the adhesive layer near the end of the CFRP splice plate.

5.3.3 Results of the 3-D, linear finite element analysis

The purpose of the finite element analysis of the steel beams was to evaluate the distribution of adhesive stresses in the splice joint under flexural loading conditions. Figure 5.20(a) – (d) show the distribution of shear, normal, longitudinal and principal stress components respectively for a 400 mm long splice plate with square plate ends. The figure also presents the corresponding stresses for a double-lap shear specimen with the same splice configuration for comparison purposes. The adhesive stresses were calculated at the adhesive-splice plate interface using the respective finite element models for the two specimen types. The applied loads for the two analyses were selected to ensure that the

tension stress in the main CFRP plate, away from the splice location, was the same for both specimen types. This was done to allow direct comparison of the adhesive stresses for both cases. For the steel beam, the local model was used to determine the stresses within 25 mm from the end of the splice plate while the global model was used to determine the stresses away from the plate end.

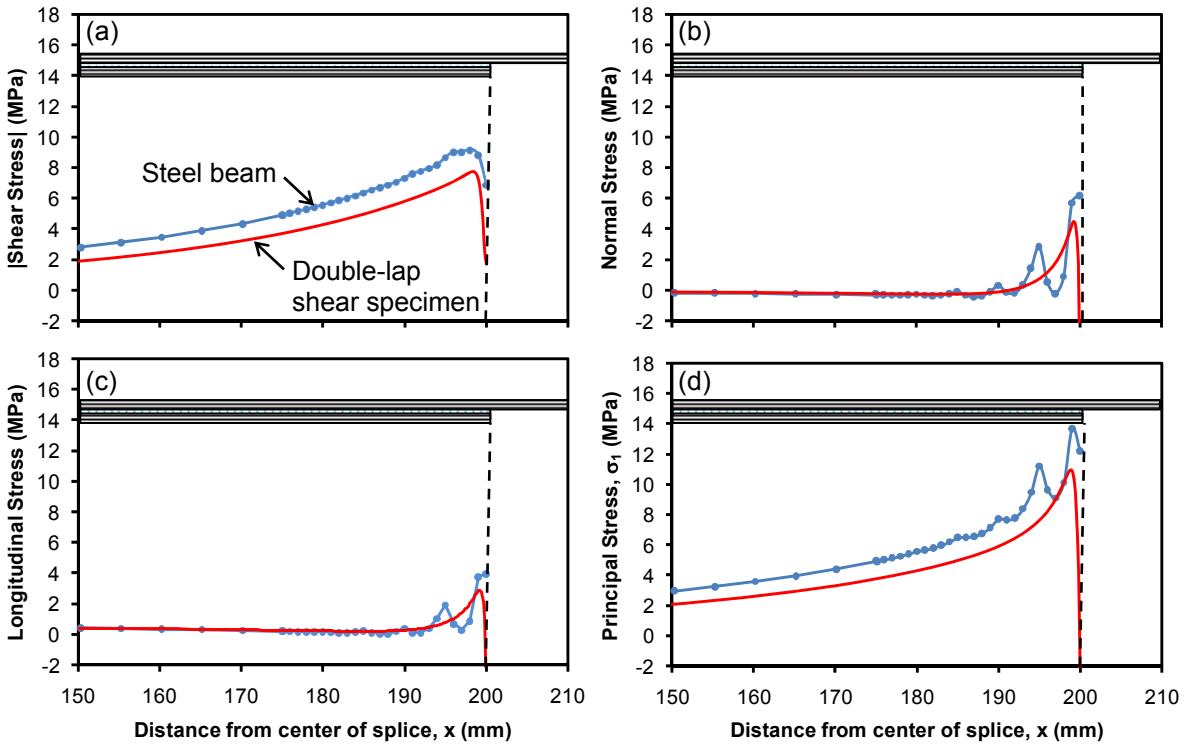

Figure 5.20 – Adhesive (a) shear, (b) normal, (c) longitudinal and (d) principal stresses for a 400 mm long splice with square plate ends

Inspection of Figure 5.20 indicates that the trends of the stresses are similar for the spliced steel beam and the double-lap shear specimen. Additionally, the magnitudes of the normal and longitudinal stress components, shown in Figure 5.20(b) and (c) are similar in both cases. This suggests that the curvature of the beam does not have a significant effect on these adhesive stress components. However, the adhesive shear and principal stresses, shown in

Figure 5.20(a) and (d) respectively, are slightly higher for the steel beam than for the double-lap shear specimen. This is mainly due to transfer of tension stresses from the tension flange of the steel beam to the CFRP splice plate through the adhesive layer. This effect can be observed by inspection of the longitudinal stresses in the tension flange of the steel beam, given in Figure 5.21. The figure indicates a reduction of the tension stresses in the steel tension flange near the end of the CFRP splice plate. This suggests that some of the tension force in the tension flange of the steel beam is being transferred to the CFRP splice plate, thereby inducing additional shear stresses in the adhesive layer. This trend is due to the localized increase of the transformed moment of inertia of the strengthened steel beam in the region of the splice plate.

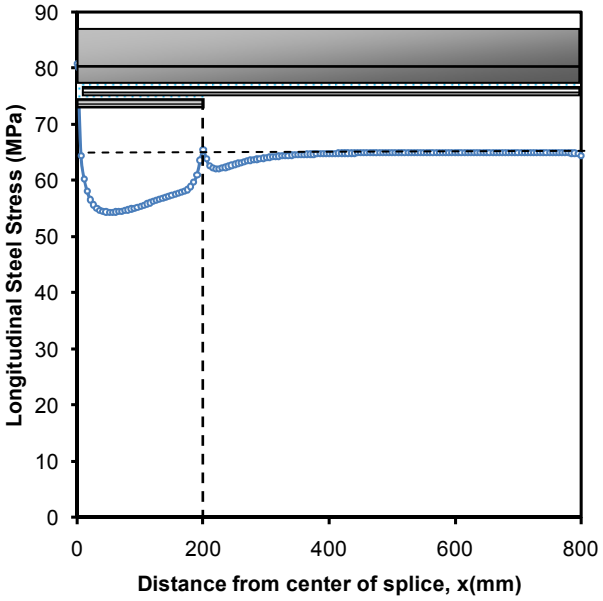

Figure 5.21 – Longitudinal stresses in the tension flange of the steel beam

The observed minor differences between the adhesive stresses for the steel beam specimens and the double-lap shear specimens are mainly due to the presence of the steel tension flange, rather than due to the nature of the applied load. The mechanisms of the stress transfer from

the main CFRP plate to the splice plate are equivalent for both types of specimens and loading.

It should be noted that in the current analysis, the splices in the beam case were located within the constant moment region of the beam with no applied shear force acting on the beam. In the case when the steel beam is also subjected to an applied shear load, additional shear stresses may develop in the adhesive layer. The magnitude of the additional shear stress can be calculated using fundamental principles of mechanics.

5.3.3.1 Effect of Taper Angle

The effect of the taper angle on the adhesive stresses was also investigated as shown in Figure 5.22. The figure presents the principal adhesive stresses at the adhesive-splice plate interface near the plate end for different taper angles. The stresses shown in the figure were determined using the local model within 25 mm of the plate end and using the global model away from the plate end. Inspection of the figure indicates the presence of a stress concentration at the interior corner of the taper similar to that obtained for the double-lap shear specimens. The figure further indicates that increasing the taper angle also increases the magnitude of the peak principal stress.

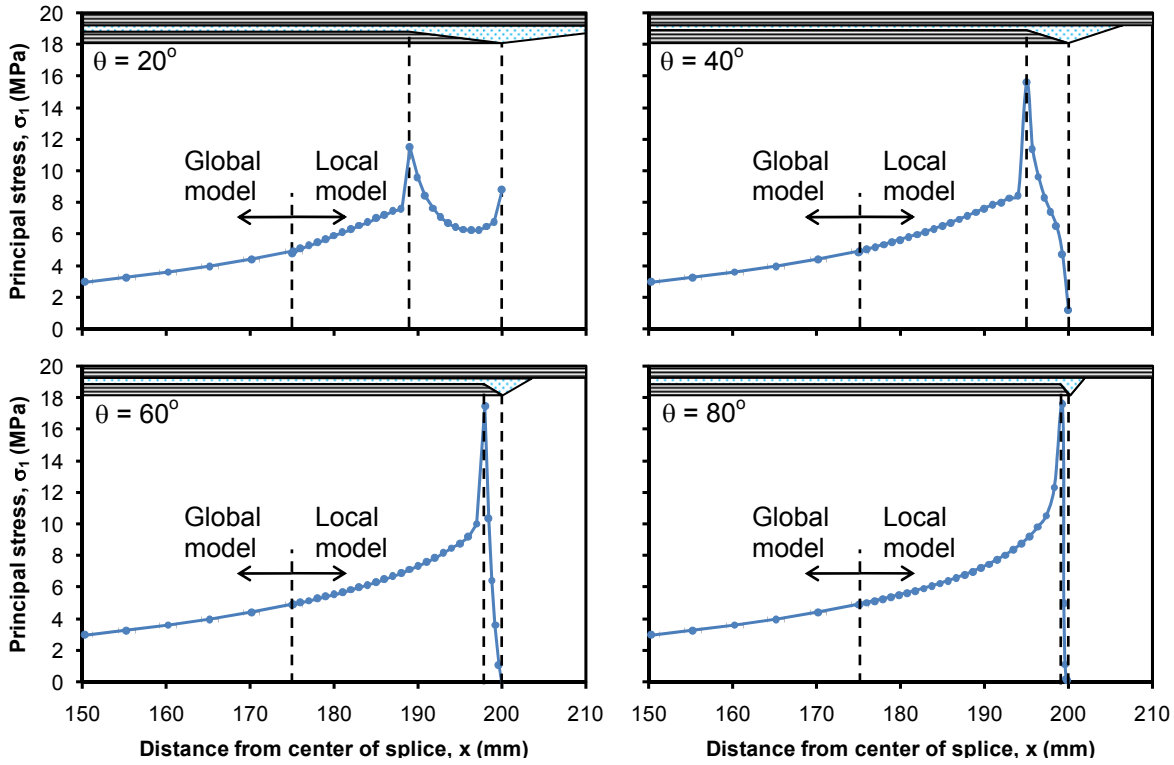

Figure 5.22 – Distribution of adhesive principal stresses for steel beams strengthened with spliced CFRP plates with different taper

Similarly to the case of the double-lap shear coupons, a stress concentration factor, ψ_θ, can be defined as in Eq. 5.3. The effect of the taper angle on the calculated stress concentration factor for the steel beam case is given in Figure 5.23. The trend of the results in the figure was extrapolated to a taper angle of 90° to represent the case of a square plate end. The relationship between the taper angle and the stress concentration factor shown in Figure 5.23 is similar to that obtained for the double-lap shear specimens and shown in Figure 5.14. Figure 5.23 also shows the proposed linear expression for the stress concentration factor given in Eq. 5.4 which closely matches the values determined from the results of the finite element analysis. This is expected based on the equivalence of the steel beams and the double-lap shear coupons which was demonstrated previously.

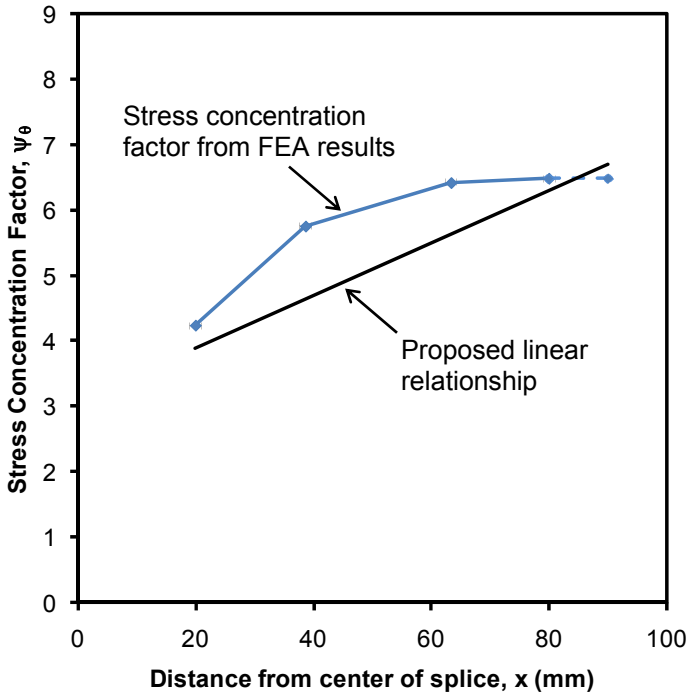

Figure 5.23 – Effect of taper angle on predicted stress concentration factor, ψ_θ, for steel beams strengthened with spliced CFRP plates

5.3.3.2 Effect of Splice Length

To evaluate the effect of the length of the splice plate on the adhesive stresses two additional analyses were conducted with an 800 mm long splice plate. The two extreme values of the taper angle, 20^o and 90^o, were considered. The calculated adhesive stresses, obtained from the finite element analysis, closely matched the stresses obtained for the 400 mm long splice plates. This suggests that increasing the splice length beyond 400 mm does not reduce the bond stresses near the plate end. This trend was confirmed experimentally since the tested beams with 400 mm and 800 mm long splice plates exhibited similar failure loads for splices with similar taper angles. This is consistent with the findings of the analysis of the double-lap shear specimens in section 5.2.2.6, which indicated a critical length of the splices of 400 mm.

5.3.3.3 Proposed Design Approach

The results of the finite element analysis indicate that the bond stresses and stress transfer mechanisms for CFRP splice are essentially equivalent for double-lap shear specimens and steel beams. Therefore, a similar design approach can be used for the two joint configurations. The typical geometry of a splice joint for a beam application is shown in Figure 5.24. Using a similar approach to that described for the double-lap shear specimens, and considering the critical length, ℓ_c, rather than the adhesive length, ℓ_a, the tension strength of the splice can be calculated as:

$$T_n = \frac{f_a \ell_c b_a}{2\psi_\theta \psi_a} \qquad \text{(Eq. 5.8)}$$

where:

f_a = adhesive tension strength

b_a = width of the adhesive joint

ℓ_c = critical length of the splice, 400 mm for the proposed CFRP system

and the stress concentrations, ψ_θ and ψ_a are as defined in equations 5.4 and 5.6 respectively.

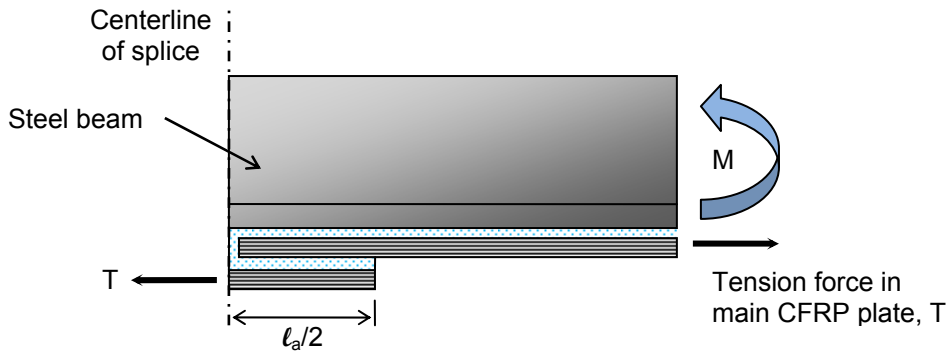

Figure 5.24 – Typical geometry of a CFRP splice in for a beam application

Thus, the proposed design approach involves locating the splices at a location where the calculated tension force in the main CFRP plate, due to the effect of the applied loads, does not exceed the ultimate tension strength of the splice, calculated using Eq. 5.7, after applying the appropriate load and reduction factors. For design purposes, a strength reduction factor, ϕ, of 0.75 is proposed which is consistent with the reduction factor used for brittle, fracture failures of steel members (AISC, 2005).

The tension force in the CFRP plate at any location along the beam can be determined based on principles of structural analysis and also based on the results of a moment curvature analysis. The moment induced at any location along the beam due to the effect of the applied loads can be obtained by structural analysis. Also, for a given steel beam section strengthened with CFRP plates, the relationship between the internal moment and the tension force in the main CFRP plate can be determined using a moment-curvature analysis (Dawood, 2005). Therefore, by correlating the results of the two analyses, the tension force in the CFRP at any location along the length of the beam can be determined.

The proposed design method was used to predict the nominal failure load of the tested steel beams with different configurations of CFRP splices. The measured and predicted failure loads are given in Table 5.2. In all cases the proposed design equation conservatively predicted the nominal capacity of the tested beams.

Table 5.2 – Comparison of test results with proposed design method for steel beams

Beam ID	G_a/t_a (N/mm^3)	ψ_a	Splice length (mm)	Taper angle	ψ_θ	Splice Tensile Strength (kN)	Failure load (kN)		Meas./ Pre.
							Meas.	Pre.	
800-S(1)	1080	1.01	800	90°	6.70	112	178	166	1.07
800-S(2)					6.70	112	205	166	1.23
800-T2				20°	3.90	193	408	285	1.42
400-S			400	90°	6.70	112	180	166	1.08
400-T2				20°	3.90	193	340	285	1.18

5.3.3.4 Numerical Illustration

The following example was developed, using the proposed design method, to illustrate the design of a CFRP splice using the proposed strengthening system for a typical steel-concrete composite beam. The cross-section of the example beam was selected to be similar to the beams tested previously by Schnerch (2005). The details of the example beam are presented in Figure 5.25.

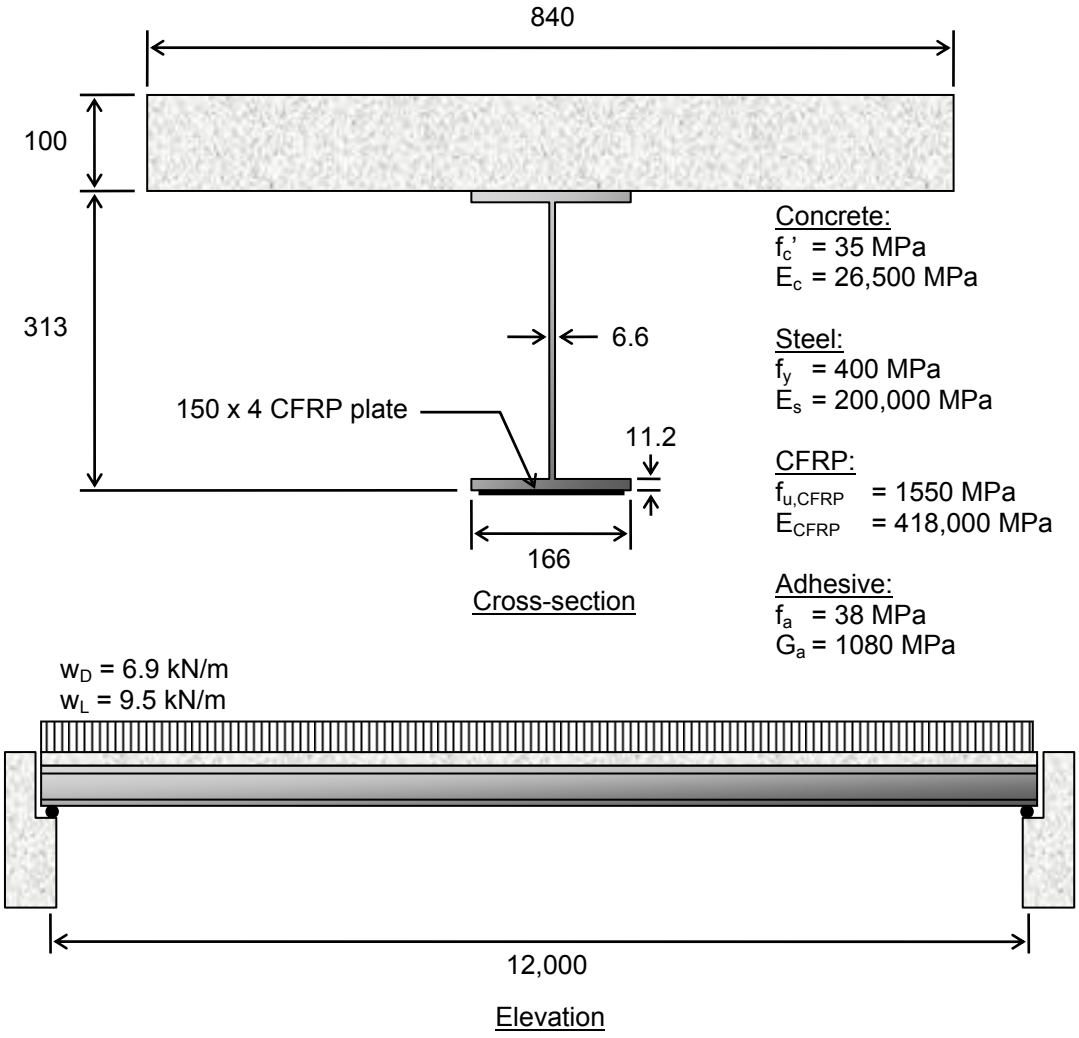

Figure 5.25 – Details of the example beam

The CFRP strengthening system was designed according to the guidelines presented by Schnerch et al. (2007). The moment-curvature response of the cross-section, given in Figure 5.26, was calculated using a spreadsheet following a similar procedure to that outlined previuosly (Dawood, 2005). For most typical repair or strengthening applications, the CFRP is installed onto the steel surface using an un-propped construction technique. Therefore, typically, the CFRP strengthening system does not support any of the applied dead load. This is represented in Figure 5.26 by the change in the slope of the moment-curvature diagram at the 110 kN-m level. This level of moment corresponds to the moment induced by the applied dead load.

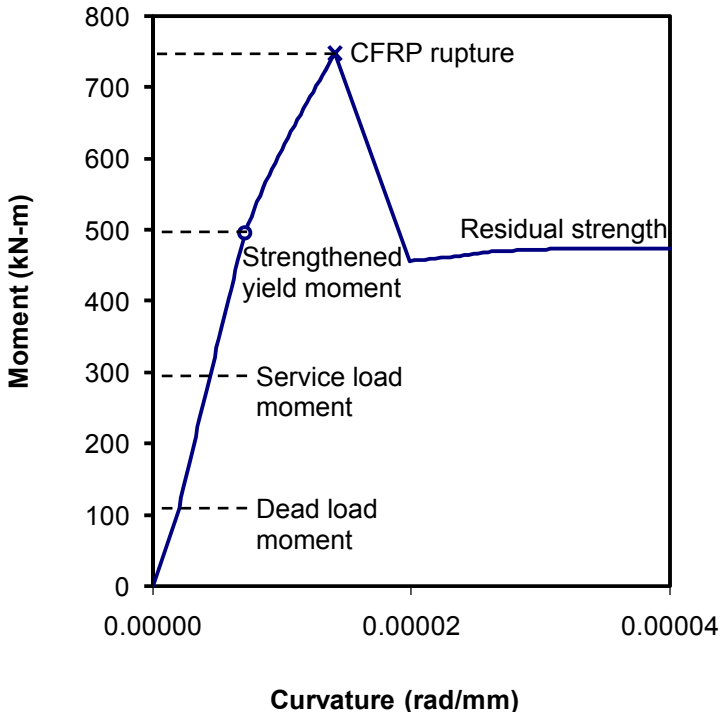

Figure 5.26 – Moment curvature response of the example beam

Using dead load and live load factors of 1.2 and 1.6 respectively, the factored moment, M_u, at the midspan cross-section of the beam was calculated as 423 kN-m.

Using a 400 mm long splice with 20° reverse tapers at all plate ends, and also using a 1 mm thick adhesive layer with a shear modulus, G_a, of 1080 MPa, similar to the proposed adhesive to be used with the strengthening system, the stress concentration factors, ψ_θ and ψ_a, can be calculated as:

$$\psi_\theta = 0.04(\theta) = 3.1$$

$$= 0.04\ (20) + 3.1$$

$$= 3.9$$

$$\psi_a = 0.0003(G_a/t_a) + 0.69$$

$$= \ 0.0003\ (1080/1) + 0.69$$

$$= 1.01$$

Using Eq. 5.8, the nominal tension strength of the splice is:

$$T_n = \frac{f_a \ell_c b_a}{2\psi_\theta \psi_a}$$

$$= \frac{(38)(400)(150)}{2(3.9)(1.01)}$$

$$= 289{,}400 \text{ N}$$

The corresponding stress and strain in the CFRP are 482 MPa and 0.00115 respectively. From the moment-curvature analysis, the applied moment acting on the strengthened section to induce a strain level in the CFRP of 0.00115 is 400 kN-m. Applying a strength reduction factor of 0.75, the moment capacity of the section at the location of the splice is 300 kN-m. Therefore, the splice should be located at a location along the beam where the moment due to the applied load will not exceed 300 kN-m, as shown in Figure 5.27.

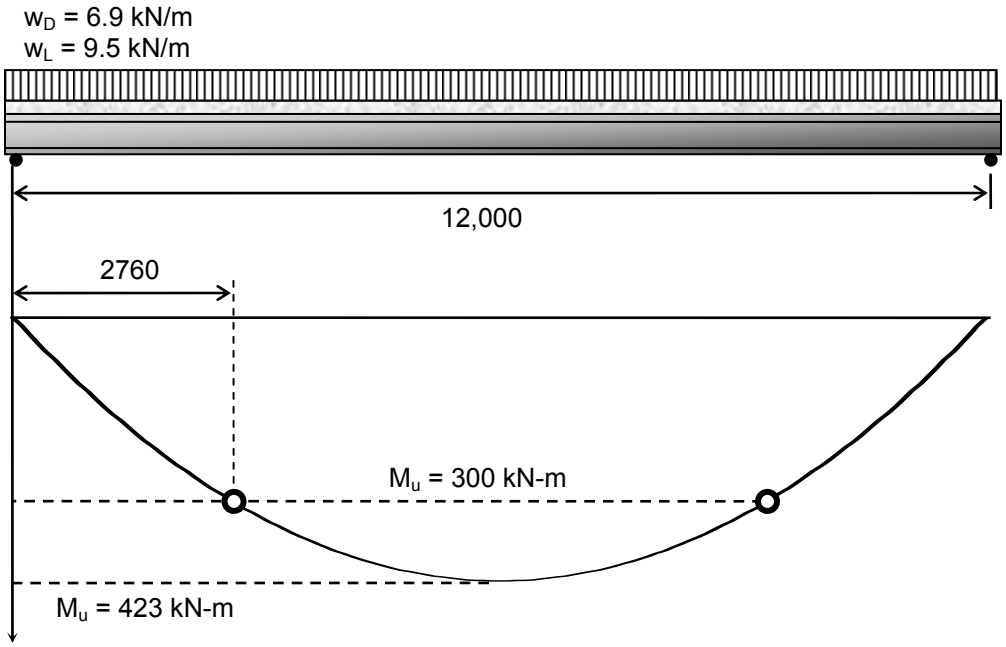

Figure 5.27 – Splice location based on the magnitude of the applied moment

Use 400 mm long splice plates with 20^o reverse tapers at all plate ends. Splices should be placed no more than 2760 mm from each support.

Chapter 6: Conclusions and Future Work

An experimental program and analytical study were conducted to evaluate the bond characteristics and splice behavior of a CFRP system for strengthening steel structures. The conclusions of the research program and future research recommendations are presented in the following sections.

6.1 SUMMARY AND CONCLUSIONS

The research presented in the first part of this dissertation was completed to study the bond characteristics and behavior of CFRP splice joints for a high modulus CFRP system proposed for strengthening of steel structures and bridges. The experimental program was conducted in two phases and included both double-lap shear specimen tests and large-scale beam tests. The parameters that were studied in the experimental program included the geometric configuration at the end of the CFRP plate, mechanical anchorage using a transverse CFRP wrap or a steel clamp, and the length of the splice plate. The analytical study consisted of a finite element analysis to evaluate the distribution of bond stresses in the adhesive for different joint configurations. The double-lap shear specimen and the beam specimen configurations, which were tested in the experimental program, were also considered in the analytical study. The main parameters considered in the analytical program included the angle of the reverse taper at the ends of the CFRP splice plate, the adhesive properties and the length of the splice plate. The research findings led to the following conclusions:

- All of the tested splices failed due to debonding of the splice plates prior to rupture of the CFRP. Since debonding was the dominant observed failure mechanism for the splice joints, an accurate understanding of the bond behavior is essential for the proper design of the splice joints to ensure satisfactory performance in service.

- Tests of the double-lap shear specimens with square main plate ends exhibited cracking of the adhesive within the center of the joint due to the presence of the stress concentration in the adhesive at that location. This cracking behavior was accurately represented by the three-dimensional, non-linear finite element analysis. The presence of the reverse tapered plate ends in the center of the splice joint helped to reduce the magnitude of the stress concentration at that location and consequently cracking was not observed for the joints with the reverse-tapered main plate ends.

- The experimental results suggested that the debonding failure mechanism initiated at one of the splice plate ends and propagated towards the center of the splice joint. This was confirmed by the three-dimensional, non-linear finite element analysis that was conducted to evaluate the cracking behavior of the double-lap shear specimens.

- The presence of the reverse tapered plate end configuration with a spew fillet at the end of the CFRP splice plates helped to approximately double the tension strength of the tested splice joints compared to the square plate end configuration. A similar trend was observed for both the double-lap shear specimens and the tested steel beam specimens.

- The finite element analysis indicated the presence of a significant stress concentration in the adhesive near the end of the CFRP splice plates. The results further indicated that the presence of the reverse taper did not affect the magnitude of the maximum shear stress near the end of the splice plates. However, the presence of the reverse taper helped to reduce the magnitude of the adhesive normal stresses. Additionally, the analysis indicated the presence of a significant longitudinal stress component near the ends of the splice plates. The presence of the reverse taper also helped to reduce the magnitude of the longitudinal stress component. Consequently, the presence of the reverse taper helped to reduce the magnitude of the adhesive principal stress concentration near the end of the splice plate. The magnitude of the stress concentration was reduced by reducing the taper angle at the end of the splice plate. A stress concentration factor is proposed to

account for the effect of the taper angle on the magnitude of the stress concentration in the adhesive.

- The finite element analysis further indicated that increasing the stiffness of the adhesive layer, by increasing the adhesive modulus or decreasing the adhesive thickness, resulted in an increase of the magnitude of the stress concentration near the end of the CFRP splice plates. A second stress concentration factor is proposed to account for the effect of the adhesive properties on the adhesive stresses near the plate end.

- The results of the finite element analysis indicate that the bond stress transfer mechanisms for the double-lap shear specimens and the CFRP splices bonded to steel beams are equivalent. Therefore, the same stress concentration factors can be used to predict the tension strength of both types of splices.

- The finite element analysis and experimental results suggest that the debonding failure of the splice joints occurs when the magnitude of the peak principal stress in the adhesive near the end of the splice plate reaches the tensile strength of the adhesive, as determined by standard tension coupon tests. A principal stress-based failure criterion is appropriate since the adhesive exhibited essentially linear-elastic, and brittle behavior.

- Based on the experimental results and the finite element analysis a design equation is proposed to calculate the tension strength for bonded double-lap shear specimens. A similar equation is proposed to calculate the tension strength of CFRP splice joints which are implemented to strengthen longer-span steel flexural members. The proposed design equations are based on the average shear stress in the adhesive layer and the proposed stress concentration factors. While the proposed equations were specifically established for the proposed CFRP strengthening system, a similar approach can be used to develop design equations for other combinations of CFRP and adhesive materials.

- Using the proposed design equation, a method is proposed to design the appropriate location for a CFRP splice joint along the length of a typical long-span steel flexural member. The design method is based on a moment curvature analysis of the strengthened section, and a structural analysis to ensure that the tension force in the CFRP strips at the location of the splice does not exceed the tension capacity of the splice joint.

- A critical overall splice length of 400 mm was defined for the proposed strengthening system. Increasing the overall length of the splice beyond the critical length did not result in a significant increase of the tension capacity of the bonded joints. Consequently, for the high modulus CFRP system tested in this research, it is recommended that a minimum overall splice length of 400 mm be used in practical applications.

- The beam test results indicated that the additional use of mechanical anchorage, by either a transverse CFRP wrap or a steel clamp assembly, did not significantly increase the strength of the splice joints. The results indicated that the transverse CFRP wrap did not have adequate stiffness to resist the peeling stresses that developed near the ends of the splice plate. Further, the presence of the transverse CFRP wrap concealed the occurrence of the debonding failure of the splice plate. The results also indicated that the effectiveness of the steel clamping system is sensitive to the installation technique used. Improper installation of the clamping system could induce tensile normal stresses near the end of the splice plate which could potentially reduce the strength of the bonded joint. Consequently the use of both methods of mechanical anchorage is not recommended until further research is conducted.

6.2 RECOMMENDED FUTURE WORK

While the current experimental program led to several interesting conclusions regarding the bond and splice behavior of CFRP materials, additional research work would also be beneficial. Recommended topics for future research include:

- Experimental investigations of the bond strength of CFRP splice joints with different taper angles between the limits of 20^o and 90^o which were tested in the current experimental program. The additional experimental results could be used to validate the proposed stress concentration factor for different taper angles.

- Experimental investigation of the bond strength of splice joints fabricated using different adhesives. Testing of adhesive with different elastic moduli and also testing splice joints with different adhesive thicknesses would be beneficial to validate the findings of the proposed analytical model. Testing of splice joints with ductile adhesives may also represent a promising way to further enhance the tension strength of splice joints. The effect of the adhesive properties on the overall splice performance should be evaluated.

- The proposed design equations were established for a specific CFRP strengthening system. However, the elastic modulus and thickness of the CFRP materials likely play an important role in the bond behavior and tension strength of the splice joints. The effect of the CFRP properties on the bond behavior should be studied in detail. The proposed model can then be modified to be generally applicable for any combination of FRP materials and adhesives.

- The potential to use mechanical anchorage as a method to enhance the tension strength of CFRP splice joints should be studied more thoroughly. The current study indicates that the design and installation of mechanical anchorage systems should be conducted with care to ensure that the system performs as intended by the designer. Further research is

necessary to develop an appropriate method to mechanically anchor CFRP materials to steel surfaces.

- The fatigue behavior of the proposed splicing system has not been studied. The fatigue performance of the proposed splicing system should be evaluated to verify the behavior under the effect of the increased live load levels which are commonly applied to strengthened members.

- All of the splices that were tested in the flexural portion of the experimental study were installed in the constant moment region of the strengthened beams. It is typically believed that the shear stresses induced in the adhesive due to the presence of an applied shear load acting on the beam are relatively small compared to the magnitude of the shear stress concentration near the end of the bonded strengthening plates. However, the bond behavior of the splice joints in the presence of an applied shear load should be tested to confirm this behavior.

- Other researchers have demonstrated that thermal stresses in bonded joints can be more severe than stresses induced by mechanical loading. This is particularly important when considering that the mechanical properties of most structural adhesives are temperature dependent. However, the effect of temperature fluctuations on bond stresses in CFRP strengthening systems for steel structures has not been studied in detail, neither experimentally nor analytically. The effect of thermally induced stresses on the bond behavior should be studied in detail before these types of strengthening systems can be widely implemented.

Part II:

Environmental Durability Study

Chapter 7: Background

The use of adhesives for bonding metallic and composite surfaces is a well established practice in the aerospace, marine, automotive and manufacturing industries. Research on the use of adhesives in these fields has been ongoing for the past 40 years. By comparison, the use of adhesives in civil engineering is a relatively new practice, particularly as related to strengthening metallic structures. Some of the experience gained from the other industries can be directly applied to civil infrastructure applications. However, characteristically the materials and methods used in civil engineering are substantially different from those used in other fields. Civil engineering applications typically employ relatively thick composite materials compared to the thin laminates used in the aerospace industry. Further, in infrastructure applications, environmental regulations and restricted accessibility to the job site limit the applicability of sophisticated chemical and electrochemical surface preparation techniques which are commonly used in other industries. While the use of elevated curing temperatures is common in other industries, cold cure two-part epoxies are used almost exclusively for strengthening bridges and structures. Therefore, while some of the advances in other industries can be applied directly, the use of adhesives and fiber reinforced polymer (FRP) materials in civil engineering presents unique challenges which must be addressed. This is particularly true when considering the environmental durability of bonded joints.

The fundamental mechanisms of degradation of adhesive joints are typically the same regardless of the specific application of the joint. In most applications, the ingress of water is of particular concern. Water can enter a bonded joint by diffusion through the adhesive, wicking along the interfaces between the adhesive and the adherends, capillary action through cracks and voids in the adhesive or absorption through porous adherends (Kinloch, 1983). Once moisture has penetrated into the joint, degradation can occur due to one of two primary mechanisms: degradation of the adhesive/adherend interface or degradation of the properties of the adhesive itself (Kinloch, 1983). At the interface degradation can occur due

to displacement of intermolecular adhesive forces or due to instability of the oxide layers on the surface of metallic adherends. Further, the presence of moisture can affect adhesive properties in a reversible manner, such as by plasticization, or in an irreversible manner, such as by chemical or physical breakdown of the adhesive. In addition, when joining dissimilar materials the possibility of galvanic corrosion should also be considered.

This chapter summarizes the significant advancements made by other researchers related to environmental durability of adhesive joints, with emphasis on adhesive joints between composite materials and steel surfaces. Each of the primary mechanisms of environmental degradation, including interfacial attack, adhesive degradation and galvanic corrosion, are discussed in detail. Recent advances in predicting the residual strength of environmentally degraded joints are also presented.

7.1 INTERFACIAL ATTACK AND SURFACE PREPARATION

Four main theories of adhesion have been proposed to describe the mechanisms of adhesion between different surfaces. These include the theory of physical adsorption, chemical bonding, electrostatic attraction and mechanical interlocking (Adams, 2005). Of these the theory of adhesion by physical adsorption is the most widely applicable. This theory suggests that adhesion is due to van der Waals forces which occur between the molecules of the two different materials across the interface between them (Owens, 1970). Van der Waals forces are the weakest of all intermolecular forces. These forces are very short ranged and are only experienced by a couple molecular layers near the interface. According to this theory, the thermodynamic work of adhesion, W_A, between two materials, B and C, is the energy required to separate the bonded interface into two separate surfaces and is given by:

$$W_A = \gamma_B + \gamma_C - \gamma_{BC} \qquad \text{(Eq. 7.1)}$$

where:

γ_B = surface free energy of surface B

γ_C = surface free energy of surface C

γ_{BC} = interfacial free energy between the two adhered surfaces

If this energy is positive, the bonded surface is stable, whereas a negative work of adhesion indicates an unstable bond which may spontaneously debond. The principal is the same if the separation occurs in the presence of a liquid; however the values γ_B and γ_C should be replaced by corresponding values for the submerged surfaces, γ_{BL} and γ_{CL}, respectively, which are typically less than their 'dry' counterparts. Owens (1970) conducted a series of tests in which a polypropylene film was coated with a polymer to validate the proposed theory. The cured system was submerged in different liquid surfactants. In all cases, when the calculated work of adhesion, W_A, was negative, the polymer spontaneously debonded from the polypropylene film upon submersion in the liquid surfactant. Other sources indicate that for epoxy/steel interfaces in the presence of water the thermodynamic work of adhesion is negative (Adams, 2005). This suggests that the bond is unstable in the presence of water which may lead to debonding. Unfortunately, the same properties which give a surface its adhesive properties also render it hydrophilic. Therefore, a surface which is chemically active and suitable for bonding may also attract moisture into the bond interface thereby reducing the thermodynamic work of adhesion.

A thorough review of the research related to adhesively-bonded joints of metals, polymers and composites was conducted by Baldan (2004a,b). It is commonly accepted that proper surface treatment is essential to ensure the long-term environmental durability of a bonded interface. Proper surface treatment of metals should produce a rough surface free from contamination with a fresh, stable oxide that has a favorable chemical composition. This can be achieved by using three basic steps: (1) remove contaminants from the surface by degreasing, (2) expose a fresh, chemically active surface and (3) modify the surface by a

chemical process to produce an interface resistant to hydration (Davis and Bond, 1999). In infrastructure applications, degreasing can typically be conducted by wiping the surface with an organic solvent such as acetone. To prevent environmental contamination, the used solvent should be collected and properly disposed.

Grit blasting is the preferred method of surface abrasion for preparation of metallic surfaces (Hollaway and Cadei, 2002, Cadei et al., 2004, Schnerch et al., 2007). Grit blasting helps to remove weak layers from the surface of the adherend and creates a rough, chemically active surface by cutting and deformation of the base material (Davis and Bond, 1999). Grits should be of adequate shape and hardness to cut rather than punch the surface (Davis and Bond, 1999). Research indicates that grit size does not affect the initial bond strength of steel and aluminum substrates (Harris and Beevers, 1999). Further, the durability of steel lap-shear joints that were immersed in 60^{o}C water was unaffected by grit size. However, bonded steel joints that were prepared using coarser grits and subjected to direct tension exhibited better durability than joints prepared with finer grits. Re-cleaning of the surface by air blowing, brushing or solvent wipe may also help to remove contaminants from the surface, but should be done with care so as not to cross-contaminate the surface or redistribute contaminants.

Several chemical and electrochemical surface preparation techniques are commonly used to modify the surface chemistry of metals in aerospace and other industries Baldan (2004a,b). However, they are of limited usefulness in civil engineering applications due to environmental restrictions, economics, and limitations on accessibility to the worksite. The use of a silane coupling agent as a primer for metallic surfaces demonstrates several distinct advantages that make it well suited for infrastructure applications. Silane can be applied by brushing onto the surface of the structure thereby minimizing the possibility of environmental contamination. When properly applied, silanes can provide bonds with durability similar to that of surfaces prepared with other chemical processes (Davis and Bond, 1999).

Silanes are monomeric silicone based chemicals similar to hydrocarbons (Dow Corning, 2005a). Organosilanes are those chemicals which have a direct bond between a silicon atom and a carbon atom in the molecule. The structure of a typical organosilane molecule is shown in Figure 7.1. These chemicals typically include similar hydrocarbon groups, called organic functional groups, to those found in organic, carbon based, compounds such as epoxy adhesives. The organic functional groups can react chemically in the same manner on the silane molecule as on an organic molecule. Therefore a primary chemical bond can form between the organic functional group on the organosilane and the adhesive. The other end of the silane molecule consists of a silicone based inorganic functional group. This functional group can react with hydroxyl groups on a metal surface to form very stable bonds. The silane molecules on the inorganic surface can also react with each other, thereby expelling water, to form a dense multimolecular siloxane network that is resistant to moisture penetration. The primary chemical bonds formed by the silane molecule are stronger, and therefore more environmentally stable, than the secondary van der Waals forces which are attributed to adhesive forces. Silanes are typically applied to a surface as a dilute solution in deionized water, methanol or another alcohol.

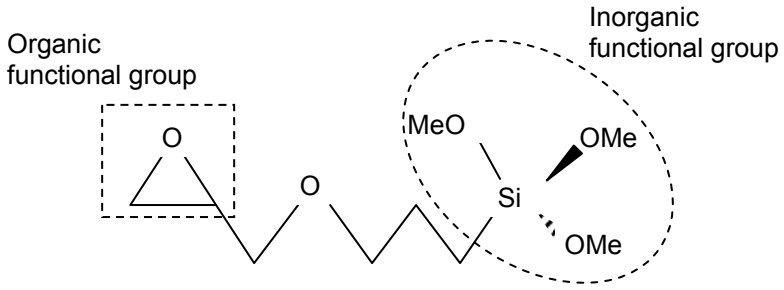

Figure 7.1 – Chemical structure of an organosilane (adapted from Dow Corning, 2005b)

When selecting a silane for a particular application, it is essential to consider the reactivity of the functional groups to ensure that the silane is capable to react with the specific adhesive and adherends used. In 1977, Gettings and Kinloch compared the surface chemistry of steel

specimens that were treated with different types of silane primers. They also conducted a series of tests to evaluate the durability of the bond between steel surfaces, which were treated with the different silanes, and an epoxy adhesive. The durability tests indicated that the only silane which enhanced the bond durability was a γ-glycidoxypropyltrimethoxy (γ-GPS) silane. The enhancement of the durability was attributed to three key processes which were not observed for the other tested silanes. The chemical analysis of the surface indicated that the treated steel surface was heavily oxidized which may have been due to complex bonding between silicon, iron and oxygen. The analysis further suggested that the silane was polymerized to form a polysiloxane structure. Finally, the presence of $FeSiO^+$ ions on the steel surface, which was not observed for any of the other tested silanes, was strong evidence for the formation of primary chemical bonds between the metal oxide and the polysiloxane primer.

Silanes can be applied to a surface directly as a pretreatment primer, as a part of a formulated primer or as an additive to an adhesive (Walker, 1990). The optimum method of application depends on the type of silane being used, the nature of the substrate and the nature of the coating or adhesive. A comprehensive experimental study was conducted to investigate the effect of different silanes and different application methods on the bond strength and durability of different coatings bonded to different substrates (Walker, 1990). The study included a total of eight different silanes, four different coatings (including two paints, an epoxy adhesive and a structural polyurethane adhesive) and four different substrates (including steel, stainless steel, aluminum and glass). The silanes were applied using two methods, directly to the surface in a dilute solution as a surface pretreatment primer and as an additive to the adhesive or coating. For the specific case of epoxy adhesives bonded to steel surfaces, the use of a γ-GPS silane as a surface pretreatment to a grit blasted steel surface increased the initial bond strength by 36 percent compared to the case without any silane. Using the same silane as an additive to the adhesive did not provide any notable increase of bond strength. The same γ-GPS silane was applied as a pretreatment to a grit blasted

stainless steel surface. The treated surface exhibited a significant enhancement of the bond durability as compared to the untreated case when exposed to a relative humidity of 100 percent at 21^{o}C for up to 150 weeks.

Other factors which influence the effectiveness of a silane as an adhesion promoter include the age of the silane solution at the time of application on the surface, the type of solvent used to prepare the silane solution, the drying time after application and the pH of the solution (Gledhill et al., 1990). Gledhill et al. tested a series of mild steel, butt joint specimens to evaluate the effect of these different parameters on the bond durability. The steel was grit blasted, solvent cleaned and pretreated with one of five different organosilanes. The adhesive joints were subsequently immersed in 60^{o}C water for 1500 hours. Untreated specimens exhibited a degradation of the bond strength of approximately 85 percent after 1500 hours of environmental exposure. The test results indicate that the greatest increase of durability is achieved when the silane was mixed in distilled water, applied to the steel surface 30 to 90 minutes after mixing and allowed to dry at 20^{o}C. Using this application procedure, the tested joints exhibited essentially no degradation of the bond strength after 1500 hours of environmental exposure. Changing the application time or drying temperature also resulted in an increase of the bond durability compared to the untreated case; however, the benefit was not as significant. Mixing the silane in an ethanol/water based solution provided essentially no improvement of the durability compared to the untreated specimens. Further, the study indicated that the pH of the solution was a function of the type of silane used and that the silane should be applied to the surface at its natural pH.

In a similar study, Abel et al. (2005) studied the effect of several parameters on the durability of aluminum joints treated with a γ-GPS silane and bonded using an epoxy adhesive. The parameters studied included the solution pH, silane concentration, nature of the solvent, hydrolysis time, drying temperature and time lag between silane application and bonding. The results indicated a complex interaction between silane concentration and pH. The

general trend indicated that with increased silane concentration, increasing the solution pH produced the best environmental durability, with all other factors being equal. The tests also suggested that the silane should be applied to the surface between 10 minutes to one hour after mixing. An additional set of tests indicated that bonding should occur within seven days after application of the silane to obtain maximum bond durability. The drying temperature did not have an effect on the bond durability. In considering the effect of the nature of the solvent, the results indicated that better joint durability was achieved when the silane was mixed in distilled water as compared to solutions prepared with a methanol/water mixture. Alternatively, tests conducted by Wang and Gupta (2005) on steel specimens treated with a γ-methacryloxypropyltrimethoxysilane (γ-MPS) and bonded to glass fiber reinforced polymers (GFRP) suggested that increasing the methanol content of the solution enhanced the bond durability.

In 2001, West tested a series of adhesives and primers to develop a CFRP system to strengthen steel bridges. A total of three adhesives, two epoxies and a methacrylate adhesive were considered in the study. Additionally, three different primers were tested including the Dow Corning Z-6040 γ-GPS silane, a silane based formulated primer and a proprietary primer designed for use with the methacrylate adhesive. Tests were conducted to evaluate the environmental durability under hot-wet and freeze-thaw conditions. The fracture toughness of the different adhesive/primer combinations was determined from the measured crack lengths at different exposure durations. The specimens that were pretreated with the Dow Corning Z-6040 γ-GPS silane and bonded with the Ciba-Geigy AV8113 epoxy adhesive exhibited the greatest bond durability under both hot-wet and freeze-thaw conditions. Based on the test results, and results of previous stages of the testing, this adhesive/silane combination was recommended to bond CFRP materials to steel surfaces for infrastructure applications. It was recommended to mix the silane to a 1 percent solution in distilled water and to allow the primer to air dry for 15 minutes prior to bonding.

In general, no single set of parameters can be universally recommended to yield optimum durability for all types of bonded joints. Rather, the silane concentration, nature of the solvent, pH and other variables are sensitive to the type of silane used, the nature of the adherends, and the type of adhesive. This is due to the complex nature of the chemical reactions which occur at the interface during the application of the silane and the subsequent bonding process. The selection of the silane and the specific mixture parameters should be selected in conjunction with the silane manufacturer while taking into account the details of the specific application (Petrie, 2007).

Fiber reinforced polymer (FRP) composite materials typically form strong, durable bonds with adhesives. For most civil applications, surface preparation by light sanding and solvent wiping is adequate. Alternatively some FRP products are fabricated with a removable peel ply which can be removed immediately prior to bonding. However, care should be taken to ensure that removal of the peel ply does not damage the surface of the FRP or leave a chemical residue.

7.2 ADHESIVE DEGRADATION

Degradation of the material properties of the adhesive can contribute to the overall joint degradation. While moisture transport can occur in a joint by many different mechanisms, diffusion of water into the adhesive appears to have a significant effect on the adhesive properties. Considerable testing has been conducted to evaluate the moisture absorption characteristics of adhesives and to correlate this with the degradation of the material properties.

Hand et al. (1991) conducted a series tests on thin films of adhesives exposed to different moisture conditions to determine the moisture absorption, stress relaxation and strength retention of six different adhesives. The test results indicated that, for the different adhesives tested, the initial moisture absorption rate was relatively high. The moisture content of the

adhesives reached levels approximately equal to the equilibrium levels within about two days. After submersion in water at room temperature for 16 days, the specimen weight increased by between 2 to 7 percent due to moisture absorption compared to the dry case. Similar results were obtained for specimens exposed to 50 % relative humidity at 50°C, however, the equilibrium moisture content was approximately half that of the immersed specimens. Due to moisture absorption the specimens swelled which caused a relaxation of stress for specimens that were subjected to a constant strain level. The reported stress relaxation was between 50 to 90 percent for the different adhesives tested. Exposure to moisture also reduced the ultimate strength of the adhesives by between 30 to 70 percent. This suggests that while moisture absorption may degrade the strength of the adhesive, the relaxation of stresses may help to reduce stress concentrations in highly stressed regions such as near plate ends.

In other tests a series of adhesive specimens were exposed to different environmental conditions, including submersion in distilled water and dilute solutions of sodium chloride for different durations (Horton et al., 1992). The test results indicated an initial increase of the weight of adhesive specimens, attributed to moisture absorption, followed by a subsequent decrease, attributed to leaching of chemicals from the adhesive. Mechanical tests indicated no degradation of the adhesive properties after exposure. However, aluminum lap joints prepared using the same adhesive exhibited significant degradation of strength after exposure which suggests that the degradation of the interface had a more significant effect on the joint durability than the degradation of the adhesive properties. The test results further indicated that exposure to sustained load accelerated the bond degradation.

A series of tests were conducted on small epoxy prisms to determine the effect of environmental exposure on the glass transition temperature and elastic modulus (De Nève and Shanahan, 1992). Test results indicated that exposure to 100% relative humidity at 70°C for approximately two months decreased the glass transition temperature from 126°C to 77°C. The exposure did not significantly affect the measured elastic modulus of the

adhesive. The degradation was attributed primarily to plasticization of the adhesive due to water uptake. Measurements of the water absorption of the adhesive indicated that, initially, the moisture uptake followed a Fickian diffusion law followed by a plateau stage and a subsequent increase of the water absorption.

Crasto and Kim (1996) tested several CFRP double-lap shear coupons which were bonded together using an epoxy adhesive and exposed to moisture conditions at different temperatures. For specimens tested at lower temperatures, the measured failure strength of fully saturated specimens was greater than that for dry specimens. This was attributed to toughening of the adhesive caused by plasticization. However, at higher test temperatures saturated specimens were weaker than dry specimens. The authors suggested that the presence of moisture in the adhesive may have reduced the glass transition temperature thereby reducing the strength of the saturated joints that were tested at higher temperatures. Alternatively, in other testing, Johnson and Butkus (1998) demonstrated that exposure to high temperature and humidity reduced the mode I fracture toughness of an epoxy adhesive by approximately 70 percent. This alternative mechanism could also possibly account for the measured strength reduction.

Knox and Cowling (2000) conducted a series of tests to evaluate the environmental degradation of epoxy tension coupons. They found that, under accelerated ageing conditions, the strength and modulus of the adhesive degraded by 20 percent and 10 percent respectively. This was attributed to plasticization of the adhesive. Similar results were obtained by Lapique and Redford (2002) who additionally noted that the environmental exposure also increased the maximum strain and ductility of the adhesive.

The results obtained by Knox and Cowling further indicated that application of a relatively low sustained load, corresponding to 20 percent of the initial adhesive strength, did not affect the adhesive durability. However, application of a relatively high load level, corresponding to 50 percent of the initial adhesive strength, significantly reduced the adhesive strength to

the point of causing spontaneous failure of the adhesive within 5 weeks of exposure for most of the tested coupons. Since most adhesive joints exhibit high bond stress concentrations near the ends of the bonded plates, environmental degradation of the highly stressed adhesives in this region could cause premature sudden failure of the bond. However, the magnitude of the stress concentration may be reduced slightly due to the localized reduction of the adhesive modulus caused by ingress of moisture near the plate end.

In the same study Knox and Cowling tested a series of steel lap-shear coupons to compare the degradation of the adhesive properties to the degradation of bonded joints. They also studied the effect of the presence of a spew fillet on the joint durability. The results suggest that while the adhesive degradation may have contributed to the overall joint degradation, it was not sufficient to account for the measured loss of strength of the joints. The authors suggested that the lap joints may also have been affected by degradation of the interfacial zone. The test results further indicated that providing an adhesive spew fillet near the end of the joint helped to increase the bond durability. The presence of the spew fillet increased the path length required for moisture to penetrate into the joint and reduced the bond stresses near the plate end. Further, removal of the fillet by machining may have exposed cracks and voids in the adhesive which could possibly have increased the moisture penetration and decreased the strength of the joints without fillets.

Colombi et al. (2005) tested a series of steel/CFRP double-lap shear coupons which were subjected to different combinations of saltwater spray and thermal cycles. The testing was conducted to evaluate the effectiveness of using CFRP materials for strengthening steel structures in civil engineering applications. The results indicated that while the environmental conditioning did not have a significant effect on the joint strength, the ductility of the bonded joints was decreased by up to 50 percent as compared to unconditioned specimens. The authors did not identify the primary mechanisms of degradation of the joints.

7.3 GALVANIC CORROSION

Galvanic corrosion can occur when two metals are coupled together and submerged in an electrolyte. Four conditions are necessary for galvanic corrosion to occur (Francis, 2000): (i) the two metals in contact must exhibit a sufficient difference of electrical potential (ii) an electrical connection must exist between the two metals, (iii) the two metals must be bridged by an electrolyte and (iv) a sustained cathodic reaction must proceed on the more electropositive metal which typically involves the consumption of dissolved oxygen. If these four conditions are satisfied, a galvanic current will form between the two metals. The current will increase the corrosion rate of the anode and may decrease or halt the corrosion of the cathode. However, passivation may occur due to the buildup of a thick oxide layer on the surface of the anode which may inhibit further corrosion.

To ensure the long-term durability of any CFRP system for strengthening steel structures galvanic corrosion between CFRP and the steel substrate must be prevented. The electropotential difference between steel and carbon is sufficiently large to drive a galvanic current (Francis, 2000). Therefore, in the presence of the remaining three conditions, accelerated corrosion of the steel is possible. In infrastructure applications, moisture may collect on the surface of a structure by condensation, due to runoff or due to spray from roadways or water bodies. Dissolved deicing chemicals, salt from marine environments or minerals leached from other sources can create an electrically conductive solution. Repeated wetting and drying of the structure would provide sufficient dissolved oxygen to drive a sustained cathodic reaction on the CFRP surface. Therefore, if the two materials are in direct electrical contact, galvanic corrosion may occur. However, the presence of an adhesive layer between the steel and the CFRP material may provide sufficient electrical insulation to prevent the formation of a galvanic current.

An experimental study was conducted to investigate the possibility of galvanic corrosion between CFRP materials and a number of different metals, which are commonly used in the

aerospace industry (Brown, 1974). Different methods of attaching the CFRP to the metal surface were considered including bolting and adhesive bonding. The couples were exposed to a number of different environments, including accelerated corrosion, industrial and marine exposure environments. For CFRP coupled to cadmium-plated mild steel, test results indicated that, for bolted joints, moderate corrosion was observed in all three environments. The results further indicated that adhesively bonding the CFRP to the steel surface helped to minimize the occurrence of galvanic corrosion. However, in this case, severe localized corrosion was observed near the edges of the CFRP plate. Specimens that were painted with epoxy paint prior to exposure exhibited essentially no corrosion in any of the exposure environments.

The effect of temperature, metal type, area ratio and environmental exposure on galvanic corrosion rates was studied for different metals coupled to two different CFRP materials (Bellucci, 1991; Bellucci, 1992). Different types of metal anodes were electrically coupled with CFRP materials and a submerged in a 3.5 percent NaCl solution. The galvanic current was measured to evaluate the extent of the galvanic corrosion. The study concluded that both aluminum and steel exhibit significant galvanic corrosion when coupled to CFRP materials. Further, increasing the ambient temperature resulted in an increase of the measured galvanic current. Measurement of the galvanic current indicated that, for steel and aluminum coupled to CFRP, increasing the cathode/anode area ratio increased the corrosion rate. For the specific case of strengthening steel bridges or structures with CFRP, the exposed area of CFRP is relatively small compared to the exposed area of steel. Therefore, the cathode/anode area ratio is relatively low which could possibly help to reduce the galvanic corrosion rate in case the two materials come into direct electrical contact.

Test results also indicated that environmental degradation of the CFRP material can lead to an increase of the corrosion rate. The authors suggested that exposure of the CFRP material to moisture can cause localized debonding between the carbon fibers and the adhesive matrix in the CFRP material. This could possibly expose more of the carbon fiber to the electrolyte,

thereby increasing the cathode/anode area ratio and consequently the corrosion rate. Additionally, diffusion of NaCl solution into the resin matrix can also reduce the electrical resistance of the CFRP and increase the galvanic current.

The galvanic coupling between steel and CFRP reinforcing bars imbedded in chloride contaminated concrete has also been studied (Torres-Acosta and Sen, 2005). Two types of steel reinforcing bars were considered: epoxy coated bars with simulated damage to the epoxy coating representing 0.1 percent of the bar surface area and plain steel bars. The simulated damage to the epoxy coating of the reinforcing bars exposed an area of steel of approximately 0.1 cm^2. The exposed surface area of the CFRP bar was approximately 32 cm^2. Therefore, in this case the cathode/anode area ratio was 320. The specimens which used plane steel bars had a cathode/anode area of approximately one. The findings indicated that the current densities were one order of magnitude higher for the damaged epoxy coated reinforcing bars. This was likely due to the excessively high cathode/anode area ratio, which has a significant effect on the corrosion rate as previously noted by other researchers. It should be noted that the cathode/anode area ratio of 320 is extremely high compared to the case when CFRP is externally bonded on the surface of a metallic structure.

Galvanic coupling has also been shown to cause damage to the cathodic CFRP materials due to the formation of the chemical products of the cathodic reaction. Several mechanisms of degradation have been reported including blistering of the FRP (Tucker and Brown, 1989) and degradation of the resin or the resin/fiber interface (Sloan and Talbot, 1992).

In one study submersion of a vinyl-ester based CFRP in natural sea water resulted in the formation of solution filled voids, or blisters, on the CFRP surface (Tucker and Brown, 1989). The authors suggested three possible mechanisms for the formation of these blisters. Pre-existing voids in the CFRP, which formed due to poor consolidation of the CFRP during fabrication, may have filled with fluid during environmental exposure. Alternatively, the blister formation may have been related to the chemistry of the vinyl-ester resin since similar

epoxy-based CFRP materials did not exhibit any voids under the same exposure conditions. Finally, the authors suggested that water-soluble molecules in the transverse glass fiber tows, which were used to hold the carbon fibers in position, may have caused diffusion of moisture into the composite which may have driven the blistering process. It was observed that specimens that were not coupled to steel did not exhibit blister formation. This suggests that, regardless of the mechanism of blister formation, the galvanic reaction between the steel and the CFRP likely modified the solution chemistry thereby promoting the formation of blisters.

In another study it was shown that the interlaminar shear strength of CFRP materials that were galvanically coupled to magnesium decreased by 30 percent (Sloan and Talbot, 1992). Analysis of the failure surface by scanning electron microscope indicated extensive debonding between the carbon fibers and the matrix near the edges of the CFRP. Chemical analysis suggested that the debonding may have been caused by the evolution of hydroxyl or perhydroxyl ions which formed as a product of the cathodic reaction on the CFRP.

To help minimize the occurrence of galvanic corrosion between steel and CFRP materials, an electrical insulator can be placed between the two materials to break the electrical contact and prevent the formation of a galvanic current. Tavakkolizadeh and Saadatmnesh studied the effect of using an epoxy adhesive as an insulator between steel and carbon fibers (2001). They found that coating the carbon fibers with a 0.25 mm thick layer of adhesive reduced the galvanic corrosion rate of steel in seawater by 21 times compared to uncoated fibers. West suggested that embedding a layer of glass fibers in the adhesive between the steel and the CFRP helped to prevent electrical contact between the two materials, particularly in locations where there may be a void in the adhesive (2001). In either case it should be noted that few materials retain their insulating properties after exposure to environmental conditions for more than a few years and therefore careful monitoring to identify and remediate galvanic corrosion should be conducted (Sloan and Talbot, 1992).

7.4 PREDICTION OF ENVIRONMENTAL DEGRADATION

To evaluate the environmental degradation of adhesively bonded systems accelerated exposure tests are conducted using severe environmental conditions. The conditions are often unrepresentative of actual environmental conditions and consequently the bond degradation may occur due to unrepresentative mechanisms. Ashcroft et al. (2001) concluded that accelerated exposure tests cannot be used to accurately predict the expected service life of bonded joints under natural environmental exposure conditions. They did, however, indicate that accelerated tests can be used to compare the relative performance of different systems, particularly if the accelerated conditions are reasonably representative of the natural conditions. More recently, researchers have looked at using different analytical methods to help predict the residual strength of bonded joints after environmental exposure.

Abdel Wahab et al. (2002) conducted a coupled diffusion/stress finite element analysis to evaluate the effect of moisture exposure on the stress distribution in steel single-lap joints. They found that after six weeks of exposure swelling of the adhesive due to moisture absorption induced compressive stresses near the plate end. These stresses helped to reduce the localized normal (peeling) stress concentrations which typically form near the end of bonded plates. Further, moisture absorption also reduced the adhesive modulus near the plate end thus further reducing the local stress concentration. Although the moisture absorption also reduced the strength of the adhesive locally, these effects counteracted each other and no degradation of joint strength was predicted. However, after longer durations of exposure, reduction of the adhesive strength due to plasticization, and perhaps reduction of the interface strength, would eventually lead to deterioration of the joint strength. These trends were also confirmed experimentally.

Chapter 8: Experimental Program

This chapter outlines the details of the experimental program that was undertaken to evaluate the environmental durability of the proposed CFRP strengthening system. The program investigated the durability of four different configurations proposed to bond the CFRP material to the steel surface. The experimental program consisted of a total of 44 steel-CFRP double-lap shear specimens. Fourteen of the double-lap shear specimens were tested under typical laboratory conditions and used as control specimens to provide a basis for comparison of the test results. The remaining 30 specimens were exposed to severe environmental conditioning to induce accelerated degradation of the bond. The specimens were subsequently tested monotonically to failure to evaluate their residual bond strength. In addition to the double-lap shear specimens, tension coupons of the steel, adhesive and CFRP materials were exposed to the same environmental conditions and tested to evaluate the effect of the environmental exposure on the material properties.

The proposed experimental program was distributed to members of the International Institute of FRP in Construction (IIFC) working group on FRP-Strengthened Metallic Structures for critical review prior to implementation of the program. The recommendations of the reviewers were considered during the development and implementation of the research.

8.1 TEST SPECIMENS

A total of 44 steel-CFRP double-lap shear specimens were tested to evaluate the environmental durability of the proposed CFRP strengthening system. The typical specimens, shown in Figure 8.1 consisted of two 9.5 mm thick x 32 mm wide steel plates bonded together using two 4 mm thick x 19 mm wide CFRP strips.

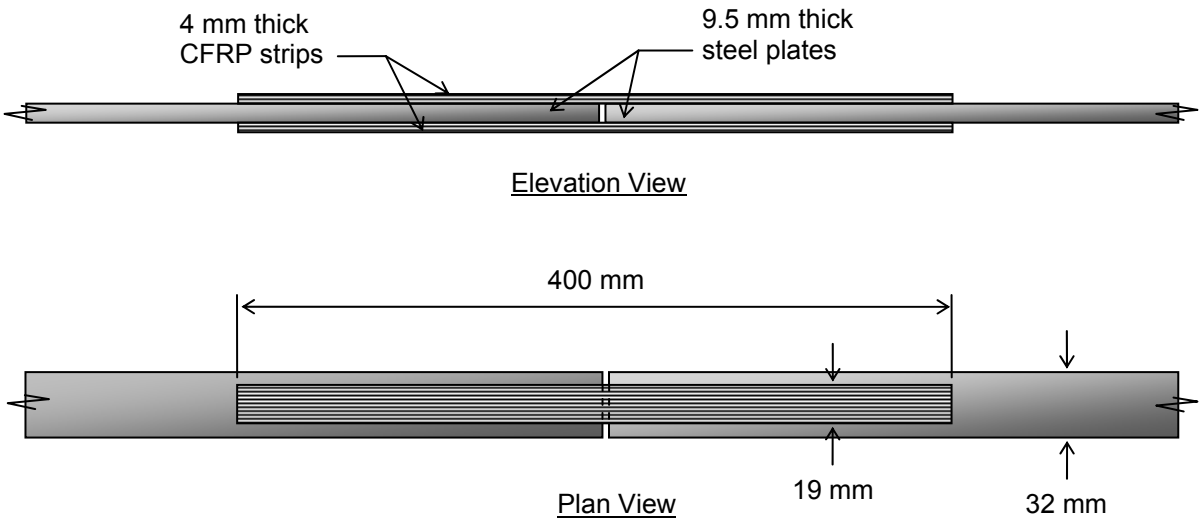

Figure 8.1 – Schematic of typical environmental durability test specimen

Four different bond configurations were considered as shown in Figure 8.2. The first configuration, Detail A, consisted of bonding the CFRP strips to the steel surface using only a relatively thin layer of adhesive. This configuration increased the possibility of direct electrical contact between the steel and the CFRP and represents a practical worst-case scenario for the occurrence of galvanic corrosion. For the second configuration, Detail AS, the steel surface was pretreated with a silane coupling agent to enhance the durability of the interfacial zone between the steel and the adhesive. Again, a relatively thin layer of adhesive was used. For Detail AG a unidirectional glass fiber layer was embedded in the adhesive between the steel and the CFRP to act as an electrical insulator between the two materials and to help reduce the possibility of galvanic corrosion. Detail AGS included both methods of environmental protection including the use of a silane adhesion promoter and the additional use of a glass fiber layer.

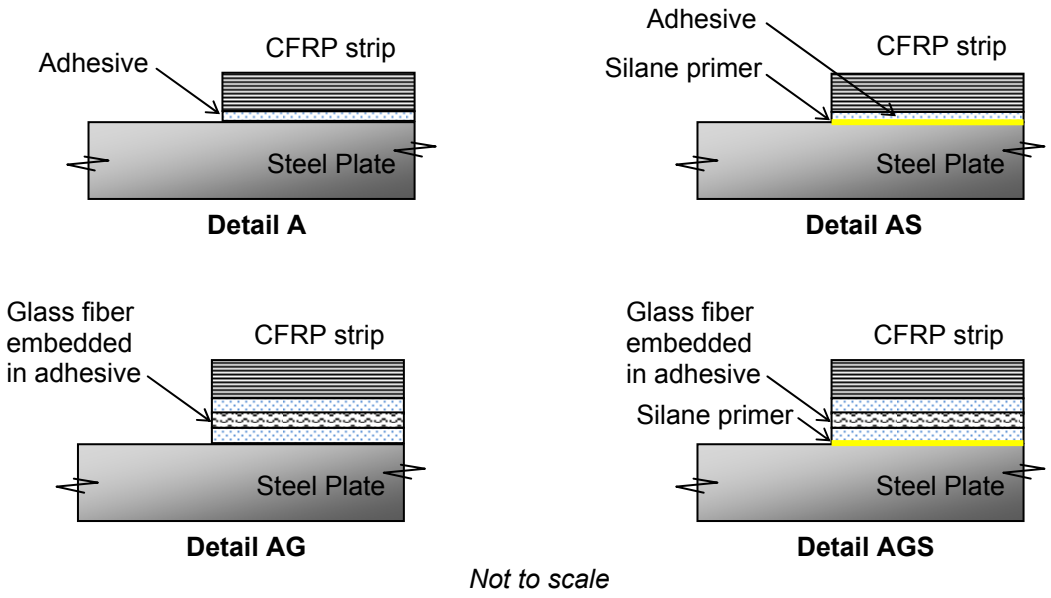

Figure 8.2 – Schematic representation of different bond configurations

To maintain consistency of the test specimens, a standard fabrication process was adopted and ten specimens were fabricated simultaneously. The surface preparation and installation technique followed the guidelines published by Schnerch et al. (2007). The steel surface was cleaned with acetone, sandblasted to a white metal finish and re-cleaned with acetone. The steel plates were aligned in a specially designed fixture and clamped in place. For the Detail AS and AGS specimens the steel surface was then treated with the Z-6040 γ-glycidoxypropyltrimethoxysilane (silane) produced by Dow Corning according the directions provided by the manufacturer. The silane was diluted in methanol to a 4 percent mixture by weight, brushed onto the steel surface and left to dry for approximately one hour according to the recommendations received from a Dow Corning representative.

The CFRP strips were prefabricated with a disposable peel-ply to protect the surface. The strips were cut to the required dimensions and the edges were wiped with methanol to remove any residual dust. The peel-ply was removed immediately prior to bonding. The

adhesive was mixed thoroughly by hand and applied to the CFRP surface. For the Detail AG and AGS specimens one layer of Fyfe Tyfo SHE-51A unidirectional glass fibers was cut to the same dimensions as the CFRP strip, pressed into the adhesive and thoroughly impregnated by pressing with a plastic spatula. Additional adhesive was applied as needed to ensure that the fibers were thoroughly impregnated. The CFRP plate was pressed onto the surface and clamped into place. The excess adhesive was removed and the specimens were left to cure in the fixture at room temperature for at least 12 hours as shown in Figure 8.3(a). The specimens were then removed and the second CFRP plate was bonded onto the opposite surface following a similar procedure. The adhesive was allowed to cure at room temperature for at least one week. Excess cured adhesive was removed from the edges of the specimen using abrasion by a hand-held rotary tool. Several typical completed specimens are shown in Figure 8.3(b).

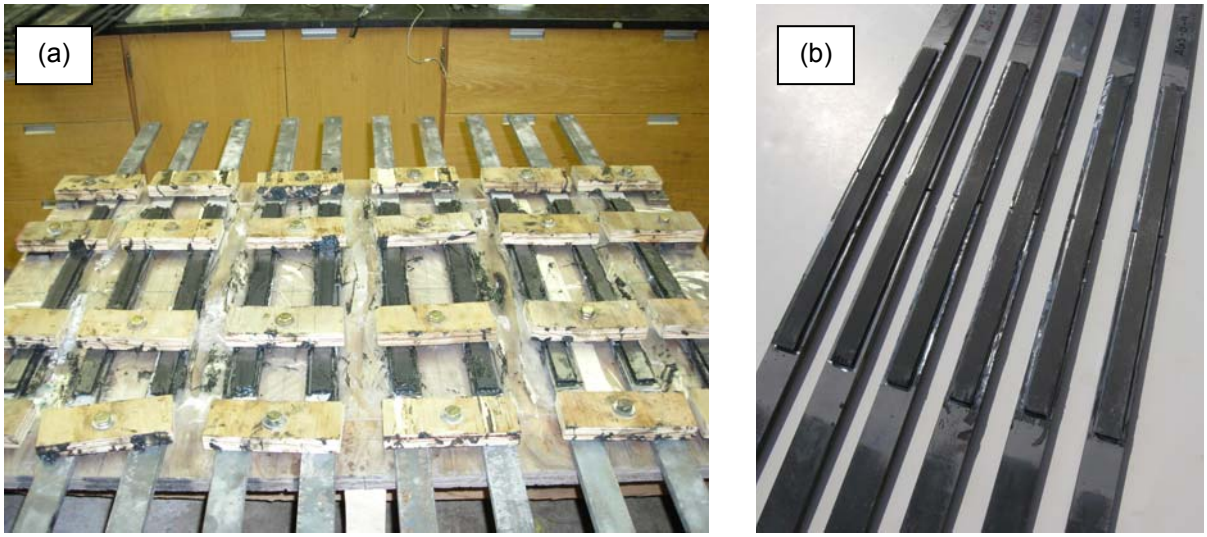

Figure 8.3 – Environmental durability test specimens (a) during fabrication and (b) completed specimens

8.2 MATERIALS

The primary materials used in the experimental program included the steel, CFRP and adhesive. Each of the materials was tested according to the appropriate ASTM standards to determine their respective mechanical properties. The results of the tests are presented in the following sections.

8.2.1 Steel Material Properties

A 9.5 mm x 32 mm hot-rolled Grade A36 steel plate was used to fabricate all of the double-lap shear specimens. The tensile properties of the steel were determined according to ASTM A370-02 using three dog-bone shaped steel tension coupons which were cut from the original plate material. The coupons were tested in tension using an 890 kN MTS hydraulic testing machine. The measured stress-strain relationship of steel in the elastic-plastic range is given in Figure 8.4. The elastic modulus of the steel was determined, by fitting a best-fit line to the elastic portion of the stress strain curves, as 215,000 MPa. The yield strength of the steel was determined, using the 0.2% offset method, as 334 MPa. The average tensile strength and ultimate strain of the steel were measured as 475 MPa and 0.35 respectively.

To evaluate the effect of environmental exposure on the material characteristics of the steel additional steel coupons were fabricated and environmentally conditioned with the double-lap shear specimens. At the conclusion of the environmental conditioning, the mass loss of the steel due to the effect of corrosion was measured according to ASTM G1-03. The coupons were soaked in a solution of 500mL distilled water, 500 mL hydrochloric acid and 3.5g hexamethylene tetramine (Cook, 2004). The coupons were soaked in the solution, abraded with a wire brush and the weight was measured. The process was repeated until there was no corrosion product visibly adhered to the specimens and the subsequent weight measurements exhibited no change. The tensile properties of the steel coupons after the

environmental conditioning and the subsequent cleaning were measured according to ASTM A370-02.

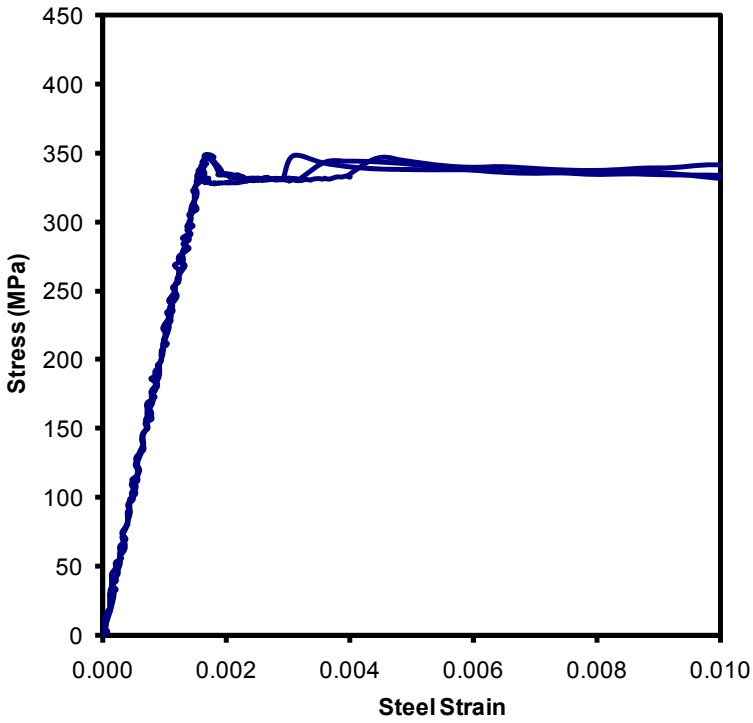

Figure 8.4 – Measured tensile stress-strain curve of the steel plate

8.2.2 CFRP Material Properties

The CFRP materials used in the experimental program were similar to those used for the bond and splice phase of the research. The CFRP materials consisted of a pultruded, high modulus CFRP material, ePLATE HM, which is distributed by Mitsubishi Chemical FP America Inc. The tensile properties of the CFRP were determined according to ASTM D3039-00. Three straight, 12 mm wide CFRP coupons were fabricated and tested in tension using an 890 kN MTS hydraulic testing machine. The measured stress-strain relationship of the CFRP up to failure is shown in Figure 8.5. The chord modulus of the CFRP was measured between strain values equivalent to 25 percent and 50 percent of the measured

ultimate strain of the CFRP respectively. The measured elastic modulus, failure strain and tension strength of the CFRP coupons are given in Table 8.1. All of the tested CFRP tension coupons failed due to rupture of the CFRP.

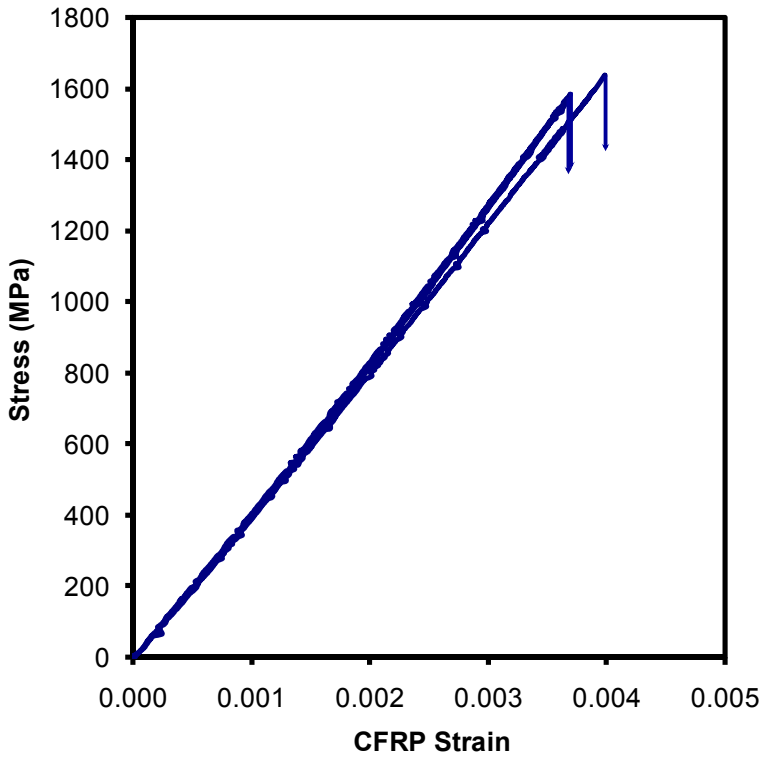

Figure 8.5 – Measured tensile stress-strain curve of the CFRP strips

Table 8.1 – Measured tensile properties of the CFRP strips

Coupon ID	Tensile Modulus (MPa)	Ultimate Tensile Strain	Tensile Strength (MPa)
CFRP-0-1	402,000	0.00398	1640
CFRP-0-2	423,000	0.00366	1570
CFRP-0-3	427,000	0.00368	1580
Average	417,000	0.00377	1600
Standard Deviation	13,000	0.00018	40
Coefficient of Variation	3.1%	4.8%	2.5%

To evaluate the effect of environmental exposure on the tensile properties of the CFRP, additional CFRP coupons were environmentally conditioned with the double-lap shear coupons and subsequently tested to failure.

8.2.3 Adhesive Material Properties

The adhesive material used in the experimental program was similar to that used for the bond and splice phase of the research. The SP systems Spabond 345 two-part epoxy adhesive was used. The tensile properties of the adhesive were determined according to ASTM D638-02. A 7.3 mm thick plate of the cured adhesive was fabricated by casting the adhesive into a rectangular mold. The adhesive was allowed to cure for one week and the dog-bone shaped tension coupons were cut from the plate. The coupons were tested in tension using a 90 kN Instron screw-driven universal testing machine. The experimentally determined stress-strain relationship of the adhesive is given in Figure 8.6. The tensile chord modulus of the adhesive was obtained between strain values corresponding to 5 percent and 20 percent of the average ultimate tension strain of the adhesive respectively. The experimentally determined elastic modulus, failure strain and tension strength of the adhesive coupons are given in Table 8.2.

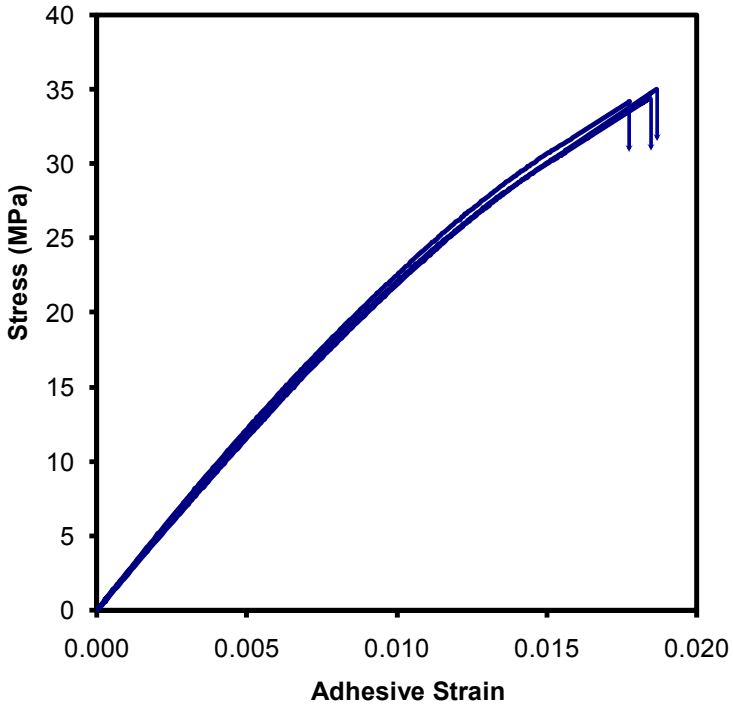

Figure 8.6 – Experimentally determined tensile stress-strain curve of the cured adhesive

Table 8.2 – Experimentally determined tensile properties of the cured adhesive

Coupon ID	Tensile Modulus (MPa)	Ultimate Tensile Strain	Tensile Strength (MPa)
Epoxy-0-1	2340	0.0186	35.1
Epoxy-0-2	2360	0.0181	34.1
Epoxy-0-3	2440	0.0178	34.2
Average	2380	0.0182	34.5
Standard Deviation	50	0.0004	0.6
Coefficient of Variation	2.1%	2.2%	1.7%

All of the tested adhesive coupons failed in a brittle manner due to rupture. Inspection of the tested coupons revealed the presence of several small air voids which formed during mixing and casting of the adhesive. The presence of these air voids may have slightly reduced the measured tensile strength and modulus of the adhesive. The presence of the air voids was consistently observed for all of the tested specimens. The primary objective of the material tests was to evaluate the effect of the environmental conditioning on the material properties

as installed. Therefore, the presence of the air voids was acceptable since it represents practical field applications. Additional adhesive coupons were also fabricated from the same original adhesive plate and environmentally conditioned with the double-lap shear specimens for subsequent material testing.

The glass transition temperature of the adhesive was determined using Differential Scanning Calorimetry according to ASTM E 1356-03 by Delson Testing Laboratories, Inc. (Ching, 2007). The specimens were fabricated from a thin film of the adhesive which was allowed to cure at room temperature for one week before sending it to the testing facility. Two specimens were taken from the film and tested independently. The specimens were both subjected to two heating scans between 40°C and 150°C. For both specimens, the first heating scan yielded a midpoint glass transition temperature, T_m, of 62°C. The first scan of the two specimens also yielded an exothermal peak at temperatures of 115°C and 117°C respectively. This suggests possible incomplete curing of the adhesive (J. Ching, personal communication, August 22, 2007, Lapique and Redford, 2002). This is expected since the adhesive was cured at room temperature and was not subjected to an elevated temperature post cure. This curing process is similar to the curing process which is typically used for strengthening typical bridges and structures. Therefore, the measured glass transition temperature, of 62°C, and the observed exothermic peak, at 115°C, are representative of the typical properties which can be expected for the adhesive in typical structural strengthening and retrofit applications.

8.3 ENVIRONMENTAL CONDITIONING

The overall testing program for the environmental durability study is given in Table 8.3. The program includes a total of 14 control specimens that were tested under laboratory conditions without any environmental conditioning. A total of 30 specimens were exposed to severe exposure conditions to accelerate the deterioration of the bond. This allowed comparison of the test results after a short duration of exposure. The accelerated exposure consisted of one

week wet/one week dry cycles in a 5% NaCl solution at a temperature of 38°C. During the wet portion of the cycle, the specimens were totally submerged in the NaCl solution and the temperature was maintained by a submersible water heater. During the dry cycle the specimens were exposed to ambient out-door temperatures. The specimens were protected from exposure to direct sunlight and rain. The experimental program was conducted from August 2, 2007 to February 11, 2008. The measured outdoor minimum, maximum and average temperatures during this period were -9°C, 40°C and 16°C respectively (National Weather Service Forecast Office, 2008). The experimental program included exposure durations of one, four and six months.

Table 8.3 – Environmental durability test matrix

Environmental Exposure	Bond Detail	Applied Load	Exposure Duration	Number of Repetitions
Control	A	T_{uA}	-	3
Laboratory Conditions	AS	T_{uAS}	-	3
	AG	T_{uAG}	-	4
	AGS	T_{uAGS}	-	4
Accelerated Exposure Wet/Dry Cycling 5% NaCl 38°C	A	0	1 month	2
			4 months	2
			6 months	2
		0.35 T_{uA}	1 month	2
			4 months	2
			6 months	2
	AS	0.35 T_{uA}	1 month	2
			4 months	2
			6 months	2
	AG	0.35 T_{uA}	1 month	2
			4 months	2
			6 months	2
	AGS	0.35 T_{uA}	1 month	2
			4 months	2
			6 months	2

The effect of sustained load on the environmental durability of the system was also considered. A total of 24 of the accelerated exposure specimens were subjected to a sustained load level of 15 kN which represents 35 percent of the average ultimate strength of the Detail A control specimens, T_{uA}. The specimens were conditioned in specially designed reinforced concrete tanks which are shown schematically in Figure 8.7. The tanks also acted as self-reacting frames to resist the applied load which was applied to the specimens. The environmental conditioning test setup is shown in Figure 8.8(a). The sustained load was applied using a specially designed fixture, shown in Figure 8.8(b), and the load level was monitored using two electrical resistance strain gauges mounted on each specimen near the loading fixture.

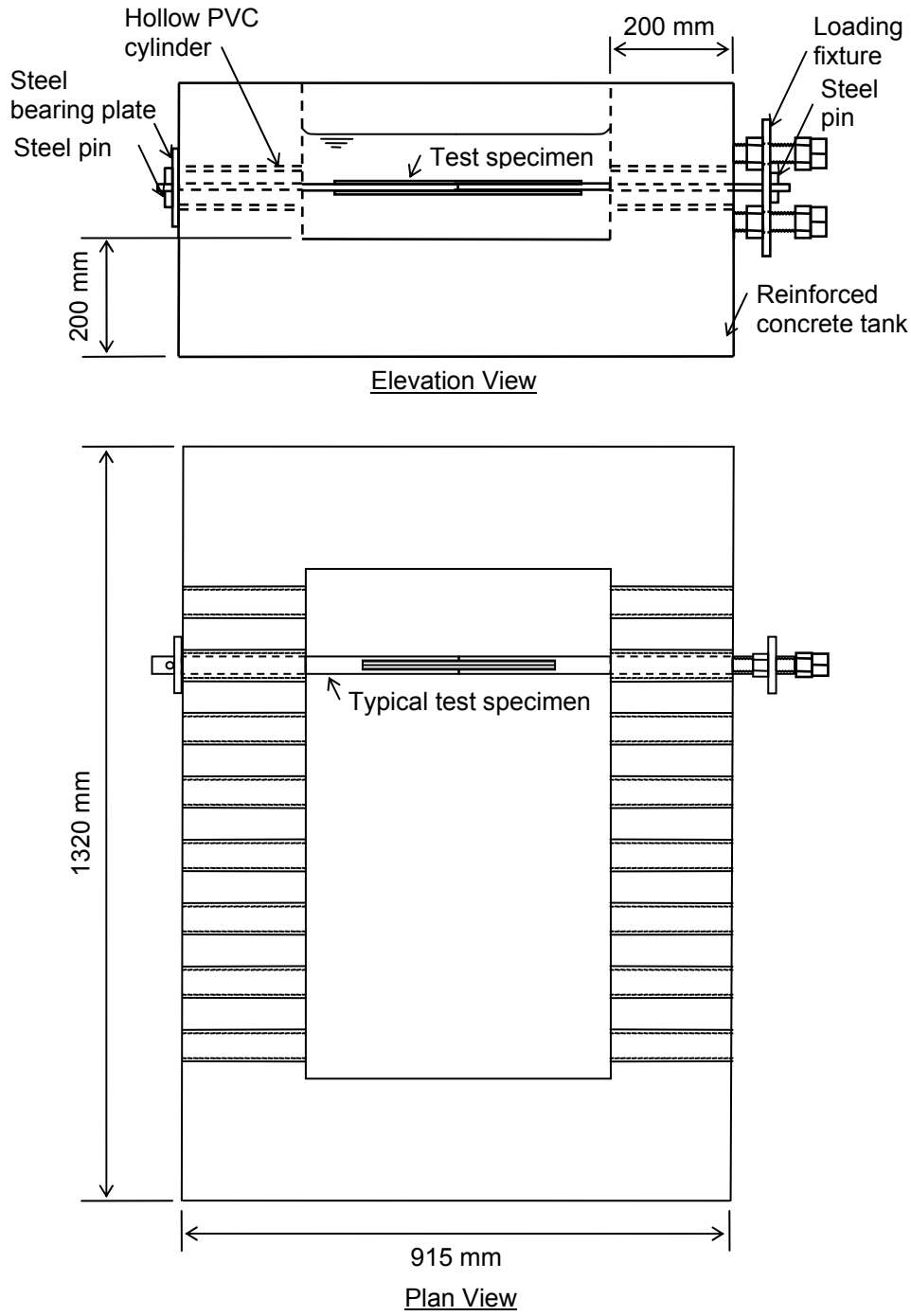

Figure 8.7 – Schematic of a typical reinforced concrete environmental conditioning tank

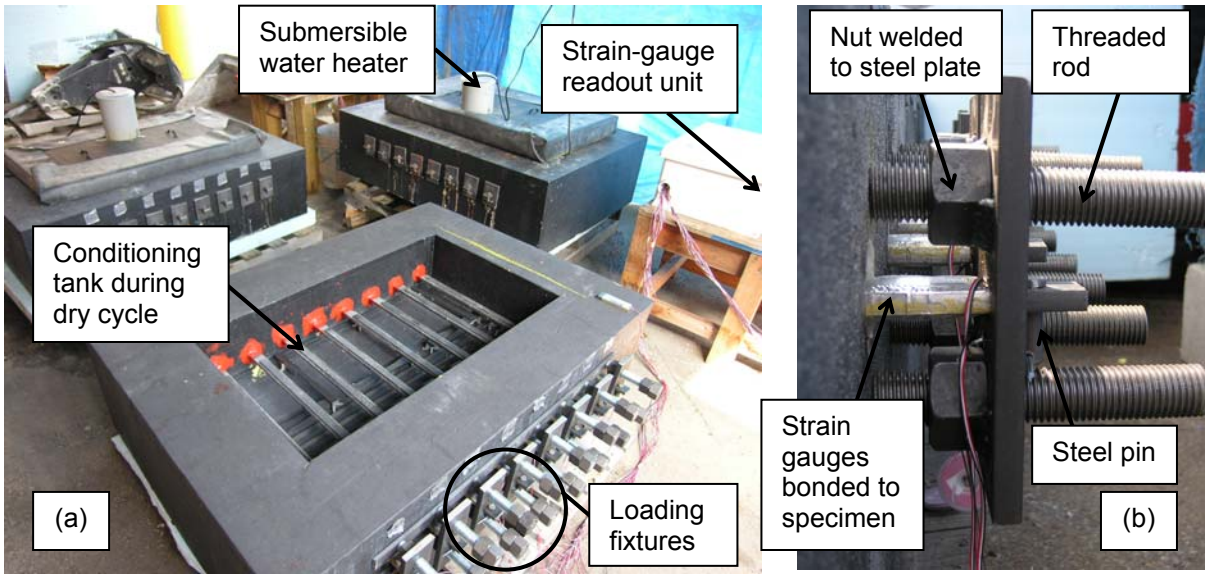

Figure 8.8 – (a) Environmental conditioning test setup and (b) loading fixtures

8.4 RESIDUAL STRENGTH TESTS

After reaching the specified duration of the environmental conditioning the specimens were loaded monotonically to failure in tension to determine the residual capacity of the bond between the steel and the CFRP. The specimens were tested using the same setup and testing procedure as the control specimen tests. All of the specimens were tested by an 890 kN hydraulic MTS testing machine using a constant displacement rate of 0.5 mm/min. The load and stroke of the machine were recorded using a data acquisition system connected to a personal computer. The initial distance between the grips of the machine, prior to loading the specimens, was set to 800 mm as shown in Figure 8.9. This was consistently maintained for all of the tested specimens, with the exception of the six Detail A specimens which were conditioned without being subjected a sustained load. Maintaining a consistent gauge length allowed direct comparison of the stroke as an indication of the degradation of the stiffness of the specimens. The six specimens that were conditioned without being subjected to a sustained load had a shorter overall length than the rest of the specimens. Therefore, these

specimens were tested with a shorter gauge length and evaluated on the basis of residual capacity only.

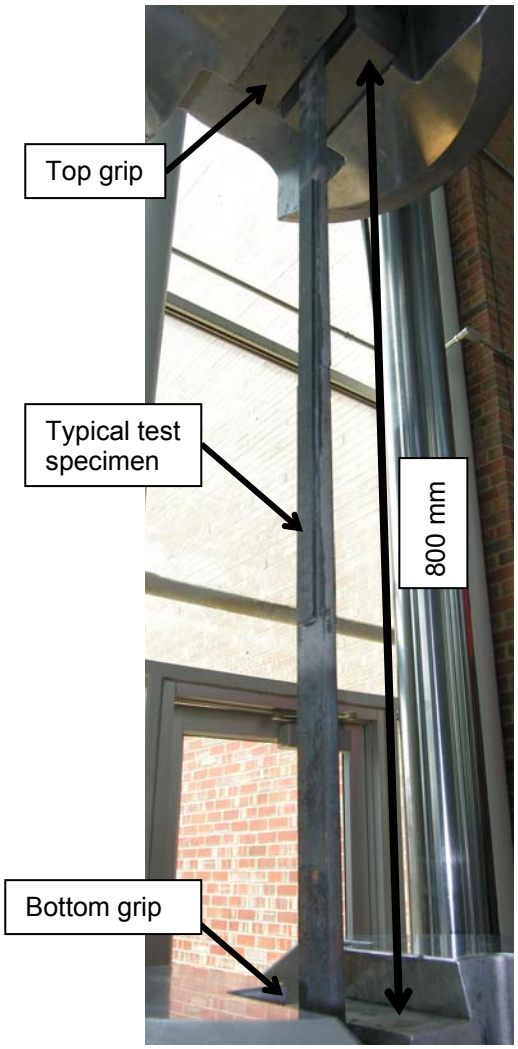

Figure 8.9 – Test setup for monotonic residual strength tests and control specimen tests

Chapter 9: Experimental Results & Discussion

This chapter presents the experimental results of the environmental durability study. The load-stroke behavior, elastic stiffness, observed failure mode and ultimate strength of the tested control specimens are presented and discussed in detail. The behavior of the specimens exposed to one month, four months and six months of environmental conditioning is summarized in subsequent sections and the detailed results are presented in Appendix B following the same sequence. The degradation of the properties of the materials due to the environmental exposure is also presented in this chapter. Finally the results of the tests for the different exposure durations are discussed and compared to the control specimens.

9.1 BEHAVIOR OF THE CONTROL SPECIMENS

A total of 14 double lap shear specimens were tested as control specimens to provide a basis for comparison of the results for the tested specimens that were subjected to severe environmental conditioning. The load-stroke behavior of the control specimens is presented in Figure 9.1(a)-(d) for the four different bond configurations tested in this phase. In general, the load-stroke behavior of all of the tested specimens was essentially linear up to failure. All of the tested double-lap shear specimens, with the exception of one of the detail AG specimens, failed due to debonding of one or both of the CFRP strips. One of the specimens with the AG bonding type failed due to yielding of the steel plate after which the specimen was unloaded.

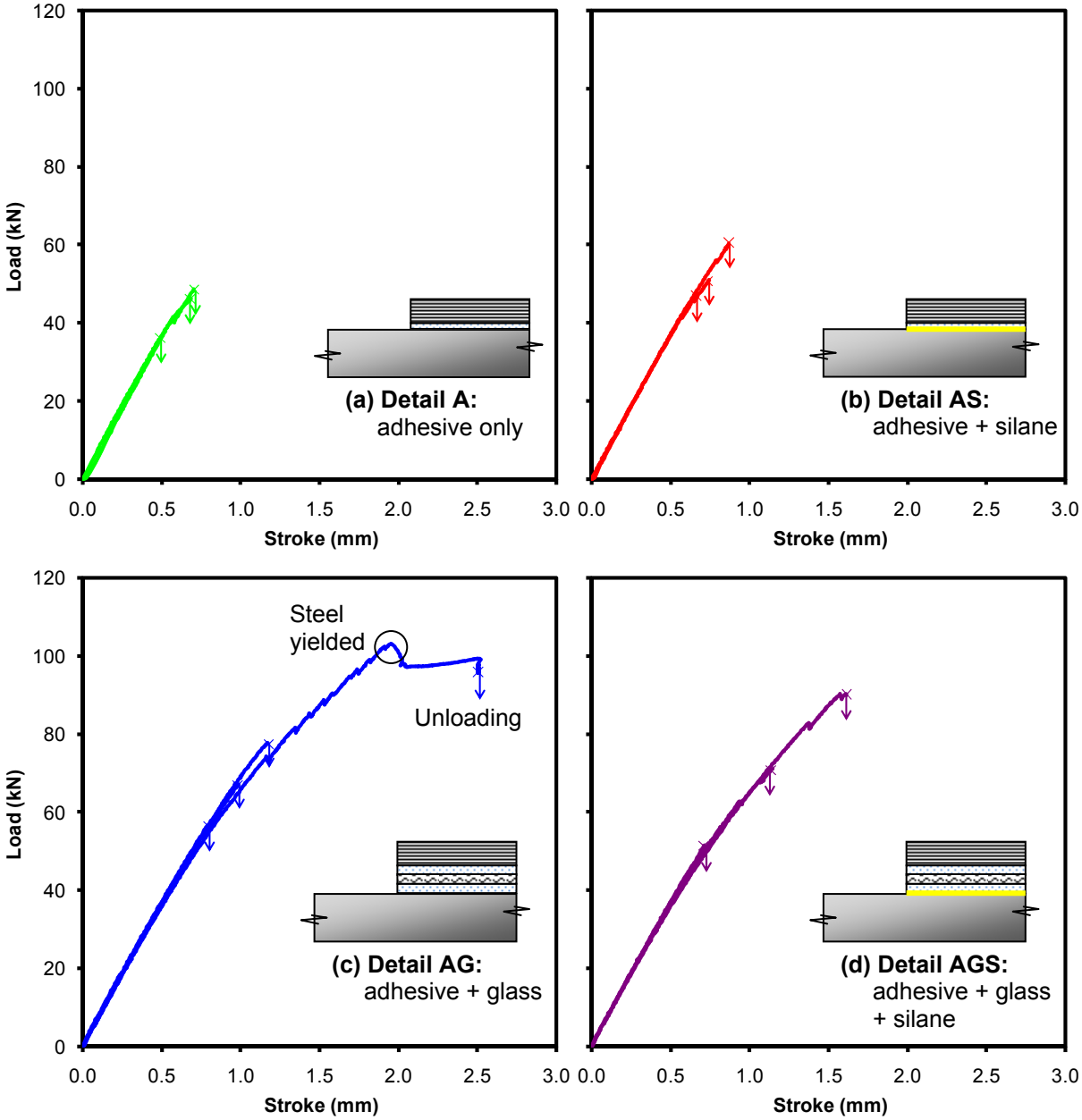

Figure 9.1 – Measured load-stroke behavior of environmental control specimens

The initial chord stiffness of the specimens, presented in Table 9.1, was determined between stroke values of 0.1 mm and 0.5 mm for the tested specimens. The measured stiffness for all of the tested specimens was comparable.

Table 9.1 – Measured chord stiffness of the environmental control specimens

Test Number	Detail A (kN/mm)	Detail AS (kN/mm)	Detail AG (kN/mm)	Detail AGS (kN/mm)
1	77.2	74.2	73.1	73.0
2	76.5	73.6	71.7	72.1
3	72.9	72.3	71.1	71.7
4	N/A*	N/A*	73.5	N/A**
Average	75.5	73.3	72.4	72.3
St. dev.	2.3	1.0	1.1	0.7
Coef. of var.	3.0%	1.3%	1.5%	0.9%

* only three specimens were tested
** data unavailable due to data acquisition error

Most of the tested control specimens failed due to debonding of one or both of the CFRP strips as shown in Figure 9.2. In the figure, the specimens are identified by a three part identifier which includes: the bond detail, a number indicating the exposure duration in months and a serial number to differentiate between multiple repetitions of the same specimen configuration. The failures typically occurred at the surface of the CFRP with a thin layer of fibers remaining attached to the steel plate. Some interfacial and combined failure modes were also observed. For the detail AG and AGS specimens, the failure typically occurred between the glass fiber layer and the CFRP with the glass fibers remaining bonded to the steel surface. Inspection of the failure surface indicated that, for some of the detail AG and AGS specimens the glass fiber sheet, which was embedded into the adhesive, shifted during fabrication. Consequently the glass fibers were only embedded into a portion of the adhesive layer and the remaining portion did not include any glass fibers.

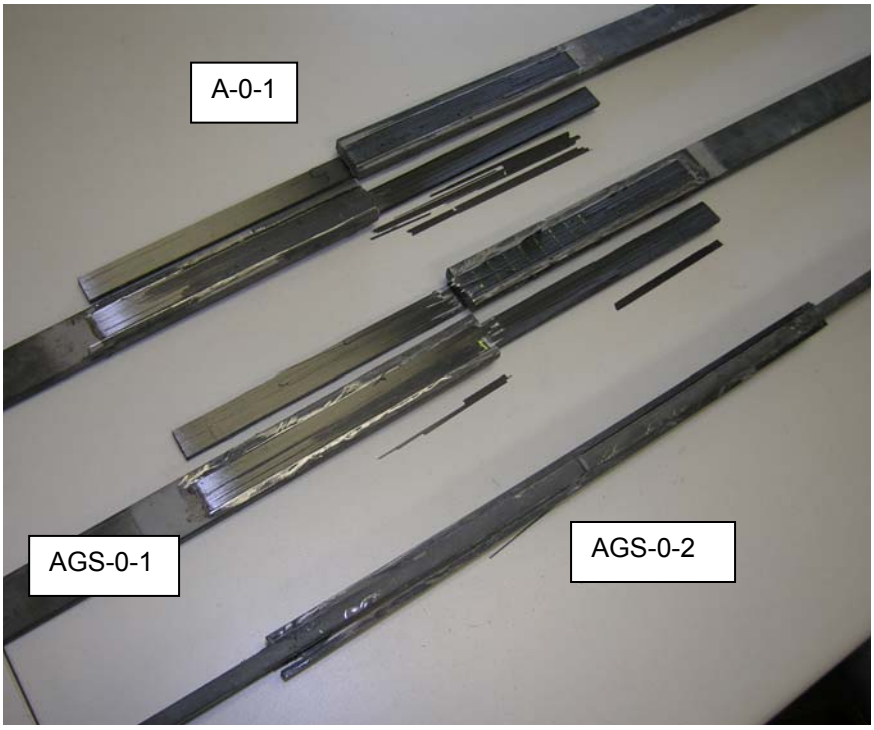

Figure 9.2 – Typical failed control specimens

The measured ultimate capacities of the tested control specimens are given in Table 9.2. Comparison of the average ultimate strength for the Detail A and Detail AS specimens suggests that the use of the silane adhesion promoter increased the average measured bond strength by 20 percent. However, when considering the scatter of the experimental results it appears that some of the observed difference may be due to the statistical variation of the bond strength rather than due to the effect of the silane adhesion promoter. Comparison of the Detail A and Detail AG specimens indicates that the presence of the glass fiber layer increased the average measured bond strength by 74 percent. The observed increase of the measured ultimate strength suggests that the presence of the glass fibers acted as reinforcement for the adhesive and retarded the propagation of cracks through the adhesive layer, similarly to the effect of reinforcing bars in concrete. However, the Detail AG specimens also exhibited a significantly higher standard deviation and coefficient of variation

than the specimens without glass fibers in the adhesive layer. The increase of the standard deviation may have possibly been due to the observed shifting of the glass fibers within the adhesive layer during fabrication which was previously noted. Comparison of the Detail AG and Detail AGS specimens indicates no significant difference of the average measured ultimate strength. Again, the observed difference is likely due to the statistical variation of the bond strength rather than due to the effect of the silane.

Table 9.2 – Measured ultimate strength of the tested control double-lap shear specimens

Test Number	Detail A (kN/mm)	Detail AS (kN/mm)	Detail AG (kN/mm)	Detail AGS (kN/mm)
1	46.2	51.2	77.5	51.5
2	48.6	46.9	56.5	71.0
3	36.3	60.4	103.1	90.0
4	N/A*	N/A*	67.0	66.2
Average	43.7	52.8	76.0	69.7
St. dev.	6.6	6.9	20	15.9
Coef. of var.	15%	13%	26%	23%

* only three specimens were tested

9.2 TEST RESULTS AFTER ONE MONTH ENVIRONMENTAL EXPOSURE

After one month of exposure, ten of the double-lap shear specimens were removed from the environmental conditioning tanks and tested monotonically to failure to evaluate the residual strength of the bond. Eight of the specimens, two of each bond configuration, were subjected to sustained loading during the environmental conditioning while the remaining two were left unloaded. Figure 9.3 shows the eight specimens, which were subjected to a sustained load during the conditioning, after removal from the environmental conditioning tank. Inspection of the figure indicates the presence of noticeable corrosion on the steel portion of the specimens. The figure also indicates deposition of corrosion products onto the surface of the FRP causing discoloration. However, there is no noticeable difference in the degree of degradation between the different bond configurations. Visual inspection of the specimens did not reveal any debonded regions or degradation of the CFRP materials.

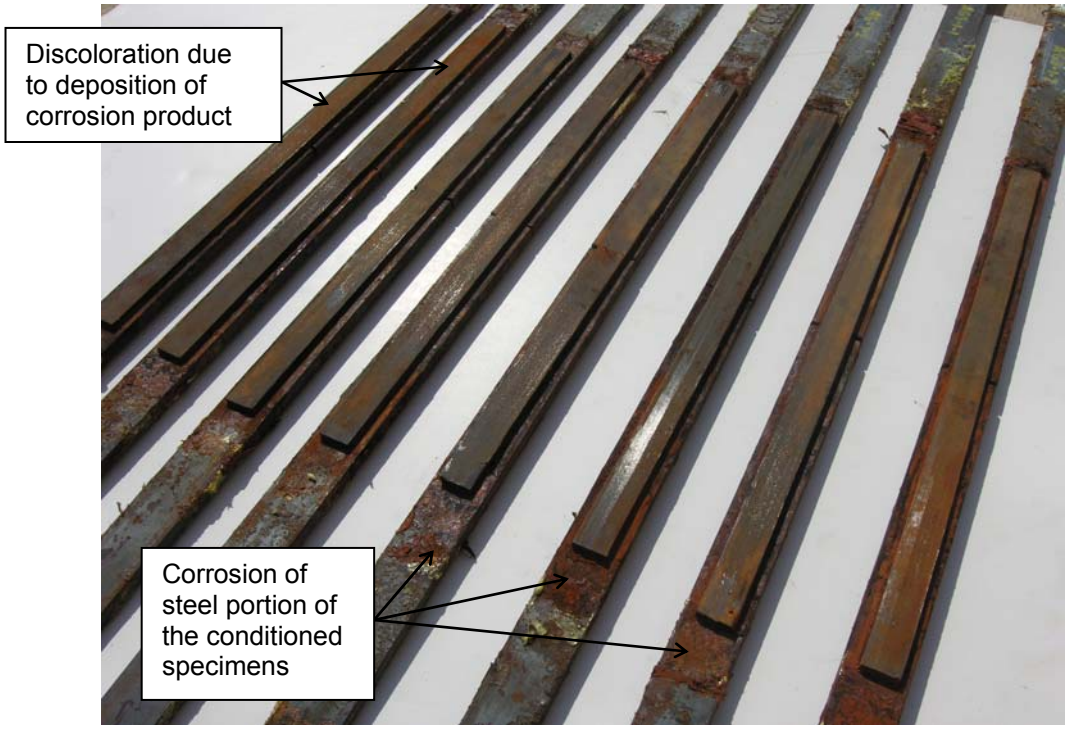

Figure 9.3 – Degradation of the test specimens after one month of environmental conditioning

Upon testing of the conditioned specimens to failure, the observed behavior was similar to that of the unconditioned control specimens. All of the specimens failed due to debonding of the CFRP strips from the steel surface. The observed failure mode was typically a shallow interlaminar failure within the CFRP with a thin layer of carbon fibers remaining bonded to the CFRP. The failure of the Detail AGS specimens, shown in Figure 9.4, occurred within the glass fiber layer with some of the glass fibers remaining bonded to the CFRP strip and some remaining bonded to the steel surface. A significant amount of dry glass fibers were observed along the failure surface indicating only partial impregnation of the glass fibers by the adhesive.

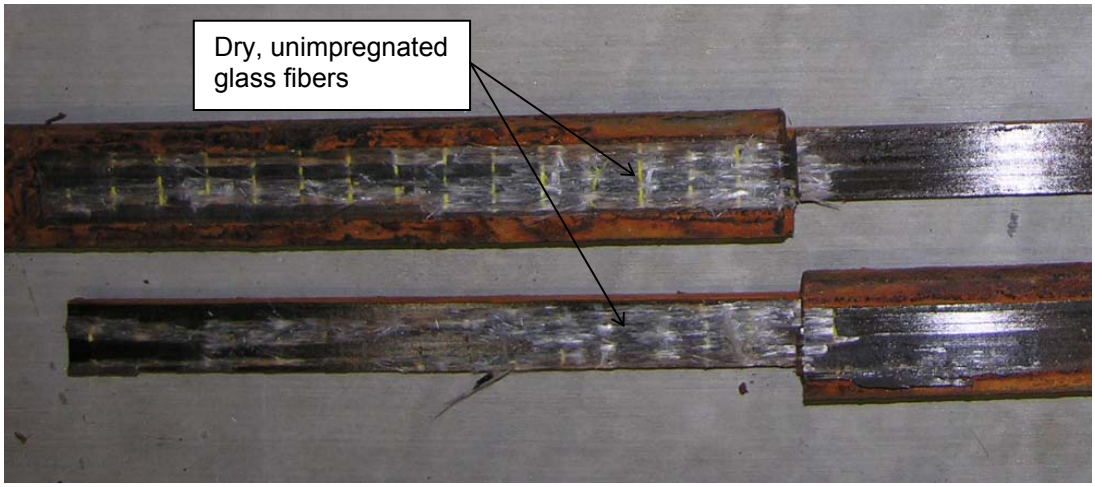

Figure 9.4 – Failure surface of the Detail AGS specimens after one month of conditioning

A detailed comparison of the test results with the results of the other tests is presented later in the chapter.

9.3 TEST RESULTS AFTER FOUR MONTHS ENVIRONMENTAL EXPOSURE

A total of ten specimens were subjected to environmental conditioning for four months. Eight of the specimens were subjected to a sustained load while two of the Detail A specimens were unloaded. After the completion of four months of environmental conditioning one of the CFRP strips for one of the loaded Detail A specimens was totally debonded from the steel surface. The failed specimen is shown in Figure 9.5 immediately after the observation of the failure. The environmental exposure obviously caused degradation of the bond which led to failure of the specimen under the effect of the 15 kN sustained load. Inspection of the remaining specimens indicated partial debonding of one of the remaining Detail A specimens which was not subjected to an applied load. The remaining specimens exhibited noticeable degradation including severe corrosion of the steel and noticeable buildup of corrosion products on and discoloration of the CFRP. No debonding was observed for any of the other specimens.

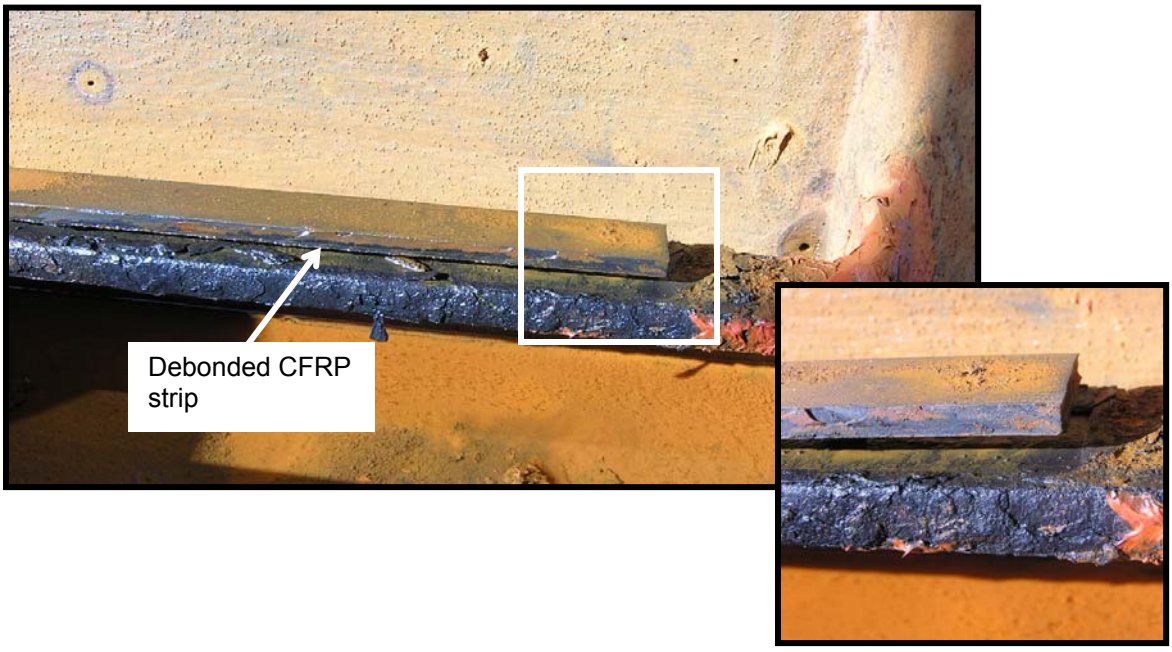

Figure 9.5 – Debonding failure of one of the Detail A specimens after four months of environmental conditioning

The specimens were subsequently tested to failure to evaluate the residual capacity of the bond between the CFRP and the steel. Similarly to the previously tested specimens, the failure mode was primarily interlaminar within the surface layers of the CFRP strip. The failure surfaces of one the Detail A, Detail AS and Detail AGS specimens are shown in Figure 9.6(a) – (c) respectively. Inspection of the failure surface of the Detail A specimen, shown in Figure 9.6(a), revealed the presence of a discolored, partially debonded region near the edges of the CFRP strip. This indicates possible ingress of moisture into the interfacial region between the adhesive and the steel. The discoloration may also possibly be due to galvanic corrosion of the steel at the interface. Inspection of the Detail AS failure surface, shown in Figure 9.6(b), revealed a complete bond between the steel and the CFRP strip without any discoloration or indication of degradation. This suggests that the presence of the silane effectively prevented ingress of moisture into the interfacial region and helped to enhance the environmental durability of the bond. Inspection of the failure surface for the

Detail AGS specimen, shown in Figure 9.6(c), revealed that the glass fiber layer within the adhesive was largely unimpregnated with adhesive. The dry glass fibers had a rust-colored discoloration which suggests wicking of moisture and deposition of corrosion product along the dry fibers.

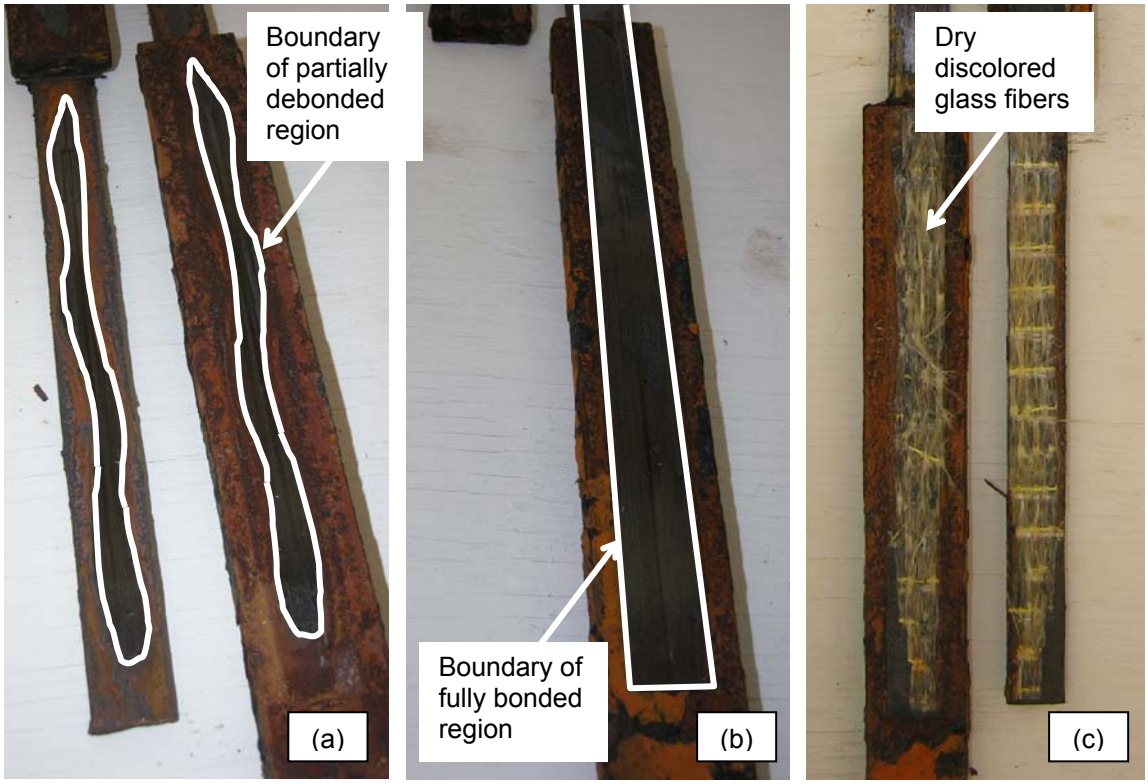

Figure 9.6 – Failure surfaces of (a) Detail A, (b) Detail AS and (c) Detail AGS specimens after four months of environmental conditioning

9.4 TEST RESULTS AFTER SIX MONTHS ENVIRONMENTAL EXPOSURE

A total of ten double-lap shear specimens were subjected to environmental conditioning for six months. Eight of the specimens were subjected to a sustained load while two specimens were not loaded. After 17 weeks of exposure, one of the loaded Detail A specimens failed by total debonding of one of the CFRP strips from the steel surface under the effect of the

sustained load. The remaining specimens were left in the environmental conditioning tank for the remainder of the six month conditioning period. Upon completion of the conditioning the specimens were removed from the tank, visually inspected and tested to failure to determine the residual bond capacity of the specimens. The visual inspection indicated that the remaining Detail A specimen that was subjected to a sustained load, and one of the unloaded specimens both exhibited partial debonding of the CFRP strips. All of the specimens had significant buildup of corrosion product on the steel with severe scaling and flaking of the surface layers of the steel. Significant deposition of the corrosion product onto the CFRP and discoloration were observed as shown in Figure 9.7. Upon testing the conditioned specimens to failure, the observed behavior and failure mode were similar to that of the specimens exposed to four months of environmental conditioning.

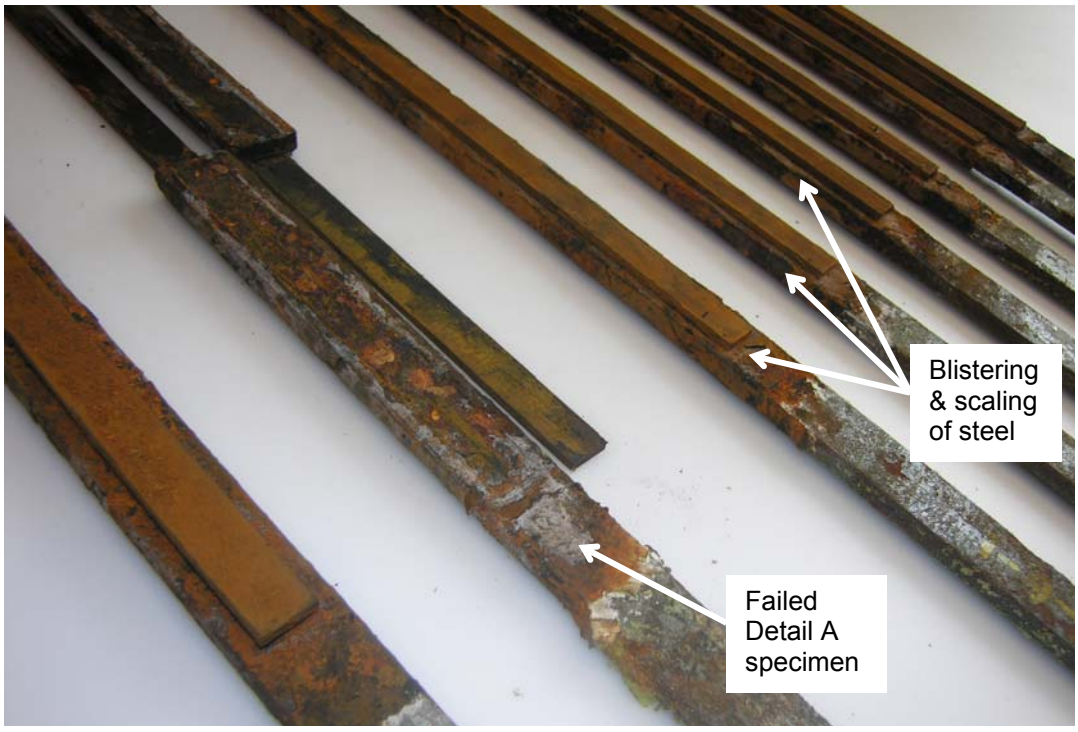

Figure 9.7 – Double-lap shear specimens after six months of environmental conditioning

9.5 MATERIAL DEGRADATION

To evaluate the effect of the environmental conditioning on the material properties of the steel, CFRP and adhesive, tension specimens of the materials were also conditioned along with the double-lap shear specimens. Three specimens of each material were conditioned for the exposure durations of one, four and six months and subsequently tested to failure to determine the failure strength, failure strain and tensile stiffness of the materials. Due to instrument failure, in some cases only two sets of test results were obtained for a given group of specimens. The steel specimens were first cleaned and weighed to evaluate the mass loss due to corrosion. The degradation of the material properties of the steel, CFRP and adhesive is presented in Figure 9.8(a), (b) and (c) respectively.

Figure 9.8(a) shows the degradation of the yield strength, stiffness and mass of the tested steel coupons for the different exposure durations considered. The values are normalized with respect to the average parameter values for the unconditioned coupons. The experimental scatter of the results is shown by the error bars in the figure. Inspection of the figure indicates that the degradation of the three parameters is comparable throughout the six month exposure duration with a maximum loss of strength, stiffness and mass of approximately 20 percent. The measured loss of the strength and stiffness of the steel are likely due to loss of cross-sectional area of the specimens due to corrosion rather than degradation of the material properties themselves.

Figure 9.8(b) shows the degradation of the strength, ultimate strain and stiffness of the CFRP specimens. It should be noted that all of the CFRP coupons which were conditioned for four months failed due to debonding of the CFRP in the grip region. Consequently, the test results were not representative of the actual material properties and, therefore, these tests were neglected. To avoid a debonding type failure, the six month coupons were first machined to a dog bone shape with a reduced section in the center portion to induce a rupture type failure mode. Prior to testing two of the coupons were damaged and, therefore, could

not be tested. The test results of the remaining coupon indicate that there was essentially no change of the material properties of the CFRP after six months of severe environmental exposure as shown in Figure 9.8(b).

Figure 9.8(c) shows the environmental degradation of the adhesive strength, failure strain and stiffness. After six months of exposure the strength, ultimate strain, and stiffness of the adhesive degraded by 10 percent, 14 percent, and 4 percent respectively. The standard deviation of the measured strength and ultimate strain also increased significantly after the four and six month exposure durations. This reflects the increased uncertainty of the material properties due to the effect of the environmental degradation. The trend of the results suggests that the measured parameter values after four months of exposure are anomalously low. This may have been due to damage of the specimens during fabrication or handling.

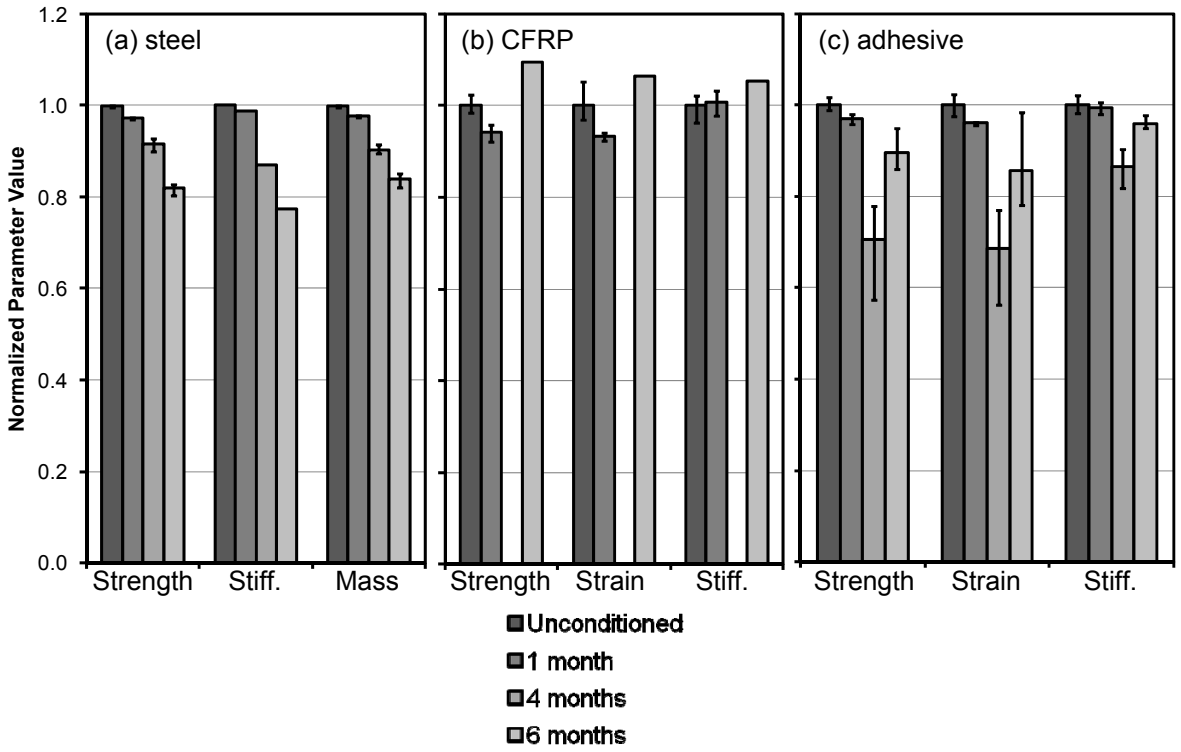

Figure 9.8 – Degradation of (a) steel, (b) CFRP and (c) adhesive material characteristics

9.6 COMPARISON AND DISCUSSION

The following section presents a comparison of the measured tensile stiffness and ultimate strength of all of the double lap shear specimens that were tested throughout the environmental durability study. The degradation of the elastic stiffness of the tested specimens is given in Figure 9.9 for each of the different tested bond details. The range of the experimental results is represented by the error bars in the figure. Inspection of the figure indicates a minimal variation of the measured stiffness for all of the tested specimens, regardless of the bond detail or the exposure duration. The one notable exception is the stiffness of the Detail A configuration after six months of conditioning. As previously noted, during the environmental conditioning one of the Detail A specimens failed under the effect of the sustained load. The remaining Detail A specimen was partially debonded at the conclusion of the conditioning. This resulted in a significant reduction of the measured stiffness of the specimen as shown in the figure.

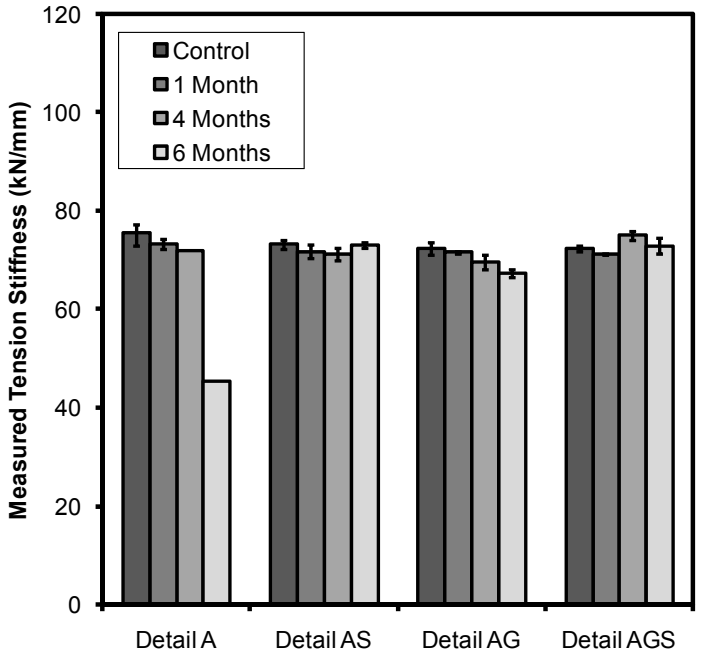

Figure 9.9 – Measured stiffness degradation of the tested bond details

The measured degradation of the tension strength of the tested double-lap shear specimens is given in Figure 9.10 for the four different bond details. Inspection of the figure reveals several interesting trends. The Detail A specimens represent typical use of the adhesive without any special arrangements to enhance the bond durability. Comparison of the test results in Figure 9.10 indicates a 60 percent reduction of the measured tension strength after six months of environmental conditioning. This highlights the need to include some form of supplemental protection to enhance the environmental durability of the system. The increase of the measured strength of the Detail A specimens after only one month of conditioning is anomalous and should not be relied on for design purposes. The measured increase of strength may represent the inherent statistical variation of the bond strength. It may also possibly be due to post curing of the adhesive due to the elevated temperature associated with the environmental conditioning.

Comparison of the results for the Detail AS specimens indicates that the presence of the silane adhesion promoter significantly enhanced the environmental durability of the bond. No significant degradation of the bond strength was measured after completion of the six month duration of the environmental conditioning.

A similar trend was observed for the Detail AG and AGS specimens. These bond details included an additional layer of glass fiber embedded in the adhesive layer. As previously noted, the presence of the glass fiber layer helped to increase the initial bond strength of the tested double-lap shear specimens. However, the measured degradation of the bond strength was 55 percent which is comparable to the degradation of the Detail A specimens. This suggests that the presence of the glass fibers did not significantly increase the durability of the system. By comparison, the Detail AGS specimens, which included both silane and glass fibers, exhibited a significant increase of the initial bond strength as compared to the Detail A specimens while exhibiting only a minimal degradation of the bond strength.

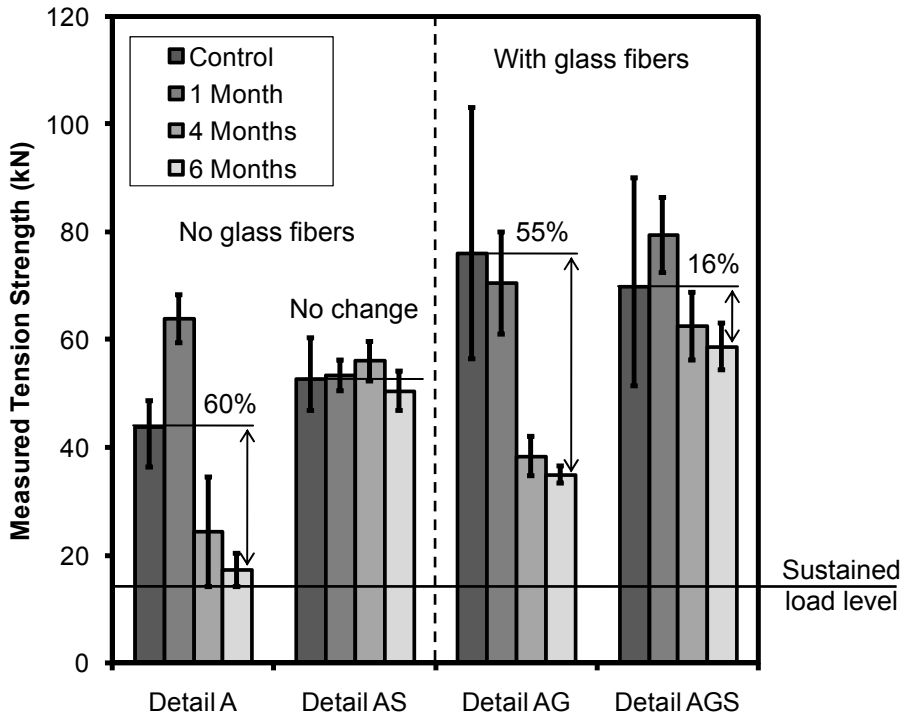

Figure 9.10 – Measured strength degradation of the tested bond details

It is interesting to note that, for the Detail A and Detail AG bond configurations, the measured degradation of the bond strength was approximately 60 percent. This is approximately six times the magnitude of the measured degradation of the adhesive tension strength. This suggests that, while degradation of the adhesive may have contributed to the bond degradation, some additional mechanisms must also have been involved. The test results indicate that pre-treating the steel surface with silane was essential to maintain the durability of the bond regardless of the presence or absence of the glass fiber layer. This suggests that the degradation of the bond strength was primarily due to ingress of moisture into the interfacial region between the steel and the adhesive. Wicking of moisture along the dry glass fibers, absorption of moisture into the adhesive and galvanic corrosion may also have affected the bond durability as observed by the failure surfaces of some of the tested double-lap shear specimens.

The effect of the sustained load on the bond durability is shown in Figure 9.11. The figure presents the measured residual tension strength of the Detail A double-lap shear specimens which were conditioned with and without the effect of the sustained load. The figure indicates that the measured average tension strength of the unloaded specimens was slightly higher than that of the loaded specimens after four and six months of conditioning. However, the variation is within the experimental scatter of the results. It is likely that the applied load level was not sufficient to induce significant cracking or distress to the bond and therefore the applied load did not have a significant effect on the bond durability.

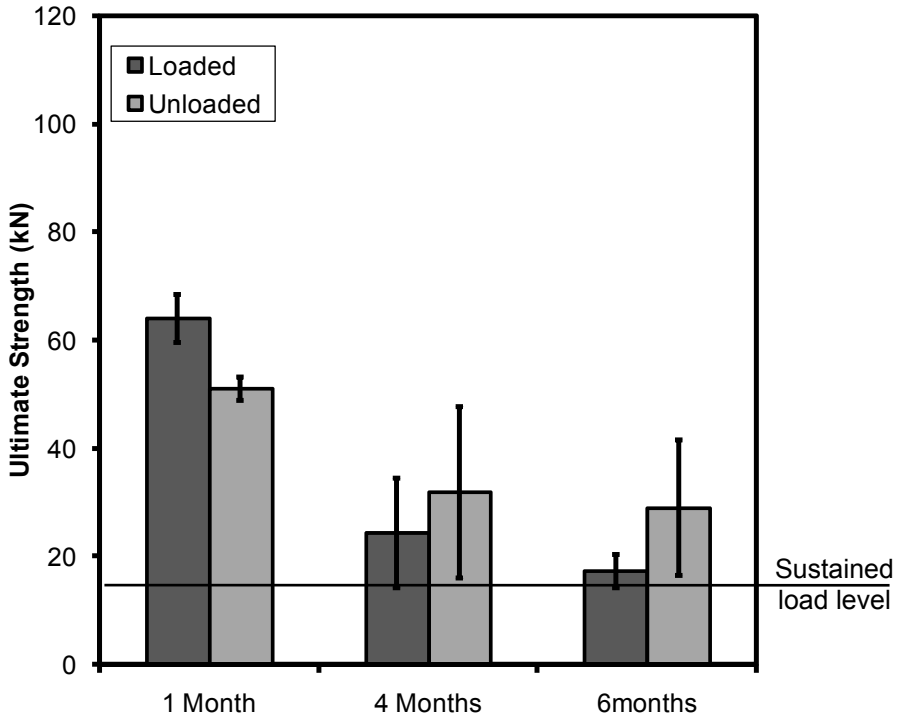

Figure 9.11 – Effect of sustained load on bond durability

Chapter 10: Conclusions and Future Work

An experimental program was conducted to evaluate the environmental durability of the bond between CFRP strips and steel surfaces. Conclusions of the research program and the recommended future work are presented in the following sections.

10.1 SUMMARY AND CONCLUSIONS

The experimental program consisted of four different configurations to bond the CFRP strips to steel surfaces. The first configuration consisted of applying a thin layer of adhesive to the steel surface without any additional methods to enhance the bond durability. The second configuration included pre-treating the steel surface with a silane coupling agent prior to applying the adhesive. In the third configuration a glass fiber layer was embedded in the adhesive layer to prevent possible galvanic degradation of the two adherends. The final configuration implemented both the silane adhesion promoter and the glass fiber layer. The research findings led to the following conclusions:

- The specimens that did not include any additional environmental protection exhibited a 60 percent reduction of the measured bond strength after six months of exposure to severe accelerated exposure conditions. The inspection of the failure surface suggested that the failure was primarily due to degradation of the interface between the adhesive and the steel surface due to moisture ingress and possibly also due to degradation of the adhesive properties.

- Pretreatment of the steel surface with a compatible silane coupling agent was essential to ensure the bond durability of the strengthening system. The Dow Corning Z-6040 γ-GPS silane enhanced the durability of the interface between the steel and the Spabond 345 epoxy adhesive. Specimens that were pretreated with silane did not exhibit any significant degradation of the bond strength after six months of severe exposure. This is

consistent with the findings of other researchers, presented in Chapter 2, which indicate that silane creates primary bonds at the steel-adhesive interface which are more environmentally stable than the van der Waals forces which are typically attributed to adhesion between dissimilar materials. The steel surface should be degreased with acetone, grit blasted and re-cleaned with acetone. The silane should be brushed onto the surface in a 4 percent solution with methanol by weight and allowed to dry for approximately one hour prior to applying the adhesive. Application of the silane onto the steel surface should occur as soon after grit blasting as possible.

- The presence of a unidirectional glass fiber layer increased the average measured initial bond strength between the steel and the adhesive by 74 percent compared to the specimens that were prepared with adhesive only. The presence of the glass fibers likely acted as reinforcement for the adhesive and helped to prevent the propagation of cracks in the adhesive layer. However, the standard deviation of the measured bond strength approximately tripled compared to the case with adhesive only. Shifting of the fibers within the adhesive layer during fabrication is believed to have lead to the significant variation of the measured bond strength. Care should be taken to ensure that the glass fibers are properly aligned and that they do not shift during installation.

- The presence of the glass fiber layer alone did not significantly enhance the environmental durability of the bonded joints. Specimens that included a glass fiber layer in the adhesive layer without pretreatment of the steel surface exhibited a 55 percent reduction of the average measured bond strength after six months of accelerated exposure. This is comparable to the measured degradation of the specimens which were bonded with adhesive only. Inspection of the failure surface indicated incomplete wetting of the fibers by the adhesive due to the high viscosity of the adhesive used. Wicking of water along the dry fibers may have contributed to the degradation of the bond.

- The combination of a glass fiber layer and the use of a silane pretreatment helped to enhance the average measured initial strength and the environmental durability of the bonded joints. After six months of severe environmental exposure the measured average bond strength decreased by 16 percent compared to the unconditioned specimens. This suggests that, while the silane pretreatment help to enhance the durability of the steel/adhesive interface, wicking of moisture along the dry fibers or possibly degradation of the adhesive properties likely still contributed to the measured bond degradation.

- Specimens with and without glass fibers exhibited similar levels of strength degradation under the effect of accelerated environmental exposure. The measured strength degradation was likely primarily due to the degradation of the steel/adhesive interface, which was prevented by the use of a silane primer. This suggests that the adhesive provided sufficient insulation between the steel surface and the CFRP material to prevent galvanic coupling of the two materials. However, the enhancement of the bond strength due to the presence of the glass fibers should be examined further.

- The measured tension strength, elastic modulus and failure strain of the adhesive decreased by 10 percent, 14 percent and 4 percent respectively after six months of severe environmental exposure. The degradation of the adhesive may have contributed to the overall degradation of the bonded specimens. However, the magnitude of the measured strength degradation is insufficient to account for the overall bond degradation. Therefore, other mechanisms of degradation must have contributed to the bond degradation as previously described.

- Application of a sustained load did not significantly accelerate the degradation of the tested specimens compared to unloaded specimens. The applied load level was equal to 35 percent of the average measured initial strength of the specimens that were bonded using adhesive only.

- The measured degradation of the stiffness of the bonded joints was negligible for all of the bond configurations studied.

- The midpoint glass transition temperature of the adhesive, T_m, was measured by Differential Scanning Calorimetry as 62°C. This should be adequate to prevent softening of the adhesive for most structural applications.

10.2 RECOMMENDED FUTURE WORK

While the current research program led to several interesting conclusions regarding the environmental durability of the proposed strengthening system, additional research work would also be beneficial. Recommended topics for future research include:

- Evaluation of the environmental durability of the strengthening system under extended exposure to natural environmental conditions. The current research work focused on evaluation of the relative performance of different bonding methods by accelerated exposure tests. However, comparably little is known about the performance of the strengthening system under natural environmental exposure conditions. Evaluation of system under natural environmental exposure may provide valuable additional information regarding the critical deterioration mechanisms that affect the performance of the strengthening system.

- Further research is needed to assess the effectiveness of embedding a glass fiber layer in the adhesive to enhance the bond strength between CFRP and steel surfaces. The findings of the current research suggest that the use of glass fibers may be beneficial to enhance the bond strength. However, further research is needed to fully understand the mechanism of action of the glass fibers. Further, the standard deviation of the measured strength of the specimens which included glass fibers may limit the applicability of this technique. Additional research is required to study the contribution of the glass fibers to

the bond strength and to develop a suitable installation method to ensure consistency of the bond strength.

- The effect of temperature changes on the bond stresses within the adhesive layer has not been investigated in detail. The effect of elevated temperature on the bond stresses due to the effect of the thermal mismatch between the steel and the CFRP should be investigated.

References

Abdel Wahab, M.M., Crocombe, A.D., Beevers, A. and Ebtehaj, K. (2002). Coupled stress-diffusion analysis for durability study in adhesively bonded joints. *International journal of Adhesion & Adhesives, 22,* 61-73.

Abel, M.L., Allington, R.P., Digby, R.P., Porrittt, N., Shaw, S.J., and Watts, J.F. (2006). Understanding the relationship between silane application conditions, bond durability and locus of failure. *International Journal of Adhesion & Adhesives, 26,* 2-15.

Adams, R.D. (Ed.). (2005). *Adhesive bonding: Science, technology and applications.* Boca Raton: CRC.

Adams, R.D., Atkins, R.W. Harris, J.A. and Kinloch, A.J. (1986). Stress analysis and failure properties of carbon-fibre-reinforced-plastic/steel double-lap joints. *Journal of Adhesion, 20,* 29-53.

Adams, R.D. and Peppiatt, N.A. (1977). Stress analysis of adhesive bonded tubular lap joints. *Journal of Adhesion, 9,* 1-18.

Albat, A.M., and Romily, D.P. (1999). A direct linear-elastic analysis of double symmetric bonded joints and reinforcements. *Composites Science and Technology, 59,* 1127-1137.

Al-Emrani, M. and Kliger, R. (2006a). Analysis of interfacial sear stresses in beams strengthened with bonded prestressed laminates. *Composites: Part B, 37,* 265-272.

Al-Emrani, M. and Kliger, R. (2006b). Experimental and numerical investigation of the behaviour and strength of composite steel-CFRP members. *Advances in Structural engineering, 9(6),* 819-830.

Al-Saidy, A.H., Klaiber, F.W. and Wipf, T.J. (2004). Repair of steel composite beams with carbon fiber-reinforced polymer plates. *Journal of Composites for Construction, 8(2),* 163-172.

American Institute of Steel Construction. (2005). *Steel Construction Manual* (13th ed.). Chicago: American Institute of Steel Construction.

Andresen, H.W. and Echtermeyer, A.T. (2006). Critical energy release rate for a CSM reinforced carbon fibre composite/steel bonding. *Composites: Part A, 37,* 742-751.

Ashcroft, I.A., Digby, R.P. and Shaw, S.J. (2001). A comparison of laboratory-conditioned and naturally-weathered bonded joints. *Journal of Adhesion, 75,* 175-201.

ASTM International. (2000). *D 3039/D 3039 M-00 Standard test method for tensile properties of polymer matrix composite materials*. West Conshohocken, PA.

ASTM International. (2003). *A 370-02 Standard test methods and definitions for mechanical testing of steel products*. West Conshohocken, PA.

ASTM International. (2003). *D 638-03 Standard test method for tensile properties of plastics*. West Conshohocken, PA.

ASTM International. (2003). *E 1356-03 Standard test method for assignment of the glass transition temperature by differential scanning calorimetry*. West Conshohocken, PA.

ASTM International. (2003). *G 1-03 Standard practice for preparing, cleaning , and evaluating corrosion test specimens*. West Conshohocken, PA.

Baldan, A. (2004a). Review adhesively-bonded joints and repairs in metallic alloys, polymers and composite materials: Adhesives, adhesion theories and surface pretreatment. *Journal of Materials Science, 39,* 1-49.

Baldan, A. (2004b). Review adhesively-bonded joints in metallic alloys, polymers and composite materials: Mechanical and environmental durability performance. *Journal of Materials Science, 39,* 4729-4797.

Bambach, M.R. and Elchalakani, M. (2007). Plastic mechanism analysis of steel SHS strengthened with CFRP under large axial deformation. *Thin-Walled Structures, 45,* 159-170.

Bambach, M.R., Elchalakani, M. Zhao, X.L. (2008). Composite steel-CFRP SHS tubes under axial impact, *Composite Structures, doi:10.1016/j.compstruct.2008.02.008.*

Bassetti, A., Nussbaumer, A. and Hirt, M.A. (2000). Crack repair and fatigue life extension of riveted bridge members using composite materials. *Bridge Engineering Conference ESE-IABSE-FIB 26-30 March 2000, Sharm El Sheikh (Egypt), 1,* 227-238.

Belingardi, G., Goglio, L. and Tarditi, A. (2002). Investigating the effect of spew and chamfer size on the stresses in metal/plastics adhesive joints. *International Journal of Adhesion & Adhesives, 22,* 273-282.

Bellucci, F. (1991). Galvanic corrosion between nonmetallic composites and metals: I effect of metal and temperature. *Corrosion Engineering, 47(10),* 808-819.

Bellucci, F. (1992). Galvanic corrosion between nonmetallic composites and metals: II effect of area ratio and environmental degradation. *Corrosion Engineering, 48(4),* 281-291.

Bocciarelli, M., Colombi, P., Fava, G. and Poggi, C. (2008). Fatigue performance of tensile steel members strengthened with CFRP plates. *Composite Structures, doi:10.1016/j.compstruct.2008.02.004.*

Brown. A.R.G. (1974). The corrosion of CFRP-to-metal couples in saline environments. *Carbon Fibres, 2nd International Conference, Proceedings, Feb. 18-20, 1974, London England,* 230-241.

Buyukozturk, O., Gunes, O., Karaca, E. (2004). Progress on understanding debonding problems in reinforced concrete and steel members strengthened using FRP composites. *Construction and Building Materials, 18,* 9-19.

Cadei, J.M.C., Stratford, T.J., Hollaway, L.C. and Duckett, W.G. (2004). *Strengthening metallic structures using externally bonded fibre-reinforced polymers*. London: CIRIA.

Carpenter, W.C. (1991). A comparison of numerous lap joint theories for adhesively bonded joints. *Journal of Adhesion, 35,* 55-73.

Chacon, A., Chajes, M., Swinehart, M., Richardson, D. and Wnczel, G. (2004). Applications of advancedcomposites to steel bridges: A case study on the Ashland Bridge (Delaware-USA). *Advanced composite materials in bridges and structures, Calgary, Alberta, July 20-23, 2004*.

Ching, J.H.C. (2007). *Test report T 40601.* Glendale, CA: Delsen Testing Laboratories, Inc.

Colombi, P. (2004). On the evaluation of compliance information for common crack growth specimens reinforced by composite patch. *International Journal of Fracture, 125,* 73-87.

Colombi, P. (2005). Plasticity induced fatigue crack growth retardation model for steel elements reinforced by composite patch. *Theoretical and Applied Fracture Mechanics, 43,* 63-76.

Colombi, P. (2006). Reinforcement delamination of metallic beams strengthened by FRP strips: Fracture mechanics based approach. *Engineering Fracture Mechanics, 73,* 1980-1995.

Colombi, P. Bassetti, A., and Nussbaumer, A. (2003a). Analysis of cracked steel members reinforced by pre-stress composite patch. *Fatigue & Fracture of Engineering Materials & Structures, 26,* 59-66.

Colombi, P. Bassetti, A., and Nussbaumer, A. (2003b). Crack growth induced delamination on steel members reinforced by prestressed composite patch. *Fatigue & Fracture of Engineering Materials & Structures, 26,* 429-437.

Colombi, P. Fanesi, E., Fava, G. and Poggi, C. (2005). Durability of steel elements strengthened by FRP plates subjected to mechanical and environmental loads. *Composites in Construction, 2005 – Third international conference, Lyon, France, July 11 – 13, 2005.*

Colombi, P. and Poggi, C. (2006a). An experimental, analytical and numerical study of the static behavior of steel beams reinforced by pultruded CFRP strips. *Composites: Part B, 37,* 64-73.

Colombi, P. and Poggi, C. (2006b). Strengthening of tensile steel members and bolted joints using adhesively bonded CFRP plates. *Construction and Building Materials, 20,* 22-33.

Cook, A.K. (2004). Evaluation of the effectiveness of surface applied corrosion inhibitors for concrete bridges. (Master's Thesis, North Carolina State University, 2004).

Crasto, A.S. and Kim, R.Y. (1996). Environmental durability of a composite-to-composite adhesive bond in infrastructure applications. *28th international SAMPE technical conference, November, 4-7, 1996*, 837-849.

Crocombe, A.D., Bigwood, D.A. and Richardson, G. (1990). Analysing structural adhesive joints for failure. *International Journal of Adhesion & Adhesives, 10(3),* 167-178.

Davis, M. and Bond, D. (1999). Principles and practices of adhesive bonded structural joints and repairs. *International Journal of Adhesion & Adhesives, 19,* 91-105.

Dawood, M., Rizkalla, S., and Sumner, E. (2007). Fatigue and overloading behavior of steel-concrete composite flexural members strengthened with high modulus CFRP materials. *Journal of Composites for Construction, 11(6),* 659-669.

Dawood, M.M.R. (2005). Fundamental behavior of steel-concrete composite beams strengthened with high modulus carbon fiber reinforced polymer (CFRP) materials. (Master's Thesis, North Carolina State University, 2005).

De Nève B., and Shanahan, M.E.R. (1992). Effects of humidity on an epoxy adhesive. *International Journal of Adhesion & Adhesives, 12(3),* 191-196.

Deng, J. and Lee, M.M.K. (2007a). Behaviour under static loading of metallic beams reinforced with a bonded CFRP plate. *Composite Structures, 78,* 232-242.

Deng, J. and Lee, M.M.K. (2007b). Fatigue performance of metallic beam strengthened with a bonded CFRP plate. *Composite Structures, 78,* 222-231.

Deng, J., Lee, M.M.K., and Moy, S.S.J. (2004). Stress analysis of steel beams reinforced with a bonded CFRP plate. *Composite Structures, 65,* 205-215.

Diaz, A.D., Hadj-Ahmed, R., Foret, G. and Ehrlacher, A. (2008). Stress analysis in a classical double lap, adhesively bonded joint with a layerwise model. *International Journal of Adhesion & Adhesives, doi:10.1016/j.ijadhadh.2008.01.004.*

Dow Corning. (2005a). *A guide to silane solutions from Dow Corning.* USA: Dow Corning. Retrieved July 14, 2008, from http://www.dowcorning.com/content/publishedlit/SILANE-GUIDE.pdf

Dow Corning. (2005b). *Product information organofunctional silanes: Dow Corning Z-6040 silane.* USA: Dow Corning. Retrieved July 14, 2008, from http://www.dowcorning.com/applications/search/products/details.aspx?prod=01011278&type=PROD

Fam, A., MacDougall, C., and Shaat, A. (2008). Upgrading steel-concrete composite girders and repair of damaged steel beams using bonded CFRP laminates. *Journal of Composites for Construction,* accepted for publication.

Fawzia, S. (2007). Bond characteristics between steel and carbon fibre reinforced polymer (CFRP) composites. (Doctoral Dissertation, Monash University, 2007).

Francis, R. (2000). *Bimetallic Corrosion: Guide to good practice in corrosion control*. Teddington, Middlesex: National Physical Laboratory. Retrieved July 14, 2008, from http://www.npl.co.uk/upload/pdf/bimetallic_20071105114556.pdf

Gao, B., Kim, J., and Leung, C.K.Y. (2006a). Optimization of tapered end design for FRP strips bonded to RC beams. *Composites Science and Technology, 66,* 1266-1273.

Gao, B., Kim, J., and Leung, C.K.Y. (2006b). Strengthening efficiency of taper ended FRP strips bonded to RC beams. *Composites Science and Technology, 66,* 2257-2264.

Gettings, M. and Kinloch, A.J. (1977). Surface analysis of polysiloxane/metal oxide interfaces. *Journal of Material Science, 12,* 2511-2518.

Gledhill, R.A., Shaw, S.J. and Tod. D.A. (1990). Durability of adhesive-bonded joints employing organosilane coupling agents. *International Journal of Adhesion & Adhesives, 10(3),* 192-198.

Golland, M. and Reissner, E. (1944). The Stresses in cemented joints. *Journal of Applied Mechanics, 11,* A17-A27.

Hand, H.M., Arah, C.O., McNamara, D.K. and Mecklenburg, M.F. (1991). Effects of environmental exposure on adhesively bonded joints. *International Journal of Adhesion & Adhesives, 11(1),* 15-23.

Harris, A.F. and Beevers, A. (1999). The effects of grit-blasting on surface properties for adhesion. *International Journal of Adhesion & Adhesives, 19,* 445-452.

Harris, J.A., and Adams, R.D. (1984). Strength prediction of bonded single lap joints by non-linear finite element methods. *International Journal of Adhesion & Adhesives, 4(2),* 65-78.

Hildebrand, M. (1994). Non-linear analysis and optimization of adhesively bonded single lap joints between fibre-reinforced plastics and metals. *International Journal of Adhesion & Adhesives, 14(4),* 261-267.

Hollaway L.C., and Cadei, J. (2002). Progress in the technique of upgrading metallic structures with advanced polymer composites. *Progress in Structural Engineering and Materials, 4,* 131-148.

Horton, T., Spinks, G.M. and Isles, N.A. (1992). Structural adhesive performance in marine environments. *Polymer International, 28(1),* 9-17.

Jiao, H., and Zhao, X.L. (2004). CFRP strengthened butt-welded very high strength (VHS) circular steel tubes. *Thin-Walled Structures, 42,* 963-978.

Johnson, W.S. and Butkus, L.M. (1998). Considering environmental conditions in the design ofbonded structures: A fracture mechanics approach. *Fatigue & Fracture of Engineering Materials & Structures, 21,* 465-478.

Jones, S.C. and Civjan, S.A. (2003). Application of fiber reinforced polymer overlays to extend steel fatigue life. *Journal of Composites for Construction, 7(4),* 331-338.

Kinloch, A.J. (Ed.). (1983). *Durability of structural adhesives.* London: Applied Science Publishers.

Knox, E.M., and Cowling, M.J. (2000). Durability aspects of adhesively bonded thick adherend lap shear joints. *International Journal of Adhesion & Adhesives, 20,* 323-331.

Lam, C.C.A., Cheng, J.J.R., Kennedy, G.D., and Yam, M.C.H. (2006). Study of stress distribution of cracked steel plate with single sided CFRP composite patching. *IABMAS 06, Third international conference on bridge maintenance, safety and management, July 16-19, 2006, Porto, Portugal.*

Lam, C.C.A., Cheng, J.J.R. and Yam, C.H.M. (2004). Study of the tensile strength of CFRP/steel double lap joints. *Advanced composite materials in bridges and structures, Calgary, Alberta, July 20-23, 2004.*

Lanier, B., Schnerch, D., and Rizkalla, S. (2008). Proposed design guidelines for strengthening of steel monopoles with high modulus CFRP materials. *Thin-walled Structures,* accepted for publication.

Lapique, F., and Redford, K. (2002). Curing effects on viscosity and mechanical properties of a commercial epoxy resin adhesive. *International Journal of Adhesion and Adhesives, 22,* 337-346.

Lee, Y., Wipf, T.J., Phares, B.M., and Klaiber, F.W. (2005). Evaluation of steel girder bridge strengthened with carbon fiber-reinforced polymer posttension bars. *Transportation Research Record: Journal of the Transportation Research Board, 1928,* 233-244.

Lenwari, A., and Thepchatri, T. (2002). Predictin of premature separation of bonded CFRP plates from strengthened steel beams using a fracture criterion. *Structural Engineering and Mechanics, 14(5),* 565-574.

Lenwari, A., Thepchatri, T., Albrecht, P. (2005). Flexural response of steel beams strengthened with partial-length CFRP plates. *Journal of Composites for Construction, 9(4),* 296-303.

Lenwari, A., Thepchatri, T., and Albrecht, P. (2006). Debonding strength of steel beams strengthened with CFRP plates. *Journal of Composites for Construction, 10(1),* 69-78.

Liu, X., Silva, P.F., and Nanni, A. (2001). Rehabilitation of steel bride members with FRP composite materials. *Proceedings of CCC 2001, Composites in Construction, Porto, Portugal, Oct. 10-12, 2001,* 613-618.

Matta, F., Karbhari, V.M., and Vitaliani, R. (2005). Tensile response of steel/CFRP adhesive bonds for the rehabilitation of civil structures. *Structural Engineering and Mechanics, 20(5),* 589-608.

Matta, F., Rizzo, P., Karbhari, V., and Lanza di Scalea, F. (2006). Acoustic emission damage assessment of steel/CFRP bonds for rehabilitation. *Journal of Composites for Construction, 10(3),* 265-274.

Mertz, D.R., and Gillespie, J.W. (1996). *Rehabilitation of steel bridge girders through the application of advanced composite materials.* Washington, D.C.: Transportation Research Board

Miller, T.C., Chajes, M.J., Mertz, D.R., and Hastings, J.N. (2001). Strengthening of a steel bridge girder using CFRP plates. *Journal of Bridge Engineering, 6(6),* 514-522.

Mosallam, A.S. (2005). Evaluation and construction of composite strengthening systems for the Sauvie Island Bridge. *FRP Composites in Civil Engineering – CICE 2004*, 715-723.

Moy, S.S.J., Hill, P., Moriarty, J., Dier, A., Kenchington, A. and Iverson, B. (2001). *ICE design and practice guide FRP composites life estension and strengthening of metallic structures* (S.S.J. Moy, Ed.). London: Thomas Telford.

National Research Council. (2007). *Guidelines for the design and construction of externally bonded FRP systems for strengthening existing structures: Metallic structures.* Rome: CNR.

National Weather Service Forecast Office. *Climate Reports* [Data Files]. Retrieved from http://www.weather.gov/climate/index.php?wfo=rah

Nouredine, A. (1996). Rehabilitation of steel bridge girders with graphite pultrusion (Master's thesis, University of Delaware, 1996).

Nozaka, K., Shield, C.K., and Hajjar, J.F. (2005). Effective bond length of carbon-fiber-reinforced polymer strips bonded to fatigued steel bridge I-girders. *Journal of Bridge Engineering, 10(2),* 195-205.

Owens, D.K. (1970). Some thermodynamic aspects of polymer adhesion. *Journal of applied polymer science, 14,* 1725-1730.

Pantelides, C.P., Nadauld, J., and Cercone, L. (2003). Repair of cracked aluminum overhead sign structures with glass fiber reinforced polymer composites. *Journal of Composites for Construction, 7(2),* 118-126.

Patnaik, A.K., and Bauer, C.L. (2004). *4th International Conference on Advanced Composite Materials in Bridges and Structures, Calgary, Alberta, July 20-23, 2004.*

Petrie, E.M., (2007). Silanes as primers and adhesion promoters for metal substrates. *Metal Finishing, 105(7-8),* 85-93.

Photiou, N.K., Hollaway, L.C., and Chryssanthopoulos, M.K. (2006a). Selection of carbon-fiber-reinforced polymer systems for steelwork upgrading. *Journal of Materials in Civil Engineering, 18(5),* 641-649.

Photiou, N.K., Hollaway, L.C., and Chryssanthopoulos, M.K. (2006b). Strengthening of an artificially degraded steel beam utilising a carbon/glass composite system. *Construction and Building Materials, 20,* 11-21.

Rabinovich, O., and Frostig, Y. (2000). Closed-form high-order analysis of RC beams strengthened with FRP strips. *Journal of Composites for Construction, 4(2),* 65-74.

Richardson, G., Crocombe, A.D., and Smith, P.A. (1993). A comparison of two- and three-dimensional finite element analyses of adhesive joints. *International Journal of Adhesion & Adhesives, 13(3),* 193-200.

Sancaktar, E. and Nirantar, P. (2003). Increasing strength of single lap joints of metal adherends by taper minimization. *Journal of Adhesion Science and Technology, 17(5),* 655-675.

Schnerch, D.A. (2005). Strengthening of Steel Structures with High Modulus Carbon Fiber Reinforced Polymer (CFRP) Materials. (Doctoral Dissertation, North Carolina State University, 2005).

Schnerch, D., Dawood, M., Rizkalla, S., and Sumner E. (2007). Proposed design guidelines for strengthening of steel bridges with FRP materials. *Construction and Building Materials, 21,* 1001-1010.

Sebastian, W.M. (2003). Nonlinear influence of contraflexure migration on near-curtailment stresses in hyperstatic FRP-laminated steel members. *Computers and Structures, 81,* 1619-1632.

Sebastian, W.M. (2005). Design of FRP strengthening in metal yield zones. *Structures and Buildings, 158(SB5),* 303-310.

Sebastian, W.M. (2006). Performance implications of imperfectly plastic material in metallic structures with nonmetallic reinforcement. *Journal of Structural Engineering, 132(2),* 237-243.

Seica, M.V. and Packer, J.A. (2007). FRP materials for the rehabilitation of tubular steel structures, for underwater applications. *Composite Structures, 80,* 440-450.

Sen, R. Liby, L., and Mullins, G. (2001). Strengthening steel bridge sections using CFRP laminates. *Composites: Part B, 32,* 309-322.

Shaat, A., and Fam, A. (2006). Axial loading tests on short and long hollow structural steel columns retrofitted using carbon fibre reinforced polymers. *Canadian Journal of Civil Engineering, 33,* 1-13.

Shaat, A. and Fam, A. (2007). Fiber-element model for slender HSS columns retrofitted with bonded high-modulus composites. *Journal of Structural Engineering, 133(1),* 85-95.

Shaat, A. and Fam, A. (2008). Repair of cracked steel girders connected to concrete slabs using carbon fiber reinforced polymer sheets. *Journal of Composites for Construction,* accepted for publication.

Shaat, A., Schnerch, D., Fam, A., and Rizkalla, S. (2004). Retrofit of steel structures using fiber reinforced polymers (FRP): State-of-the-Art. *Transportation Research Board, Annual Meeting, Washington, D.C.*

Shen, H., Teng, J.G., and Yang, J. (2001). Interfacial stresses in beams and slabs bonded with thin plate. *Journal of Engineering Mechanics, 127(4),* 399-406.

Silvestre, N., Young, B., and Camotim, D. (2008). Non-linear behavior and load-carrying capacity of CFRP-strengthened lipped channel steel columns. *Engineering Structures, doi:10.1016/j.engstrucu.2008.02.010.*

Sloan, F.E., and Talbot, J.B. (1992) Corrosion of graphite-fiber reinforced composites I – Galvanic coupling damage. *Corrosion Engineering, 48(10),* 830-839.

Smith, S.T., and Teng, J.G. (2001). Interfacial stresses in plated beams. *Engineering Structures, 23,* 857-871.

Stratford, T., and Cadei, J. (2006). Elastic analysis of adhesion stresses for the design of a strengthening plate bonded to a beam. *Construction and Building Materials, 20,* 34-45.

Täljsten, B. (1997). Defining anchor lengths of steel and CFRP plates bonded to concrete. *International Journal of Adhesion & Adhesives, 17(4),* 319-327.

Tavakkolizadeh, M. and Saadatmanesh, H. (2001). Galvanic corrosion of carbon and steel in aggressive environments. *Journal of Composites for Construction, 5(3),* 200-210.

Tavakkolizadeh, M. and Saadatmanesh, H. (2003a). Fatigue strength of steel girders strengthened with carbon fiber reinforced polymer patch. *Journal of Structural Engineering, 129(2),* 186-196.

Tavakkolizadeh, M. and Saadatmanesh, H. (2003b). Repair of damaged steel-concrete composite girders using carbon fiber-reinforced polymer sheets. *Journal of Composites for Construction, 7(4),* 311-322.

Tavakkolizadeh, M., and Saadatmanesh, H. (2003c). Strengthening of steel-concrete composite girders using carbon fiber reinforced polymers sheets. *Journal of Structural Engineering, 129(1),* 30-40.

The Institution of Structural Engineering. (1999). *Guide to the structural use of adhesives.* London: The Institution of Structural Engineering.

Torres-Acosta, A.A., and Sen, R. (2005). Electrochemical behavior ofcoupled carbon fiber-reinforced polymer (CFRP) rods in concrete. *Journal of Applied Electrochemistry, 35,* 529-537.

Tucker, W.C., and Brown, R. (1989). Blister formation on graphite/polymer composites galvanically coupled with steel in seawater. *Journal of Composite Materials, 23,* 389-395.

Walker, P. (1991). Organosilanes as adhesion promoters. *Journal of Adhesion Science and Technology, 5(4),* 279-305.

Wang, J. Rider, A.N., Heller, M., and Kaye, R. (2005). Theoretical and experimental research into optimal edge taper of bonded repair patches subject to fatigue loadings. *International Journal of Adhesion & Adhesives, 25,* 410-426.

Wang, X. and Gupta, V. (2005). Construction and characterization of chemically joined stainless steel/E-glass composite sections. *Mechanics of Materials, 37,* 1198-1209.

West, T.D. (2001). Enhancement to the bond between advanced composite materials and steel for bridge rehabilitation. (Master's Thesis, University o Delaware, 2001).

Wipf, T.J., Phares, B.M., Klaiber, F.W., Al-Saidy, A.H., and Lee, Y. (2005). Strengthening steel girder bridges with carbon fiber-reinforced polymer plates. *Transportation Research Board – 6th International Bridge Engineering Conference: Reliability, Security and Sustainability in Bridge Engineering,* 435-447.

Xia, S.H., and Teng, J.G. (2005). Behaviour of FRP-to-steel bonded joints. *Proceedings of the international symposium on bon behaviour of FRP in structures (BBFS 2005),* 419-426.

Youssef, M.A. (2006). Analytical prediction of the linear and nonlinear behavior of steel beams rehabilitated using FRP sheets. *Engineering Structures, 28,* 903-911.

Zhai, L.L., Ling, G.P. and Wang, Y.W. (2007). Effect of nano-Al_2O_3 on adhesion strength of epoxy adhesive and steel. *International Journal of Adhesion & Adhesives, 28,* 23-28.

Zhao, X. and Zhang, L. (2007). State-of-the-art review on FRP strengthened steel structures. *Engineering Structures, 29,* 1808-1823.

Zhao, X., Fernando, D., and Al-Mahaidi, D. (2006). CFRP strengthened RHS subjected to transverse end bearing force. *Engineering Structures, 28,* 1555-1565.

Appendices

Appendix A. Detailed Results of the Splice Beam Tests

The detailed results of the steel beams that were tested to study the bond behavior of spliced CFRP plates are presented in this appendix following the order of the discussion in Chapter 4. The measured strains and calculated shear stresses are presented for the 400-S, 800-S(1), 400-T2, 800-T2 and 800-U splice configurations.

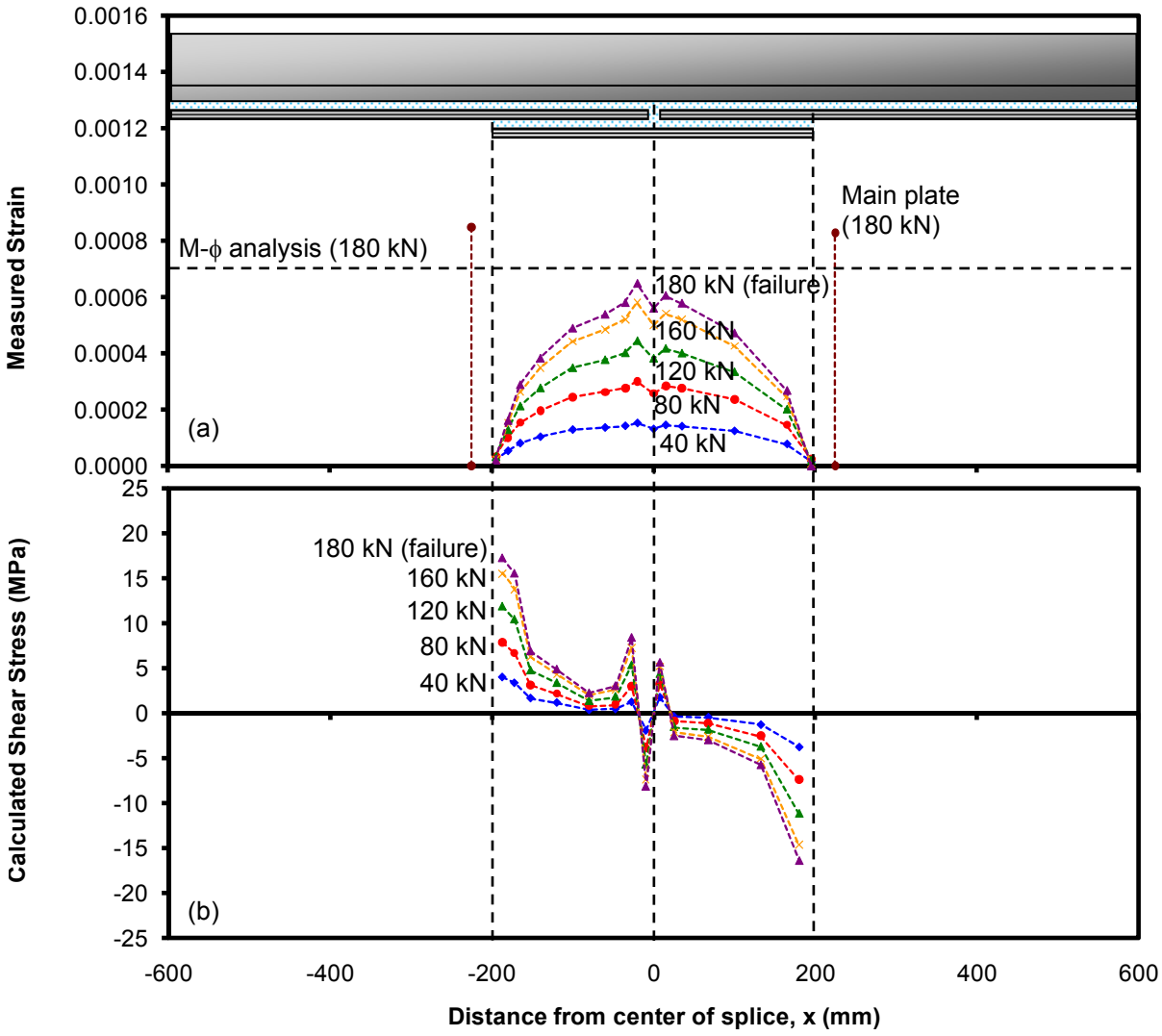

Figure A.1 – Results for beam splice configuration 400-S (a) Measured strains at the surface of the CFRP splice plate and (b) calculated shear stress distribution in the adhesive

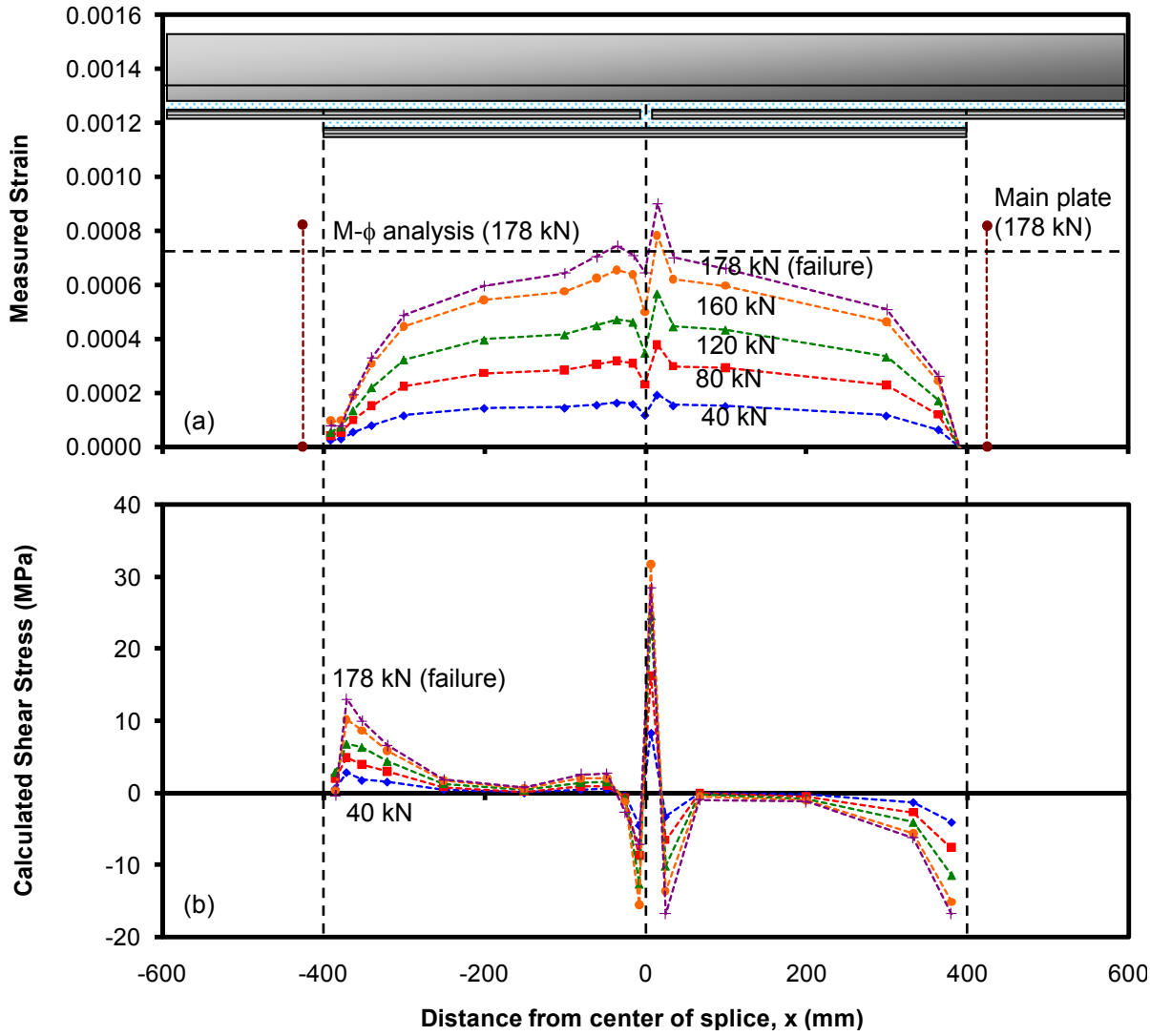

Figure A.2 – Results for beam splice configuration 800-S(1) (a) Measured strains at the surface of the CFRP splice plate and (b) calculated shear stress distribution in the adhesive

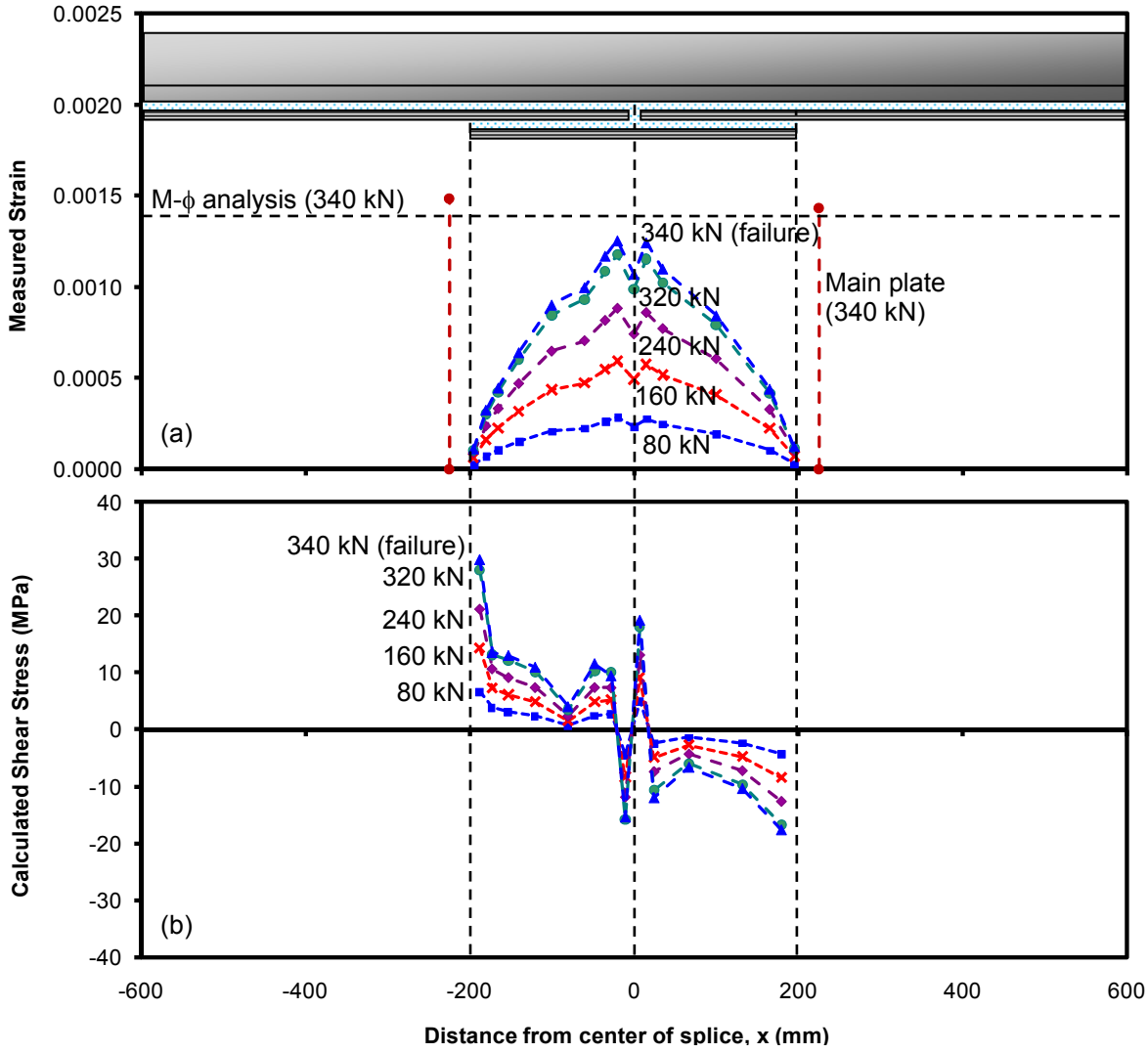

Figure A.3 – Results for beam splice configuration 400-T2 (a) Measured strains at the surface of the CFRP splice plate and (b) calculated shear stress distribution in the adhesive

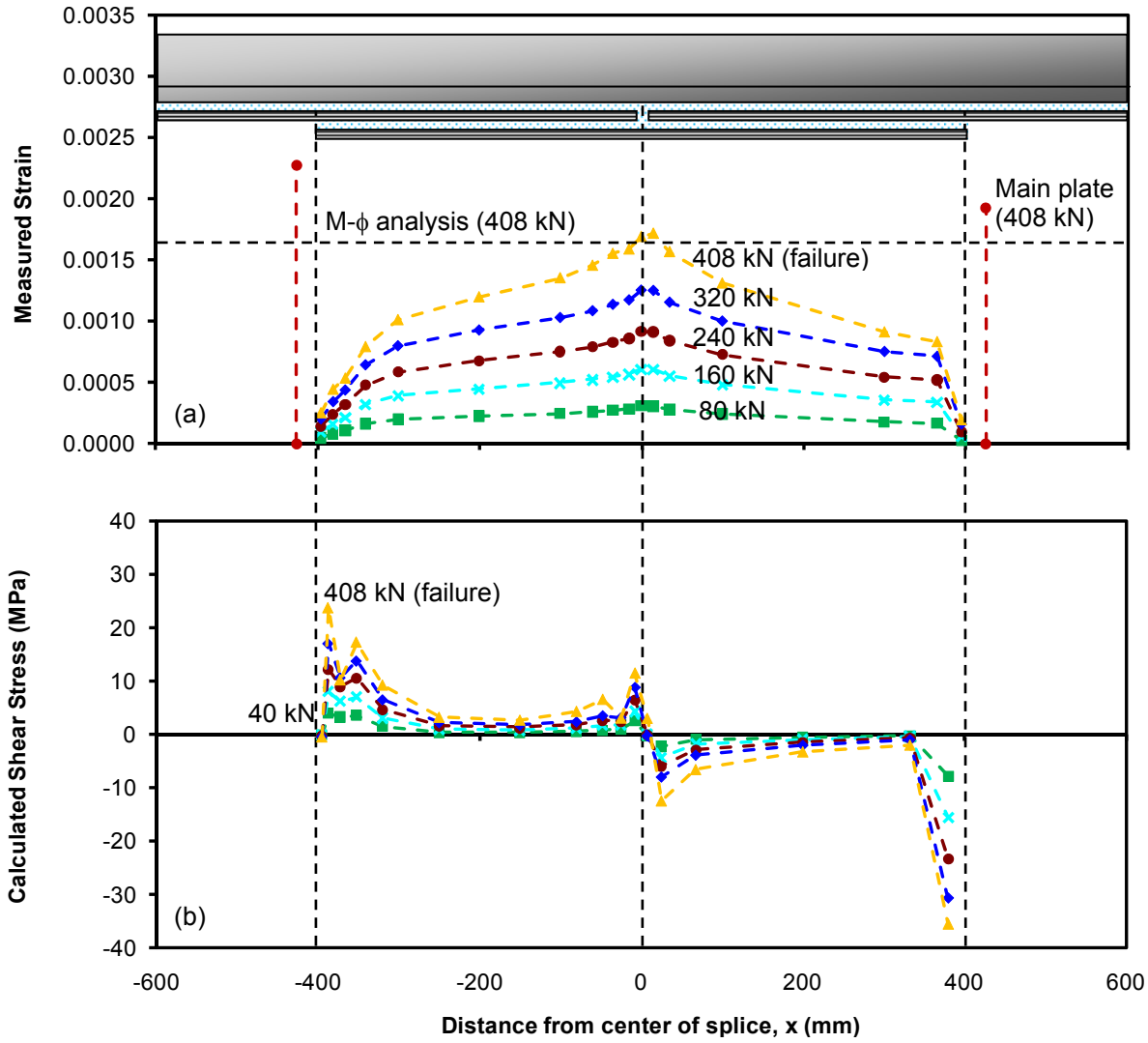

Figure A.4 – Results for beam splice configuration 800-T2 (a) Measured strains at the surface of the CFRP splice plate and (b) calculated shear stress distribution in the adhesive

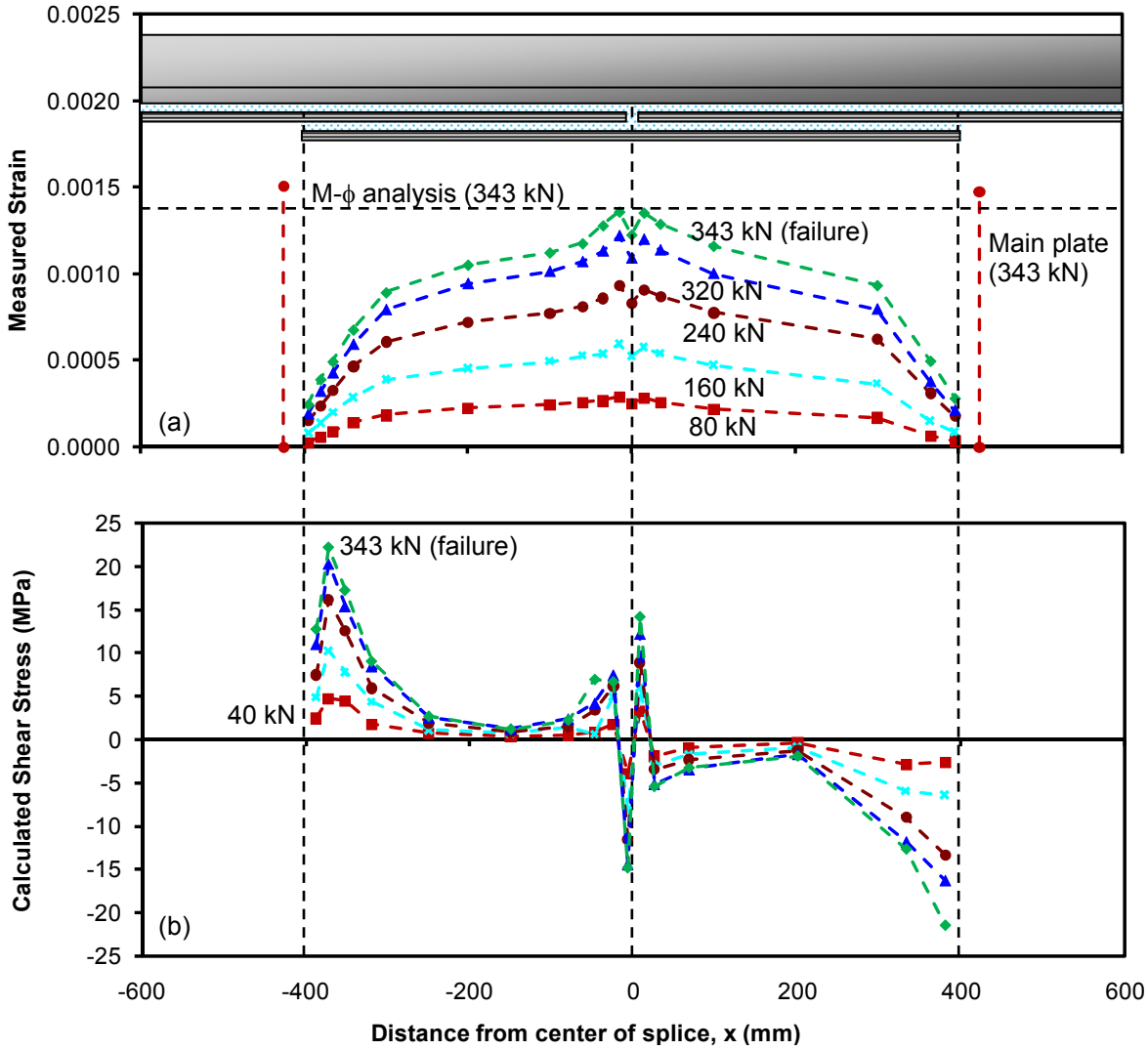

Figure A.5 – Results for beam splice configuration 800-U (a) Measured strains at the surface of the CFRP splice plate and (b) calculated shear stress distribution in the adhesive

Appendix B. Detailed Results of the Environmental Durability Study

The detailed results of the double-lap shear coupons that were tested for the environmental durability study are presented in this appendix following the order of the discussion in Chapter 9. The results of the specimens exposed to one, four and six months of environmental conditioning are presented respectively.

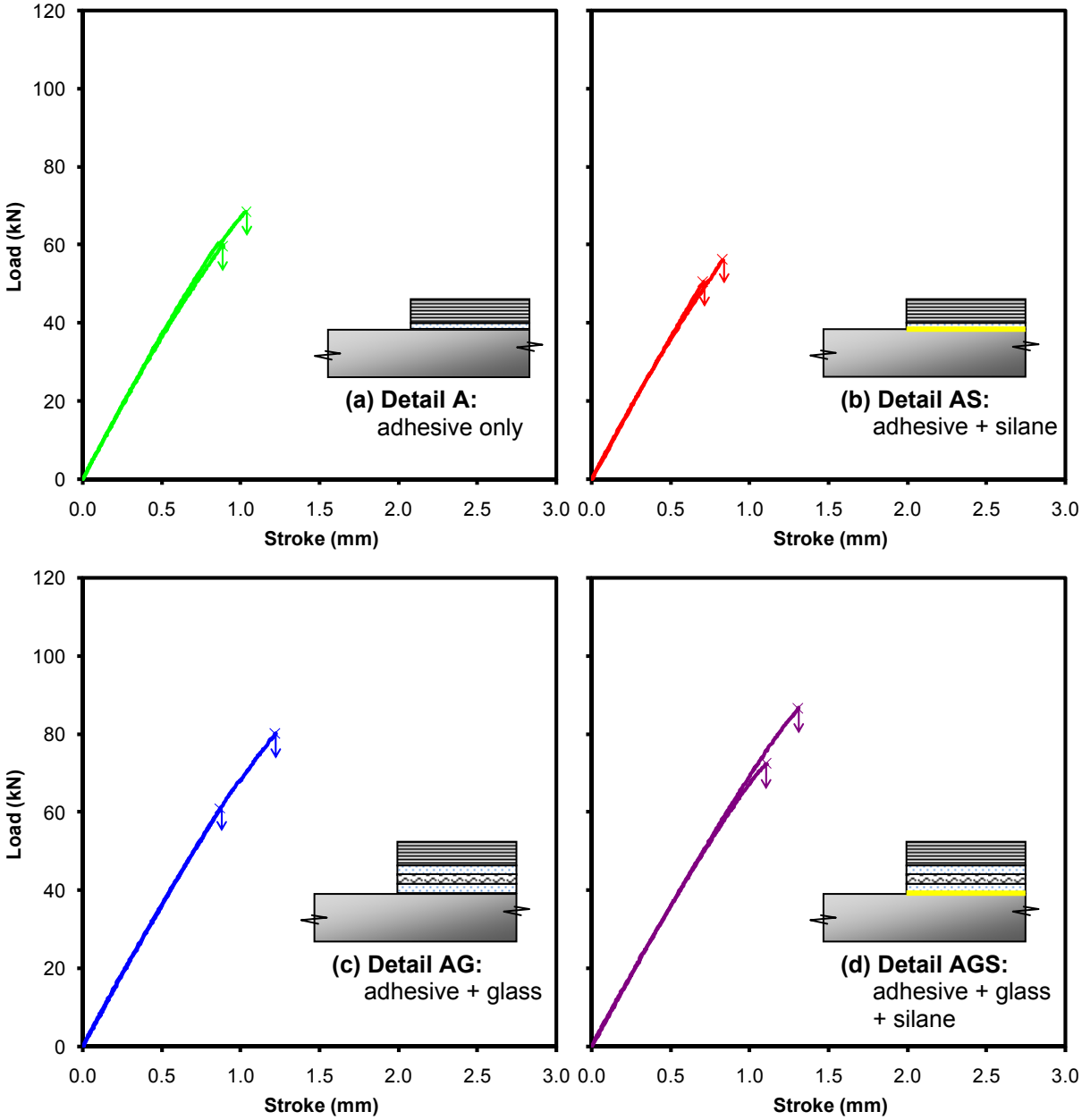

Figure B.1 – Measured load-stroke behavior of specimens subjected to one month of environmental conditioning

Table B.1 – Measured chord stiffness of specimens subjected to one month of environmental conditioning

Test Number	Detail A (kN/mm)	Detail AS (kN/mm)	Detail AG (kN/mm)	Detail AGS (kN/mm)
1	74.3	73.0	71.3	71.4
2	72.2	70.3	71.7	71.0
Average	73.2	71.7	71.5	71.2
St. dev.	1.5	1.9	0.3	0.3
Coef. of var.	2.0%	2.6%	0.4%	0.4%

Note: The stiffness of the two unloaded specimens is not presented due to the shorter specimen length used for those tests.

Table B.2 – Measured ultimate strength of specimens subjected to one month of environmental conditioning

Test Number	Detail A (kN/mm)	Detail AS (kN/mm)	Detail AG (kN/mm)	Detail AGS (kN/mm)
1	68.4	50.5	61.1	86.4
2	59.5	56.2	80.1	72.4
3*	48.8	N/A	N/A	N/A
4*	53.2	N/A	N/A	N/A
Average	57.5	53.3	70.6	79.4
St. dev.	8.5	4.0	13.4	9.9
Coef. of var.	15%	7.5%	19%	13%

* unloaded during conditioning

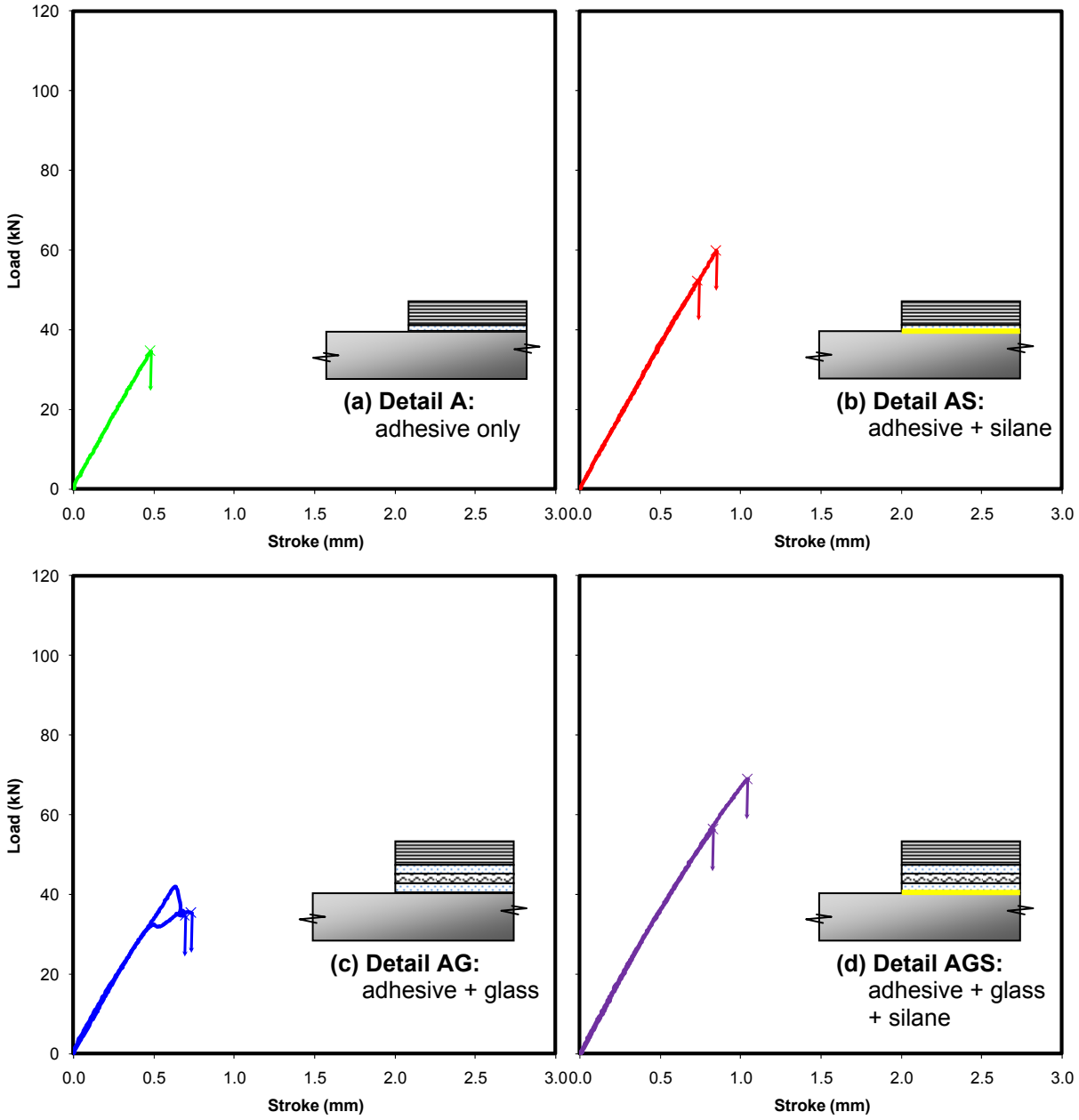

Figure B.2 – Measured load-stroke behavior of specimens subjected to four months of environmental conditioning

Table B.3 – Measured chord stiffness of specimens subjected to four months of environmental conditioning

Test Number	Detail A (kN/mm)	Detail AS (kN/mm)	Detail AG (kN/mm)	Detail AGS (kN/mm)
1	N/A*	72.4	68.1	75.9
2	71.9	70.0	71.2	74.1
Average	-	71.2	69.6	75.0
St. dev.	-	1.7	2.2	1.3
Coef. of var.	-	2.3%	3.2%	1.7%

* data unavailable, failed during conditioning

Note: The stiffness of the two unloaded specimens is not presented due to the shorter specimen length used for those tests.

Table B.4 – Measured ultimate strength of specimens subjected to four months of environmental conditioning

Test Number	Detail A (kN/mm)	Detail AS (kN/mm)	Detail AG (kN/mm)	Detail AGS (kN/mm)
1	15.0*	59.8	34.7	68.9
2	34.5	52.4	42.0	56.3
3**	15.9	N/A	N/A	N/A
4**	47.6	N/A	N/A	N/A
Average	28.3	56.1	38.3	62.6
St. dev.	15.7	5.2	5.2	8.9
Coef. of var.	56%	9.3%	14%	14%

* failed due to sustained load during conditioning

** unloaded during conditioning

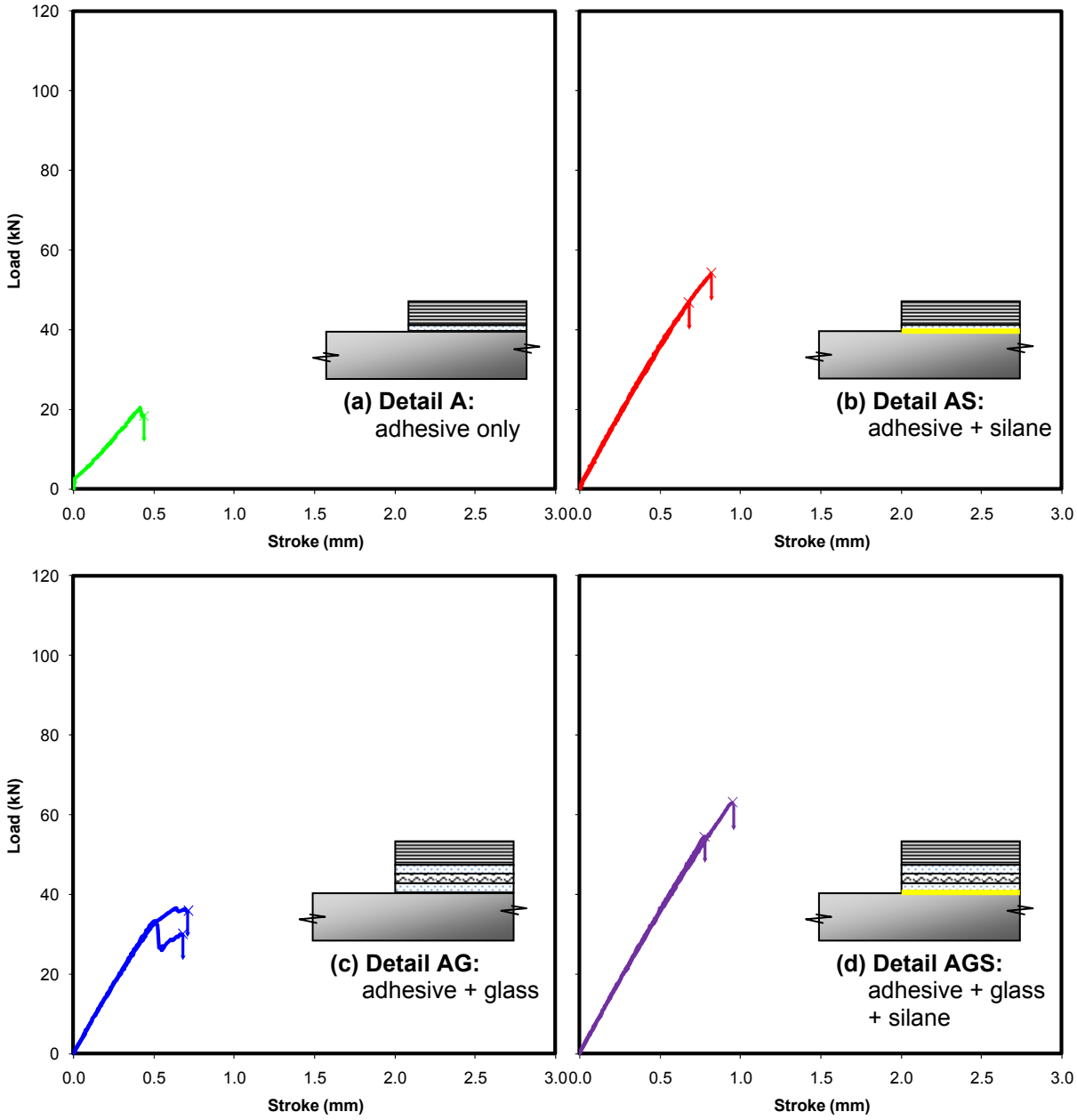

Figure B.3 – Measured load-stroke behavior of specimens subjected to six months of environmental conditioning

Table B.5 – Measured chord stiffness of specimens subjected to six months of environmental conditioning

Test Number	Detail A (kN/mm)	Detail AS (kN/mm)	Detail AG (kN/mm)	Detail AGS (kN/mm)
1	45.3*	72.6	68.1	74.5
2	N/A**	73.6	66.6	71.3
Average	-	73.1	67.3	72.9
St. dev.	-	0.7	1.0	2.3
Coef. of var.	-	1.0	1.5	3.1

* CFRP partially debonded during environmental conditioning
** data unavailable, failed during conditioning

Note: The stiffness of the two unloaded specimens is not presented due to the shorter specimen length used for those tests.

Table B.6 – Measured ultimate strength of specimens subjected to six months of environmental conditioning

Test Number	Detail A (kN/mm)	Detail AS (kN/mm)	Detail AG (kN/mm)	Detail AGS (kN/mm)
1	20.3	46.8	33.3	54.5
2	15.0*	54.1	36.6	63.0
3**	41.5	N/A	N/A	N/A
4**	16.5	N/A	N/A	N/A
Average	23.3	50.4	35.0	58.7
St. dev.	12.3	5.2	2.3	6.0
Coef. of var.	53%	10%	6.5%	10%

* failed due to sustained load during conditioning
** unloaded during conditioning